January 2015

Impact of Polymers on the Solution Crystal Growth Rate of a Poorly Water-Soluble Active Pharmaceutical Ingredient

Caitlin J. Schram
Purdue University

Graduate School Form 30
Updated 1/15/2015

PURDUE UNIVERSITY
GRADUATE SCHOOL
Thesis/Dissertation Acceptance

This is to certify that the thesis/dissertation prepared

By Caitlin J. Schram

Entitled
Impact of Polymers on the Solution Crystal Growth Rate of a Poorly Water-Soluble Active Pharmaceutical Ingredient

For the degree of Doctor of Philosophy

Is approved by the final examining committee:

Stephen P. Beaudoin
Chair

Lynne S. Taylor

Zoltan K. Nagy

Gintaras V. Reklaitis

To the best of my knowledge and as understood by the student in the Thesis/Dissertation Agreement, Publication Delay, and Certification Disclaimer (Graduate School Form 32), this thesis/dissertation adheres to the provisions of Purdue University's "Policy of Integrity in Research" and the use of copyright material.

Approved by Major Professor(s): Stephen P. Beaudoin

Approved by: John A. Morgan 12/5/2015
Head of the Departmental Graduate Program Date

IMPACT OF POLYMERS ON THE SOLUTION CRYSTAL GROWTH RATE OF A POORLY WATER-SOLUBLE ACTIVE PHARMACEUTICAL INGREDIENT

A Dissertation

Submitted to the Faculty

of

Purdue University

by

Caitlin J. Schram

In Partial Fulfillment of the

Requirements for the Degree

of

Doctor of Philosophy

December 2015

Purdue University

West Lafayette, Indiana

I dedicate this dissertation to my parents, for providing me with the tools and confidence to succeed in everything I dare to accomplish, to my sisters, Emily and Kristin, for being my role models and my biggest fans, and to Jin for supporting me unconditionally throughout this crazy adventure.

ACKNOWLEDGEMENTS

I would like to thank my advisors, Stephen Beaudoin and Lynne Taylor for their guidance throughout this project. This work would not have been possible without their constant support and leadership.

I would also like to express my gratitude to my fellow members of the Beaudoin and Taylor research groups, for their constant willingness to lend a helping hand when needed, and to the undergraduate researchers who assisted me in the lab. In particular, Ryan Smyth, who worked diligently to gather some of the data presented in this dissertation.

I would also like to thank Purdue University and the School of Chemical Engineering for the opportunity to study in this program. I have grown immensely as a researcher over the past few years and I am very grateful to Purdue for investing in me.

Finally, I would like to acknowledge our sources of funding. The Graduate Assistantship in Areas of National Need program from the Department of Education (award number P200A090335), the National Science Foundation through grant numbers EEC-0540855 and IIP- 1152308 and the National Institutes of Health Grant R41GM100657-01A1. Without their financial support, this work would not have been possible.

TABLE OF CONTENTS

Page

Page

Page

Page

LIST OF TABLES

LIST OF FIGURES

Figure Page

Appendix Figure

Appendix Figure Page

Appendix Figure Page

LIST OF SYMBOLS

A	total crystal surface area	j	solute mass flux
A_{hkl}	individual crystal face area	k_B	Bolzmann constant
a_b	bulk solute activity	k_d	mass transfer rate coefficient
a*	equilibrium solute activity	k_r	integration rate coefficient
a	size of a growth unit	L	distance between active sites
C	concentration	l	distance between adsorbed polymers
C_b	bulk concentration	m	crytsal mass
C_I	interface concentration	R	gas constant
C*	equilibrium concentration	R_e	Reynold's number
D	diffusion coefficient	R_G	crystal growth rate
Da	Damköhler number	R_0	crystal growth rate of pure drug
E_g	polymer effectiveness ratio	R_P	crystal growth rate with polymers
G	face growth rate	$R_{q,av}$	average surface roughness
G_0	face growth rate of pure drug	r	integration rate order
G_P	face growth rate with polymers	r_d	disk radius
g	overall growth rate order	r_h	hydrodynamic radius of solute
h	height of a growth step	r_p	radius of a polymer globule
h_p	height of a polymer globule	S	supersaturation ratio

S_m	entropy of melting	ζ	crystal density
T	temperature	η	dynamic viscosity
T_m	melting temperature	θ	polymer surface coverage (model)
V	volume of spherical cap	μ	chemical potential
V	step growth rate	ν	kinematic viscosity
V_0	step growth rate of pure drug	ρ	step radius of curvature
V_P	step growth rate with polymers	ρ_c	critical nucleus radius
v_y	axial velocity component	σ	crystallization driving force
X	mole fraction aqueous solubility	Υ	activity coefficient
y	axial direction	Υ_b	bulk activity coefficient
α	impurity effectiveness factor	Υ^*	equilibrium activity coefficient
γ	edge free energy	Φ	polymer surface coverage (measured)
δ_H	hydrodynamic boundary layer	ω	angular velocity

ABSTRACT

Schram, Caitlin J. Ph.D., Purdue University, December 2015. Impact of Polymers on the Solution Crystal Growth Rate of a Poorly Water-Soluble Active Pharmaceutical Ingredient. Major Professors: Stephen Beaudoin, Lynne Taylor.

Poor aqueous solubility is a major impediment to the oral delivery of over 75% of pharmaceutical compounds currently under development. The bioavailability of these compounds can be enhanced with the use of supersaturating dosage forms, due to their high flux rates across the gastrointestinal tract membrane. However, the success of this strategy hinges on the ability to inhibit crystallization of the supersaturated drug solutions. Polymers can be used to inhibit crystallization and prolong supersaturation, however the mechanisms of polymer inhibition are not yet fully understood. Therefore it is desirable to understand the attributes that render a polymer effective. In this work, the crystal growth rate of a poorly soluble pharmaceutical compound, felodipine, was measured in the presence of various polymers. The growth rate studies were performed using a rotating disk apparatus so that the growth kinetics could be controlled and mathematically modeled. It was found that both polymer ionization state and polymer hydrophobicity greatly impacted polymer effectiveness. Investigation of these systems with atomic force microscopy (AFM) revealed that these properties significantly impacted adsorbed polymer conformation. The polymers that adsorbed in an extended

chain conformation were able to achieve a higher degree of surface coverage than those that adsorbed in a coiled globule formation. The surface coverage was found to directly correlate to polymer effectiveness. By modeling this correlation using the Kubota-Mullin model, polymer effectiveness could be predicted when surface coverage was known. This research also assessed the ability of a polymer to impact crystal morphology. It was found that when polymers were present during crystal evolution from an amorphous melt, they were able to impact the size and shape of the resulting crystals. This in turn influenced the rate of crystal growth from supersaturated solutions.

CHAPTER 1. LITERATURE REVIEW

1.1 Introduction

Many factors determine the rate and extent of absorption of an active pharmaceutical ingredient (API) from the gastrointestinal (GI) tract.[1,2] Fundamentally, the API must be able to permeate through the GI tract membrane, and possess adequate aqueous solubility.[3] Thus, a poorly soluble drug will have limited bioavailability, posing a challenge for oral dosage formulations. Modification of the solid state, for example, formulation as an amorphous solid, can increase solubility[4–6] without compromising permeability.[7]

The amorphous form possesses higher free energy and enthalpy compared to the crystalline form, and has no long-range molecular order.[8–10] Thus, the energy required to dissolve an amorphous solid is significantly decreased relative to the crystalline form. Upon dissolving, the amorphous solid can generate a supersaturated solution.[11] The supersaturated solution of a drug has a greater thermodynamic activity than its saturated solution, which can increase absorption.[12–14] However, supersaturated solutions will quickly crystallize due to the increased activity; therefore, methods to slow crystallization and prolong supersaturation are of great interest. One such method is the use of additives, such as polymers, which can effectively inhibit crystal growth and stabilize supersaturated solutions by adsorbing to growth sites.[15–17]

The overall objective of the work presented in this dissertation was to provide valuable insight into the specific mechanisms by which polymers can inhibit crystal growth in solution. Recent studies on polymer inhibition, which will be reviewed in the following sections, showed that polymer effectiveness varied greatly for a given API. Certain polymer properties that impacted effectiveness were identified, however, the details of how these properties contributed to effectiveness were unclear. The work presented in this dissertation reveals that polymer conformation and consequently, surface coverage, are key determinants of polymer effectiveness.

1.2 Broader Impact

Many industries, including fine chemicals, microelectronics, food, and pharmaceuticals, require the ability to control crystallization processes.[18] This is because crystal form dictates the physical and chemical properties of a compound. In the pharmaceutical field, manipulating crystal form can be used as a means to enhance the bioavailability of oral dosage forms. This is important because it is estimated that about 75% - 90% of promising drug candidates have poor aqueous solubility[6,19] This compromises their absorption due to their inability to dissolve in the aqueous gastrointestinal lumen[5]. Therefore, methods to enhance the solubility, such as utilizing the amorphous form of the API, are necessary in order to ensure that pharmaceutical companies can put promising drug candidates on the market.

Two recently approved therapies highlight the importance of solid form manipulation. Vemurafenib is able to treat tumors by inhibiting mutations of the protein kinase B-RAF, common in melanoma. In its crystalline form, this compound yielded

modest drug exposure, so there was little tumor regression. But higher drug exposure was achieved by reformulating vemurafenib as micro-precipitated bulk powder (MBP). Thus, by utilizing the amorphous form, the bioavailability was proven to increase tenfold causing tumors to shrink significantly.[20]

Another example is telaprevir, a treatment for the hepatitis C virus. In its crystalline form, telaprevir exhibited a lower aqueous solubility than that of marble. However, formulating this API as an amorphous spray dried suspension with a stabilizing polymer and surfactant greatly improved its bioavailability, such that the sustained viral response (SVR) rates in patients treated with the new telaprevir formulation was 60-70%.[21]

Both of the therapies mentioned above are used to treat serious, life-threatening diseases. The ability to improve the bioavailability of these drugs and others that suffer from low solubility, has significant implications for patients seeking life-saving treatments.

1.3 The Amorphous Form

Solubility can be expressed as[19,22]

$$\ln X = -\frac{\Delta S_m (\mathrm{T}_m - \mathrm{T})}{\mathrm{RT}} - \ln \Upsilon \qquad (1.1)$$

where X is the mole fraction aqueous solubility, ΔS_m is the entropy of melting, T_m is the melting temperature, R is the gas constant, T is the temperature, and Υ is the activity

coefficient. This expression assumes that heat capacity is independent of temperature. The second term in the equation reflects the affinity of the solute for the solvent, or the lyophilicity, which can either hinder or aid solubility.

The first term in equation (1.1) reflects the crystallinity of the solid.[22] In crystalline solids, molecules are arranged in a tightly packed lattice formation (Figure 1.1a), maximizing a molecule's interactions with neighboring molecules, and increasing overall stability of the solid. Amorphous solids on the other hand lack long-range molecular order (Figure 1.1b), and are considered a supercooled liquid or a glass.[8] Thus an amorphous solid does not exhibit a phase transition to the liquid state and the first term in equation (1.1) can be neglected thereby increasing the mole fraction solubility.

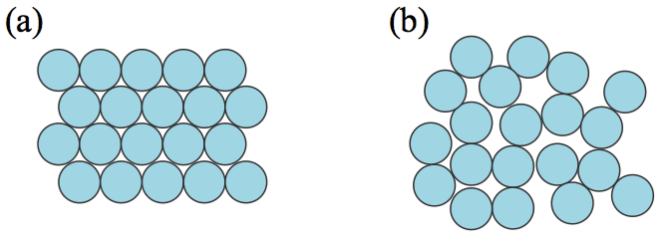

Figure 1.1. Molecular arrangements of (a) a crystalline solid, and (b) an amorphous solid

In other words, for a solid to enter into solution, the interactions between molecules must be disrupted. Due to the lack of long-range order in an amorphous solid, less energy is required (i.e. it is more favorable) to disrupt the intramolecular bonds. Upon dissolving, the amorphous solid can generate a supersaturated solution,[11] which has greater thermodynamic activity than a saturated solution resulting in higher membrane

flux rates, and therefore, higher absorption.[12–14] However, supersaturated solutions will crystallize rapidly due to the increased thermodynamic driving force, threatening the efficacy of this formulation strategy.[23] Therefore, it is necessary to stabilize the supersaturated solution by inhibiting crystal growth for a sufficient amount of time, such that the solute can permeate the GI tract membrane and be absorbed successfully.

1.4 Crystal Growth Theory

The thermodynamic driving force for crystal growth, σ, is the chemical potential difference between a supersaturated and saturated solution of a given substance, Δμ.[24] This can be expressed in dimensionless form in terms of solute activity:[25,26]

$$\sigma = \frac{\Delta\mu}{RT} = \ln\left(\frac{a_b}{a^*}\right) \qquad (1.2)$$

where a_b is the solute activity in the bulk solution, a* is the equilibrium solute activity, R is the gas constant, and T is the temperature. Equivalently, the driving force can be expressed in terms of the activity coefficient, Υ, and concentration, C:[24,26]

$$\ln\left(\frac{a_b}{a^*}\right) = \ln\left(\frac{\Upsilon_b C_b}{\Upsilon^* C^*}\right) \qquad (1.3)$$

Activities and activity coefficients are difficult to obtain. Therefore, the driving force is often expressed in terms of only the concentration ratio (eq 1.4a and 1.4b) or the concentration gradient (eq 1.4c):

$$\sigma \approx \ln\left(\frac{C_b}{C^*}\right) \quad (1.4a)$$

$$\sigma \approx \frac{C_b}{C^*} = \mathrm{S} \quad (1.4b)$$

$$\sigma \approx C_b - C^* \quad (1.4c)$$

where S is the supersaturation ratio. Such expressions for the driving force in terms of concentration assume that $\Upsilon_b \approx \Upsilon^*$ which is valid for ideal solutions with low supersaturation (S<1).[27]

The overall crystal growth rate, R_G, which is the rate of mass deposition, m, onto the crystal over time, t, is expressed in terms of the driving force as[24]

$$\mathrm{R_G} = k_G \mathrm{A}\sigma^g = \frac{\mathrm{dm}}{\mathrm{dt}} \quad (1.5)$$

where k_G is the growth rate coefficient, A is the crystal surface area, and g is the overall growth order.

Crystallization occurs by two distinct phenomena: nucleation and growth. Nuclei must be present in order for growth to occur. Nucleation is the materialization of a new solid phase from the supersaturated phase.[26] Nuclei can form by the union of solute molecules in an uncontaminated homogeneous solution (primary homogeneous nucleation). It can be instigated by an impurity that provides an existing surface for solute molecules to attach to (primary heterogeneous nucleation). Or it can be induced by seeds of the material placed in the supersaturated solution (secondary nucleation).[24]

Once the nucleus reaches a critical size in solution, growth can begin. There are many mechanisms for crystal growth described in the literature. Adsorption layer theories are widely accepted and they are based on the adsorption of solute molecules onto the crystal face starting from a two-dimensional nucleus of critical radius, ρ_c. The critical radius will depend on several properties of the compound as well as the environment:[15]

$$\rho_c = \frac{\gamma a}{k_B \mathrm{T}(\ln \mathrm{S})} \qquad (1.6)$$

Here, γ is the edge free energy of the compound, a is the area that a growth unit occupies on a crystal, k_B is the Boltzmann constant, and T is the solution temperature.

In the step-growth theory developed by Kossel,[28] growth units will attach at the highest energy 'kink' sites, and continue in a linear step-wise fashion across the width of the face, creating steps that are monoatomic in height. In the birth and spread mechanism, nuclei form at the edges or on faces of the crystals and monolayer growth proceeds in all directions from these nuclei.[24,29] Knowledge of adsorption layer theories provides a basis for understanding additive inhibition theory (Section 1.5). The work shown in Chapter 6 of this dissertation provides evidence of these growth mechanisms for the systems studied.

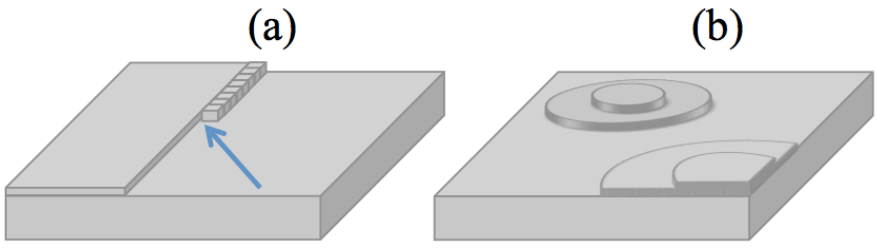

Figure 1.2. Illustrations of the (a) step-growth mechanism, where the arrow is highlighting a kink site, and (b) the birth and spread mechanism.

The rate of crystal growth can be expressed by combining equations (1.4c) and (1.5):

$$\mathrm{R_G} = k_G \mathrm{A}(C_b - C^*)^g \qquad (1.7)$$

Equation (1.7) is the overall growth rate expression, however, crystal growth involves two separate steps, which are considered to occur in series. First, solute diffuses to the solid-liquid interface (Figure 1.2a), then it integrates into the crystal lattice. Figure 1.2b illustrates the integration process. According to the Gibbs-Volmer theory, once the solute arrives at the interface, it can diffuse over the surface until it finds a site to link into the lattice.[24]

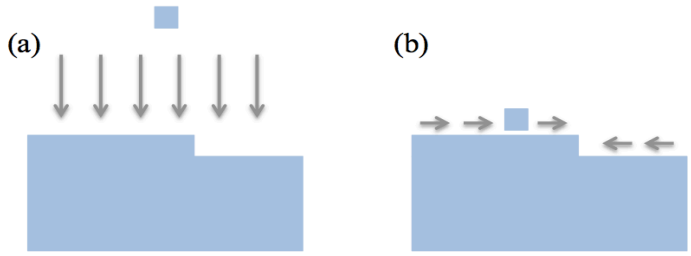

Figure 1.3. Illustrations of the two steps of a crystal growth process: (a) mass transfer of solute to the interface and (b) integration of solute into the crystal lattice

Each growth step has a different rate associated with it and a different driving force. Equation (1.7) can then be separated into two steps:[24,26]

$$\mathrm{R_G} = k_d \mathrm{A}(C_b - C_I) \qquad (1.8)$$

$$\mathrm{R_G} = k_r \mathrm{A}(C_I - C^*)^r \qquad (1.9)$$

Equation (1.8) represents the rate of mass transfer, where k_d is the mass transfer rate coefficient, and C_I is the concentration at the solid-liquid interface. Equation (1.9) represents the rate of integration, where k_r is the integration rate coefficient, and r is the integration rate order.

When the rate of mass transfer is slower (i.e. the mass transfer step offers more resistance), the growth process is considered to be 'mass transfer controlled.' When the integration step offers more resistance, the growth process is 'integration controlled.' In the case of integration-controlled growth, the concentration at the interface, C_I will approach the bulk concentration, C_b, and equation (1.9) can be approximated as

$$\mathrm{R_G} = k_r \mathrm{A}(C_b - C^*)^r \qquad (1.10)$$

The Damköhler number (Da) is used to compare the relative contribution of each step:

$$\mathrm{Da} = \frac{k_r (C_b - C^*)^{r-1}}{k_d} \qquad (1.11)$$

Thus, when Da is large, growth is mass transfer controlled ($k_d << k_r$) and when Da is small, growth is integration controlled ($k_r << k_d$).[26] The objective of the work presented in Chapter 3 was to separate the roles of mass transfer and integration so that integration-controlled growth rates could be studied.

1.5 Additive Inhibition: Theory and Model

Supersaturated solutions will crystallize over time, compromising absorption. Thus, methods to slow crystallization and prolong supersaturation are of great interest. Additives, such as polymers, can effectively inhibit crystal growth and stabilize supersaturated solutions by competing for growth unit adsorption sites.[15–17] To effectively inhibit growth, the impurities do not need to cover the entire crystal surface, rather they merely need to disturb the flow of growth layers.[24] Cabrera and Vermilyea first proposed the pinning mechanism (Figure 1.4) which was then modified by Kubota and Mullin.

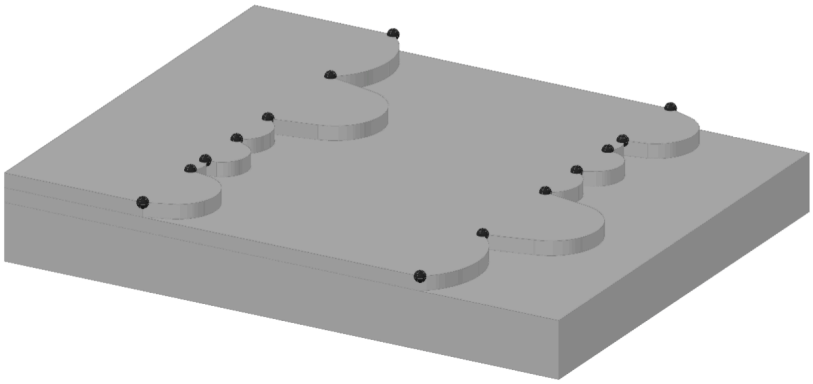

Figure 1.4. Depiction of the pinning mechanism due to additive adsorption.

In this mechanism, the impurities adsorb at kink sites along the steps at an average distance, l, apart. This forces the steps to curve, thus slowing step advancement. The radius of curvature of a pinned step, ρ, is equal to $l/2$. If $\rho \leq \rho_c$ (the critical nucleus radius), then step advancement will stop completely. Therefore, Kubota and Mullin have expressed the step velocity in the presence of additives, V_P, relative to the step velocity of the pure system, V_0, in terms of ρ_c and l:[15,30]

$$\frac{V_P}{V_0} = 1 - \frac{\rho_c}{l} \qquad (1.12)$$

Expressing the step velocities in the absence and presence of impurities as a ratio is useful because V_0/V_P is a measure of additive effectiveness. When $V_0/V_P > 1$, the additive is considered effective at slowing crystal growth.

For many systems, at low supersaturations, additives can slow crystal growth significantly, or even stop it completely. However, at high supersaturations, the same additive may completely lose its effect.[31–33] This impact of supersaturation can be explained by equations (1.6) and (1.12). With an increase in S, ρ_c will decrease, thus reducing the effectiveness of the additives.

Combining equations (1.6) and (1.12), V_P/V_0 can instead be expressed in terms of the useful parameters α, the impurity effectiveness factor, and θ, the impurity fractional coverage,

$$\frac{V_P}{V_0} = 1 - \alpha\theta \qquad (1.13a)$$

$$\alpha = \frac{\gamma a}{k_B \mathrm{T}(\ln \mathrm{S})\mathrm{L}} \qquad (1.13b)$$

$$\theta = \frac{\mathrm{L}}{l} \qquad (1.13c)$$

where L is the average distance between active sites available for impurity adsorption.[15] Expressing V_P/V_0 as equation (1.13a) rather than (1.12) is useful because growth inhibition can be then expressed in terms of the impurity fractional coverage, θ, which assumes linear adsorption along the steps. This form of the expression is also useful because impurities act only at certain sites, not all available active sites. This is reflected

in the parameter, L, which will vary for each additive-drug combination. Therefore α takes into account the active sites specific to the system under study.[30]

The rate of step growth, *V*, can be difficult to measure experimentally. Thus, Kubota and Mullin replaced the relative step velocity V_P/V_0 by the relative face growth rate G_P/G_0 under the assumption that *V* is proportional to G. This holds true if the growth proceeds by single-layer step growth and if the step heights remain constant.

It is even easier to experimentally determine overall mass growth rates, R_G, than individual face growth rates. Garside describes the following relationship between R_G and face growth rate, G:[26]

$$R_G = \frac{\zeta}{A}\sum G \cdot A_{hkl} \qquad (1.14)$$

where ζ is the crystal density, A is the total crystal surface area, and A_{hkl} represents the areas of all the individual faces. Therefore equation (1.13a) can be expressed in terms of the overall crystal growth rates in the presence (R_P) and absence (R_0) of impurities as

$$\frac{R_P}{R_0} = 1 - \alpha\theta \qquad (1.15)$$

if the following assumptions hold true: the ratio of crystal density to total crystal surface area (ζ/A) does not change when impurities are added to the system, and the areas of the individual faces (A_{hkl}) do not change with the addition of impurities.

1.6 Polymer Inhibition of Crystal Growth

It has become increasingly more common to use polymeric additives as crystal growth inhibitors. Polymer adsorption onto a crystal is driven by the change in free

energy, ΔG due to favorable polymer-surface interactions. Adsorption causes the polymer to lose entropy, which is unfavorable. Therefore, adsorption must be enthalpically driven in order for the process to be favorable. In other words, the interaction energy between the polymer and drug must be large enough to overcome the entropy loss. Components of the interaction energy can include electrostatic, chemical, hydrophobic, and hydrogen bonding interactions.[34]

The polymer-surface interactions will be influenced not only by the properties of the drug and polymer, but also by the liquid medium. If the interactions between the polymer and solvent are unfavorable, the polymer will want to minimize its interactions with the medium by adsorbing to the solid. If the polymer-solvent interactions are favorable, adsorption is less likely, unless the polymer can form even more favorable interactions with the drug than with the medium.[35]

Recently, there have been increased efforts to determine the factors that impact a polymer's effectiveness as a crystal growth inhibitor. Studies have shown that the hydrophobicity match between the polymer and the drug is of fundamental importance.[36,37] Ilevebare *et al*. have demonstrated that for moderately hydrophobic drugs, the most effective polymers also possessed moderate hydrophobicity. In general for these systems, very hydrophobic polymers were ineffective, as were very hydrophilic polymers. This result could be explained by the adsorption theory described in the preceding paragraph. It is likely that very hydrophilic polymers will interact primarily with the solvent and little adsorption will occur. Very hydrophobic polymers, on the other hand, may be driven to adsorb, however they may adsorb in globular formations, severely

decreasing surface coverage.[37] The objective of the work presented in Chapter 5 of this dissertation was to provide evidence of these phenomena.

The above findings suggest that hydrophobic forces may be the key driving force for polymer adsorption in solution. However it has also been shown that specific surface-polymer interactions, such as hydrogen bonding, can drive adsorption from solution as well.[38,39] It is already well known that specific interactions are key for polymer effectiveness in amorphous solid dispersions (amorphous drug dispersed in a polymeric matrix).[40,41] Studies on solid dispersions have demonstrated the importance of the relative functional group chemistries of the drug and polymer.[42] According to Black and Davey, effective polymers in solution should contain a part similar to the drug molecule – the part that adsorbs to the crystal – and the part that emerges from the crystal should be different enough from the host molecule that its binding energy is modified, contributing to less favorable incorporation of growth units.[17]

In a recent study by Ilevbare *et al*., it was observed that the presence of ionizable functional groups on a polymer and a higher degree of substitution increased polymer effectiveness.[37] The authors completed a subsequent study comparing the effectiveness of several ionizable polymers at two pH conditions, above and below the pKa of the functional groups.[33] The polymers were consistently more effective at the higher pH where they were ionized, despite having similar extent of adsorption to the crystal.

It was hypothesized from these findings that pH most likely affected the adsorbed polymer conformation.[43–45] Ionic polymers, or polyelectrolytes can undergo reversible conformation changes with an increase or decrease in pH due to shifts in charge density of ionizable groups.[45,46] The objective of the work presented in Chapters 4 and 5 of this

dissertation was to gain more insight into the relationship between polymer conformation and crystal growth inhibition.

Due to the effect polymers can have on the advancement of growth steps, over time the polymers can impact crystal morphology. Some studies have found that the presence of impurities alter crystal size and shape.[36] Holder and Winkler found that polymers selectively poisoned the 011 face of n-paraffin wax. The crystals proceeded to grow only in the remaining crystallographic planes and the thus the polymers modified the crystal habit. Land *et al* and Gratz and Hillner found in their respective studies that impurities distorted the shape of macrosteps, or terraces. The objective of the work presented in Chapter 6 of this dissertation was to evaluate the impact of changes in crystal morphology due to polymer surface poisoning on crystal growth rates.

References

(1) Yu, L. X.; Lipka, E.; Crison, J. R.; Amidon, G. L. Transport Approaches to the Biopharmaceutical Design of Oral Drug Delivery Systems: Prediction of Intestinal Absorption. *Adv. Drug Deliv. Rev.* **1996**, *19*, 359–376.

(2) Dahan, A. S.; Amidon, G. L. Gastrointestinal Dissolution and Absorption of Class II Drugs. *Drug Bioavailab. Estim. Solubility, Permeability, Absorpt. Bioavailability, Vol. 40, Second Ed.* **2009**, 33–51.

(3) Amidon, Gordon L., Lennernas, Hans, Shah, Vinod P., Crison, J. R. A Theoretical Basis for a Biopharmaceutic Drug Classification: The Correlation of in Vitro Drug Product Dissolution and in Vivo Bioavailability, 1995, 413–420.

(4) Yu, L. Amorphous Pharmaceutical Solids: Preparation, Characterization and Stabilization. *Adv. Drug Deliv. Rev.* **2001**, *48*, 27–42.

(5) Kim, K. T.; Lee, J. Y.; Lee, M. Y.; Song, C. K.; Choi, J.; Kim, D. Solid Dispersions as a Drug Delivery System. *J. Pharm. Investig.* **2011**, *41*, 125–142.

(6) Babu, N. J.; Nangia, A. Solubility Advantage of Amorphous Drugs and Pharmaceutical Cocrystals. *Cryst. Growth Des.* **2011**, *11*, 2662–2679.

(7) Yalkowsky, S. H. Perspective on Improving Passive Human Intestinal Absorption. *J. Pharm. Sci.* **2012**, *101*, 3047–3050.

(8) Hancock, B. C.; Zografi, G. Characteristics and Significance of the Amorphous State in Pharmaceutical Systems. *J. Pharm. Sci.* **1997**, *86*, 1–12.

(9) Leuner, C.; Dressman, J. Improving Drug Solubility for Oral Delivery Using Solid Dispersions. *Eur. J. Pharm. Biopharm.* **2000**, *50*, 47–60.

(10) Bhugra, C.; Pikal, M. J. Role of Thermodynamic, Molecular, and Kinetic Factors in Crystallization From the Amorphous State. *J. Pharm. Sci.* **2008**, *97*, 1329–1349.

(11) Pouton, C. W. Formulation of Poorly Water-Soluble Drugs for Oral Administration: Physicochemical and Physiological Issues and the Lipid Formulation Classification System. *Eur. J. Pharm. Sci.* **2006**, *29*, 278–287.

(12) Takano, R.; Takata, N.; Saito, R.; Furumoto, K.; Higo, S.; Hayashi, Y.; Machida, M.; Aso, Y.; Yamashita, S. Quantitative Analysis of the Effect of Supersaturation on in Vivo Drug Absorption. *Mol. Pharm.* **2010**, *7*, 1431–1440.

(13) Gao, P.; Guyton, M. E.; Huang, T.; Bauer, J. M.; Stefanski, K. J.; Lu, Q. Enhanced Oral Bioavailability of a Poorly Water Soluble Drug PNU-91325 by Supersaturatable Formulations. *Drug Dev. Ind. Pharm.* **2004**, *30*, 221–229.

(14) Davis, A. F.; Hadgraft, J. Effect of Supersaturation on Membrane Transport: 1. Hydrocortisone Acetate. *Int. J. Pharm.* **1991**, *76*, 1–8.

(15) Kubota, N. Effect of Impurities on the Growth Kinetics of Crystals. *Cryst. Res. Technol.* **2001**, *36*, 749–769.

(16) Ziller, K. H.; Rupprecht, H. Control of Crystal Growth in Drug Suspensions: 1) Design of a Control Unit and 2) Application to Acetaminophen Suspensions. *Drug Dev. Ind. Pharm.* **1988**, *14*, 2341–2370.

(17) Black, S. N.; Davey, R. J.; Halcrow, M. The Kinetics of Crystal Growth in the Presence of Tailor-Made Additives. *J. Cryst. Growth* **1986**, *79*, 765–774.

(18) Braatz, R. D. Advanced Control of Crystallization Processes. *Annu. Rev. Control* **2002**, *26 I*, 87–99.

(19) Williams, H. D.; Trevaskis, N. L.; Charman, S. a; Shanker, R. M.; Charman, W. N.; Pouton, C. W.; Porter, C. J. H. Strategies to Address Low Drug Solubility in Discovery and Development. *Pharmacol. Rev.* **2013**, *65*, 315–499.

(20) Bollag, G.; Hirth, P.; Tsai, J.; Zhang, J.; Ibrahim, P. N.; Cho, H.; Spevak, W.; Zhang, C.; Zhang, Y.; Habets, G.; et al. Clinical Efficacy of a RAF Inhibitor Needs Broad Target Blockade in BRAF-Mutant Melanoma. *Nature* **2010**, *467*, 596–599.

(21) Kwong, A. D.; Kauffman, R. S.; Hurter, P.; Mueller, P. Discovery and Development of Telaprevir: An NS3-4A Protease Inhibitor for Treating Genotype 1 Chronic Hepatitis C Virus. *Nat. Biotechnol.* **2011**, *29*, 993–1003.

(22) Jain, N.; Yalkowsky, S. H. Estimation of the Aqueous Solubility I: Application to Organic Nonelectrolytes. *J. Pharm. Sci.* **2001**, *90*, 234–252.

(23) Alonzo, D. E.; Gao, Y.; Zhou, D.; Mo, H.; Zhang, G. G. Z.; Taylor, L. S. Dissolution and Precipitation Behavior of Amorphous Solid Dispersions. *J. Pharm. Sci.* **2011**, *100*, 3316–3331.

(24) Mullin, J. W. *Crystallization, 4th Ed.*; Butterworth-Heinemann: Woburn, MA, 2001.

(25) Mullin, J. W.; Sohnel, O. Expressions of Supersaturation in Crystallization Studies. *Chem. Eng. Sci.* **1977**, *32*, 683–686.

(26) Garside, J.; Mersmann, A.; Nyvlt, J. *Measurement of Crystal Growth and Nucleation Rates, 2nd Ed.*; Institute of Chemical Engineers: London, 2002.

(27) Mohan, R.; Myerson, A. S. Growth Kinetics: A Thermodynamic Approach. *Chem. Eng. Sci.* **2002**, *57*, 4277–4285.

(28) Kossel, V. W. Zur Energetik von Oberflachenvorgangen. *Ann. Phys.* **1934**, *5*, 457–480.

(29) Van der Eerden, J. P.; Bennema, P.; Cherepanova, T. A. Survey of Monte Carlo Simulations of Crystal Surfaces and Crystal Growth. *Prog. Cryst. Growth Charact.* **1978**, *1*, 219–254.

(30) Kubota, N.; Mullin, J. W. A Kinetic Model for Crystal Growth from Aqueous Solution in the Presence of Impurity. *J. Cryst. Growth* **1995**, *152*, 203–208.

(31) Kubota, N.; Yokota, M.; Mullin, J. W. The Combined Influence of Supersaturation and Impurity Concentration on Crystal Growth. *J. Cryst. Growth* **2000**, *212*, 480–488.

(32) Kubota, N.; Yokota, M.; Mullin, J. W. Supersaturation Dependence of Crystal Growth in Solutions in the Presence of Impuritity. *J. Cryst. Growth* **1997**, *0248*.

(33) Ilevbare, G. a.; Liu, H.; Edgar, K. J.; Taylor, L. S. Inhibition of Solution Crystal Growth of Ritonavir by Cellulose Polymers – Factors Influencing Polymer Effectiveness. *CrystEngComm* **2012**, *14*, 6503–6514.

(34) Somasundaran, P.; Krishnakumar, S. Adsorption of Surfactants and Polymers at the Solid-Liquid Interface. *Colloids Surf., A* **1997**, *124*, 491–513.

(35) Holmberg, K.; Jonsson, B.; Kronberg, B.; Lindman, B. *Surfactants and Polymers In Aqueous Solutions, 2nd Ed.*; John Wiley & Sons, LTD: Chichester, 2003.

(36) Zimmermann, A.; Millqvist-Fureby, A.; Elema, M. R.; Hansen, T.; Müllertz, A.; Hovgaard, L. Adsorption of Pharmaceutical Excipients onto Microcrystals of Siramesine Hydrochloride: Effects on Physicochemical Properties. *Eur. J. Pharm. Biopharm.* **2009**, *71*, 109–116.

(37) Ilevbare, G. A.; Liu, H.; Edgar, K. J.; Taylor, L. S. Understanding Polymer Properties Important for Crystal Growth Inhibition - Impact of Chemically Diverse Polymers on Solution Crystal Growth of Ritonavir. *Cryst. Growth Des.* **2012**, *12*, 3133–3143.

(38) Ilevbare, G. A.; Liu, H.; Edgar, K. J.; Taylor, L. S. Impact of Polymers on Crystal Growth Rate of Structurally Diverse Compounds from Aqueous Solution. *Mol. Pharm.* **2013**, *10*, 2381–2393.

(39) Zhang, Q.; Zhang, T.; Ge, J.; Yin, Y. Permeable Silica Shell through Surface-Protected Etching. *Nano Lett.* **2008**, *8*, 2867–2871.

(40) Kestur, U. S.; Taylor, L. S. Role of Polymer Chemistry in Influencing Crystal Growth Rates from Amorphous Felodipine. *CrystEngComm* **2010**, *12*, 2288.

(41) Eerdenbrugh, B. Van; Taylor, L. S. An Ab Initio Polymer Selection Methodology to Prevent Crystallization in Amorphous Solid Dispersions by Application of Crystal Engineering Principles. *CrystEngComm* **2011**, *13*, 6171.

(42) Raghavan, S.; Trividic, A.; Davis, A.; Hadgraft, J. Crystallization of Hydrocortisone Acetate: Influence of Polymers. *Int. J. Pharm.* **2001**, *212*, 213–221.

(43) Yuan, W.; Zhang, J.; Zou, H.; Shen, T.; Ren, J. Amphiphilic Ethyl Cellulose Brush Polymers with Mono and Dual Side Chains: Facile Synthesis, Self-Assembly, and Tunable Temperature-pH Responsivities. *Polymer (Guildf).* **2012**, *53*, 956–966.

(44) Wu, W.; Liu, J.; Cao, S.; Tan, H.; Li, J.; Xu, F.; Zhang, X. Drug Release Behaviors of a pH Sensitive Semi-Interpenetrating Polymer Network Hydrogel Composed of Poly(vinyl Alcohol) and Star poly[2-(dimethylamino)ethyl Methacrylate]. *Int. J. Pharm.* **2011**, *416*, 104–109.

(45) Etika, K. C.; Cox, M. A.; Grunlan, J. C. Tailored Dispersion of Carbon Nanotubes in Water with pH-Responsive Polymers. *Polymer (Guildf).* **2010**, *51*, 1761–1770.

(46) Roiter, Y.; Minko, S. AFM Single Molecule Experiments at the Solid-Liquid Interface: In Situ Conformation of Adsorbed Flexible Polyelectrolyte Chains. *J. Am. Chem. Soc.* **2005**, *127*, 15688–15689.

CHAPTER 2. METHODS AND MATERIALS

2.1 Rotating Disk Apparatus Theory

Crystal growth rates are impacted by the rate of solute mass transfer to the crystal interface, and rate of integration into the lattice, as explained in Chapter 1. A rotating disk apparatus (RDA) can be utilized to separate the roles of mass transfer and integration because it induces controlled forced convection. The rotation of the disk draws the fluid up in the axial direction toward the surface then throws it outward in the radial and tangential directions across the disk surface[1] (see Figure 2.1). Thus, the rate of the mass transfer step will depend on the angular velocity, ω, of the rotating disk.

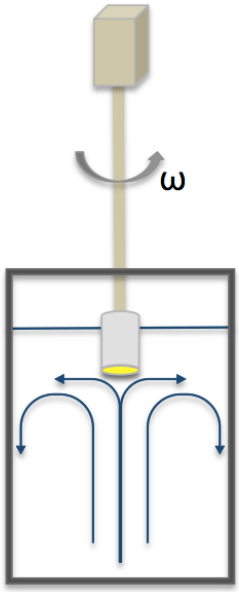

Figure 2.1 Schematic of a rotating disk apparatus.

The Navier-Stokes and continuity equations for the fluid motion due to a rotating disk have been solved,[2–5] and the axial velocity component, v_y, was determined to be:[1]

$$v_y \approx -0.51\sqrt{\frac{\omega^3}{\nu}}y^2 \quad \text{for } y \ll \sqrt{\frac{\nu}{\omega}} \tag{2.1}$$

where ν is the kinematic viscosity of the solution. Since forced convection toward the disk is in the axial (y) direction only, the concentration will not be a function of the radial or tangential directions. Thus, the Navier-Stokes convective diffusion equation (in cylindrical coordinates) becomes:

$$v_y \frac{\partial C}{\partial y} = D\frac{\partial^2 C}{\partial y^2} \tag{2.2a}$$

with the boundary conditions

$$y = 0,\ C = 0 \tag{2.2b}$$

$$y \to \infty,\ C = C_b \tag{2.2c}$$

where D is the diffusion coefficient of the solute in the solution. Solving for the concentration, C, and combining with equation (2.1), then differentiating to obtain mass flux, j, to the disk surface, the result is:[1]

$$j = D\left(\frac{\partial C}{\partial y}\right) = 0.6205D^{2/3}\nu^{-1/6}\omega^{1/2}C_b \tag{2.3}$$

Thus, the mass transfer rate coefficient, k_d depends on ω according to the following relationship:[6,7]

$$k_d = 0.6205D^{2/3}\nu^{-1/6}\omega^{1/2} \tag{2.4}$$

Therefore, when the crystal growth rate is mass transfer-controlled, it will depend on the rotational speed of the disk, ω, according to equation (2.4). As ω continues to increase, it will reach a critical velocity, ω_c, where the growth rate plateaus because it is no longer dependent on disk rotational speed. Above ω_c the growth rate is now limited by how quickly solute can integrate into the crystal lattice. Thus, the correlation between crystal growth rate, R_G and $\omega^{1/2}$ should follow the trend shown in Figure 2.2.

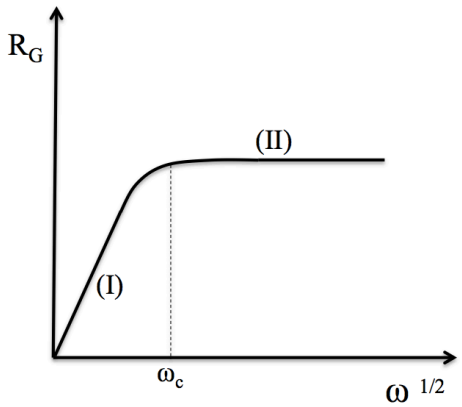

Figure 2.2. Theoretical correlation between growth rate and RDA rotational speed, showing mass transfer-controlled growth (I) and integration-controlled growth (II). ω_c denotes the critical disk rotational speed above which the growth rate is independent of the rotational speed.

In order for equation (2.4) to accurately describe the mass transfer, several criteria must be met:[8]

i) Flow over the disc must be laminar.

ii) Edge effects must be negligible.

iii) The disc must be planar.

iv) The disc surface must be 'smooth'.

v) The fluid must be considered an 'infinite expanse'

Explanations for how these criteria are met will be given in Chapter 3. In that chapter, a rotating disk apparatus was utilized to isolate the rate of integration and extract kinetic growth parameters. Once the integration-controlled growth regime was determined, the growth rate experiments in the following chapters were performed at rotational speeds above ω_c. This is because the integration rate is the step that is impacted by polymer adsorption.

2.2 Atomic Force Microscopy

Atomic Force Microscopy (AFM) is a widely-used scanning probe microscopy. This method can perform force measurements as well as topographical imaging. In this study, the mode of interest is imaging. The sample is placed on a piezoelectric column which can move in the x-, y-, and z-directions. A flexible cantilever tip placed above the sample interacts with the surface. A laser reflects off the cantilever to a photodetector. Therefore, as the cantilever moves due to attractive or repulsive forces from the surface, the deflections are recorded.[9] The deflections are combined with the x-, y-, and z-positions on the surface to create a topographical map. Analysis of topographical images can reveal surface roughness properties.

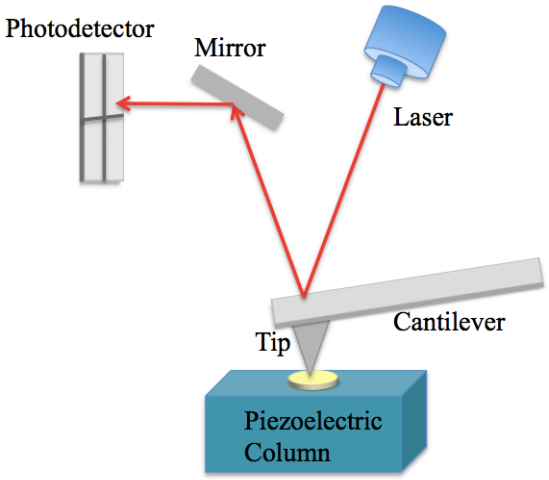

Figure 2.3: Schematic of an atomic force microscope

For this study, the AFM was run in tapping mode, during which the cantilever oscillates at a resonant frequency. The phase response of the oscillating cantilever is of particular interest. During imaging, the phase lag between the excitation force and cantilever oscillation is recorded to produce a phase-contrast image. This phase lag is very useful to reveal differences in material properties. Thus, it is good for differentiating between surface components, revealing variations that the height measurements may not detect.[10] This is particularly useful for detecting polymers because the viscoelasticity will differ from that of the drug surface.

AFM coupled with infrared spectroscopy (AFM-IR) was also used in this work. The sample was illuminated from below with a laser, causing the sample to expand and contract. The amount of expansion and contraction correlated to how much IR illumination the sample absorbed at the particular wavelength. The AFM cantilever probe would oscillate due to the expansion and the amplitude of oscillation was recorded. This method was useful for chemically characterizing submicron polymer domains.

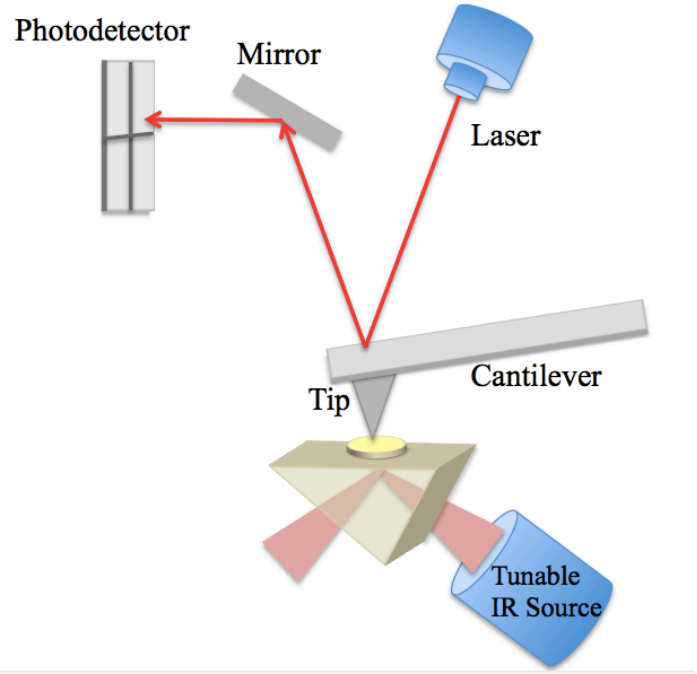

Figure 2.4. Schematic of AFM coupled with infrared spectroscopy

2.3 Materials

The active pharmaceutical ingredient utilized as a model compound in this study was felodipine, a calcium channel blocker which treats hypertension. Felodipine has a low equilibrium solubility (C* = 0.5μg/ml at 25°C.[11]) and its crystal growth and nucleation kinetics have been well-studied.[11–13] The polymers used in this study were hydroxypropylmethyl cellulose acetate succinate (HPMCAS) grade LF, hydroxypropylmethyl cellulose (HPMC), polyvinylpyrrolidone (PVP), poly(acrylic acid) (PAA), poly(vinyl acetate) (PVAc) poly(vinylpyrrolidone vinyl acetate) (PVPVA), and poly(2-vinylpyridine) (P2VP). The chemical structures of felodipine and these polymers are displayed in Figure 2.5.

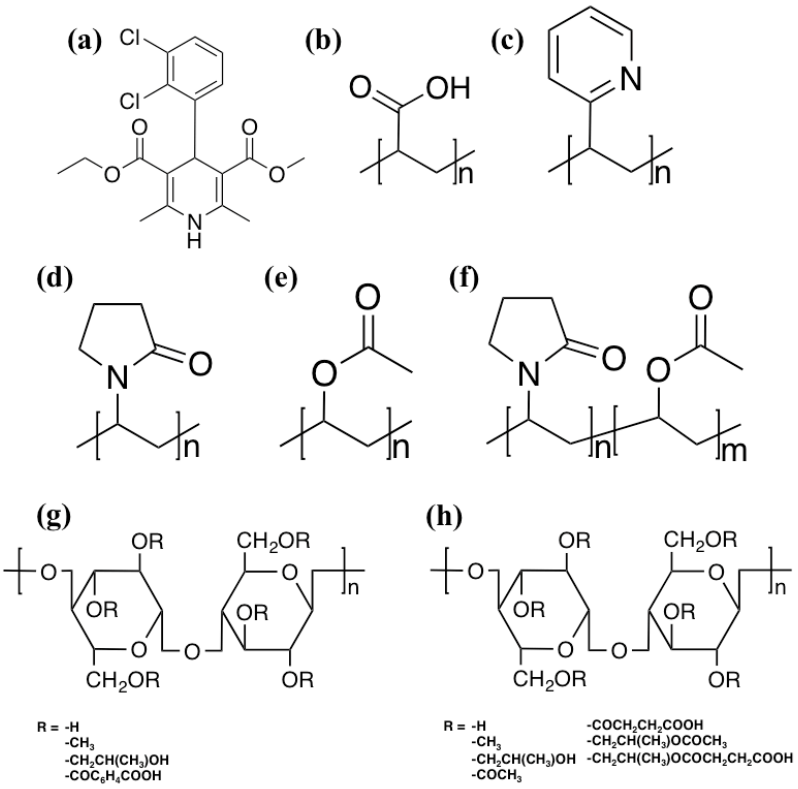

Figure 2.5. Chemical structures of (a) felodipine, (b) PAA, (c) P2VP, (d) PVP, (e) PVAc, (f) PVPVA, (g) HPMC, (h) HPMCAS

References

(1) Levich, V. *Physicochemical Hydrodynamics*; Prentice-Hall, Inc.: Englewood Cliffs, 1962.

(2) von Karman, T. Über Laminare Und Turbulente Reibung *Z. Angew. Math. Mech.* **1921**, *1*, 233–252.

(3) Cochran, W. G.; Goldstein, S. The Flow due to a Rotating Disc. *Math. Proc. Cambridge Philos. Soc.* **1934**, *30*, 365-375.

(4) White, R. The Fluid Motion Due to a Rotating Disk. *J. Electrochem. Soc.* **1976**, *123*, 383-385.

(5) Newman, J. Schmidt Number Correction for the Rotating Disk. *J. Phys. Chem.* **1966**, *70*, 1327–1328.

(6) Chang, F.; Abbad, M. Modelling Mass Transfer in a Rotating Disk Reaction Vessel. *KSG* **2011**, 1-17.

(7) Beaudoin, S. P.; Grant, C. S.; Carbonell, R. G. Removal of Organic Films from Solid Surfaces Using Aqueous Solutions of Nonionic Surfactants. 2. Theory. *I&EC Res.* **1995**, *34*, 3318–3325.

(8) Garside, J.; Mersmann, A.; Nyvlt, J. *Measurement of Crystal Growth and Nucleation Rates, 2nd Ed.*; Institute of Chemical Engineers: London, 2002.

(9) Niemantsverdriet, J. W. *Spectroscopy in Catalysis*; Wiley-VCH, 2007.

(10) Babcock, K. L.; Prater, C. B. Phase Imaging : Beyond Topography. *Science (80).*

(11) Alonzo, D. E.; Raina, S.; Zhou, D.; Gao, Y.; Zhang, G. G. Z.; Taylor, L. S. Characterizing the Impact of Hydroxypropylmethyl Cellulose on the Growth and Nucleation Kinetics of Felodipine from Supersaturated Solutions. *Cryst. Growth Des.* **2012**, *12*, 1538–1547.

(12) Rumondor, A. C. F.; Jackson, M. J.; Taylor, L. S. Effects of Moisture on the Growth Rate of Felodipine Crystals in the Presence and Absence of Polymers. *Cryst. Growth Des.* **2010**, *10*, 747–753.

(13) Kestur, U. S.; Taylor, L. S. Role of Polymer Chemistry in Influencing Crystal Growth Rates from Amorphous Felodipine. *CrystEngComm* **2010**, *12*, 2390-2397.

CHAPTER 3. UNDERSTANDING CRYSTAL GROWTH KINETICS IN THE ABSENCE AND PRESENCE OF A POLYMER USING A ROTATING DISK APPARATUS

This chapter is a preprint with minor modifications of a manuscript submitted to *Crystal Growth and Design* with the same title by: Caitlin J. Schram, Ryan J. Smyth, Lynne S. Taylor, and Stephen P. Beaudoin

3.1 Abstract

Polymer inhibition of crystal growth from supersaturated solutions is an important area of study, particularly in the pharmaceutical field. Polymers can be used to modify crystal morphology or to slow crystal growth with the goal of enhancing oral drug absorption. In order to fully understand the effect of polymers on crystal growth it is important to understand the kinetics of the integration step. In this study, a rotating disk apparatus is used to isolate the integration step from the diffusion step so that the integration kinetics can be determined for growth rates in the absence and presence of polymers. The results indicate that the presence of polymers in solution greatly impacts the integration step, and has no impact on the mass transfer kinetics.

3.2 Introduction

Solution crystallization is a phenomenon central to many industries and fields of research. It is highly desirable to be able to manipulate a crystallization process because it can have a large impact on the physicochemical properties, and therefore the quality, of the product.[1] Modification of crystal growth can be achieved through changes in the process environment, such as temperature or solvent. Another increasingly common approach to manipulate crystal form is to use polymeric additives.[2,3]

In the pharmaceutical field, polymers can be used to slow crystal growth rates and maintain supersaturated solutions *in vivo*, which will ultimately enhance drug delivery.[4,5] The use of this approach is of special interest for drugs that exhibit poor aqueous solubility, and thus are formulated as amorphous solids.[6–8] In order to effectively inhibit crystal growth, it is important to have a good understanding of the kinetics of crystallization as well as a mechanistic understanding of how polymers inhibit growth.

Crystal growth occurs by two phenomena in series: transport of solute to the crystal-liquid interface, and integration of solute into the lattice.[9,10] It is likely that polymers inhibit growth by inhibiting the integration step, because they compete with growth units for active sites on the surface.[11–13] Once adsorbed to a site, they create a mechanical barrier for further growth units to attach at that site.[13] It is therefore important to isolate the integration step to better study polymer inhibition. This can be done using a rotating disk apparatus.[10] Rotating disks have traditionally been used to study the kinetics of chemical or electrochemical reactions.[14,15] Relatively few studies have used rotating disks to study crystal growth,[16,17] and currently this technique has not been used to study polymer inhibition of crystal growth.

The objective of this work was to measure crystal growth rates of a poorly water-soluble drug in the absence and presence of a polymer using a rotating disk apparatus. This will provide insight into the kinetics of crystal growth when polymers are present in the system, therefore providing a better mechanistic understanding of how polymers inhibit crystal growth.

3.3 Experimental Section

3.3.1 Materials

Felodipine was provided by Attix (Toronto, Ontario, Canada). Methanol (HPLC grade) was purchased from Avantor Performance Materials (Center Valley, PA). Hydroxypropylmethyl cellulose acetate succinate (HPMCAS) LF grade, M_w 18 000 g mol^{-1}, was supplied in powder form by Shin-Etsu Chemical Co, Ltd. (Tokyo, Japan). 50 mM pH 6.8 phosphate buffer was used as the crystallization medium in all growth experiments. HPMCAS was pre-dissolved in the buffer for experiments where crystal growth rates were measured in the presence of polymer. The molecular structures of felodipine and HPMCAS are given in Figure 2.5.

3.3.2 Rotating Disk Apparatus

The experimental apparatus is illustrated in Figure 3.1a. The rotating disk apparatus (RDA) was provided by Princeton Applied Research (Oak Ridge, TN. Model #616). Seed crystals were mounted on a disk in a custom-made holder at the bottom of the RDA shaft, which rotated with angular velocity, ω. The disk was submerged in buffer solution (60 mL) containing dissolved felodipine alone, or containing both dissolved

felodipine and dissolved HPMCAS. The solution was contained in a jacketed beaker connected to a circulating water bath held at a constant temperature, 25°C. A UV probe, which was used to measure the amount of dissolved felodipine in solution (see section 3.3.3), was also submerged in the solution.

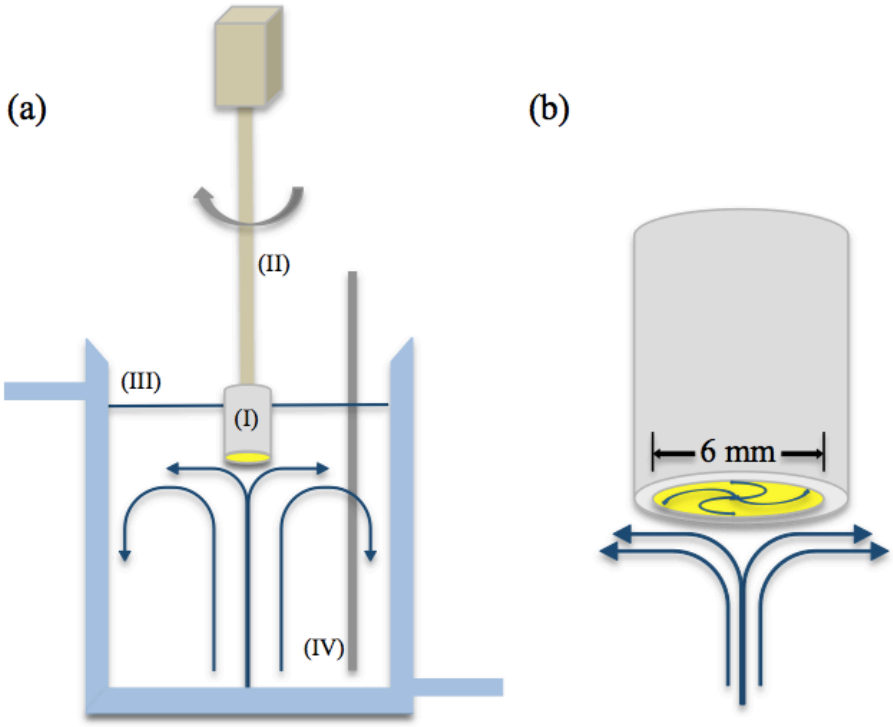

Figure 3.1. (a) Schematic of the experimental system, showing the seed crystal holder (I), rotating shaft (II), jacketed vessel (III), and UV probe (IV); and (b) close-up image of custom-made seed crystal holder. Liquid flow patterns induced by the rotating disk are also shown.

Figure 3.1b shows an image of the custom-made Teflon seed crystal holder that was mounted at the bottom of the rotating shaft. Felodipine crystals, as supplied by the manufacturer were melted and poured into the custom holder. The surface of the melt was flattened using a glass coverslip and the melt was allowed to solidify. The surface must be completely flat and flush with the rim of the holder in order to fulfill criterion *(iii)* below, and therefore be suitable for use in the rotating disk apparatus. The amorphous

felodipine surface was then re-crystallized by exposure to an atmosphere of 75% relative humidity.

Several criteria must be met in the execution of experiments in order mass transfer to be accurately described by equation (2.4):

i) Flow over the disk must be laminar.[18]

This criterion is met if $Re_{disk} = \frac{r_d{}^2 \omega}{\nu} < 2x10^5$. The radius, r_d, of the disk used in this study was 3 mm, and the highest rotational speed used was ω = 733 rad/s. (The value of *v* is given in Table 3.1). Thus the maximum $Re_{disk} = 7.2x10^3$ which is $< 2x10^5$, therefore all experiments were run well within the laminar region. Additionally, Re_{disk} should remain above $1x10^2$ to avoid effects of natural convection. This condition was also satisfied since the minimum value of Re_{disk} at the lowest rotational speed used, ω = 20.9 rad/s, is $2.1x10^2$.

ii) Edge effects must be negligible.[18,19]

To meet this criterion, the radius of the disk, r_d, must be $> \delta_H$, where δ_H is the hydrodynamic boundary layer, which can be expressed as $\delta_H = 3.6\left(\frac{\nu}{\omega}\right)^{0.5}$.

The lowest rotational speed used in this study was ω = 20.9 rad/s, which yields δ_H = 0.75 mm. Thus r = 3 mm > δ_H for all experiments.

iii) The disk must be planar.[10]

This criterion was satisfied due to the methods employed for seed crystal preparation as explained above.

iv) The disk surface must be 'smooth.'[10]

This criterion is met if the average height of the roughness elements of the crystal surface, $R_{q,av} < \delta_H$. Characterization with atomic force microscopy of seed crystals revealed $R_{q,av}$ = 32.6 nm. The hydrodynamic boundary layer will be at a minimum at the highest rotational speed, ω = 733rad/s. At this speed, δ_H = 0.11 mm which is greater than $R_{q,av}$. Thus, this criterion was satisfied.

v) The fluid must be considered an infinite expanse.[19]

This criterion is met if the distance from the disk surface to the reservoir walls, and the distance from the disk to the air-solution interface are both >> δ_H. δ_H will be at a maximum at the lowest rotational speed, ω = 20.9 rad/s, which yields δ_H = 0.75 mm. Thus, this criterion was met by ensuring that the distance from the disk to the walls and from the disk to the solution interface were at least 7.5 mm.

3.3.3 Crystal Growth Rate Measurements

The growth rate of felodipine was measured in the absence and presence of HPMCAS. A stock solution of 10 mg/mL solubilized felodipine was prepared by dissolving felodipine in methanol. Supersaturated aqueous solutions were then generated by adding a small amount of the felodipine stock solution to pH 6.8 buffer alone, or buffer containing pre-dissolved HPMCAS (5 µg/mL). The equilibrium concentration, *C**, of felodipine is approximately 0.5 µg/mL at 25°C.[20] The experiments performed to determine the effect of rotational speed on the growth rate were carried out at initial bulk

concentration, C_b = 2 μg/mL. Experiments performed to determine the integration rate constant, k_r, and growth order, r, were carried out at C_b = 1 μg/mL, 1.5 μg/mL, 2 μg/mL, 2.5 μg/mL, and 3 μg/mL.

The concentration of felodipine in solution as a function of time was measured to determine a desupersaturation profile. This profile is considered to be directly proportional to the growth rate of felodipine, R_G. Immediately after generation of supersaturated solutions, desupersaturation profiles were measured using a CCD Array UV-vis Spectrometer (SI Photonics, Tuscon, AZ). The intensity of an absorbance peak of felodipine (wavelength 238 nm) was recorded at 10-second intervals for 1 hour. Calibration solutions, prepared in methanol, were used to correlate peak intensity to concentration. The slope of the resulting concentration v. time curve was recorded as the growth rate, R_G. All experiments were performed in triplicate.

3.4 Results and Discussion

The growth rate of felodipine was measured at various rotational speeds using a rotating disk apparatus. A plot of felodipine growth rate as a function of rotational speed, $\omega^{1/2}$, is shown in Figure 3.2. The results show that at first the growth rate increases linearly with increasing rotational speed. Eventually, the growth rate plateaus, remaining at a constant value, independent of ω.

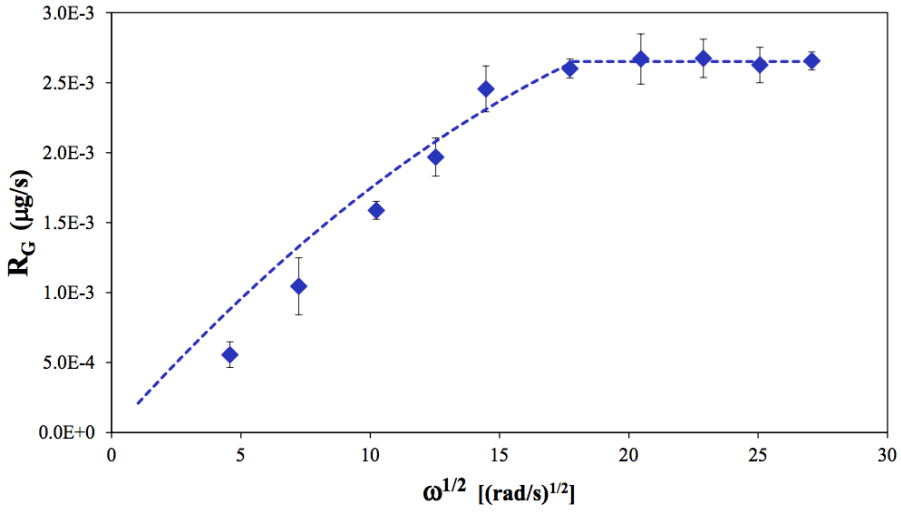

Figure 3.2. Plot of felodipine crystal growth rate (initial C_b = 2 µg/mL) as a function of RDA rotational speed. Experimental growth rates (blue ◆) were measured in triplicate and error bars indicate one standard deviation from the mean. The theoretical curve (dashed line) was generated from equations (3.1) and (1.10).

The observed experimental trend is in agreement with rotating disk apparatus theory (Figure 2.2). At lower rotational speeds, the crystal growth rate is limited by the rate of mass transfer of solute to the solid-liquid interface. Thus, as the rotational speed increases, so does the forced convection rate, which increases the overall crystal growth rate. At higher rotational speeds, the crystal growth rate is limited by the rate of integration of growth units into the crystal lattice. This rate is independent of bulk fluid velocity, thus the rate remains constant as rotational speed increases.

For mass transfer-controlled growth, the growth rate can be expressed by equation (1.8), wherein the rate coefficient, k_d, depends on $\omega^{1/2}$ according to equation (2.4). Combining equations (1.8) and (2.4) results in the following expression which relates the overall growth rate, R_G to the rotational speed, $\omega^{1/2}$:

$$R_G = 0.6205 D^{2/3} \nu^{-1/6} \omega^{1/2} A(C_b - C_I) \qquad (3.1)$$

Equation (3.1) was used to model the experimentally determined growth rates of felodipine at rotational speeds below $\omega^{1/2} = 17.7$ (rad/s)$^{1/2}$. The diffusion coefficient, D, was estimated using the Stokes-Einstein equation:

$$D = \frac{k_B T}{6\pi\eta r_h} \qquad (3.2)$$

where k_B is the Boltzmann constant, T is the temperature, η is the dynamic viscosity of the medium, and r_h is the hydrodynamic radius of a felodipine growth unit in solution. The numerical values of the constant parameters used in equations (3.1) and (3.2) are given in Table 3.1.

Table 3.1. Values used in equations (3.1) and (3.2) to calculate mass transfer-controlled crystal growth rates of felodipine.

Parameter	Value
ν	9.15 x 10^{-7} m^2/s
A	2.83 x 10^{-5} m^2
C_b	2 μg/mL
k_B	1.38 x 10^{-23} J/K
T	298.15 K
η	9.10 x 10^{-4} Pa•s
r_h	3.50 x 10^{-10} m

The value of T and C_b were set experimentally, and C_b is the initial bulk concentration of felodipine. A is the nominal cross sectional area of the crystalline surface. The values of η and ν were found in the literature for water at 25°C.[21] The value of r_h was estimated using the crystal structure visualization software Mercury,[22] wherein the 'measure distances' tool was used to measure the length of a felodipine molecule.

The concentration at the interface, C_I is not a constant. It will increase and approach the bulk concentration, C_b as the rotational speed increases,[10] bringing more solute to the interface. Thus, the boundary conditions for C_I are:

$$\omega = 0;\ C_I = C^* \qquad (3.3a)$$

$$\omega \rightarrow \infty;\ C_I \rightarrow C_b \qquad (3.3b)$$

The relationship between C_I and ω was determined to be

$$C_I = C^* + 0.024\omega^{1/2} \qquad (3.4)$$

Theoretical growth rates were determined for $0 < \omega^{1/2} < 17.7$ (rad/s)$^{1/2}$ by substituting equation (3.4) for C_I along with the values given in Table 3.1 and the calculated value of D into equation (3.1). The theoretical curve is plotted (dotted line) along with the experimental values in Figure 3.2.

For $\omega^{1/2} > 17.7$ (rad/s)$^{1/2}$ the growth rate plateaus at a constant value. Here, the growth rate is limited by the rate at which growth units can integrate into the lattice. This growth rate can be described by equation (1.10). In order to model the integration-

controlled growth rate using this equation, the rate coefficient, k_r, and the integration order, r, must be known. These can be determined experimentally by measuring the crystal growth rate at various supersaturation conditions at a rotational speed above 17.7 $(rad/s)^{1/2}$ (when growth is integration-controlled). Since the growth rate correlates to (C_b - C^*) according to equation (1.10), plotting R_G/A v. (C_b - C^*) (Figure 3.3) allows for extrapolation of the values of k_r and r by determining the equation of the best-fit curve. (Equation 3.5).

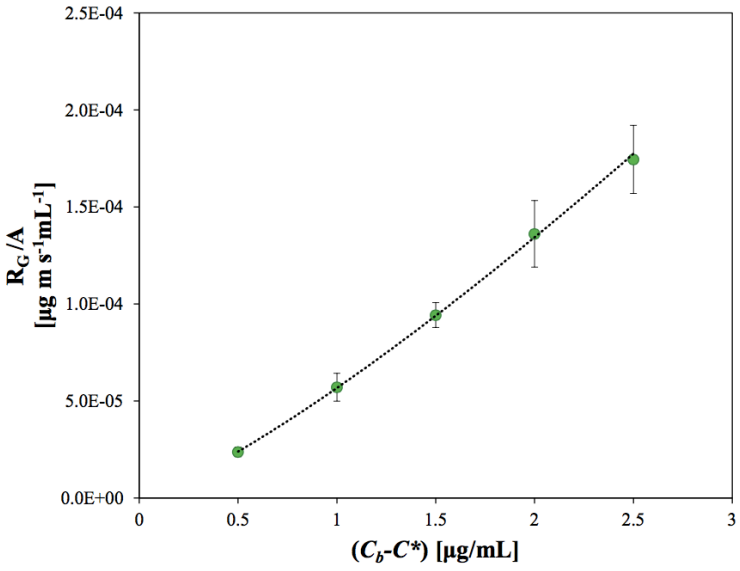

Figure 3.3. Plot of integration-controlled growth rate as a function of the concentration gradient utilized to extrapolate the values of k_r and r. Measurements were performed in triplicate and error bars indicate one standard deviation from the mean.

$$\frac{R_G}{A} = k_r(C_b - C^*)^r = 5.67\text{x}10^{-5}(C_b - C^*)^{1.24} \qquad (3.5)$$

Thus according to equation (1.10), k_r is equal to the coefficient in equation (3.5), 5.7 x 10^{-5} m/s, and r is equal to the exponent, 1.24. Plugging these values along with the

values of A, C_b, and C^* into equation (1.10), the theoretical integration-controlled growth rate was determined to be $R_G = 2.56 \times 10^{-3}$ μg/s, which agrees quite well with the experimentally determined growth rates, as shown by the dotted line in Figure 3.2.

The Damköhler number, Da, which represents the ratio of the integration and mass transfer rate coefficients (equation 1.11), was plotted as a function of RDA rotational speed. The result is shown in Figure 3.4.

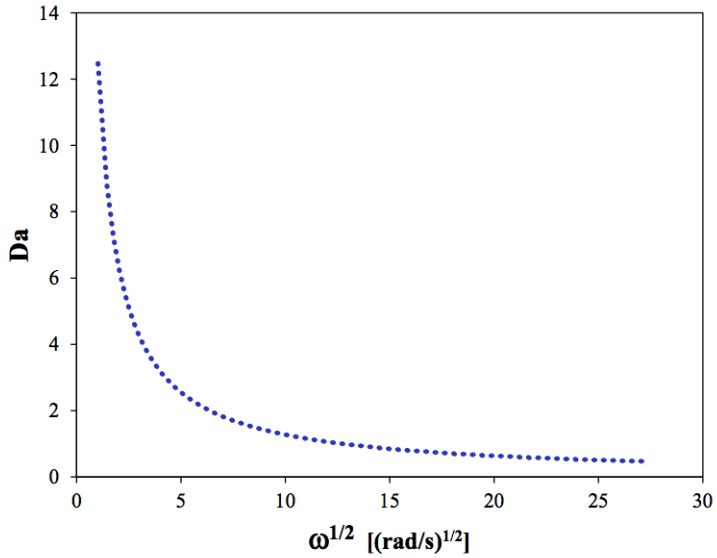

Figure 3.4. Plot of the Damköhler number as a function of rotational speed showing the transition from mass transfer to integration-controlled growth.

In agreement with RDA theory, at low rotational speeds, Da is large, indicating mass transfer-controlled growth ($k_r >> k_d$). As rotational speed increases, Da becomes smaller. This indicates that the growth rate switches over to being controlled by the integration step ($k_d >> k_r$).

The good agreement between the experimentally-measured growth rates of felodipine and the theoretically-determined growth rates (from equations 3.1 and 1.10)

validate the use of the rotating disk apparatus to extract kinetic information. Thus, using this method to measure crystal growth rates in the presence of a polymer should provide insight into growth inhibition.

The growth rate of felodipine was measured at various rotational speeds in the presence of the polymer HPMCAS. The results are presented in Figure 3.5 along with the pure felodipine growth rate results for comparison.

The observed and predicted growth rates in the presence of HPMCAS follow the same overall trend as those of the pure drug; at first there is a linear increase in growth rate with rotational speed until the growth rate reaches a plateau indicating integration control. However, the magnitude of the growth rate at all rotational speeds is reduced due to the adsorption of HPMCAS on active sites at the solid-liquid interface. The adsorbed polymer creates a barrier, preventing felodipine growth units from attaching to the crystal, thereby slowing crystal growth.[11] Evidence of HPMCAS adsorption to felodipine has been confirmed using atomic force microscopy (AFM),[23] and these results will be shown in Chapters 4 and 5.

As will be discussed in more detail in Chapter 5, the fraction of felodipine surface covered by adsorbed polymers was measured using AFM for nine different polymer systems. It was found that adsorbed polymer surface coverage, Φ, correlated linearly to polymer effectiveness, R_G/R_P, where R_P is the growth rate of felodipine in the presence of polymers (see Figure 5.5). This correlation was then modeled using the approach developed by Kubota and Mullin[11,13] (equation 1.15). Briefly, all parameters in the model were known or could be determined experimentally (see Table 5.2) except the distance between adsorbed polymers, *l*. Thus, values for *l* were fitted to determine a general

relationship between *l* and Φ (equation 5.3). Substituting this into the model, it was determined that polymer effectiveness, R_G/R_P, is related to fractional polymer surface coverage, Φ, according to the following relationship:[24]

$$\frac{R_G}{R_P} = 3.918\Phi + 1 \qquad (3.6)$$

Applying this relationship to the current study, theoretical R_P values could be calculated from the theoretical R_G values determined in this study and the experimentally measured HPMCAS fractional surface coverage (see Chapter 5), $\Phi = 0.53$.[24] This curve is plotted along with the experimental values in Figure 3.5 (red dotted line).

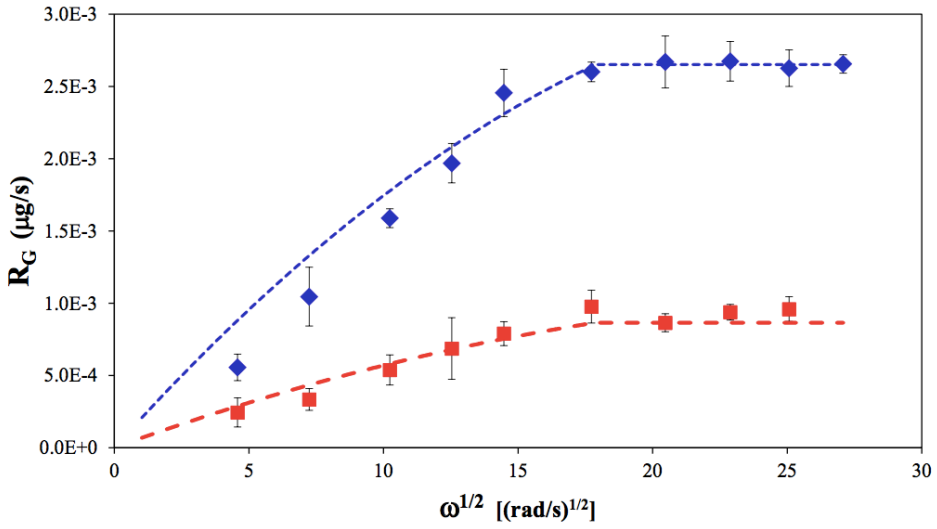

Figure 3.5. Plot of felodipine crystal growth rate (initial C_b = 2 µg/mL) as a function of RDA rotational speed. Experimental growth rates in the absence (blue ◆) and presence (red ■) of HPMCAS were measured in triplicate and error bars indicate one standard deviation from the mean. The theoretical curve for pure felodipine growth rates (blue - -) was generated from equations (3.1) and (1.10). The theoretical curve for growth in the presence of HPMCAS (red − −) was generated from equation (3.6).

It can be seen that the theoretical curve agrees with the experimental data regardless of whether the growth is mass transfer or integration controlled. This result confirms that the reduction in growth rate when polymers are present is purely a surface coverage effect even when the growth rate is mass transfer controlled. Thus, from equation (1.8), the reduction in growth rate can be attributed to a reduction in the nominal surface area available for integration, A, due to polymer adsorption at active growth sites, as well as changes in the interface concentration, C_I. The rate coefficient, k_d, however, will remain the same as the pure drug rate coefficient at each rotational speed, ω. This implies that polymers do not impact the kinetics of the mass transfer step.

The integration constants, k_r and r, for growth in the presence of HPMCAS were determined using the same approach used to determine the pure drug growth constants. The resulting values are displayed in Table 3.2 along with the integration constants of pure felodipine.

Table 3.2. Integration constants for felodipine crystal growth in the absence and presence of HPMCAS

	k_r (m/s)	r
Pure felodipine growth	5.7×10^{-5}	1.24
Growth with HPMCAS	1.4×10^{-5}	1.75

The rate constant, k_r, was reduced for growth in the presence of HPMCAS, and the integration order, r was increased. The rate of integration depends on how quickly a solute molecule can position itself in the crystal lattice. This rate will decrease due to the presence of adsorbed polymers because as growth units diffuse across the surface in

search of active sites, the number of available sites will be reduced. This barrier to integration created by the adsorption of HPMCAS is reflected in the change to k_r.

The increase in the integration order, r, may be due to a shift in growth mechanism when polymers are present. Crystal growth of the pure drug proceeds in a linear step-wise fashion as described in Chapter 1 (Section 1.4). When HPMCAS is present, the steps are pinned and are forced to curve. Thus the presence of adsorbed polymers can result in a shift in growth mechanism, which will likely impact the order of integration.

Previous studies in which overall crystal growth rates were measured in the absence and presence of polymers have shown that the overall growth order (g in equation 1.7) increases when polymers are present, indicating a shift toward integration-controlled growth.[20] Studying growth with an RDA and isolating the integration step confirms that when polymers are present, the integration step is slowed. Thus, it offers more resistance to the overall growth rate resulting in the shift toward integration control.

3.5 Conclusions

A rotating disk apparatus was used to study the kinetics of crystal growth of felodipine in the absence and presence of the polymer, HPMCAS. The use of the RDA enabled the isolation of the mass transfer and integration steps so that the kinetic rate constants for each step could be determined. In the presence of polymer, it was shown that the felodipine crystal growth rate was slowed in both the mass transfer-controlled, and integration-controlled regions due to adsorption of the polymer on the crystal surface.

The use of this technique in crystal growth inhibition studies can enhance our understanding of the effects of polymers on growth kinetics.

References

(1) Vippagunta, S. R.; Brittain, H. G.; Grant, D. J. W. Crystalline Solids. *Adv. Drug Deliv. Rev.* **2001**, *48*, 3–26.

(2) Sangwal, K. Effects of Impurities on Crystal Growth Processes. *Prog. Cryst. Growth Charact. Mater.* **1996**, *32*, 3–43.

(3) Kulak, A. N.; Iddon, P.; Li, Y.; Armes, S. P.; Co, H.; Paris, O.; Wilson, R. M.; Meldrum, F. C. Continuous Structural Evolution of Calcium Carbonate Particles : A Unifying Model of Copolymer-Mediated Crystallization. *J. Am. Chem. Soc.* **2007**, *129*, 3729–3736.

(4) Moser, K.; Kriwet, K.; Kalia, Y. N.; Guy, R. H. Stabilization of Supersaturated Solutions of a Lipophilic Drug for Dermal Delivery. *Int. J. Pharm.* **2001**, *224*, 169–176.

(5) Raghavan, S.; Trividic, A.; Davis, A.; Hadgraft, J. Crystallization of Hydrocortisone Acetate: Influence of Polymers. *Int. J. Pharm.* **2001**, *212*, 213–221.

(6) Babu, N. J.; Nangia, A. Solubility Advantage of Amorphous Drugs and Pharmaceutical Cocrystals. *Cryst. Growth Des.* **2011**, *11*, 2662–2679.

(7) Murdande, S. B.; Pikal, M. J.; Shanker, R. M.; Bogner, R. H. Solubility Advantage of Amorphous Pharmaceuticals. *J. Pharm. Sci.* **2010**, *99*, 1254–1264.

(8) Hancock, B. C.; Zografi, G. Characteristics and Significance of the Amorphous State in Pharmaceutical Systems. *J. Pharm. Sci.* **1997**, *86*, 1–12.

(9) Mullin, J. W. *Crystallization, 4th Ed.*; Butterworth-Heinemann: Woburn, MA, 2001.

(10) Garside, J.; Mersmann, A.; Nyvlt, J. *Measurement of Crystal Growth and Nucleation Rates, 2nd Ed.*; Institute of Chemical Engineers: London, 2002.

(11) Kubota, N. Effect of Impurities on the Growth Kinetics of Crystals. *Cryst. Res. Technol.* **2001**, *36*, 749–769.

(12) Anklam, M. R.; Firoozabadi, A. An Interfacial Energy Mechanism for the Complete Inhibition of Crystal Growth by Inhibitor Adsorption. *J. Chem. Phys.* **2005**, *123*, 144708.

(13) Kubota, N.; Mullin, J. W. A Kinetic Model for Crystal Growth from Aqueous Solution in the Presence of Impurity. *J. Cryst. Growth* **1995**, *152*, 203–208.

(14) Melville, J.; Goddard, J. D. A Solid-Liquid Phase-Transfer Catalysis in Rotating-Disk Flow. *Ind. Eng. Chem. Res.* **1988**, *27*, 551–555.

(15) Chang, F.; Abbad, M. Modelling Mass Transfer in a Rotating Disk Reaction Vessel. **2011**.

(16) Chianese, A. Growth and Dissolution of Sodium Perborate in Aqueous Solutions by Using the RDC Technique. *J. Cryst. Growth* **1988**, *91*, 39–49.

(17) Bourne, J. R.; Davey, R. J.; Gros, H.; Hungerbuhler, K. The Rotating Disc Configuration in the Measurement of Crystal Growth Kinetics from Solution. *J. Cryst. Growth* **1976**, *34*, 221–229.

(18) Levich, V. *Physicochemical Hydrodynamics*; Prentice-Hall, Inc.: Englewood Cliffs, 1962.

(19) Cochran, W. G.; Goldstein, S. The Flow due to a Rotating Disc. *Math. Proc. Cambridge Philos. Soc.* **1934**, *30*, 365.

(20) Alonzo, D. E.; Raina, S.; Zhou, D.; Gao, Y.; Zhang, G. G. Z.; Taylor, L. S. Characterizing the Impact of Hydroxypropylmethyl Cellulose on the Growth and Nucleation Kinetics of Felodipine from Supersaturated Solutions. *Cryst. Growth Des.* **2012**, *12*, 1538–1547.

(21) Perry, Robert, H.; Green, Don, W. *Perry's Chemical Engineers' Handbook*; seventh.; McGraw-Hill: New York, 1997.

(22) Macrae, C. F.; Edgington, P. R.; McCabe, P.; Pidcock, E.; Shields, G. P.; Taylor, R.; Towler, M.; van de Streek, J. Mercury: Visualization and Analysis of Crystal Structures. *J. Appl. Cryst.* **2006**, *39*, 453–457.

(23) Schram, C. J.; Beaudoin, S. P.; Taylor, L. S. Impact of Polymer Conformation on the Crystal Growth Inhibition of a Poorly Water-Soluble Drug in Aqueous Solution. *Langmuir* **2015**, *31*, 171–179.

(24) Schram, C. J.; Taylor, L. S.; Beaudoin, S. P. Influence of Polymers on the Crystal Growth Rate of Felodipine – Correlating Adsorbed Polymer Surface Coverage to Solution Crystal Growth Inhibition. *Langmuir* **2015**, *31*, 11279–11287.

CHAPTER 4. IMPACT OF POLYMER CONFORMATION ON THE CRYSTAL GROWTH INHIBITION OF A POORLY WATER-SOLUBLE DRUG IN AQUEOUS SOLUTION

This chapter is a reprint with minor modifications of a manuscript published in *Langmuir* in December 2014 with the same title by: Caitlin J. Schram, Stephen P. Beaudoin, and Lynne S. Taylor.

4.1 Abstract

Poor aqueous solubility is a major hindrance to oral delivery of many emerging drugs. Supersaturated drug solutions can improve passive absorption across the gastrointestinal tract membrane as long as crystallization can be inhibited, enhancing the delivery of such poorly soluble therapeutics. Polymers can inhibit crystallization and prolong supersaturation, therefore it is desirable to understand the attributes which render a polymer effective. In this study, the conformation of a polymer adsorbed to a crystal surface, and its impact on crystal growth inhibition was investigated. The crystal growth rate of a poorly soluble pharmaceutical compound, felodipine, was measured in the presence of hydroxypropyl methylcellulose acetate succinate (HPMCAS) at two different pH conditions: pH 3 and pH 6.8. HPMCAS was found to be a less effective growth rate inhibitor at pH 3, below its pKa. It was expected that the ionization state of HPMCAS would most likely influence its conformation at the solid-liquid interface. Further

investigation with atomic force microscopy (AFM) revealed significant differences in the conformation of HPMCAS adsorbed to felodipine at the two pH conditions. At pH 3, HPMCAS formed coiled globules on the surface, whereas at pH 6.8, HPMCAS adsorbed more uniformly. Thus it appeared that the reduced effectiveness of HPMCAS at pH 3 was directly related to its conformation. The globule formation leaves many felodipine growth sites open and available for growth units to attach, rendering the polymer less effective as a growth rate inhibitor.

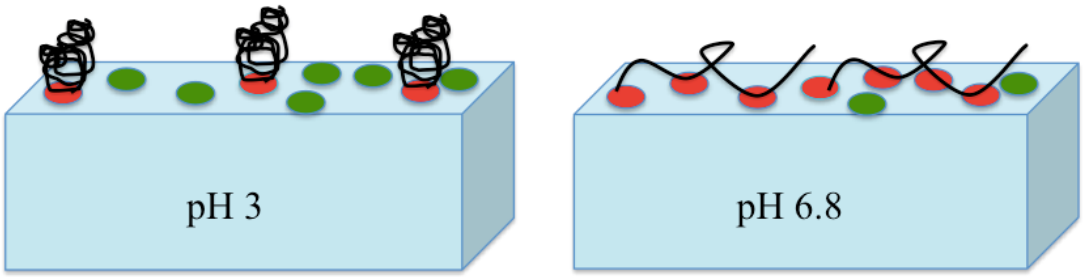

Figure 4.1. Schematic showing the change in polymer conformation at the two pH conditions studied.

4.2 Introduction

Manipulating crystal formation is of fundamental importance to several fields including biomineralization, organic electronics and drug delivery. While the impact of polymers on inorganic crystallization[1,2] and the effect of low molecular weight additives on organic crystallization[3,4] have been widely studied, polymeric modification of crystallization in aqueous solutions of low molecular weight organic molecules is not widely understood.

There is growing interest in combining polymers with poorly water soluble drugs to form amorphous drug-polymer blends, with the goal of enhancing oral

bioavailability.[5,6] The amorphous system is expected to generate a supersaturated solution *in vivo* upon dissolution.[7,8] This is because the amorphous form possesses higher free energy and enthalpy compared to the crystalline form, and has no long-range molecular order.[9–11] Thus, the energy required to dissolve an amorphous solid is significantly decreased relative to the crystalline form. Supersaturated solutions lead to higher membrane flux rates and hence can significantly improve passive drug absorption.[5,6,12–14] Therefore, amorphous drug-polymer blends can be used to improve the delivery of drugs with solubility-limited absorption. This is a pressing issue since it is estimated that up to 80% of investigational drugs have suboptimum aqueous solubility[15]. The success of this strategy can be highlighted with two examples of recently approved therapies: the protease inhibitor telaprevir[5] which is used to treat hepatitis C infections, and the B-Raf inhibitor, vemurafenib,[6] used for melanoma. Both were developed as amorphous formulations in order to achieve adequate clinical efficacy, which could not be achieved with a crystalline form of the drug.

The supersaturated solutions generated from amorphous solids will typically crystallize very rapidly because of the strong thermodynamic driving force.[8] Consequently, employing additives that slow crystallization is critical when using supersaturating dosage forms. Additives can effectively stabilize supersaturated solutions by either disrupting nucleation, or inhibiting crystal growth by adsorbing to growth sites and acting as a mechanical barrier[16–18] Recently, there have been increased efforts to determine the factors that impact the effectiveness of polymers as a crystal growth inhibitors. Key factors thought to be of importance are the hydrophobicity match between the polymer and drug,[19,20] and the ability of the polymer to form specific interactions via

hydrogen bonds to the drug.[21,22] In a recent study, it was observed that pH impacted the effectiveness of several ionizable polymers.[23] The polymers were consistently more effective at higher pH where they were highly ionized, despite having a similar extent of adsorption to the crystal at both pH values. A number of studies have shown that pH affects polymer conformation.[24–26] When a polymer is ionized, the charged functional groups will self-repulse, causing the polymer chain to extend. In the unionized state, the polymer will coil due to intramolecular hydrogen bonding.[26] Roiter and Minko confirmed these conformational transitions of poly(2-vinylpyridine) chains in aqueous solution as a function of pH using atomic force microscopy (AFM).[27]

The objective of this study was to investigate the conformation of polymers on the surface of a drug crystal as a function of pH. It is hypothesized that pH influences the conformation of the adsorbed polymers at the solid-liquid interface, and that these changes in polymer conformation impact their ability to inhibit crystal growth. To test this hypothesis, the growth rate of the model compound, felodipine, was measured in the absence and presence of the ionic polymer, hydroxypropyl methylcellulose acetate succinate (HPMCAS) at different pH conditions. The conformation of HPMCAS adsorbed to felodipine at these same pH conditions was characterized using AFM phase imaging.

4.3 Experimental Section

4.3.1 Materials

Felodipine was provided by Attix (Toronto, Ontario, Canada). Methanol was purchased from Avantor Performance Materials (Center Valley, PA). The carboxylated polymer used in this study was hydroxypropylmethyl cellulose acetate succinate

(HPMCAS) grade LF, M_W 18,000 g mol^{-1}, provided by Shin-Etsu Chemical Co, Ltd. (Tokyo, Japan) in powder form. The crystallization and adsorption media used in the growth and AFM experiments were 50 mM pH 3 phosphate buffer and 50 mM pH 6.8 phosphate buffer. The chemical structures of felodipine and HPMCAS are shown in Figure 2.5.

4.3.2 Crystal Growth Rate Measurements

The effectiveness of HPMCAS as a crystal growth inhibitor was investigated at pH 3 and pH 6.8 by measuring the growth rate of felodipine in the absence and presence of HPMCAS. The pH values of 3 and 6.8 were chosen for this study because HPMCAS grade LF has a pKa of 5.5. Thus HPMCAS will be in different ionization states at the two experimental pH values. The concentration of felodipine in solution as a function of time was measured to create a desupersaturation profile. This profile is considered to be directly proportional to the overall growth rate of felodipine. The effectiveness (E_g) of HPMCAS was then expressed as a ratio of the measured growth rates

$$E_g = \frac{R_0}{R_p} \qquad (4.1)$$

where R_0 and R_P represent the growth rate of felodipine in the absence and presence of HPMCAS respectively. Therefore, when $E_g > 1$, the polymer is considered to be effective.

Felodipine seed crystals were prepared by first melting felodipine crystals, as supplied from the manufacturer, and re-crystallizing the melt by exposure to an

atmosphere of 75% relative humidity. Seed crystals were mounted on a rotating disc apparatus (RDA) which was set to a constant rotational speed, 1000 rpm, to ensure that the growth rate coefficent, k_G, (equation 1.7) remained constant between experiments.[28–30] A stock solution of 10 mg/mL solubilized felodipine was prepared by dissolving felodipine in methanol. Supersaturated aqueous solutions were then generated by adding stock solution to pH 6.8 or pH 3 buffer. For felodipine, the equilibrium concentration, *C** is approximately 0.5 µg/mL at 25°C.[31] The initial felodipine solution concentration for growth experiments was 4 µg/mL in the absence and presence of 5 µg/mL HPMCAS. Stock solutions of 5 µg/mL HPMCAS were generated by dissolving the powder as provided in pH 6.8 or pH 3 buffer and mixing for 24 hours. The aqueous solubility of HPMCAS is poor at pH 3 compared to pH 6.8. Thus, highly concentrated solutions at pH 3 appear cloudy. However, at the low HPMCAS concentration used in this study (5 µg/mL), the solution is clear, indicating the polymer is completely dissolved and does not form agglomerates in solution at the experimental concentration.

Desupersaturation profiles were measured using a CCD Array UV-vis Spectrometer (SI Photonics, Tuscon, AZ) under isothermal conditions (25°C). Data collection began immediately after generation of supersaturated solutions. The intensity of an absorbance peak of felodipine (wavelength 360) was recorded at 10-second intervals for 1 hour. All experiments were performed in triplicate. Calibration solutions, prepared in methanol were used to correlate peak intensity to concentration. The slope of the resulting concentration v. time curve was recorded as the growth rate, R_0 or R_P in the absence or presence of HPMCAS respectively.

4.3.3 Atomic Force Microscopy

Atomic force microscopy (Figure 2.3) (MultiMode 8 AFM, Bruker Corporation, Technology Forest, TX) was used to characterize adsorbed HPMCAS on crystallized felodipine. HPMCAS was added to phosphate buffer (0.2mg/mL) and dissolved by stirring for up to 24 hours. Seed crystals grown from the melt were exposed to polymer solutions using the RDA at 200 rpm for 2 hours. The surface was not allowed to dry after adsorption. Samples were removed from the RDA holder and characterization with AFM commenced immediately. Images were taken in fluid using Tapping Mode with NPG-10 silicon nitride triangular probes (Bruker Corporation, Technology Forest, TX) with 0.24 N/m spring constant and 30 nm radius of curvature. The scan rate was set to 0.4 Hz and scan resolution was set to 512 x 512 pixels^2. Characterization was conducted in the same liquid as that used for adsorption. For samples characterized at both pH conditions, the pH of the medium was increased using sodium hydroxide. No polymers were present in the bulk solutions added to the fluid cell during imaging. Height images and phase images were taken simultaneously. Incubation times ranged from 3-5 hours. No changes in the drug surface were detected over this timeframe.

4.3.4 AFM Coupled with Infrared Spectroscopy

Infrared images coupled with AFM (Figure 2.4) were obtained using nanoIR AFM (Anasys Instruments, Santa Barbara, CA). Images were acquired using C-450 silicon cantilever probes in contact mode. An OPO nanosecond laser illuminated the sample at wavelengths characteristic to felodipine and HPMCAS. Upon irradiation, the sample expanded and contracted depending on how much infrared illumination was

absorbed, causing the AFM cantilever probe to oscillate a corresponding amount.[32] Using this approach, IR spectra from sub micron domains can be obtained. IR spectra and images were thus obtained by recording the amplitude at various sample locations. IR spectra from 1620 to 1800 cm^{-1} were acquired in increments of 4 cm^{-1} with 128 laser pulses per wavelength. IR images were obtained by irradiating the sample at 1700 cm^{-1} and 1720 cm^{-1} at a scan rate of 0.1Hz.

4.3.5 AFM-IR Sample Preparation

Samples characterized with AFM-IR were prepared directly on a ZnSe prism. A small drop of a 5 mg/mL methanolic solution of felodipine was placed on the prism and allowed to evaporate, creating a smooth, thin crystalline film. The method used to adsorb HPMCAS to the film was designed to mimic the adsorption method for samples characterized with fluid cell AFM. The ZnSe prism was suspended in buffer solution containing dissolved HPMCAS at a concentration of 0.2 mg/mL, such that the crystalline film was in contact with the solution. The solution was stirred for 1 hour. Upon removal from contact with the solution, the prism was dried with nitrogen to remove remaining liquid and any HPMCAS that was not adsorbed.

4.4 Results and Discussion

4.4.1 Polymer Effectiveness

Plots of felodipine concentration as a function of time in the absence and presence of dissolved HPMCAS are shown in Figure 4.2. The slopes of the profiles for pure felodipine (R_0) and felodipine in the presence of HPMCAS (R_P) were measured from the

data. Table 4.1 displays the values of R_0/R_P in order to compare the effectiveness of HPMCAS at reducing the growth rate of crystalline felodipine at pH 3 and pH 6.8. While $R_0/R_P > 1$ at both pH conditions, indicating that growth is reduced, the effectiveness at pH 3 is decreased by a factor of about 1.8. A similar trend was observed for ritonavir and several carboxylated cellulose polymers.[23,33] In these studies, the authors determined that the decrease in effectiveness was not due to a decrease in adsorption at the lower pH condition. Rather, the authors speculated that the difference in effectiveness might be due to changes in polymer conformation.

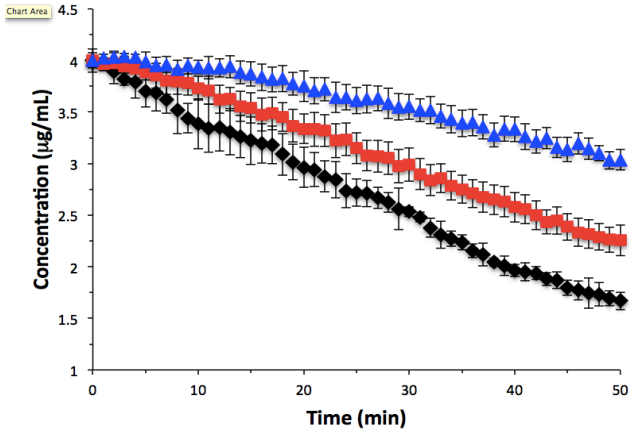

Figure 4.2. Desupersaturation of felodipine (initial S of 8) in the absence of HPMCAS (♦), and in the presence of 5 µg/mL HPMCAS at pH 3 (red ■) and pH 6.8 (blue ▲). Crystal growth rate experiments were performed in triplicate, and each data point represents the mean. Error bars indicate one standard deviation from the mean.

Table 4.1. Effectiveness crystal growth rate ratio ($E_g = R_0/R_P$) of HPMCAS for felodipine at pH 3 and pH 6.8.

pH	R_0/R_P
3	1.28
6.8	2.29

The pKa of HPMCAS is 5.5, therefore, it is nearly completely ionized at pH 6.8, and unionized at pH 3. Based on this information, and the literature previously mentioned[24–27] it is hypothesized that HPMCAS will be in an extended chain conformation at pH 6.8, and form compact coils at pH 3.

4.4.2 Polymer Conformation

Atomic force microscopy (AFM) was used to analyze the conformation of adsorbed HPMCAS on felodipine, and to provide insight into how the conformation impacts polymer effectiveness. It should be noted that AFM analysis revealed the same felodipine crystal morphology regardless of growth conditions (pH or presence of additives), therefore changes to crystal morphology is likely not the cause of changes in growth rate. Figures 4.3a and 4.3b show AFM phase contrast images of the polymer adsorbed to the crystal surface at pH 3 and 6.8. A phase contrast image of the pure drug with no adsorbed polymer is shown in Figure 4.3c for comparison. Phase contrast imaging is sensitive to changes in material properties, such as viscoelasticity,[34] making it an ideal method for detecting adsorbed polymers.

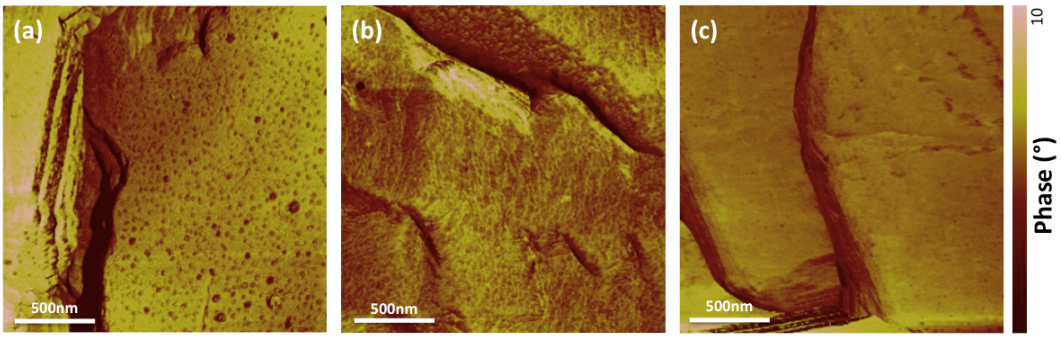

Figure 4.3. 2µm x 2µm AFM phase images of (a) HPMCAS adsorbed to felodipine at pH 3, (b) HPMCAS adsorbed to felodipine at pH 6.8, (c) felodipine with no HPMCAS adsorbed. Images were captured in liquid at room temperature with an incubation time of about 3 hours.

The results qualitatively confirm differences in HPMCAS conformation at the solid-liquid interface as a function of pH. The dark spots in Figure 4.3a are evidence of distinct globules of HPMCAS adsorbed to the crystalline drug surface at pH 3. In contrast, at pH 6.8, the AFM reveals dark shading (Figure 4.3b), over the entire surface. This dark shading is not present in the image of pure drug (Figure 4.3c), thus it is indicative of extended polymer chains dispersed across the drug surface. These results are in qualitative agreement with the proposed hypothesis. Specifically, the adsorbed polymer, when ionized, extends itself across the surface in order to isolate the charges present on its functional groups, while the unionized polymer does not suffer from internal electrostatic repulsion and can remain coiled.

Quantitative analysis of the topography of HPMCAS adsorbed to felodipine at both pH conditions can provide insight into how these changes in conformation impact the effectiveness of HPMCAS. Cross sections of the surface topography at both pH conditions are presented in Figure 4.4. The cross section of the surface at pH 6.8 (Figure 4.4a), reveals a relatively even height distribution and small topographical features up to about 0.8nm in height. The molecular diameter of glucose (an approximate surrogate for the monomer units of HPMCAS) is about 0.75 nm, which is consistent with these height variations. Thus it can be deduced that the polymer chains lay parallel to the surface, and therefore may be able to cover multiple growth sites.

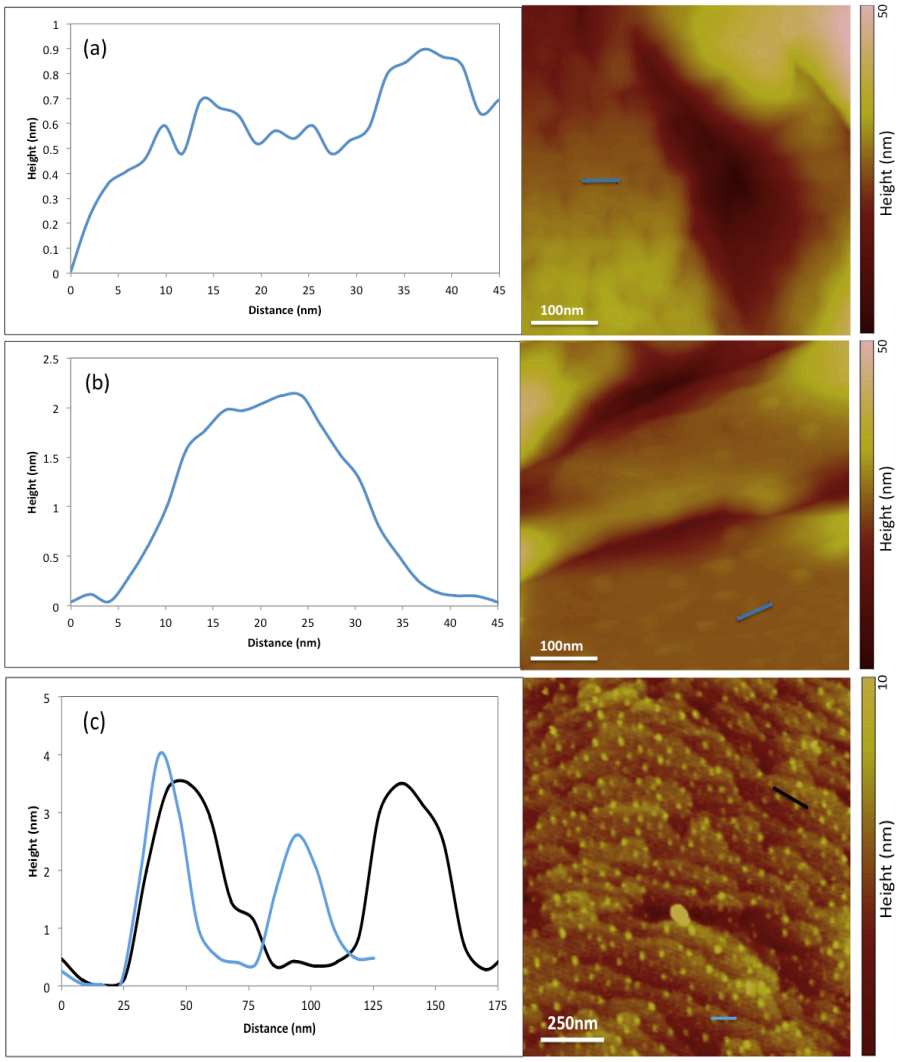

Figure 4.4. AFM cross-sectional height analyses of HPMCAS adsorbed to felodipine at (a) pH 6.8, revealing a relatively even height distribution, and at (b and c) pH 3 illustrating sample globule dimensions and standard distances between adjacent globules. AFM images were captured in liquid at room temperature with an incubation time of 3-5 hours.

Figure 4.4b shows a cross section of the surface at pH 3. Instead of many small topographical features, one large feature is present which has a radius of about 17 nm and a height of about 2 nm, providing an example of the size and shape of the adsorbed polymer globules at pH 3. The average radius, r_p, of all globules present on a 1.5µm x 1.5µm area was determined to be 15.4 nm using ImageJ analysis[35] as shown in Figure 4.5.

The average polymer globule height, h_p, was found to be 2.98 nm using cross-sectional analysis. These dimensions were applied to determine the average globule volume by modeling the globule as a spherical cap:[36]

$$V = \frac{1}{6}\pi h_p(3{r_p}^2 + {h_p}^2) \qquad (4.2)$$

From this equation, the average globule volume was determined to be 1.05×10^{-3} nm^3. Given this volume as well as the polymer density and molecular weight provided by the manufacturer, it was determined that an average of ~46 HPMCAS molecules were present in each globule.

Figure 4.4c provides an illustration of the distance between globules on the crystalline drug surface at pH 3, whereby it can be seen that the distance between any two globules ranged from 25-50 nm. Further analysis using ImageJ (Figure 4.5) revealed the average distance between globules to be about 44 nm.

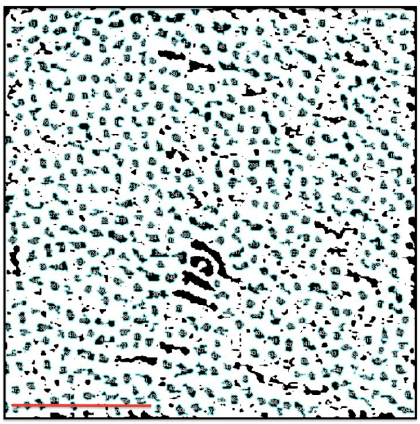

Figure 4.5. ImageJ analysis of HPMCAS adsorbed to felodipine at pH 3. Analysis reveals polymer surface coverage and average globule size. Scale bar is 500 nm.

These results provide a mechanistic understanding of the role of polymer conformation on growth inhibition. The fact that multiple polymer molecules are present in each globule at pH 3 explains why polymer adsorption did not decrease at the lower pH condition in the study by Ilevbare *et al.* previously mentioned.[23] The key consideration is the large distance between globules at pH 3. These spaces between globules leave a large number of felodipine growth sites open and available for growth units to attach; the molecular diameter of a felodipine molecule is about 0.9 nm, which is approximately 50 times smaller than the determined average distance between globules. From equations (1.15) and (1.13c), it is clear that as this average distance between globules, l, increases, the ratio R_P/R_0 increases. Thus, the effectiveness factor, E_g (equation 4.1) will be reduced at pH 3, which agrees with the results displayed in Figure 4.2 and Table 4.1. Conversely, the extended polymer chain conformation observed at pH 6.8 should have the ability to block more than one growth site, either by adsorbing to multiple sites, or by creating a barrier for growth units attaching to neighboring sites due to the extension of the chain, rendering it more effective at pH 6.8.

To determine if adsorbed polymer conformation is reversible, HPMCAS was adsorbed to felodipine at pH 3, and the topography was immediately characterized with AFM in pH 3 solution. The pH of the solution over the sample was then increased to pH 6.8 and the topography of the same location on the sample was characterized again. The results, displayed in Figure 4.6, show a change upon increasing the pH. At pH 3, the coiled polymer chains, are revealed as distinct spots in Figure 4.6a. Despite the presence of less obvious spots in the phase image at pH 6.8 (Figure 4.6b), the corresponding topographical scan at pH 6.8 (Figure 4.6d) reveals that the polymers are no longer

arranged in a compact globular formation. This change in conformation is especially clear when compared to the topography at pH 3 (Figure 4.6c).

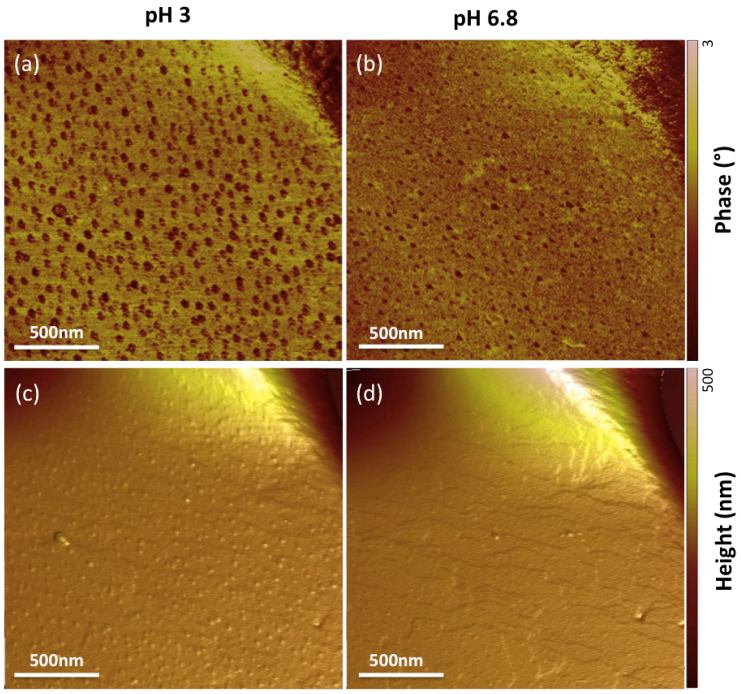

Figure 4.6. (a) 2µm x 2µm AFM phase image and (c) corresponding 3D height image topography of HPMCAS adsorbed to felodipine at pH 3. (b) AFM phase image and (d) corresponding 3D height image topography of the same area after the pH of the system was increased to 6.8. Images were captured in liquid at room temperature with an incubation time of 5 hours.

Computation of the root mean square roughness of a 1.5µm x 1.5µm area at both pH conditions reveal a 29.3% decrease in surface roughness at pH 6.8 compared to pH 3. This quantitatively confirms that the polymer chains are no longer coiled when the pH is increased to 6.8. Polymer adsorption is considered to be irreversible, however, it is possible that after the pH increases, polymer chains that were previously coiled in a globule but not adsorbed will diffuse into the bulk solution and adsorb elsewhere on the surface. However, the phase image at pH 6.8 (Figure 4.6b) reveals dark spots, unlike

Figure 4.3b. It can be deduced that these spots in Figure 4.6b represent a large density of extended polymer chains in the location of the pre-existing globules. This result suggests that when the polymers become ionized and extend, it is not likely that they migrate away from their original cluster to open growth sites on the surface within the timeframe of these experiments. Rather, they extend to occupy growth sites in the local vicinity of their original deposition coordinate.

To summarize, the conformation of HPMCAS adsorbed on a crystalline felodipine surface is pH-dependent. At pH 6.8, above its pKa, HPMCAS is ionized, therefore its functional groups will self-repulse and the polymer chains will extend. This has a favorable effect on the polymer's ability to inhibit crystal growth because it allows for more extensive growth site coverage for a given mass of deposited polymer. At pH 3, below its pKa, HPMCAS is unionized, and the polymer chains remain coiled due to intramolecular bonding. It is now known that multiple coils will combine, forming globules on the surface of the drug. This has an unfavorable impact on the polymer's ability to inhibit crystal growth because it leaves growth sites vacant for drug growth units to attach.

4.4.3 Chemical Identification of Polymer Adsorption

To confirm chemically that HPMCAS adsorbs to felodipine, the drug was characterized with infrared spectroscopy coupled with AFM (AFM-IR) before and after exposure to HPMCAS in solution at pH 6.8. Due to the nature of the measurement, samples could not be characterized in liquid. Following polymer adsorption, the surface was dried with nitrogen resulting in agglomeration of HPMCAS molecules on the surface,

as revealed by the large aggregates in the topographical image (Figure 4.7). Therefore it should be noted that AFM-IR experiments were completed for the purpose of chemical characterization only, not to gain any conformational information. The corresponding color-coded spectra in Figure 4.7 reveal that the large agglomerates on top of the smooth drug layer exhibit an absorbance peak at 1720 cm^{-1} (green and black) which arises from the carbonyl group found in HPMCAS, confirming that the aggregates are polymer. In contrast, spectra taken at various positions on what is expected to be the pure drug layer (blue and red) do not have a peak at 1720 cm^{-1}, but do exhibit four absorbance peaks from 1650 – 1700 cm^{-1}, which arise from felodipine functional groups. The spectra taken on the HPMCAS agglomerates also show absorption bands from 1650 – 1700 cm^{-1}, characteristic of felodipine. The presence and reduced height of these peaks can be attributed to the fact that the IR laser must pass through the drug layer underneath adsorbed HPMCAS. Thus, at these locations, the sample exhibited absorbance at the characteristic drug frequencies in addition to the characteristic polymer frequency. However, the presence of adsorbed HPMCAS considerably dampened the signal arising from the drug that reached the AFM tip.

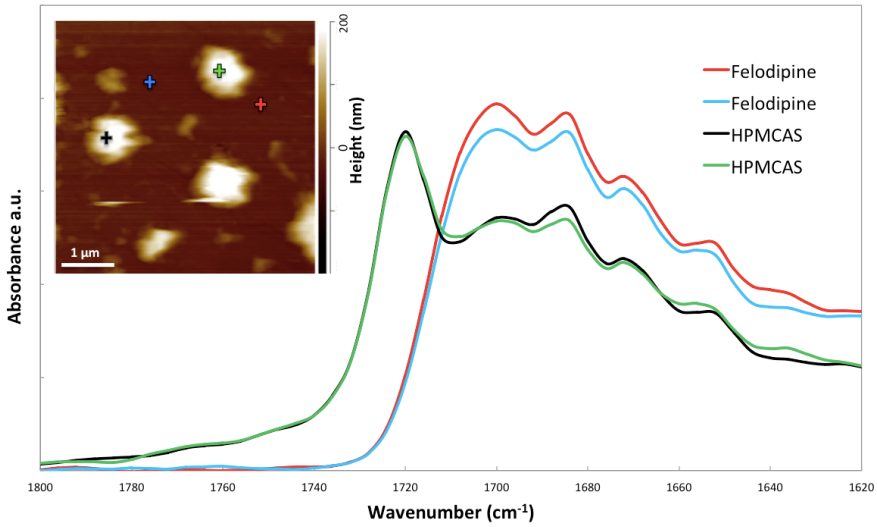

Figure 4.7. AFM-IR spectra from 1620-1800 cm^{-1} of felodipine (red and blue) and HPMCAS adsorbed to felodipine (green and black), and their corresponding locations on the AFM height image.

Figure 4.8 shows the chemical images captured as the sample was selectively illuminated at 1700 cm^{-1} and 1720 cm^{-1}, wavenumbers characteristic of felodipine and HPMCAS respectively. Pure felodipine was characterized prior to HPMCAS adsorption (Figure 4.8a). Illumination at 1700 cm^{-1} reveals a uniform absorbance at this wavelength, as expected for a chemically homogeneous surface. The sample was illuminated again at 1700 cm^{-1} after exposure to HPMCAS. The result, Figure 4.8b, now reveals dampened absorptivity (purple) when the AFM tip encountered a polymer agglomerate. This same area was irradiated at 1720 cm^{-1}, (Figure 4.8c), and it is immediately clear that the resulting image is the inverse of that shown in Figure 4.8b. There was strong absorptivity (orange) when the tip encountered a polymer agglomerate, and little absorptivity at this wavenumber on the drug crystal surface. The absence of signal from some of the smaller HPMCAS features in Figure 4.8c is due to the lesser thickness of these small

agglomerates compared to the drug layer. Since the IR laser passes through both layers, the signal that reaches the AFM tip is dominated by the thicker drug layer.

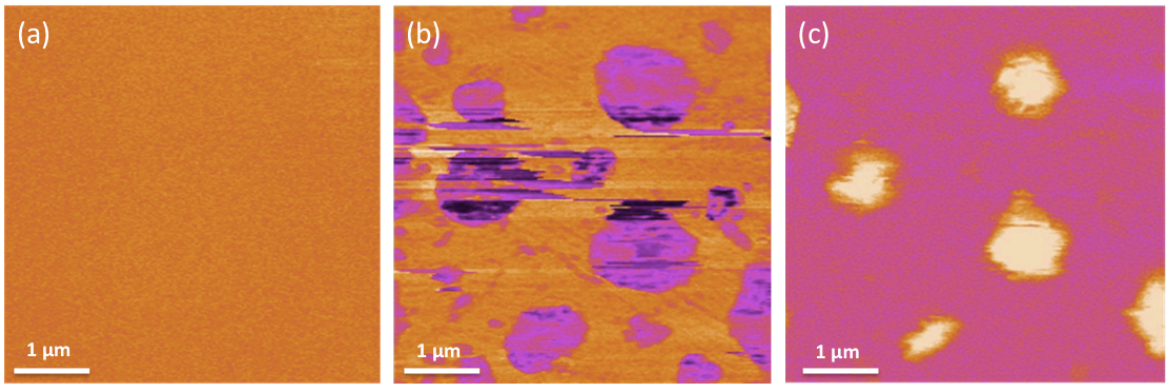

Figure 4.8. 5µm x 5µm AFM-IR chemical images of (a) pure felodipine illuminated at 1700 cm^{-1} (b) felodipine after exposure to HPMCAS illuminated at 1700 cm^{-1} and (c) 1720 cm^{-1}.

These results provide clear evidence that HPMCAS adsorbs to felodipine under the conditions specified in the current study. After exposure to HPMCAS, agglomerates were present on the felodipine surface, whereby submicron chemical imaging confirmed the chemical identity of the agglomerates.

4.5 Conclusions

When the moderately hydrophobic carboxylated cellulose polymer, HPMCAS, was not ionized in aqueous solution, it was found to adsorb onto the surface of crystalline felodipine in the form of compact coils resulting in distinct polymer globules with poor total surface coverage. In contrast, when ionized, HPMCAS chains extended, presumably due to charge repulsion between molecules, resulting in a more uniform surface coverage. In concert, it was noted that the inhibitory effect of HPMCAS on the solution crystal

growth of felodipine was considerably diminished at a low pH when the polymer is not ionized relative to at a higher pH when the polymer is ionized. Thus it is apparent that the reduced inhibitory impact of the polymer on crystal growth at low pH arises from the globule formation which leaves many growth sites available on the crystal; in contrast more growth sites are blocked when the polymer is more evenly distributed on the surface as a consequence of repulsive interactions and growth rate is more effectively reduced. The insights gained from this study with felodipine and HPMCAS can be applied to other drug-polymer systems, and can be used to identify polymers which both adsorb to the crystal surface and provide a high degree of surface coverage. This will ultimately improve the delivery of poorly water soluble therapeutics, which rely on the creation of supersaturated solutions to drive passive absorption across the gastrointestinal tract membrane.

Notes

Several crystallographic planes were identified as being present on the recrystallized amorphous films, as determined by measuring the angles between the faces (Figure 4.9 and Table 4.2). Polymer adsorption was observed, for example, on the (1 1 -1), (1 -2 -2), and (1 -1 1) faces. Each of these faces presents a different surface chemistry (Figures 4.10 – 4.12), with potential exposure of multiple functional groups including methyl, chlorine, and oxygen atoms. No difference could be discerned in the density of HPMCAS adsorption between these three faces, suggesting that adsorption is nonspecific.

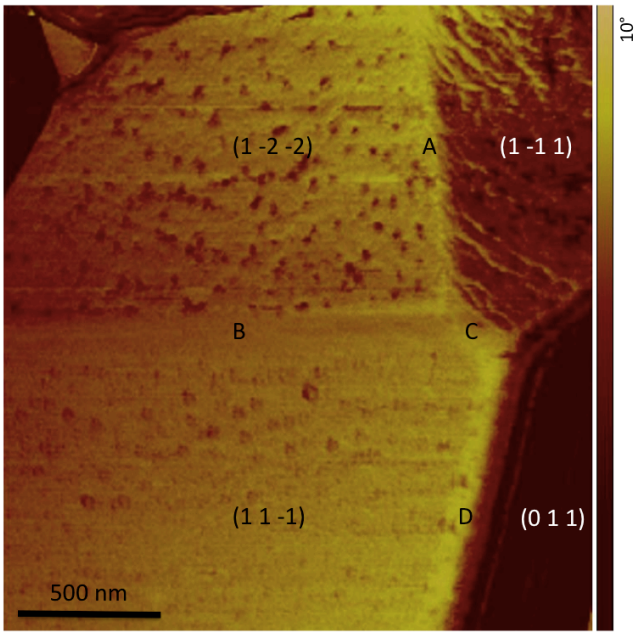

Figure 4.9. 2µm x 2µm AFM phase image of HPMCAS adsorbed to a felodipine crystallite at pH 3. The crystallite was formed following recrystallization of the amorphous material by exposure to buffer solution. The image reveals that HPMCAS adsorbs with comparable density to multiple crystal faces. The corresponding crystallographic planes were determined from the angles between crystal faces as reported in Table 4.2.

Table 4.2. The measured angles between faces of the felodipine single crystal shown in Figure 4.9, compared to the predicted angles between crystallographic planes. Angles were measured from the corresponding AFM height image using cross sectional analysis. Small discrepancies between measured and predicted values are due to instrument error and limitations of the top-down cross sectional analysis method.

Angle	Measured with AFM	Predicted
A	100.1°	97.66°
B	87.6°	86.8°
C	75.5°	75.66°
D	103.5°	103.23°

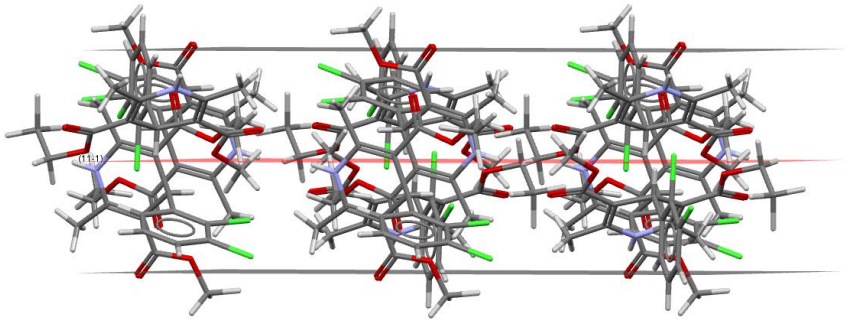

Figure 4.10. Surface chemistry of the (1 1 -1) face. Methyl groups and oxygen atoms are exposed at the surface.

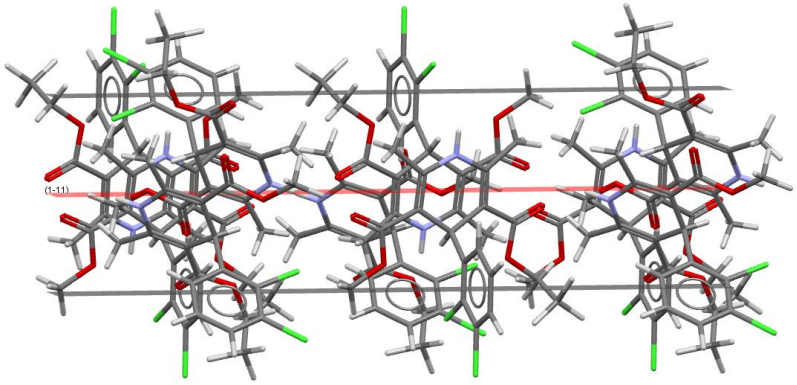

Figure 4.11. Surface chemistry of the (1 -1 1) face. Chlorine atoms and methyl groups are exposed at the surface.

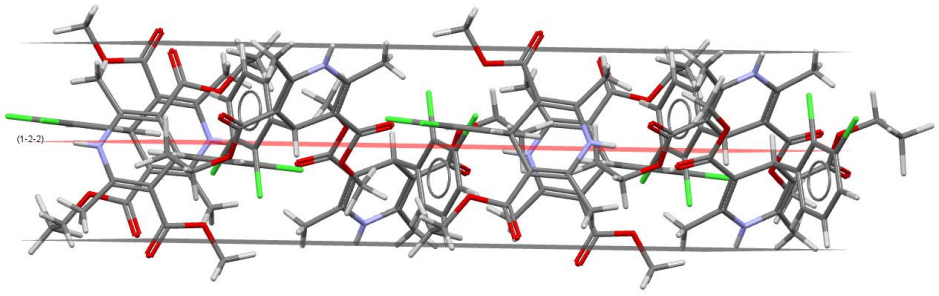

Figure 4.12. Surface chemistry of the (1 -2 -2) face. Methyl groups, amine groups, and oxygen atoms are exposed at the surface. The varying surface chemistry between this face and the (1 1 -1) and (1 -1 1) faces suggests that HPMCAS adsorption is non-specific.

References

(1) Kulak, A. N.; Iddon, P.; Li, Y.; Armes, S. P.; Co, H.; Paris, O.; Wilson, R. M.; Meldrum, F. C. Continuous Structural Evolution of Calcium Carbonate Particles : A Unifying Model of Copolymer-Mediated Crystallization. *J. Am. Chem. Soc.* **2007**, *129*, 3729–3736.

(2) Colfen, H.; Antonietti, M. Crystal Design of Calcium Carbonate Microparticles Using Double-Hydrophilic Block Copolymers. *Langmuir* **1998**, *14*, 582–589.

(3) Lahav, M.; Addadi, L.; Leiserowitz, L. Chemistry at the Surfaces of Organic Crystals. *Proc. Natl. Acad. Sci. USA* **1987**, *84*, 4737–4738.

(4) Weissbuch, I.; Addadi, L.; Lahav, M.; Leiserowitz, L. Molecular Recognition at Crystal Interfaces. *Science (80-.).* **1991**, *253*, 637–645.

(5) Kwong, A. D.; Kauffman, R. S.; Hurter, P.; Mueller, P. Discovery and Development of Telaprevir: An NS3-4A Protease Inhibitor for Treating Genotype 1 Chronic Hepatitis C Virus. *Nat. Biotechnol.* **2011**, *29*, 993–1003.

(6) Bollag, G.; Hirth, P.; Tsai, J.; Zhang, J.; Ibrahim, P. N.; Cho, H.; Spevak, W.; Zhang, C.; Zhang, Y.; Habets, G.; et al. Clinical Efficacy of a RAF Inhibitor Needs Broad Target Blockade in BRAF-Mutant Melanoma. *Nature* **2010**, *467*, 596–599.

(7) Pouton, C. W. Formulation of Poorly Water-Soluble Drugs for Oral Administration: Physicochemical and Physiological Issues and the Lipid Formulation Classification System. *Eur. J. Pharm. Sci.* **2006**, *29*, 278–287.

(8) Hancock, B. C.; Parks, M. What Is the True Solubility Advantage for Amorphous Pharmaceuticals? *Pharm. Res.* **2000**, *17*, 397–404.

(9) Hancock, B. C.; Zografi, G. Characteristics and Significance of the Amorphous State in Pharmaceutical Systems. *J. Pharm. Sci.* **1997**, *86*, 1–12.

(10) Leuner, C.; Dressman, J. Improving Drug Solubility for Oral Delivery Using Solid Dispersions. *Eur. J. Pharm. Biopharm.* **2000**, *50*, 47–60.

(11) Bhugra, C.; Pikal, M. J. Role of Thermodynamic, Molecular, and Kinetic Factors in Crystallization From the Amorphous State. *J. Pharm. Sci.* **2008**, *97*, 1329–1349.

(12) Takano, R.; Takata, N.; Saito, R.; Furumoto, K.; Higo, S.; Hayashi, Y.; Machida, M.; Aso, Y.; Yamashita, S. Quantitative Analysis of the Effect of Supersaturation on in Vivo Drug Absorption. *Mol. Pharm.* **2010**, *7*, 1431–1440.

(13) Gao, P.; Guyton, M. E.; Huang, T.; Bauer, J. M.; Stefanski, K. J.; Lu, Q. Enhanced Oral Bioavailability of a Poorly Water Soluble Drug PNU-91325 by Supersaturatable Formulations. *Drug Dev. Ind. Pharm.* **2004**, *30*, 221–229.

(14) Davis, A. F.; Hadgraft, J. Effect of Supersaturation on Membrane Transport: 1. Hydrocortisone Acetate. *Int. J. Pharm.* **1991**, *76*, 1–8.

(15) Babu, N. J.; Nangia, A. Solubility Advantage of Amorphous Drugs and Pharmaceutical Cocrystals. *Cryst. Growth Des.* **2011**, *11*, 2662–2679.

(16) Kubota, N. Effect of Impurities on the Growth Kinetics of Crystals. *Cryst. Res. Technol.* **2001**, *36*, 749–769.

(17) Ziller, K. H.; Rupprecht, H. Control of Crystal Growth in Drug Suspensions: 1) Design of a Control Unit and 2) Application to Acetaminophen Suspensions. *Drug Dev. Ind. Pharm.* **1988**, *14*, 2341–2370.

(18) Black, S. N.; Davey, R. J.; Halcrow, M. The Kinetics of Crystal Growth in the Presence of Tailor-Made Additives. *J. Cryst. Growth* **1986**, *79*, 765–774.

(19) Zimmermann, A.; Millqvist-Fureby, A.; Elema, M. R.; Hansen, T.; Müllertz, A.; Hovgaard, L. Adsorption of Pharmaceutical Excipients onto Microcrystals of Siramesine Hydrochloride: Effects on Physicochemical Properties. *Eur. J. Pharm. Biopharm.* **2009**, *71*, 109–116.

(20) Ilevbare, G. A.; Liu, H.; Edgar, K. J.; Taylor, L. S. Understanding Polymer Properties Important for Crystal Growth Inhibition - Impact of Chemically Diverse Polymers on Solution Crystal Growth of Ritonavir. *Cryst. Growth Des.* **2012**, *12*, 3133–3143.

(21) Addadi, L.; Berkovitch-Yellin, Z.; Domb, N.; Gati, E.; Lahav, M.; Leiserowitz, L. Resolution of Conglomerates by Stereoselective Habit Modification. *Nature* **1982**, *296*, 21–26.

(22) Raghavan, S.; Trividic, A.; Davis, A.; Hadgraft, J. Crystallization of Hydrocortisone Acetate: Influence of Polymers. *Int. J. Pharm.* **2001**, *212*, 213–221.

(23) Ilevbare, G. a.; Liu, H.; Edgar, K. J.; Taylor, L. S. Inhibition of Solution Crystal Growth of Ritonavir by Cellulose Polymers – Factors Influencing Polymer Effectiveness. *CrystEngComm* **2012**, *14*, 6503–6514.

(24) Yuan, W.; Zhang, J.; Zou, H.; Shen, T.; Ren, J. Amphiphilic Ethyl Cellulose Brush Polymers with Mono and Dual Side Chains: Facile Synthesis, Self-Assembly, and Tunable Temperature-pH Responsivities. *Polymer (Guildf).* **2012**, *53*, 956–966.

(25) Wu, W.; Liu, J.; Cao, S.; Tan, H.; Li, J.; Xu, F.; Zhang, X. Drug Release Behaviors of a pH Sensitive Semi-Interpenetrating Polymer Network Hydrogel Composed of Poly(vinyl Alcohol) and Star poly[2-(dimethylamino)ethyl Methacrylate]. *Int. J. Pharm.* **2011**, *416*, 104–109.

(26) Etika, K. C.; Cox, M. A.; Grunlan, J. C. Tailored Dispersion of Carbon Nanotubes in Water with pH-Responsive Polymers. *Polymer (Guildf).* **2010**, *51*, 1761–1770.

(27) Roiter, Y.; Minko, S. AFM Single Molecule Experiments at the Solid-Liquid Interface: In Situ Conformation of Adsorbed Flexible Polyelectrolyte Chains. *J. Am. Chem. Soc.* **2005**, *127*, 15688–15689.

(28) Bourne, J. R.; Davey, R. J.; Gros, H.; Hungerbuhler, K. The Rotating Disc Configuration in the Measurement of Crystal Growth Kinetics from Solution. *J. Cryst. Growth* **1976**, *34*, 221–229.

(29) Beaudoin, S. .; Grant, C. S.; Carbonell, R. G. Removal of Organic Films from Solid Surfaces Using Aqueous Solutions of Nonionic Surfactants. 2. Theory. *I&EC Res.* **1995**, *34*, 3318–3325.

(30) Chianese, A. Growth and Dissolution of Sodium Perborate in Aqueous Solutions by Using the RDC Technique. *J. Cryst. Growth* **1988**, *91*, 39–49.

(31) Alonzo, D. E.; Raina, S.; Zhou, D.; Gao, Y.; Zhang, G. G. Z.; Taylor, L. S. Characterizing the Impact of Hydroxypropylmethyl Cellulose on the Growth and Nucleation Kinetics of Felodipine from Supersaturated Solutions. *Cryst. Growth Des.* **2012**, *12*, 1538–1547.

(32) Harrison, A. J.; Bilgili, E. a; Beaudoin, S. P.; Taylor, L. S. Atomic Force Microscope Infrared Spectroscopy of Griseofulvin Nanocrystals. *Anal. Chem.* **2013**, *85*, 11449–11455.

(33) Ilevbare, G. A.; Liu, H.; Edgar, K. J.; Taylor, L. S. Impact of Polymers on Crystal Growth Rate of Structurally Diverse Compounds from Aqueous Solution. *Mol. Pharm.* **2013**, *10*, 2381–2393.

(34) Schmitz, I.; Schreiner, M.; Friedbacher, G.; Grasserbauer, M. Phase Imaging as an Extension to Tapping Mode AFM for the Identification of Material Properties on Humidity-Sensitive Surfaces. *Appl. Surf. Sci.* **1997**, *115*, 190–198.

(35) Abramoff, M. D.; Magalhaes, P. J.; Ram, S. J. Image Processing with ImageJ. *Biophotonics Int.* **2004**, *11*, 36–42.

(36) Walker, G. M.; Beebe, D. J. A Passive Pumping Method for Microfluidic Devices. *Lab Chip* **2002**, *2*, 131–134.

CHAPTER 5. INFLUENCE OF POLYMERS ON THE CRYSTAL GROWTH RATE OF FELODIPINE: CORRELATING ADSORBED POLYMER SURFACE COVERAGE TO SOLUTION CRYSTAL GROWTH INHIBITION

This chapter is a reprint with minor modifications of a manuscript published in *Langmuir* in September 2015 with the same title by: Caitlin J. Schram, Lynne S. Taylor, and Stephen P. Beaudoin.

5.1 Abstract

The bioavailability of orally administered drugs that exhibit poor aqueous solubility can be enhanced with the use of supersaturating dosage forms. Stabilization of these forms by preventing or inhibiting crystallization in solution is an important area of study. Polymers can be used to stabilize supersaturated systems, however the properties that impact their effectiveness as crystal growth rate inhibitors are not yet fully understood. In this study, the impact of various polymers on the crystal growth rate of felodipine and the conformation of these polymers adsorbed to crystalline felodipine was investigated in order to gain a mechanistic understanding of crystal growth inhibition. It was determined that polymer hydrophobicity impacted polymer adsorption as well as adsorbed polymer conformation. Polymer conformation impacts its surface coverage, which was shown to directly correlate to the polymer's effectiveness as a growth rate

inhibitor. By modeling this correlation, it is possible to predict polymer effectiveness given the surface coverage of the polymer.

5.2 Introduction

The crystal form of a compound can greatly impact its physical, chemical, and mechanical properties. Therefore, the ability to manipulate crystallization from supersaturated solutions is of importance to many industries. In the pharmaceutical field, controlling crystal formation is fundamental to optimizing drug formulation and delivery.[1] In particular, there is growing interest in slowing or inhibiting crystallization of organic molecules using polymeric additives.[2–4]

The ability to inhibit crystallization is desirable because nearly 80% of investigational drugs have suboptimal aqueous solubility.[5] Formulating a drug as an amorphous solid can result in increased dissolution rates and the generation of a supersaturated solution.[6–8] In this form, the drug will permeate across gastrointestinal (GI) tract membranes at a faster rate, thereby greatly increasing absorption.[9,10] A major challenge to the utilization of supersaturating delivery systems, however, is the difficulty in maintaining supersaturation, because of the driving force for crystallization.[11,12] Thus, preventing crystallization to maintain supersaturation is crucial to increasing drug exposure.

Additives, such as polymers can inhibit crystallization and stabilize supersaturated solutions.[13] While many studies have been conducted to identify effective polymers, the key properties that render a polymer effective are not widely understood. Several recent

studies determined that polymer hydrophobicity can greatly impact effectiveness,[3,14,15] however the explanation for this phenomenon has not yet been determined.

The objective of this study was to investigate the adsorbed conformation of a group of polymers of varying hydrophobicity on the surface of crystalline drug, and the corresponding effect of this adsorption on crystal growth. A polymer's adsorbed conformation has been shown to influence its ability to inhibit crystal growth.[16] Therefore, it is hypothesized that polymer hydrophobicity will greatly impact adsorbed polymer conformation, consequently influencing the effectiveness as a growth inhibitor.

5.3 Experimental Section

5.3.1 Materials

Felodipine was provided by Attix (Toronto, Ontario, Canada). Methanol (HPLC grade) was purchased from Avantor Performance Materials (Center Valley, PA). The polymers used in this study were hydroxypropylmethyl cellulose acetate succinate (HPMCAS) LF grade, M_w 18 000 g mol^{-1} and hydroxypropylmethyl cellulose (HPMC) 606 grade (Shin-Etsu Chemical Co, Ltd., Tokyo, Japan), polyvinylpyrrolidone (PVP), M_w 40 000 g mol^{-1}, polyacrylic acid (PAA) M_w 450 000 g mol^{-1}, and poly(vinyl pyrrolidone vinyl acetate) (PVPVA), M_w 50 000 g mol^{-1} (Sigma-Aldrich Co., St. Louis, MO), and poly(2-vinylpyridine) (P2VP), M_w 40 000 g mol^{-1} and polyvinyl acetate (PVAc), M_w 90 000 g mol^{-1} (Polysciences Inc., Warrington, PA). The crystallization and adsorption media used in all experiments was 50 mM pH 6.8 phosphate buffer. The chemical structures of felodipine and the polymers used in this study are given in Figure 2.5.

5.3.2 Crystal Growth Rate Measurements

The growth rate of felodipine was measured in the absence and presence of the polymers shown in Figure 2.5. The concentration of felodipine in solution as a function of time was measured to determine a desupersaturation profile. This profile is considered to be directly proportional to the overall growth rate of felodipine. The effectiveness (E_g) of each polymer can then be expressed as a ratio of the measured growth rates

$$E_g = \frac{R_0}{R_P} \tag{5.1}$$

where R_0 and R_P represent measured growth rates of felodipine in solution in the absence and presence of polymer respectively. Therefore, when $E_g > 1$, the polymer is considered to be effective.

Felodipine seed crystals were prepared by first melting felodipine crystals, as supplied from the manufacturer, in a custom PTFE holder and re-crystallizing the melt by exposure to an atmosphere of 75% relative humidity. This yielded a flat surface of well-defined and consistent surface area. Seed crystals in the holder were mounted on a rotating disc apparatus (RDA) (Princeton Applied Research, model 616), which was set to a constant rotational speed, 6000 RPM, to ensure that the measured growth rate was independent of mass transfer and reflected the rate of integration only. A stock solution of 10 mg/mL solubilized felodipine was prepared by dissolving felodipine in methanol. Supersaturated aqueous solutions were then generated by adding a small amount of the felodipine stock solution to pure pH 6.8 buffer, or buffer containing pre-dissolved polymers. The initial solution concentration for growth experiments was 2 μg/mL. The

equilibrium concentration of felodipine is approximately 0.5 μg/mL at 25°C,[17] thus the experiments were carried out at initial S = 4. Polymers were pre-dissolved in pH 6.8 buffer to create stock solutions with concentrations of 5 and 10 μg/mL.

Desupersaturation profiles were measured using a CCD Array UV-vis Spectrometer (SI Photonics, Tuscon, AZ) under isothermal conditions (25°C). Data collection began immediately after generation of supersaturated solutions. The intensity of an absorbance peak of felodipine (wavelength 238 nm) was recorded at 10-second intervals for 1 hour. All experiments were performed in triplicate. Calibration solutions, prepared in methanol were used to correlate peak intensity to concentration. The slope of the resulting concentration v. time curve was recorded as the growth rate, R_0 or R_P in the absence or presence of polymers.

5.3.3 Atomic Force Microscopy

Atomic force microscopy (Figure 2.3) (MultiMode 8 AFM, Bruker Corporation, Technology Forest, TX) was used to characterize adsorbed polymers on crystallized felodipine. Seed crystals grown from the melt were exposed for two hours to the same polymer stock solutions used for growth experiments. Samples were removed from the RDA holder and characterization with AFM commenced immediately. The surface was not allowed to dry after adsorption, and images were taken in the same liquid as that used for the adsorption step. Characterization was done using Tapping Mode with NPG-10 (0.24 N/m spring constant, 30 nm radius of curvature) or SNL-10 (0.24 N/m spring constant, 10 nm radius of curvature) silicon nitride triangular probes (Bruker Corporation, Technology Forest, TX). The scan rate was set to 0.4 Hz and scan resolution was set to

512 x 512 pixels^2. Height images and phase contrast images were obtained simultaneously. Phase contrast imaging is sensitive to changes in material properties, such as viscoelasticity,[18] thus it is an ideal method for detecting adsorbed polymers.

5.3.4 Determination of Polymer Surface Coverage

AFM phase contrast images were analyzed using ImageJ[19]. Each image was converted to an 8-bit bichromatic image such that polymers stood out as black objects on a white background. The threshold limits were set to be consistent between all systems such that the analysis could eliminate felodipine surface effects and accurately represent the size of polymers as shown in the phase contrast images. The software could then determine the percentage of the image area occupied by black pixels.

5.3.5 Contact Angle Measurements

Contact angle measurements of DI water and ethylene glycol on a crystalline felodipine surface were taken in order to determine the surface energy of felodipine. Measurements were taken under ambient conditions using a Ramé-Hart model 500 goniometer and DROPimage advanced software. Ten drops were measured for each liquid, and a total of ten measurements were taken per drop in order to obtain an average contact angle for each of the two liquids on felodipine. The surface energy was then estimated using the harmonic mean approach, or two liquid method proposed by Wu.[20] This approach uses the harmonic mean of the disperse and polar components of both the liquid and solid surface tensions to determine the solid-liquid interfacial tension. The

surface energy can then be determined from the calculated interfacial tension and measured contact angles using Young's equation.[21]

5.3.6 Determination of Felodipine Growth Unit Size

The size of a felodipine growth unit was determined using the crystal structure visualization software, Mercury.[22] The molecular structure of felodipine (form DONTIJ) was provided by the Cambridge Crystallographic Data Centre (CCDC) structural database. The measure distances tool in Mercury was used to determine the length and width of a felodipine molecule. These measurements were used to calculate the area occupied by a growth unit on a crystal surface.

5.4 Results and Discussion

Polymer adsorption to a solid-liquid interface is driven by energetically favorable interactions between the polymer and solid as influenced by the medium. In short, whether or not a polymer will adsorb to a solid is determined by how favorably the polymer interacts with the solid compared to how favorably it interacts with the solvent.[23] In a poor solvent, the polymer will want to escape the medium and will consequently adsorb to the surface.[24] However, even in a good solvent, a polymer will adsorb if it forms more favorable intermolecular interactions with the solid than with the solvent. These can include electrostatic interactions, hydrogen-bonding interactions, and chemical interactions.[23]

5.4.1 Impact of Polymer Hydrophobicity on Adsorption

The crystal growth rate of pure felodipine (R_0) and the growth rate of felodipine in the presence of polymers (R_P) were measured to determine the growth rate ratio, R_0/R_P, which indicates polymer effectiveness (equation 5.1). The results are shown in Figure 5.1, arranged in order of increasing polymer hydrophobicity. The order was determined from previously published solubility parameters calculated for each polymer.[25]

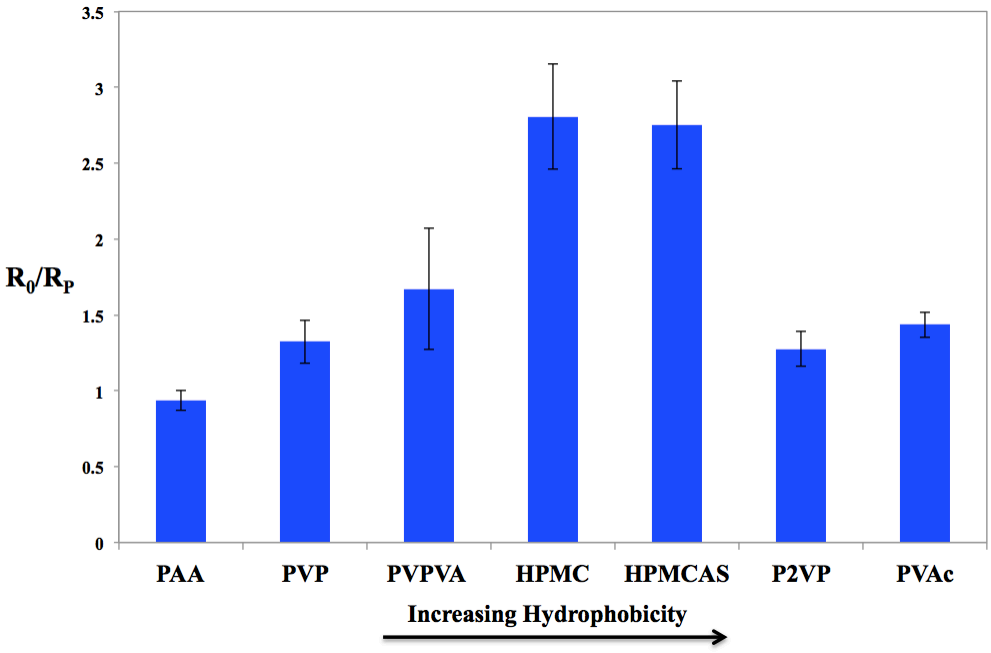

Figure 5.1. Effectiveness crystal growth rate ratio of felodipine at initial S of 4 with various polymers present at a concentration of 5 µg/mL. Growth rate experiments were performed in triplicate and each column represents the mean. Error bars indicate standard error of the mean.

Figure 5.1 shows that polymer hydrophobicity plays an important and complex role in polymer effectiveness. The very hydrophilic and hydrophobic polymers are relatively ineffective (E_g ~1-1.5), whereas the moderately hydrophobic polymers are two to three times more effective. A similar trend was observed in a previous study for the

API ritonavir.[15] In this study, the authors hypothesized that polymer hydrophobicity may affect the extent of adsorption of polymer to the drug.

To test this hypothesis, each polymer was adsorbed to felodipine and subsequently analyzed with atomic force microscopy (AFM). The results for select systems are presented in Figure 5.2 along with a pure felodipine surface (Figure 5.2e) for comparison.

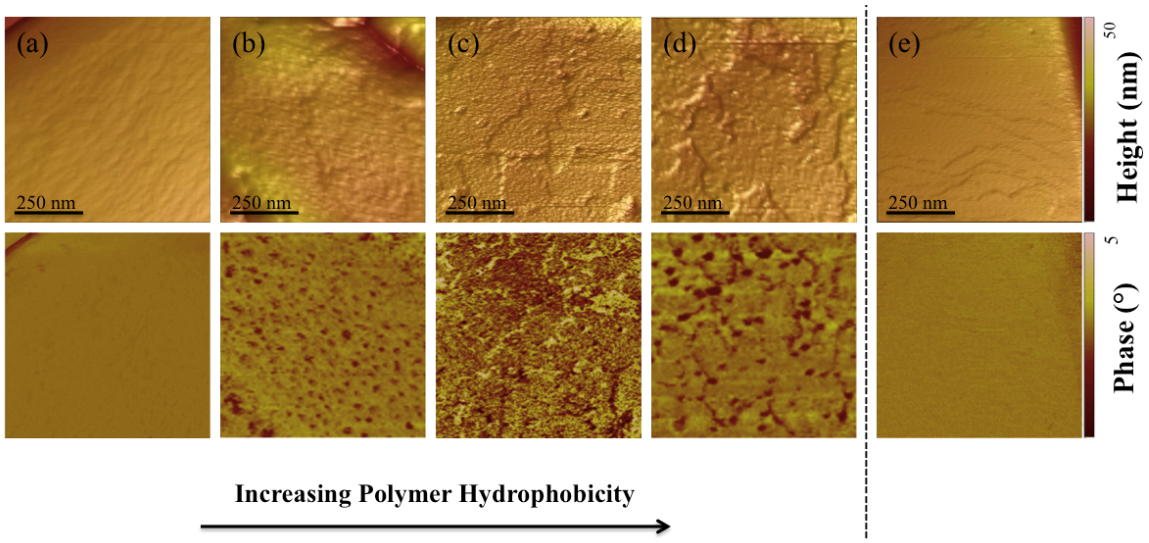

Figure 5.2. 750 nm x 750 nm AFM height and corresponding phase contrast images of felodipine after exposure to (a) PAA, (b) PVP, (c) HPMCAS, and (d) PVAc, and (e) pure felodipine with no exposure to polymers. Images were captured in liquid at room temperature with an incubation time of 4-5 h.

The very hydrophilic polymer PAA (Figure 5.2a) shows no evidence of adsorption to crystalline felodipine. This explains why PAA has no effect on the growth rate of felodipine ($R_0/R_P = 1$). Very hydrophilic polymers such as PAA interact favorably with water; therefore PAA has little driving force to adsorb to the drug surface. At the other end of the spectrum, PVAc, a very hydrophobic polymer, shows evidence of

adsorption (Figure 5.2d), however, it adsorbs in aggregates. This can be seen from the dark spots in the phase image as well as the raised globules in the corresponding 3D height image. A similar result was observed by Amiel *et al.* for hydrophobic polymers.[26] This result suggests that hydrophobic polymers such as PVAc are driven to adsorb to the drug surface in order to minimize interactions with water. The adsorbed aggregated conformation also reflects the polymer's desire to minimize surface contact with water. Therefore, although PVAc is present on the drug surface, the poor surface coverage due to aggregation results in poor growth rate inhibition as shown in Figure 5.1.

Of the four systems shown, HPMCAS, which is a moderately hydrophobic polymer, adsorbs with the highest degree of surface coverage, as evidenced by the relatively uniform dark shading in the AFM phase image (Figure 5.2c). This result suggests that HPMCAS has a certain hydrophilic/hydrophobic balance necessary to not only drive adsorption to the surface but to interact favorably with both the drug and the aqueous medium once adsorbed. The height image reveals no obvious surface features, suggesting that HPMCAS chains are spread fairly flat on the surface. This was shown to be the case for HPMCAS at pH 6.8 in Chapter 4. Because HPMCAS contains both hydrophobic and hydrophilic functional groups and favorably interacts with both the aqueous medium and the more hydrophobic drug surface, it provides a high degree of surface coverage, and is a more effective growth rate inhibitor (Figure 5.1).

Although PVP is a very hydrophilic polymer, AFM characterization reveals that it adsorbs to felodipine (Figure 5.2b). This suggests that PVP adsorption to felodipine may be driven by specific interactions between the polymer and drug. Previous studies have provided evidence of PVP adsorption due to hydrogen bonding.[14,27,28] Karavas *et al*.

confirmed that PVP interacts with felodipine via a hydrogen bond, which forms between the carbonyl group of PVP and the amino group of felodipine.[29] In fact, their results indicated that PVP forms two specific interactions with felodipine. The second interaction could be formed with the amide group of PVP.[30]

It is possible that the adsorption of PVP to felodipine is due in part to hydrophobic effects as well. PVP has been known to adsorb to hydrophobic surfaces, such as graphite in water. According to Esumi *et al.*, graphite preferentially interacts with PVP over water due to the solid's hydrophobic nature.[31] Thus, PVP adsorption to graphite is not a result of poor polymer-solvent interactions, but due to unfavorable surface-solvent interactions. This effect could contribute in concert with hydrogen bonding to the adsorption of PVP on hydrophobic felodipine.

Although PVP adsorbs to felodipine, it has limited impact on the growth rate (Figure 5.1) due to its aggregated conformation (Figure 5.2b). This conformation is a result of hydrophobic effects. The hydrophilic polymer forms aggregates in order to minimize contact with the hydrophobic drug surface.[32]

In summary, the results indicate that polymer hydrophobicity is an important factor which influences polymer effectiveness due to its impact on adsorption and adsorbed polymer conformation. Very hydrophilic polymers will likely not adsorb because they prefer to remain in solution. As polymer hydrophobicity increases, it is more likely to interact with the drug in order to minimize contact with the aqueous solution. Polymer hydrophobicity also impacts the polymer's adsorbed conformation. Very hydrophobic polymers will aggregate to minimize interactions with the aqueous medium whereas more hydrophilic polymers will aggregate to minimize contact with the

hydrophobic drug surface. Polymers with intermediate hydrophobicity will interact favorably with both the medium and the drug surface, resulting in a spread out conformation. These variations in conformation impact the polymer surface coverage, which influences growth rate inhibition.

In Figure 5.1, the growth rate results of felodipine with PVPVA, the random co-polymer of PVP and PVAc, reveal that PVPVA is a better growth rate inhibitor than the same concentration of either PVP or PVAc alone. This is most likely because PVPVA has a higher net driving force for adsorption than PVP or PVAc alone. PVPVA adsorption to felodipine is driven by the combination of hydrophobic interactions (PVAc units) and specific interactions (PVP units), resulting in greater overall surface coverage.

Greater surface coverage by PVPVA suggests that PVP and PVAc may adsorb to different felodipine sites. To gain more insight into this, crystal growth rates were measured in the presence of a polymer mixture composed of equal parts PVP and PVAc at two different concentrations. The results are displayed in Figure 5.3 along with the results for PVPVA, PVP, and PVAc for comparison.

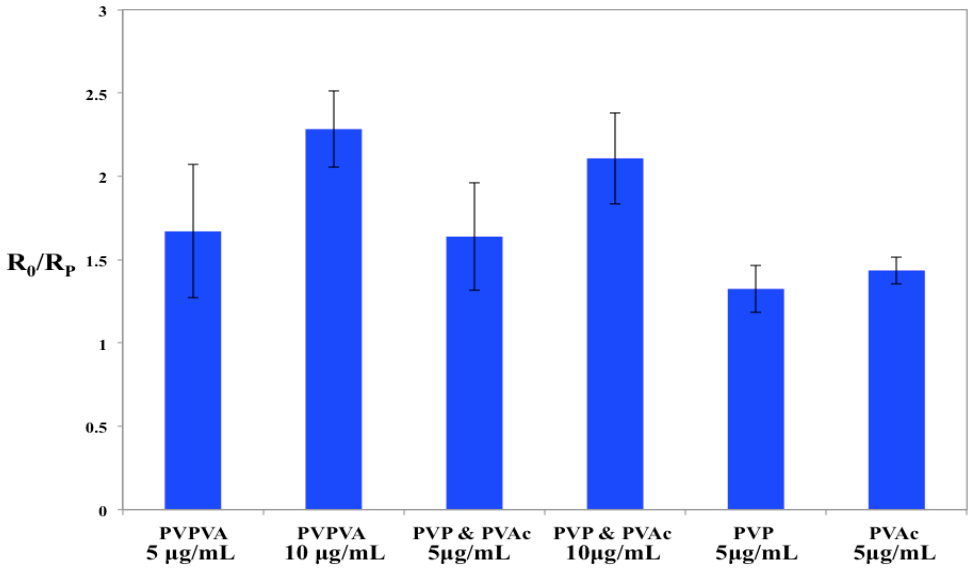

Figure 5.3. Effectiveness crystal growth rate ratio of felodipine at initial S of 4 with various polymers present at a total polymer concentration of 5 or 10 µg/mL. Growth rate experiments were performed in triplicate and each column represents the mean. Error bars indicate standard error of the mean.

The results indicate that the polymer mixture at both 5 and 10 µg/mL total concentrations have the same effect on the growth rate of felodipine as the copolymer. The fact that the polymer mixture is also able to achieve greater coverage than the same concentration of PVP or PVAc alone suggests that PVP and PVAc are able to bind to different felodipine sites and do not necessarily compete for equally energetic sites on the surface.

5.4.2 Polymer Surface Coverage

To determine the surface coverage of each polymer adsorbed to felodipine, Φ, samples were characterized with AFM phase imaging. It should be noted that the surface coverage is a physical parameter that describes simply the macroscopic fraction of the felodipine surface covered by polymer, while θ, the fractional coverage as defined by the

Kubota-Mullin model (equation 1.15), represents the ratio of the average distance between sites available for impurity adsorption to the average distance between adsorbed impurities (as described in equation 1.13c). While these parameters may be proportional, they are not identical. The AFM images were then analyzed using ImageJ analysis.[19] The results are presented in Figure 5.4 in order of increasing polymer coverage. Table 5.1 displays the fractional coverage values determined from ImageJ.

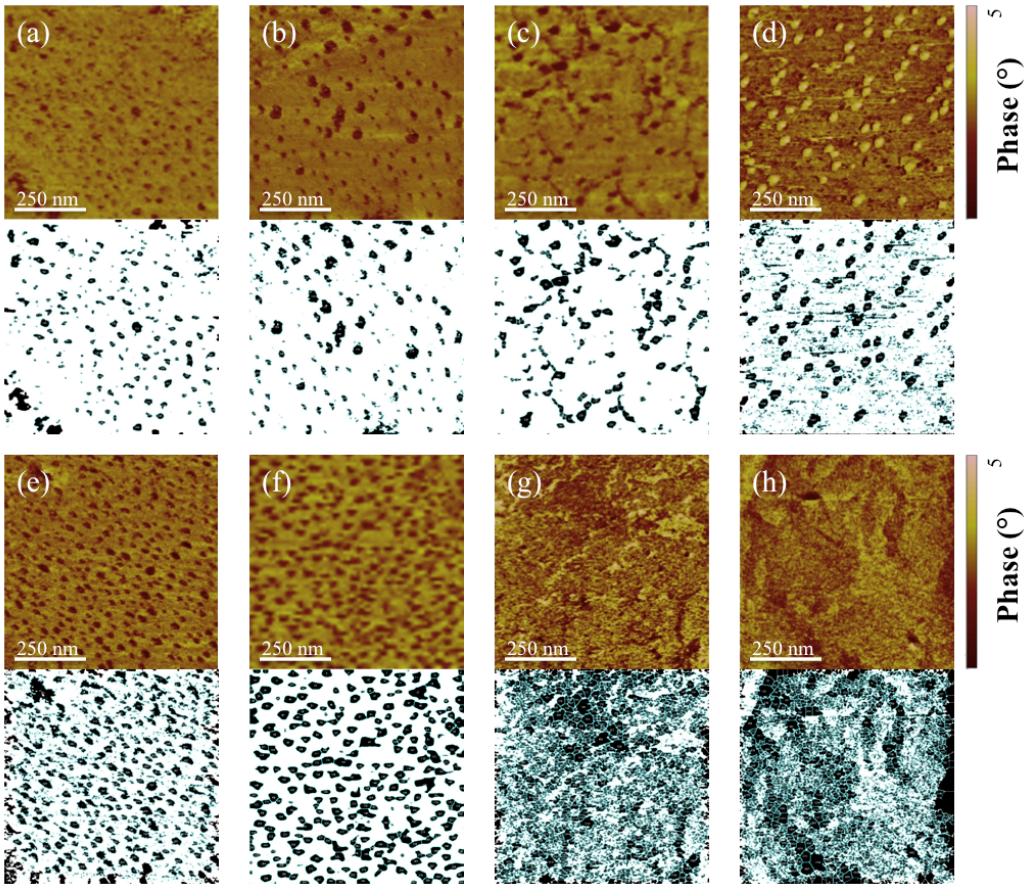

Figure 5.4. 750 nm x 750 nm AFM phase images and corresponding ImageJ analysis images of (a) PVP, (b) P2VP, (c) PVAc, (d) PVPVA, (e) PVP + PVAc (10 µg/mL), (f) PVPVA (10 µg/mL), (g) HPMCAS, (h) HPMC adsorbed to crystalline felodipine. Polymer solution concentrations were 5 µg/mL unless otherwise indicated. AFM images were captured in liquid at room temperature with an incubation time of 4-5 h.

Table 5.1. Fractional surface coverage values for each polymer adsorbed to felodipine determined using ImageJ analysis. Values given are the average of three measurements.

Polymer	Φ
PAA	0
PVP	0.08 ± 0.008
P2VP	0.10 ± 0.014
PVAc	0.14 ± 0.007
PVPVA	0.19 ± 0.025
PVP + PVAc (10 μg/mL)	0.28 ± 0.021
PVPVA(10 μg/mL)	0.31 ± 0.018
HPMCAS	0.53 ± 0.025
HPMC	0.54 ± 0.008

These results, when compared to the growth rate results presented in Figures 5.1 and 5.3, indicate that there is a correlation between polymer coverage and polymer effectiveness. The polymers that adsorb with higher coverage are the most effective growth rate inhibitors, and polymers that adsorb with the lowest coverage are less effective. Plotting polymer effectiveness, R_0/R_P, as a function of fractional surface coverage (Figure 5.5) reveals that there is a linear correlation between polymer coverage and polymer effectiveness as a growth rate inhibitor.

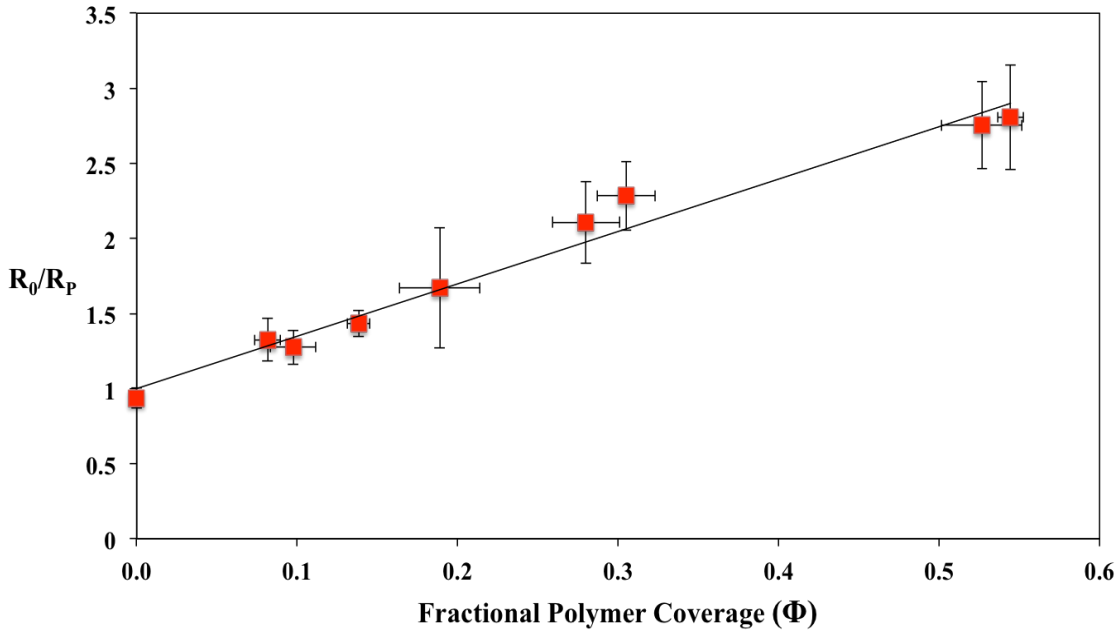

Figure 5.5. Plot of crystal growth rate ratios (polymer effectiveness) as a function of fractional polymer coverage, demonstrating a linear correlation. Error bars indicate standard error from the mean.

5.4.3 Modeling the Correlation between Growth Rate and Polymer Coverage

According to the Kubota-Mullin model, a greater fractional coverage by the polymer, θ, will result in a reduced growth rate when polymer is present, R_P, as shown in equation (1.15). As mentioned above, the definition of fractional coverage expressed in the model, θ, is the ratio of the average distance between available sites for adsorption and the average distance between adsorbed polymers. This is different from the definition of polymer surface coverage, Φ, which is a parameter that is determined experimentally. However the two parameters are expected to be proportional. Modeling the experimental results using the Kubota-Mullin model can confirm this proportionality.

Equation (1.15) can be applied in the current study because the first condition given in Section 1.5 is satisfied by the fact that seed crystals were grown in a holder of constant area for all experiments. The second condition is assumed to be true based on observations made with atomic force microscopy. There was no noticeable difference in surface area of the individual felodipine faces for the imaged systems with adsorbed polymer compared to the pure drug system. Thus, equations (1.15), (1.13b), and (1.13c) were combined to give the following expression:

$$\frac{R_P}{R_0} = 1 - \frac{\gamma a}{k_B \mathrm{T}(\ln \mathrm{S})(\theta l)}\theta \qquad (5.2)$$

The value of each parameter, except the average distance between adsorbed polymers, *l*, was known or experimentally determined. The values of these constants are given in Table 5.2. Temperature supersaturation, S, were determined from the experimental conditions. The size of a felodipine growth unit, *a*, was determined using the crystal structure visualization software Mercury,[22] as explained in section 5.3.6. To determine the surface energy of crystalline felodipine, γ, the contact angles of two different liquids on a crystalline felodipine surface were measured with a goniometer. γ was then calculated from the measured contact angles using the harmonic mean approach[20] as outlined in section 5.3.5.

Table 5.2. Values used in equation (5.2)

Constant Parameter	Value
γ	3.9E-20 J/nm
a	0.584 nm^2
k	1.38E-23 J/K
T	298.15 K
lnS	1.39

The average distance between polymers, l, varies for each system and is dependent on polymer surface coverage. Thus, it was necessary to determine a relationship between l and Φ. Values of l for all polymer systems except PVPVA at initial concentration 10 µg/mL were fitted to equation (5.2) to minimize the residual error at each value of Φ such that the experimental and theoretical values of R_0/R_P converged. These fitted values for l were then plotted against Φ as shown in Figure 5.6, resulting in the power relation given in equation (5.3).

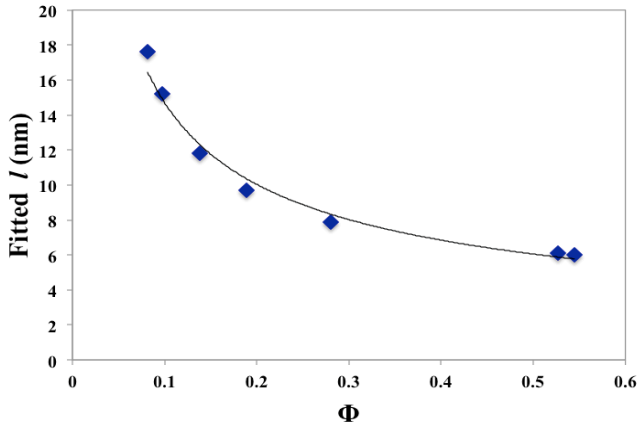

Figure 5.6. Values determined for the average distance between polymers plotted against Φ.

$$l = 4.13\Phi^{-0.55} \qquad (5.3)$$

With this general expression to relate *l* and Φ, the unknown parameter, *l*, in equation (5.2) can be determined from the measured surface coverage. Substituting this relation into equation (5.2) for *l* produces the theoretical values for R_0/R_P plotted in Figure 5.7. It can be seen that by using this model, the theoretical values for R_0/R_P are in good agreement with the experimental values.

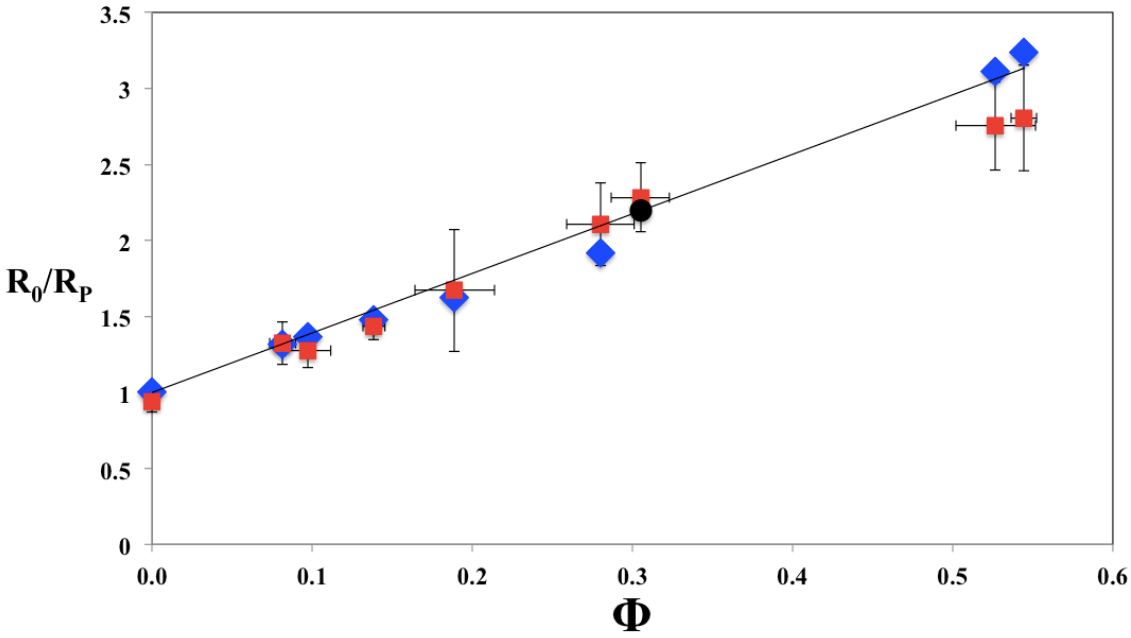

Figure 5.7. Plot comparing experimental R_0/R_P values (red ■) to theoretical R_0/R_P values (blue ♦) determined using the Kubota-Mullin model, and the predicted effectiveness of 10 µg/mL PVPVA (●).

The agreement between experimental and theoretical results suggests that the model should be able to predict polymer effectiveness given the AFM determined

fractional coverage of the polymer. To demonstrate the predictive ability of the model, the equation of the best-fit line for the linear theoretical relationship was determined to be

$$\frac{R_0}{R_P} = 3.918\Phi + 1 \qquad (5.4)$$

Entering the experimentally determined Φ for PVPVA (initial concentration 10 μg/mL) adsorbed to felodipine into equation (5.4) results in a predicted R_0/R_P value, which is in good agreement with the experimental value (Figure 5.7). This suggests that a polymer's effectiveness can be accurately predicted using this model.

In summary, the results shown in Figure 5.7 provide clear evidence that there is a linear correlation between polymer effectiveness (R_0/R_P) and polymer surface coverage. This correlation can be modeled using the Kubota-Mullin model whereby the distance between polymers depends on the polymer surface coverage according to the relation given in equation (5.3). Thus, using this model, polymer effectiveness can be accurately predicted if the polymer surface coverage is known.

5.5 Conclusions

In this study, the ability of a group of polymers with varying hydrophobicity to inhibit the crystal growth rate of felodipine in aqueous solution was assessed. The results indicated that moderately hydrophobic polymers were two to three times more effective than the very hydrophilic or very hydrophobic polymers. It was concluded that polymer hydrophobicity drives adsorption and also impacts adsorbed polymer conformation. In

addition, polymer fractional surface coverage was shown to correlate linearly to polymer effectiveness. This correlation can be modeled using the Kubota-Mullin model, and used to predict polymer effectiveness when surface coverage is known.

The results of this study provide a better mechanistic understanding of the process by which polymers can effectively inhibit crystal growth. Specifically, they demonstrate that surface coverage due to adsorbed conformation is a critical determinant of effectiveness. This knowledge can aid in polymer selection during formulation of drug products.

References

(1) Blagden, N.; de Matas, M.; Gavan, P. T.; York, P. Crystal Engineering of Active Pharmaceutical Ingredients to Improve Solubility and Dissolution Rates. *Adv. Drug Deliv. Rev.* **2007**, *59*, 617–630.

(2) Ziller, K. H.; Rupprecht, H. Control of Crystal Growth in Drug Suspensions: 1) Design of a Control Unit and 2) Application to Acetaminophen Suspensions. *Drug Dev. Ind. Pharm.* **1988**, *14*, 2341–2370.

(3) Raina, S. A.; Van Eerdenbrugh, B.; Alonzo, D. E.; Mo, H.; Zhang, G. G. Z.; Gao, Y.; Taylor, L. S. Trends in the Precipitation and Crystallization Behavior of Supersaturated Aqueous Solutions of Poorly Water-Soluble Drugs Assessed Using Synchrotron Radiation. *J. Pharm. Sci.* **2015**, *104*, 1981–1992.

(4) Moser, K.; Kriwet, K.; Kalia, Y. N.; Guy, R. H. Stabilization of Supersaturated Solutions of a Lipophilic Drug for Dermal Delivery. *Int. J. Pharm.* **2001**, *224*, 169–176.

(5) Babu, N. J.; Nangia, A. Solubility Advantage of Amorphous Drugs and Pharmaceutical Cocrystals. *Cryst. Growth Des.* **2011**, *11*, 2662–2679.

(6) Murdande, S. B.; Pikal, M. J.; Shanker, R. M.; Bogner, R. H. Solubility Advantage of Amorphous Pharmaceuticals. *J. Pharm. Sci.* **2010**, *99*, 1254–1264.

(7) Hancock, B. C.; Parks, M. What Is the True Solubility Advantage for Amorphous Pharmaceuticals? *Pharm. Res.* **2000**, *17*, 397–404.

(8) Yu, L. Amorphous Pharmaceutical Solids: Preparation, Characterization and Stabilization. *Adv. Drug Deliv. Rev.* **2001**, *48*, 27–42.

(9) Yalkowsky, S. H. Perspective on Improving Passive Human Intestinal Absorption. *J. Pharm. Sci.* **2012**, *101*, 3047–3050.

(10) Takano, R.; Takata, N.; Saito, R.; Furumoto, K.; Higo, S.; Hayashi, Y.; Machida, M.; Aso, Y.; Yamashita, S. Quantitative Analysis of the Effect of Supersaturation on in Vivo Drug Absorption. *Mol. Pharm.* **2010**, *7*, 1431–1440.

(11) Matteucci, M. E.; Miller, M. A.; Williams III, R. O.; Johnston, K. P. Highly Supersaturated Solutions of Amorphous Drugs Approaching Predictions from Configurational Thermodynamic Properties. *J. Phys. Chem. B* **2008**, *112*, 16675–16681.

(12) Kim, S.; Myerson, A. S. Metastable Solution Thermodynamic Properties and Crystal Growth Kinetics. *Ind. Eng. Chem. Res.* **1996**, *35*, 1078–1084.

(13) Kubota, N. Effect of Impurities on the Growth Kinetics of Crystals. *Cryst. Res. Technol.* **2001**, *36*, 749–769.

(14) Ilevbare, G. A.; Liu, H.; Edgar, K. J.; Taylor, L. S. Impact of Polymers on Crystal Growth Rate of Structurally Diverse Compounds from Aqueous Solution. *Mol. Pharm.* **2013**, *10*, 2381–2393.

(15) Ilevbare, G. A.; Liu, H.; Edgar, K. J.; Taylor, L. S. Understanding Polymer Properties Important for Crystal Growth Inhibition - Impact of Chemically Diverse Polymers on Solution Crystal Growth of Ritonavir. *Cryst. Growth Des.* **2012**, *12*, 3133–3143.

(16) Schram, C. J.; Beaudoin, S. P.; Taylor, L. S. Impact of Polymer Conformation on the Crystal Growth Inhibition of a Poorly Water-Soluble Drug in Aqueous Solution. *Langmuir* **2015**, *31*, 171–179.

(17) Alonzo, D. E.; Raina, S.; Zhou, D.; Gao, Y.; Zhang, G. G. Z.; Taylor, L. S. Characterizing the Impact of Hydroxypropylmethyl Cellulose on the Growth and Nucleation Kinetics of Felodipine from Supersaturated Solutions. *Cryst. Growth Des.* **2012**, *12*, 1538–1547.

(18) Schmitz, I.; Schreiner, M.; Friedbacher, G.; Grasserbauer, M. Phase Imaging as an Extension to Tapping Mode AFM for the Identification of Material Properties on Humidity-Sensitive Surfaces. *Appl. Surf. Sci.* **1997**, *115*, 190–198.

(19) Abramoff, M. D.; Magalhaes, P. J.; Ram, S. J. Image Processing with ImageJ. *Biophotonics Int.* **2004**, *11*, 36–42.

(20) Wu, S. Calculation of Interfacial Tension in Polymer Systems. *J. Polym. Sci. Part C Polym. Symp.* **1971**, *34*, 19–30.

(21) Gindl, M.; Sinn, G.; Gindl, W.; Reiterer, A.; Tschegg, S. A Comparison of Different Methods to Calculate the Surface Free Energy of Wood Using Contact Angle Measurements. *Colloids Surf., A* **2001**, *181*, 279–287.

(22) Macrae, C. F.; Edgington, P. R.; McCabe, P.; Pidcock, E.; Shields, G. P.; Taylor, R.; Towler, M.; van de Streek, J. Mercury: Visualization and Analysis of Crystal Structures. *J. Appl. Cryst.* **2006**, *39*, 453–457.

(23) Somasundaran, P.; Krishnakumar, S. Adsorption of Surfactants and Polymers at the Solid-Liquid Interface. *Colloids Surf., A* **1997**, *124*, 491–513.

(24) Holmberg, K.; Jonsson, B.; Kronberg, B.; Lindman, B. *Surfactants and Polymers In Aqueous Solutions, 2nd Ed.*; John Wiley & Sons, LTD: Chichester, 2003.

(25) Purohit, H. S.; Taylor, L. S. Phase Separation Kinetics in Amorphous Solid Dispersions Upon Exposure to Water. *Mol. Pharm.* **2015**, *12*, 1623–1635.

(26) Amiel, C.; Sikka, M.; Schneider, J. W.; Tsao, Y.; Tirrell, M.; Mays, J. W. Adsorption of Hydrophilic-Hydrophobic Block Copolymers on Silica from Aqueous Solutions. *Macromolecules* **1995**, *28*, 3125–3134.

(27) Zhang, Q.; Zhang, T.; Ge, J.; Yin, Y. Permeable Silica Shell through Surface-Protected Etching. *Nano Lett.* **2008**, *8*, 2867–2871.

(28) Pattanaik, M.; Bhaumik, S. K. Adsorption Behaviour of Polyvinyl Pyrrolidone on Oxide Surfaces. *Mater. Lett.* **2000**, *44*, 352–360.

(29) Karavas, E.; Ktistis, G.; Xenakis, A.; Georgarakis, E. Effect of Hydrogen Bonding Interactions on the Release Mechanism of Felodipine from Nanodispersions with Polyvinylpyrrolidone. *Eur. J. Pharm. Biopharm.* **2006**, *63*, 103–114.

(30) Hosono, T.; Tsuchiya, S.; Matsumaru, H. Model of Interaction of Ajmaline with Polyvinylpyrrolidone. *J. Pharm. Sci.* **1980**, *69*, 824–826.

(31) Esumi, K.; Ishizuki, K.; Otsuka, H.; Ono, M.; Ichikawa, S.; Yanase, C. The Effect of Binary Solvents on Adsorption of Poly(vinylpyrrolidone) on Titanium Dioxide and Graphite Particles. *J. Colloid Interface Sci.* **1996**, *178*, 549–554.

(32) Freij-Larsson, C.; Nylander, T.; Jannasch, P.; Wesslén, B. Adsorption Behaviour of Amphiphilic Polymers at Hydrophobic Surfaces: Effects on Protein Adsorption. *Biomaterials* **1996**, *17*, 2199–2207.

CHAPTER 6. POLYMER INHIBITION OF CRYSTAL GROWTH BY SURFACE POISONING

This chapter is a preprint with minor modifications of a manuscript submitted to *Crystal Growth & Design* with the same title by: Caitlin J. Schram, Stephen P. Beaudoin, and Lynne S. Taylor.

6.1 Abstract

Controlling the rate of crystal growth from supersaturated solutions is a desirable capability in the pharmaceutical field. The biological absorption of poorly-soluble drugs can be enhanced by inhibiting crystal growth and prolonging the duration of supersaturated solutions formed *in vivo* by dissolving supersaturating dosage forms. The use of polymeric additives to slow crystal growth is an emerging area of interest, yet the mechanisms of polymer inhibition are still being explored. In this study, the ability of a polymer to poison crystal growth and impact crystal morphology is assessed for felodipine crystallized from the amorphous material under different conditions. It was found that when polymers are present during crystal evolution from an amorphous solid exposed to water, they can impact the size and shape of the resulting crystals. This in turn influences the subsequent rate of crystal growth from supersaturated solutions. Therefore, when testing the ability of polymers to impact crystal growth, and the impact of crystal seeds on the rate of desupersaturation, the crystallization conditions and treatment of the

seed crystals should be carefully considered in order to better evaluate the desupersaturation risk for supersaturating dosage forms.

6.2 Introduction

Control of crystallization from supersaturated solutions is essential in many industries. In the pharmaceutical field, crystallization control is important for manufacturing purposes, and as a means of enhancing drug delivery. The bioavailability of BCS Class II drug compounds is limited by their ability to dissolve to sufficiently high concentrations in the gastrointestinal tract,[1] therefore these compounds are often formulated as amorphous solids in order to improve solubility.[2,3] The higher free energy of the amorphous form compared to the crystalline form allows for increased dissolution rates and the generation of supersaturated solutions *in vivo*.[4–6] Thus, this strategy has been found to increase drug absorption because supersaturated solutions can achieve superior membrane transport.[7–9] However, rapid crystallization of these supersaturated solutions *in vivo* threatens the efficacy of this formulation strategy.[10] Thus, the ability to inhibit crystal nucleation or growth to prolong supersaturation is desirable.

The ability of additives to modify crystal growth has been recognized for several decades.[11,12] Additives can adsorb at active sites of growing crystals and impact growth either by altering the crystal's interfacial energy,[13] or by pinning growth steps, thus reducing the rate of step advancement.[14] Polymers in particular have been successful at poisoning crystals, thereby reducing growth rates and stabilizing supersaturated solutions when added to the growth medium.[15–17] Previous works have shown that their success

depends on their ability to adsorb to the crystal surface and achieve a high degree of surface coverage.[18,19]

Additives such as polymers can also modify crystal morphology at the macroscopic scale.[20–22] Adsorption of polymers and their subsequent effect on the advancement of steps of monomolecular height can impact the evolution of macrosteps, or terraces.[21] Polymers have been shown to impede growth of specific crystal faces so that growth continues only in the direction of certain crystallographic planes, thus resulting in habit modification.[20]

For amorphous formulations, crystal seeds may form during manufacturing or storage, or during the dissolution process. Therefore, there is interest in understanding how low levels of crystallinity can impact desupersaturation rates, and how polymers can retard this process. However, there is little understanding of how crystal seeds with different origins may impact the desupersaturation rate. It is likely that crystal seeds formed by crystallization of an amorphous drug will be different from material produced through conventional solvent crystallization, and that the presence of a polymer during the crystallization process (a polymer will be present in the majority of amorphous formulations) will further impact the seed characteristics.

The goal of this work was to study polymer poisoning of crystal surfaces formed under different crystallization conditions and relate the changes in crystal morphology to variances in solution crystal growth rates. Polycrystalline surfaces of the active pharmaceutical ingredient (API) felodipine were grown from the amorphous melt in the absence and presence of the polymer HPMCAS. The crystalline surfaces were then exposed to supersaturated solutions of felodipine in the absence and presence of

HPMCAS and crystal growth rates were measured under carefully controlled hydrodynamic conditions. The surfaces were also characterized with atomic force microscopy (AFM). It was hypothesized that AFM characterization would reveal differences in crystal morphologies at the macroscopic scale as well as crystal growth mechanisms at the microscopic scale due to differences in how the polymer interacts with the drug at the molecular level. These variances were expected to impact crystal growth rates from supersaturated solutions.

6.3 Experimental Section

6.3.1 Materials

The model poorly water-soluble API used in this study, felodipine, was purchased from Attix Pharmaceuticals (Toronto, Ontario, Canada). Methanol (HPLC grade), used to dissolve felodipine and create supersaturated solutions, was purchased from Avantor Performance Materials (Center Valley, PA). The polymer used in this study, hydroxypropylmethyl cellulose acetate succinate (HPMCAS) LF grade, M_w 18 000 g mol^{-1}, was supplied by Shin-Etsu Chemical Co, Ltd. (Tokyo, Japan) in a powder form. 50 mM pH 6.8 phosphate buffer with or without pre-dissolved HPMCAS was used as the medium for seed crystal growth from the amorphous melt, as well as for supersaturated solution crystal growth experiments. 50 mM pH 3 phosphate buffer was used as the medium for seed crystal growth from the amorphous solid dispersions. The molecular structures of felodipine and HPMCAS are given in Figure 2.5.

6.3.2 Seed Crystal Preparation

Amorphous felodipine was prepared by melting the crystalline material from the supplier and pouring the melt onto AFM pucks (Ted Pella, Inc. Redding, CA), which sat inside custom-made cylindrical Teflon holders. The custom holders were necessary for crystal growth experiments using a rotating disk apparatus, explained further in Section 6.3.3. Amorphous solid dispersions were made by grinding a 10% w/w mixture of HPMCAS powder and felodipine crystals using a mortar and pestle. The ground mixture was then melted and poured in the custom holders in the same manner as for the pure drug. Before the melts of pure drug or polymer/drug mixtures cooled, the surfaces were flattened using a glass coverslip, then allowed to cool before removal of the coverslip.

Polycrystalline surfaces were prepared from amorphous felodipine using four different methods. The methods, outlined below are also illustrated in Figure 6.1.

i) Amorphous felodipine was exposed to aqueous phosphate buffer (pH 6.8) for up to 24 hours, allowing the surface to fully crystallize.

ii) Amorphous felodipine was exposed to aqueous phosphate buffer (pH 6.8) for up to 24 hours, allowing the surface to fully crystallize. The crystalline surface was then exposed to buffer containing 5 μg/mL dissolved HPMCAS for three hours to allow maximum adsorption of the polymer onto the crystal surface, prior to commencing crystal growth rate experiments.

iii) Amorphous felodipine was exposed to aqueous phosphate buffer (pH 6.8) containing 5 μg/mL dissolved HPMCAS for up to 24 hours, allowing the surface to fully crystallize.

iv) An amorphous solid dispersion of felodipine and HPMCAS was exposed to aqueous phosphate buffer (pH 3) for up to a week, allowing the surface to fully crystallize.

These various preparation methods were chosen to explore the role of polymer in impacting the growth surface produced upon crystallization of the amorphous material. Method (*i)* serves as the control, method (*ii)* allows for evaluation of the impact of pre-poisoning on the subsequent growth rate, while methods (*iii)* and (*iv)* enable assessment of the impact of having a polymer present when crystallization first occurs from the amorphous solid. Method (*iv)* represents the most likely scenario for an amorphous formulation, while methods (*i)* and (*ii)* more closely represents the type of approaches previously used to evaluate the impact of polymers on crystal growth.

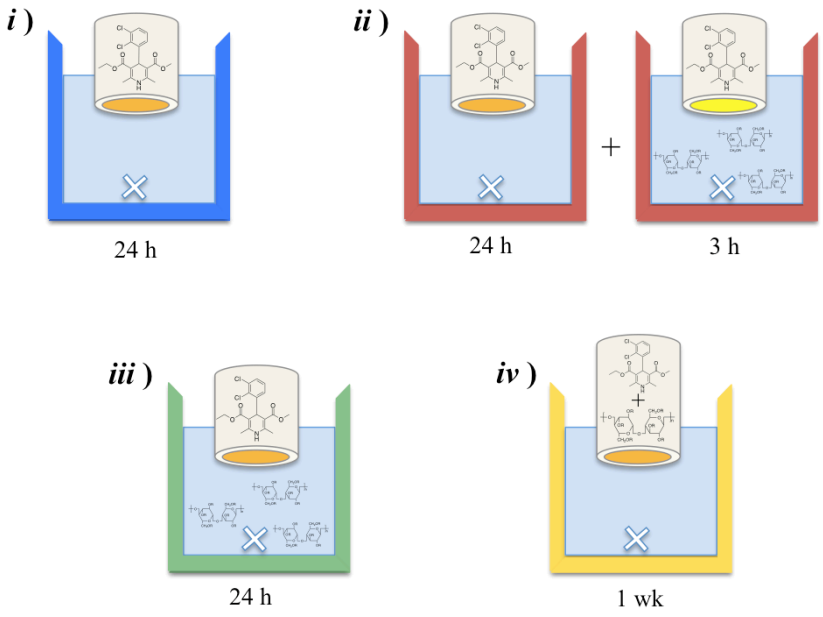

Figure 6.1. Illustrations depicting the different preparation methods of crystalline felodipine surfaces used in growth rate studies. The methods are described in Section 6.3.2. Beakers are color-coded to match the results presented in Section 6.4. Orange felodipine surfaces indicate that the surface was amorphous and the yellow surface indicates that the surface was crystalline.

6.3.3 Crystal Growth Rate Measurements

Solution crystal growth rates of felodipine were measured in the absence and presence of dissolved HPMCAS. To generate supersaturated solutions, a small amount of a stock solution of 10 mg/mL solubilized felodipine in methanol was added to pH 6.8 buffer alone, or buffer containing 5 µg/mL pre-dissolved HPMCAS or 100 µg/mL pre-dissolved SDS. The equilibrium concentration, C_{eq}, of felodipine is approximately 0.5 µg/mL at 25°C,[15] and the generated bulk concentration, C, for growth experiments was 2 µg/mL. Thus the experiments were performed at S = 4.

Immediately after generation of supersaturated solutions, the polycrystalline surfaces prepared using the methods explained in Section 6.3.2 were exposed to the supersaturated solution. The concentration of felodipine as a function of time was measured to determine a desupersaturation profile, which is proportional to the growth rate. The custom-made Teflon holders containing the polycrystalline surfaces were mounted to a rotating disk apparatus (RDA) (Princeton Applied Research, Oakridge, TN. Model #616). The RDA was set to a constant rotational speed, 3000 rpm, at which there was no effect of the rate of solute mass transfer to the solid-liquid interface.[23] Thus, the growth rates measured were determined purely by the rate of solute integration; the step impacted by polymer adsorption.

Desupersaturation profiles were measured using a CCD Array UV-vis Spectrometer (SI Photonics, Tuscon, AZ). The intensity of an absorbance peak of felodipine (wavelength 238 nm) was recorded at 10-second intervals for 1 hour. All experiments were performed in triplicate. Calibration solutions, prepared in methanol, were used to correlate peak intensity to concentration. The slope of the resulting

concentration v. time curve was recorded as the growth rate, R_0 or R_P, where R_0 is the growth rate of felodipine crystals prepared with method *(i)* in supersaturated solutions containing no HPMCAS (*i.e.* the only growth experiment in which HPMCAS was not present in solution or on the seed crystals). R_P represents the growth rate for all other experiments where HPMCAS is present on the seed crystals or dissolved in solution, or both. R_P also represents the growth rate for experiments where SDS was dissolved in solution. The values of R_P obtained were then compared to R_0 by taking the ratio of the two.

$$E_g = \frac{R_0}{R_P} \tag{6.1}$$

This gives the polymer effectiveness, E_g, in order to compare how effectively HPMCAS poisons felodipine crystal growth for each of the conditions studied. The larger the value of E_g, the more effectively HPMCAS has poisoned the surface and retarded crystal growth and hence the rate of desupersaturation.

6.3.4 Surface Characterization with Atomic Force Microscopy

Atomic force microscopy (Figure 2.3) (Multimode 8 AFM, Bruker Corporation, Technology Forest, TX) was used to characterize the crystalline surfaces following the growth experiments. Samples, which were already mounted on AFM pucks in the holder, were removed from the holder and immediately characterized in the same liquid used for growth experiments to ensure there was no surface dissolution. Characterization was performed using Tapping Mode. SNL-10 (0.24 N/m spring constant, 10 nm radius of

curvature) or NPG-10 (0.24 N/m spring constant, 30 nm radius of curvature) silicon nitride triangular probes (Bruker Corporation, Technology Forest, TX). Scan resolution was set to 512 x 512 pixels^2 with scan rates of 0.4 – 0.5 Hz.

Height images, amplitude images, and phase images were obtained simultaneously for each system. Height and amplitude both provide information on topographical changes of the surface. The amplitude is the raw feedback of tip deflection due to these changes; whereas height scans are the output of the tip deflection calibrated to a z-scale in order to generate 3D topographical images. Phase contrast imaging is sensitive to changes in material properties on the surface, thus it can be used to detect adsorbed polymers.

Images were analyzed using NanoScope Analysis (v1.5, Bruker Corporation, Technology Forest, TX). Surface areas were determined using the software's Roughness Analysis tool after images were normalized to a midline. Surface height features were measured using the software's Cross Section tool.

6.3.5 Contact Angle Measurements

The contact angles of DI water and ethylene glycol on a crystalline felodipine surface grown from amorphous material in aqueous buffer were measured in order to determine the surface energy of crystalline felodipine. A Ramé-Hart model 500 goniometer (Ramé-Hart Instrument co., Succasunna, NJ) and DROPimage advanced software were used. Ten contact angle measurements were taken for ten drops of each of the two liquids. From these results, an average contact angle for each of the two liquids

on felodipine was determined. The surface energy was then estimated using the harmonic mean approach proposed by Wu.[24]

6.3.6 Determination of Felodipine Growth Unit Size

The size of a felodipine growth unit was determined using the crystal structure visualization software, Mercury.[25] The measure distances tool was used to measure the length and width of a felodipine molecule (form DONTIJ from the Cambridge Crystallographic Data Centre (CCDC) structural database). Using these measurements, the area occupied by a growth unit on a crystal surface was calculated.

6.4 Results and Discussion

6.4.1 Growth Rate Results

Polycrystalline felodipine surfaces were exposed to supersaturated solutions of felodipine in the absence and presence of HPMCAS, and the crystal growth rate of felodipine was subsequently measured. The polycrystalline felodipine surfaces were prepared using four different methods (outlined in Section 6.3.2 and shown pictorially in Figure 6.1) in order to compare the impact of crystal preparation conditions on subsequent solution crystal growth rates, specifically the impact of having polymer present when the crystals first form from the amorphous material. Figure 6.2 shows the results of the growth rate studies, which are presented as the effectiveness ratio, R_0/R_P, defined in Section 6.3.3. Each of the four preparation methods is represented by a different color in Figure 6.2. The columns overlaid with a grid pattern represent growth

rates measured in the presence of HPMCAS in solution, whereas the columns with no pattern have only felodipine in solution.

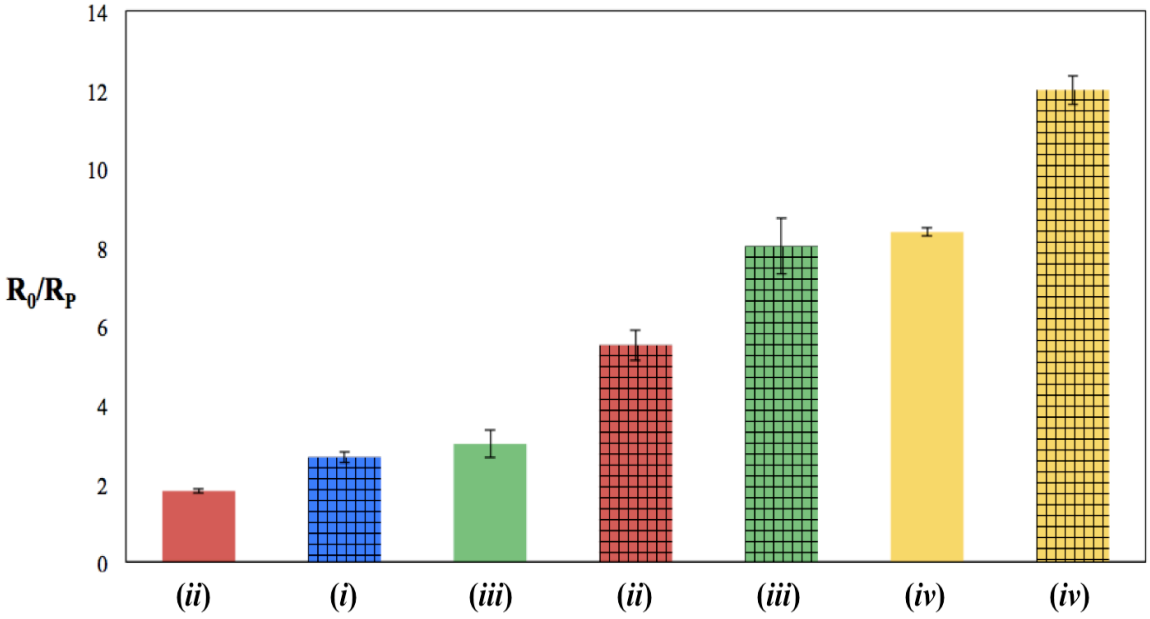

Figure 6.2. Crystal growth rates of felodipine (S=4) presented as a ratio of the pure felodipine growth rate over the growth rate of crystals poisoned by HPMCAS (the effectiveness ratio). Gridded columns have 5 µg/mL HPMCAS present in solution during the growth rate measurements whereby samples were prepared using methods (*i-iv)*. Non-gridded columns represent the same samples, which were crystallized using methods (*i-iv*), but where subsequent growth rate measurements were performed in a solution free of polymer. Experiments were performed in triplicate and each column represents the mean. Error bars indicate the standard deviation.

The results in Figure 6.2 are presented in order of increasing effectiveness, E_g, which ranges from about 2 to 12. It is clear that crystal preparation method greatly impacted effectiveness. Additionally, whether or not HPMCAS was present in solution during growth also greatly impacted the resultant effectiveness factor. To understand mechanistically how crystal preparation environment produces these differences in polymer growth inhibition effectiveness, the systems were analyzed with atomic force

microscopy. The growth rate results will be presented again in subgroups in order to focus on each preparation method separately.

6.4.2 HPMCAS Pre-adsorbed on Seed Crystals

Seed crystals were grown from amorphous felodipine immersed in liquid buffer, and then exposed to a solution containing dissolved HPMCAS for several hours (method *ii*). Thus, HPMCAS should have attained maximum surface coverage through adsorption to the crystal surface, before exposure to felodipine supersaturated solutions, which will drive new growth. Figure 6.3 compares the growth rate results for samples prepared with this method with the result for seed crystals grown in liquid with no HPMCAS pre-adsorbed (method *i*).

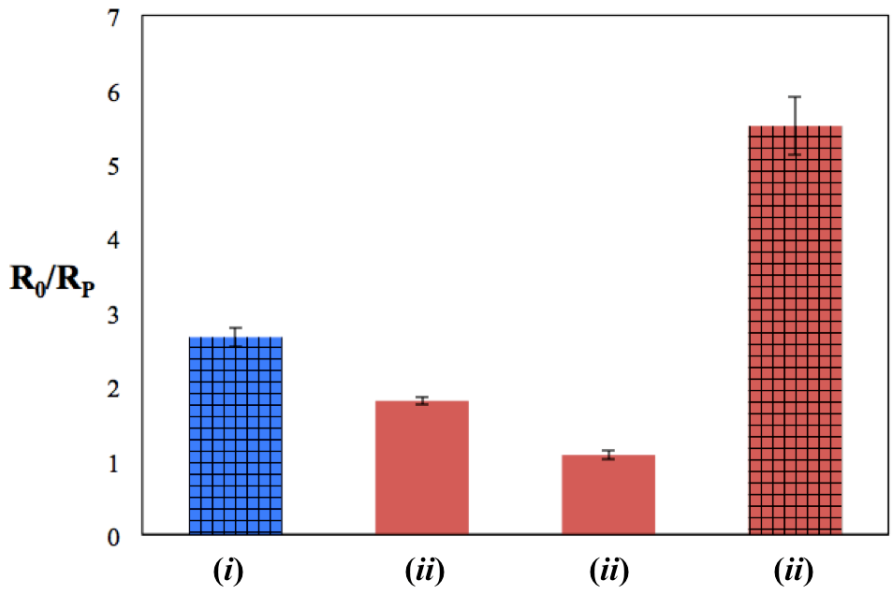

Figure 6.3. Effectiveness growth rate ratios for felodipine poisoned by HPMCAS. Effectiveness ratios of surfaces prepared using method (*ii*) are compared to method (*i*). Gridded columns have 5 µg/mL HPMCAS present in solution during growth rate determination experiments. Experiments were performed in triplicate and each column represents the mean. Error bars indicate the standard deviation.

The results indicate that when HPMCAS was pre-adsorbed on the crystalline felodipine surface and the growth rate was determined with HPMCAS in solution (red, gridded column), growth was considerably slower relative to the sample where HPMCAS was not pre-adsorbed and growth was measured with HPMCAS in solution (blue, gridded column). This result is anticipated since HPMCAS can attain greater surface coverage, and therefore more effectively pin growth steps when it has had time to reach a maximum surface coverage through the initial equilibration of the crystal surface with a solution containing polymer. However, when HPMCAS is not pre-adsorbed, it must compete with felodipine growth units for adsorption to active sites (blue, gridded column), and the polymer cannot block as many growth sites and therefore will not be as effective.

The impact of first poisoning the surface by pre-adsorption of polymer, followed by growth experiments in a fresh solution containing no polymer was also examined. It is generally accepted that polymers adsorb irreversibly,[26] therefore, the pre-adsorbed HPMCAS should remain adsorbed to the surface when exposed to fresh buffer, and would be expected to have some impact on growth rate. Interestingly, when HPMCAS was pre-adsorbed and growth was measured with no HPMCAS in solution (red column on the left), the effectiveness was reduced compared to the sample prepared the same way, but with HPMCAS in solution during growth (red, gridded column). The growth rate was also more effectively reduced for a fresh crystal surface exposed to a supersaturated solution containing HPMCAS (blue, gridded column). This result indicates that the presence of HPMCAS in solution during the growth rate measurement is a key determinant of effectiveness, regardless of the pre-equilibration step.

AFM characterization of the crystalline surfaces after growth (Figure 6.4) provided insight into these results. Figure 6.4a is an image of a felodipine surface crystallized from the amorphous material from a solution free of polymer. The height features show monomolecular steps, which extend across the crystal face, providing evidence of step growth.

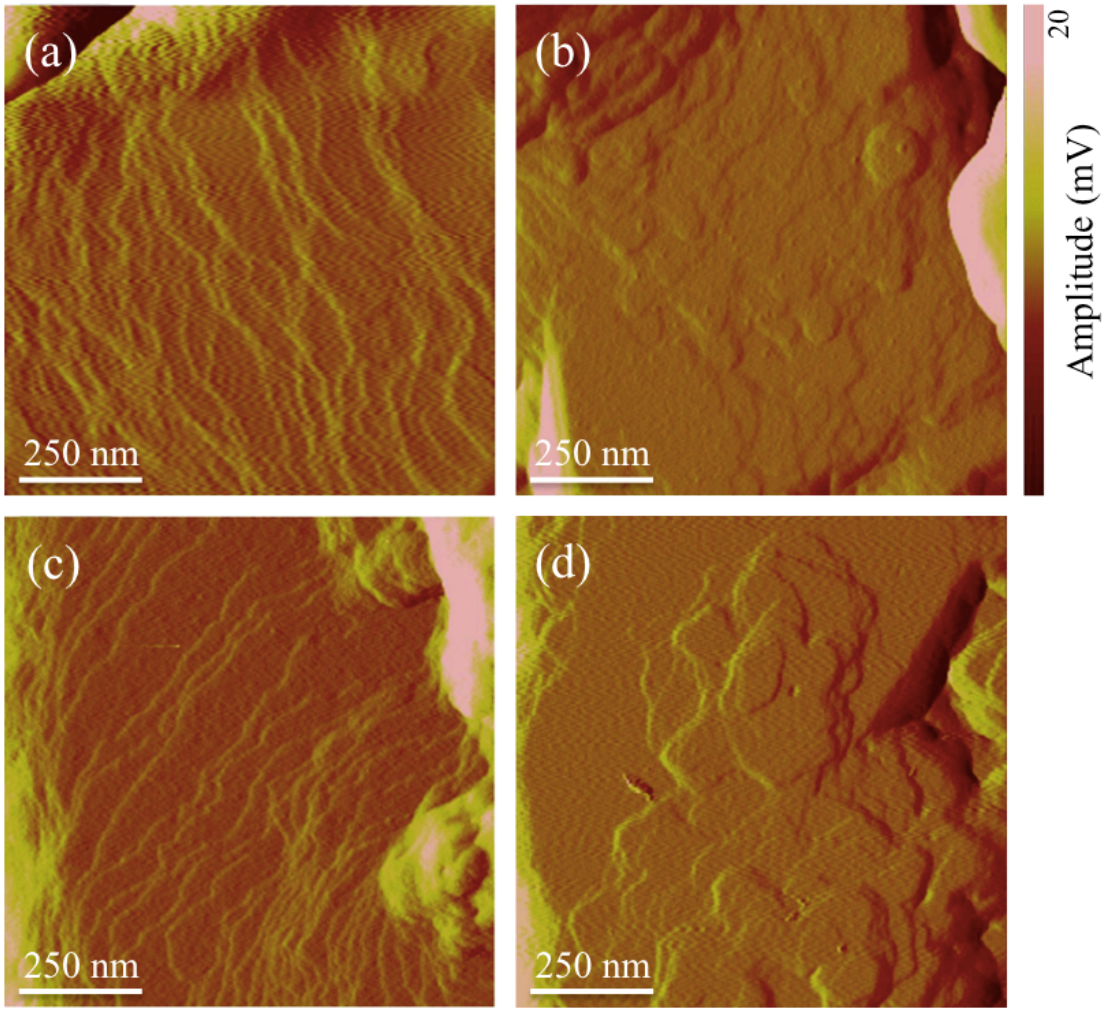

Figure 6.4. 1 µm x 1 µm AFM amplitude images characterizing a single felodipine crystal face after one hour of growth from the supersaturated solution at initial S=4. (a) and (b) were prepared using method (*i*) and (c) and (d) were prepared using method (*ii*). Only (b) and (d) had HPMCAS (5µg/mL) present in the supersaturated solution during crystal growth. Images were captured in liquid at room temperature with an incubation time of about 3 h.

Figure 6.4b shows the result of AFM characterization after the growth experiment in which HPMCAS was present in solution during growth rate measurements (there was no HPMCAS pre-adsorbed on the surface; this sample corresponds to the blue gridded column in Figure 6.3). The steps along the crystal face in Figure 6.4b look very different from those in Figure 6.4a. Instead of relatively even and linear steps across the face, the layers appear to be pinned at several points along each step, providing evidence of the pinning mechanism discussed in Section 1.5 and depicted in Figure 1.4. The result suggests that HPMCAS adsorbed at active growth sites along the steps and effectively pinned them, thereby slowing step advancement and increasing the step curvature. This explains the measured reduction in growth rate when HPMCAS was present in solution during the growth rate experiments.

Figure 6.4c shows the result of AFM surface characterization after growth of the felodipine crystal surface in a supersaturated solution which did not contain any polymer, whereby the initial crystal surface had pre-adsorbed HPMCAS (corresponding to the first red column in Figure 6.3). The surface appears very similar to that of felodipine crystallized completely in the absence of polymer (Figure 6.4a), and provides insight into why the effectiveness of this system is so low (Figure 6.3). Although HPMCAS was pre-adsorbed onto the crystalline surface, felodipine growth was able to continue as if there was no polymer present on the surface. This suggests that when there is no polymer in the supersaturated solution competing for growth sites, a felodipine layer can grow over the adsorbed polymer molecules that are present on the crystal surface due to the pre-adsorption step.

A second growth experiment, which was conducted immediately after the first growth experiment in a freshly supersaturated felodipine solution, confirmed that this is the case. The result, displayed in Figure 6.3 (second red column from the left) reveals an effectiveness ratio close to 1, that is, the pre-adsorbed polymer had no effect on the growth rate. It can therefore be concluded that during the first growth experiment, felodipine growth unit attachment was slowed slightly by the presence of the pre-adsorbed polymer molecules, but nevertheless a pure drug layer was able to grow on top of the initially poisoned surface, creating a fresh surface for growth. Thus, in the second growth experiment, there was no inhibition of growth at all because the surface was essentially free of polymer. A similar result was observed in a study by Gratz and Hilner,[22] in which re-growth was observed on poisoned crystals when introduced to a fresh supersaturated solution. This result points to the importance of having dissolved polymer present in solution during growth for effective inhibition.

Of all the growth rate results shown in Figure 6.3, the case where HPMCAS was present in the supersaturated solution during growth combined with pre-adsorption onto the surface (red, gridded column) achieved the greatest growth inhibition. Figure 6.4d reveals the AFM characterization of this sample after growth. The surface appears different from both of the previously discussed poisoned surfaces. Growth layers do not appear as steps traversing across the entire width of the face. Instead, they seem to originate from a point and grow outward in all directions, similar to the birth and spread mechanism (Figure 1.3b).[11] Thus, when polymers are covering the surface prior to drug growth, and competing with drug growth units in solution for active sites, it appears that step pinning is so effective, it forces the entire step to curve rather than only forcing

localized curves along a linear step. This provides clear evidence that surface poisoning by polymers can change how the crystals evolve.

6.4.3 Seed Crystals Grown in HPMCAS Solution

The next logical step of investigation was to evaluate how polymers might disrupt the crystal surface during the initial crystallization from the amorphous material. Thus seed crystals were grown from amorphous felodipine in a solution containing dissolved polymers (method *iii*). The subsequent solution growth rate results for these crystals in the absence and presence of dissolved HPMCAS are presented in Figure 6.5. The growth rates of these surfaces are again compared to the growth rate of a surface crystallized initially in buffer and then further grown in the presence of HPMCAS (method *i*).

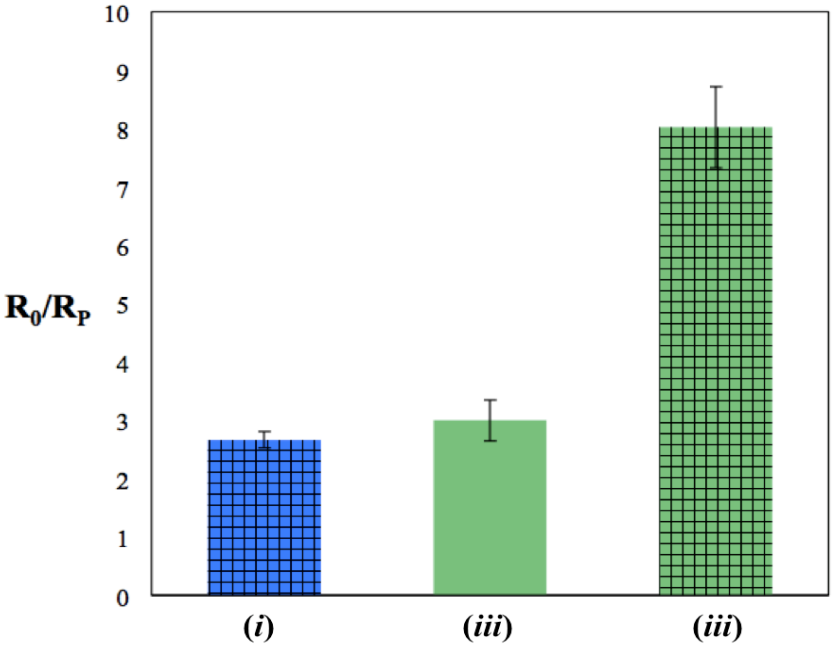

Figure 6.5. Effectiveness growth rate ratios for felodipine poisoned by HPMCAS. Effectiveness ratios of surfaces prepared using method (*iii*, green columns) are compared to method (*i*, blue column). Gridded columns had 5 μg/mL HPMCAS present in solution during the growth rate measurements. Experiments were performed in triplicate and each column represents the mean. Error bars indicate the standard deviation.

The results in Figure 6.5 indicate that when seed crystals were initially formed in the presence of HPMCAS (gridded green column), the growth rate was considerably slower (higher effectiveness) than for seed crystals grown in pure buffer (gridded blue column), when HPMCAS was not present in solution during the growth rate determination. Just growing the crystals from the amorphous material in the presence of HPMCAS appeared to impact their ability to subsequently grow when exposed to a fresh supersaturated solution without polymer (green column).

To understand the impact of HPMCAS on seed crystal growth from amorphous felodipine, the crystal surfaces were characterized with AFM. The resulting 3D topographical maps are shown in Figure 6.6, and they indicate that the presence of HPMCAS in the solution greatly impacts the size and shape of the resulting seed crystals that form from the amorphous drug. When grown in pure buffer solution (Figure 6.6a), the felodipine crystals had much larger macroscopic features than when they were grown in a solution containing HPMCAS (Figure 6.6b). This suggests that the HPMCAS in solution interfered with the growth mechanism, and impacted how the crystals evolved.

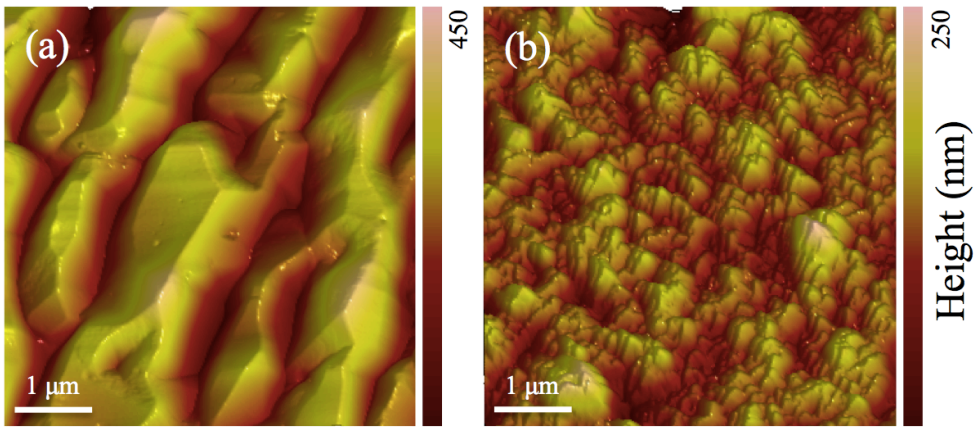

Figure 6.6. 5 µm x 5 µm AFM 3D topographical maps of polycrystalline felodipine surfaces prepared using (a) method (*i*) and (b) method (*iii*). Images were captured in liquid at room temperature with an incubation time of 2-3 h.

The morphology in Figure 6.6b could be the macroscopic effect of the growth pattern shown in Figure 6.4d. Since the crystals grew from amorphous felodipine in the presence of HPMCAS, which may have adsorbed to the surface prior to crystallization, it is likely that the polymer had an even more disruptive effect on crystal morphology, preventing the development of continuous, linear layer growth characteristic of the system crystallized in the absence of polymer, instead causing the growth of curved steps. Thus it is likely that the effect seen in Figure 6.4d is magnified in Figure 6.6b, whereby the crystallites were forced to grow vertically, similar to island growth, instead of horizontally as layers, as for the polymer-free crystalline surface. Consequently, the surface is composed of rough, spike-like features, rather than the large flat features seen in Figure 6.6a.

The surface areas of both images were determined using roughness analysis (explained in Section 6.3.4), and the values are displayed in Table 6.1. It can be seen that despite the differences in morphology, the surfaces have very similar areas, therefore a surface area difference cannot explain the differences in the measured growth rates (Figure 6.5), as one might expect given their relationship (equation 1.5). Instead, the growth rate differences must arise based on the relative availability of active growth sites for the different morphologies. The larger seed crystallites (Figure 6.6a), which grew at a faster rate from the supersaturated solution, have large faces, each of which contain many steps that extend across the face. The smaller crystallites (Figure 6.6b) cannot have such long, uninterrupted steps, resulting in fewer accessible high-energy sites and slower growth.

Table 6.1. Surface area values

Figure	A (μm^2)
6.6a	33.4
6.6b	31.2

6.4.4 Seed Crystals Grown from Amorphous Solid Dispersions

For amorphous solid dispersion (ASD) formulations, crystals will most likely evolve from the ASD during production, storage or the hydration step of the dissolution process, and it is of interest to determine the extent to which crystals evolved from this environment can lead to desupersaturation. Thus, seed crystals were grown from amorphous solid dispersions containing felodipine and HPMCAS (method *iv*). When the crystallized ASD was exposed to supersaturated solutions of felodipine, the resulting growth rate inhibition (yellow columns) was even greater than for the previously discussed case of seed crystals grown from a pure felodipine melt in the presence of HPMCAS (green columns). This is displayed in Figure 6.7. For the case where HPMCAS was present in solution during growth (yellow, gridded column), the effectiveness ratio is 12, indicating a very significant reduction in growth rate due to highly effective surface poisoning by the polymer.

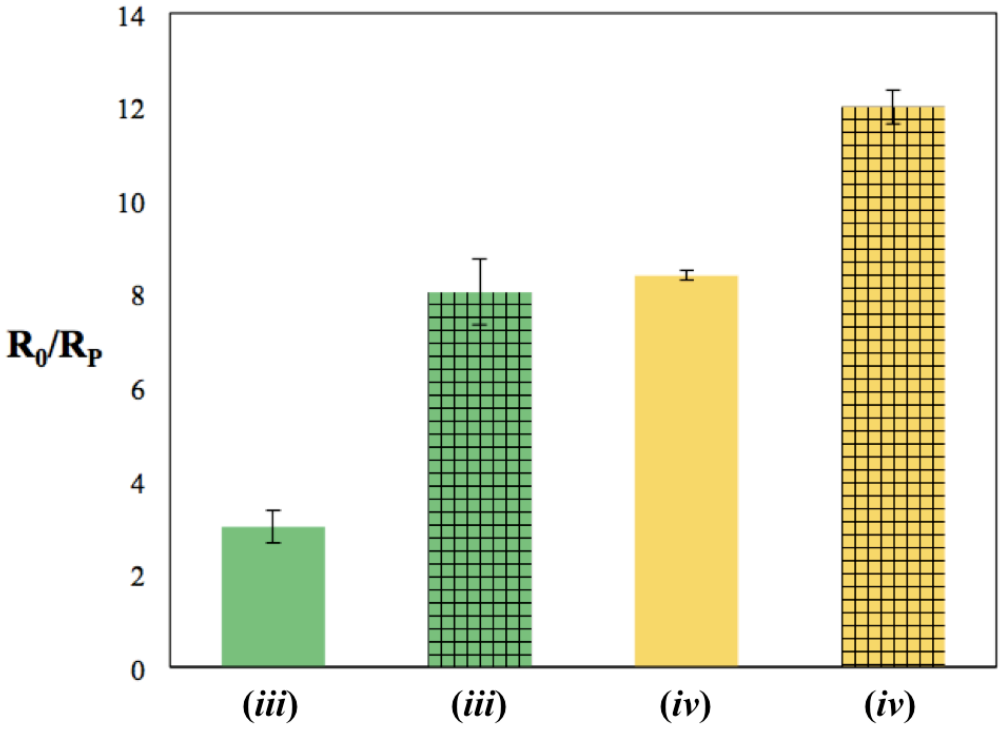

Figure 6.7. Effectiveness growth rate ratios for felodipine poisoned by HPMCAS. Effectiveness ratios of surfaces prepared using method (*iv*) are compared to method (*iii*). Gridded columns have 5 μg/mL HPMCAS present in solution during growth. Experiments were performed in triplicate and each column represents the mean. Error bars indicate the standard deviation.

Such effective surface poisoning is likely due to the fact that an ASD is an intimate mixture of API and polymer. In previous studies that have assessed the ability of polymers to stabilize ASDs, it was found that the more effective stabilizers could form strong specific interactions with the API.[27,28] These interactions between polymer and drug can disrupt crystal evolution more effectively than any of the methods previously discussed where the polymer is only present in the solution phase, and not mixed with the amorphous drug. Based on the results presented in Section 6.4.3, it was hypothesized that the surface features of seed crystals grown from an ASD would be even smaller than the features of seed crystals grown in polymer solution (method *iii*).

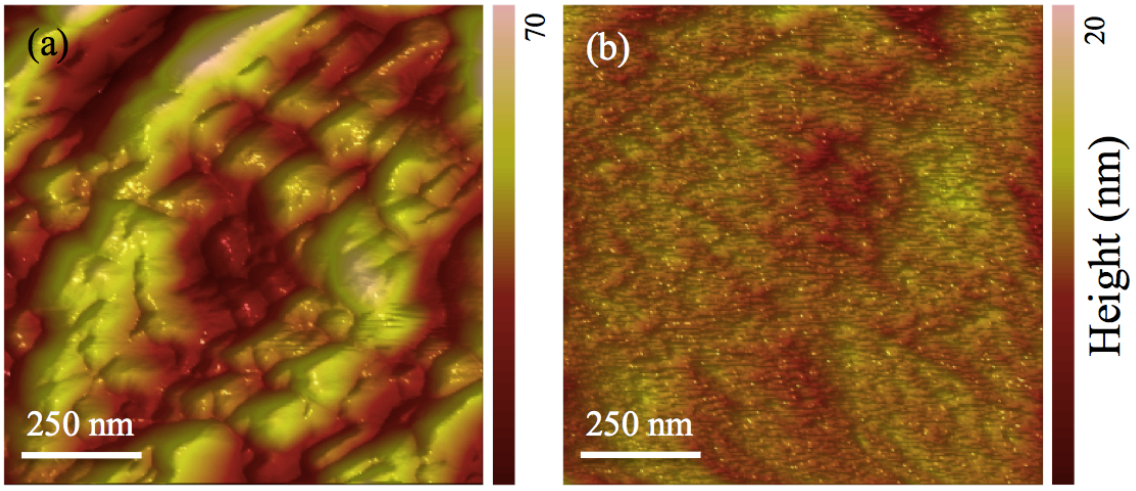

Figure 6.8. 1 μm x 1 μm AFM 3D height images of polycrystalline felodipine surfaces prepared using (a) method (*iii*) and (b) method (*iv*). Images were captured in liquid at room temperature with an incubation time of 2-3 h.

AFM height characterization (Figure 6.8) confirmed this hypothesis. Seed crystals grown from the ASD (Figure 6.8b) had much smaller features than seed crystals grown from a felodipine melt in HPMCAS solution (Figure 6.8a). (Note that the scan area of Figure 6.8 is smaller than that of Figure 6.6). The very small features in Figure 6.8b appear to be a result of the pinning mechanism. Cross-sectional analysis was performed to determine if the features were monomolecular in height. Two examples of the results obtained from the analysis are shown in Figure 6.9. Table 6.2 displays the average value of the step height, h, determined from the analysis along with the average value of h for the pinned steps of the system shown in Figure 6.4b for comparison. The analysis indicates that the average height features of these systems are similar and are both comparable to the molecular length of felodipine, which is about 0.8 nm. Thus, it was concluded that the small, rounded surface features in Figure 6.8b are the result of step pinning.

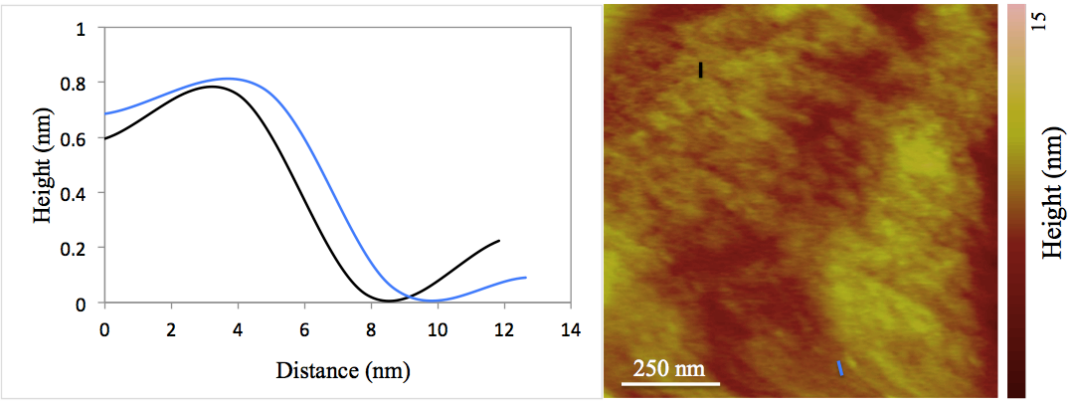

Figure 6.9. AFM cross-sectional height analysis of steps on a crystalline surface grown from an ASD of felodipine and HPMCAS.

Table 6.2. Values of *h* and *l* determined from AFM cross-sectional analysis.

Figure	*h* (nm)	*l* (nm)
6.8b	0.77 ± 0.2	15.8 ± 7.4
6.4b	0.81 ± 0.2	68.5 ± 9.4

According to the Kubota-Mullin model, which describes growth inhibition by adsorbed impurities such as polymers, a smaller radius of curvature, ρ, of a pinned step results in better growth inhibition, and $\rho = l/2$, where *l* is the average distance between adsorbed polymers. If $l \leq \rho_c$ (the critical nucleus radius) then step advancement will stop (equation 1.12).[14] Thus, values of *l* were determined by measuring the step radii using cross-sectional analysis. The results for both the crystals grown from the ASD, and for the pinned steps shown in Figure 6.4b are presented in Table 6.2.

The average distance between adsorbed polymers for the surface grown from the ASD was more than four times smaller than that of the pinned steps in Figure 6.4b (the result of growth in the presence of HPMCAS on a crystalline face grown from pure

amorphous felodipine exposed to just buffer). The critical nucleus radius, ρ_c, was calculated using equation (1.6) in order to compare its value to these measured values of *l*. The quantities used in equation (1.6) are listed in Table 6.3, and explanations for how values of γ and *a* were obtained are given in Sections 6.3.5 and 6.3.6.

Table 6.3. Values used to calculate ρ_c (equation 1.6)

Parameter	Value
γ	3.9×10^{-20} J/nm
a	0.584 nm^2
k	1.38×10^{-23} J/K
T	298.15 K
lnS	1.39

The critical nucleus radius for felodipine at the current experimental conditions was determined to be ρ_c = 3.98 nm. Comparing this to the measured values of *l* (displayed in Table 6.2), ρ_c is smaller than both values, explaining why felodipine growth was not stopped completely in either case. However, the value of *l* for the ASD is much closer to ρ_c, providing quantitative validation for why the effectiveness ratio of the ASD was about three times greater in the absence of HPMCAS (yellow column compared to blue gridded column in Figure 6.2), and nearly five times greater in the presence of HPMCAS (yellow gridded column compared to the blue gridded column in Figure 6.2).

6.4.5 Impact of Growth Environment

Thus far, the impact of the environment during crystallization of amorphous felodipine has been shown to be of great importance to the morphology of the resultant crystalline surface, with surface poisoning effects by HPMCAS being readily apparent. This in turn impacts how quickly the crystals can grow in a supersaturated solution. The other important factor highlighted in the results so far is the presence of dissolved HPMCAS in solution, which competes with felodipine growth units for active growth sites on the surface, reducing the rate of crystal growth. The results indicated that when HPMCAS was present in the growth medium, it could continue to effectively poison the surface and dictate how the crystals evolved. However, for the cases where HPMCAS was incorporated onto the crystal surface, but was not present in the growth medium, felodipine could deposit as fresh layers on top of the poisoned surface and the impact of surface poisoning by the polymer was reduced. This highlights the importance of the solution growth environment.

To further probe the importance of growth environment, felodipine crystal growth rates (of seed crystals prepared using method *i*) were measured in the presence of the surfactant, SDS. Surfactants are frequently present in solution both during *in vitro* testing of amorphous formulations and *in vivo*, and may even be added to the formulation The results are presented in Figure 6.10 along with the result for growth in the presence of HPMCAS alone for comparison.

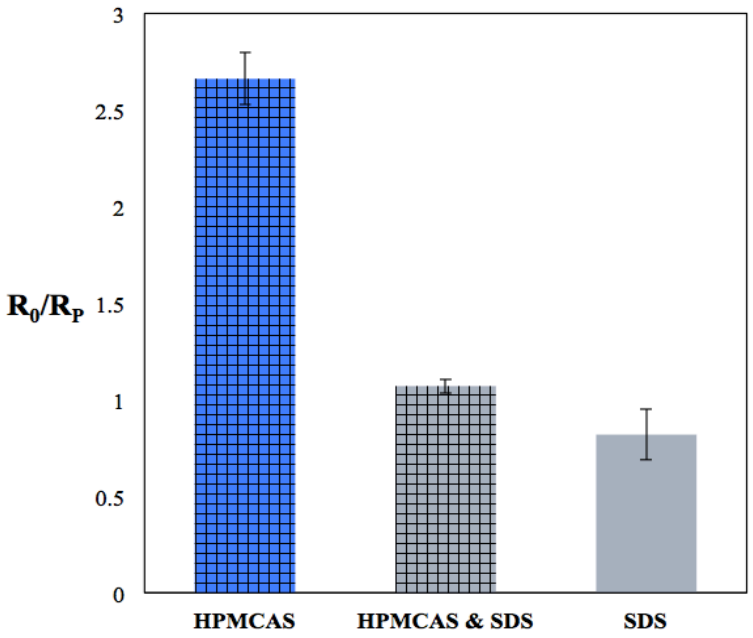

Figure 6.10. Effectiveness growth rate ratios for felodipine in the presence of SDS (100 µg/mL) and/or HPMCAS (5µg/mL). Felodipine surfaces for all experiments were prepared using method (*i*). Gridded columns have HPMCAS present in solution during growth. Experiments were performed in triplicate and each column represents the mean. Error bars indicate the standard deviation.

For the case where SDS and HPMCAS were both present in solution, crystal growth was faster than for the case of HPMCAS alone. It was hypothesized that this could be due to the possibility that SDS prevents HPMCAS from adsorbing on the surface via steric hindrance by adsorbed SDS molecules. However, AFM phase characterization, which is sensitive to surface material properties, provided evidence that this was not the case. Figure 6.11 shows AFM phase contrast imaging of a pure felodipine surface (Figure 6.11a), a felodipine surface after exposure to HPMCAS (Figure 6.11b), and a felodipine surface after exposure to a mixture of HPMCAS and SDS (Figure 6.11c). It can be seen that Figures 6.11b and 6.11c look similar, wherein both exhibit dark shading indicative of adsorbed HPMCAS. By comparison, the pure

drug surface does not have this dark shading. If SDS prevented the adsorption of HPMCAS, Figure 6.11c would be expected to look similar to Figure 6.11a.

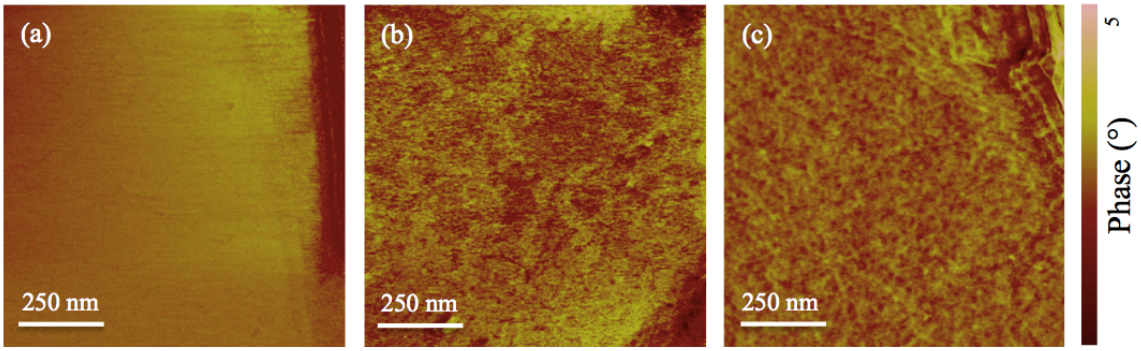

Figure 6.11. 1μm x 1μm AFM phase images of (a) a pure felodipine crystal face, (b) a felodipine crystal face after exposure to HPMCAS (5 μg/mL), and (c) a felodipine crystal face after exposure to a mixture of HPMCAS (5 μg/mL) and SDS (100 μg/mL). Images were captured in liquid at room temperature with an incubation time of 2-3 h.

A possible explanation for the increase in growth rate in the presence of SDS could be a change in the interfacial energy of felodipine in contact with water due to the adsorbed surfactant. Thus, the growth rate of felodipine was measured in the presence of SDS only. It can be seen in Figure 6.10 that the effectiveness ratio, $R_0/R_P < 1$, indicating that the growth rate when SDS was present was actually faster than the growth rate of the pure drug. A similar result was observed by Chen *et al.* where some surfactants were shown to accelerate crystallization.[29] This result can be explained by a reduction in the interfacial energy, γ, by the surfactant, thereby decreasing the critical nucleus radius (equation 1.6).

This result highlights the importance of the crystallization medium. Drug formulations include several excipients, and often surfactants are used as solubilizing

agents.[30] If a formulation includes a combination of polymer and a surfactant such as SDS, this could potentially negatively impact stabilization of the supersaturated solution once the drug has dissolved *in vivo*, and thereby decrease drug absorption.

6.5 Conclusions

The ability of the polymer HPMCAS to poison felodipine crystals was assessed. Polycrystalline felodipine surfaces were prepared from amorphous material using four different methods involving exposure to aqueous solutions with and without HPMCAS and it was found that the solution growth rates of the resultant crystals varied greatly. Characterization of the surfaces with atomic force microscopy revealed discernible differences in the morphology of the surfaces as well as the growth mechanisms. It was concluded that surface poisoning by polymers can have a large impact on crystal morphology and consequently, crystal growth rates.

In addition, it was found that the presence of HPMCAS in solution during growth reduced growth rates, regardless of the surface preparation method. AFM characterization revealed that when crystals were grown in solution in the absence of HPMCAS, fresh layers of drug were able to grow on top of the poisoned surface. When HPMCAS was present in solution during crystal growth, evidence of step pinning was observed, explaining the reduced crystal growth rates. This study highlights that seed crystals prepared in different environments have different abilities to subsequently grow, a factor that should be considered when evaluating polymers as growth rate inhibitors, and evaluating the risk of desupersaturation from amorphous formulations containing residual

crystals. The insights gained from this study can be used to control crystallization and improve the delivery of therapeutics with poor aqueous solubility.

References

(1) Dahan, A. S.; Amidon, G. L. Gastrointestinal Dissolution and Absorption of Class II Drugs. *Drug Bioavailab. Estim. Solubility, Permeability, Absorpt. Bioavailability, Vol. 40, Second Ed.* **2009**, 33–51.

(2) Hancock, B. C.; Parks, M. What Is the True Solubility Advantage for Amorphous Pharmaceuticals? *Pharm. Res.* **2000**, *17*, 397–404.

(3) Hancock, B. C.; Zografi, G. Characteristics and Significance of the Amorphous State in Pharmaceutical Systems. *J. Pharm. Sci.* **1997**, *86*, 1–12.

(4) Simonelli, A. P.; Mehta, S. C.; Higuchi, W. I. Dissolution Rates of High Energy Sulfathiazole--Povidone Coprecipitates II: Characterization of Form of Drug Controlling Its Dissolution Rate via Solubility Studies. *J. Pharm. Sci.* **1976**, *65*, 355–361.

(5) Kennedy, M.; Hu, J.; Gao, P.; Li, L.; Ali-Reynolds, A.; Chal, B.; Gupta, V.; Chandra, M.; Mahajan, N.; Akrami, A.; et al. Enhanced Bioavailability of a Poorly Soluble VR1 Antagonist Using an Amorphous Solid Dispersion Approach: A Case Study. *Mol. Pharm.* **2008**, *5*, 981–993.

(6) Alonzo, D. E.; Gao, Y.; Zhou, D.; Mo, H.; Zhang, G. G. Z.; Taylor, L. S. Dissolution and Precipitation Behavior of Amorphous Solid Dispersions. *J. Pharm. Sci.* **2011**, *100*, 3316–3331.

(7) Corrigan, O. I.; Farvar, M. A.; Higuchi, W. I. Drug Membrane Transport Enhancement Using High Energy Drug Polyvinylpyrrolidone (PVP) Co-Precipitates. *Int. J. Pharm.* **1980**, 229–238.

(8) Yalkowsky, S. H. Perspective on Improving Passive Human Intestinal Absorption. *J. Pharm. Sci.* **2012**, *101*, 3047–3050.

(9) Raina, S. A.; Zhang, G. G. Z.; Alonzo, D. E.; Wu, J.; Zhu, D.; Catron, N. D.; Gao, Y.; Taylor, L. S. Enhancements and Limits in Drug Membrane Transport Using Supersaturated Solutions of Poorly Water Soluble Drugs. *J. Pharm. Sci.* **2014**, *103*, 2736–2748.

(10) Alonzo, D. E.; Zhang, G. G. Z.; Zhou, D.; Gao, Y.; Taylor, L. S. Understanding the Behavior of Amorphous Pharmaceutical Systems during Dissolution. *Pharm. Res.* **2010**, *27*, 608–618.

(11) Mullin, J. W. *Crystallization, 4th Ed.*; Butterworth-Heinemann: Woburn, MA, 2001.

(12) Addadi, L.; Berkovitch-Yellin, Z.; Weissbuch, I.; van Mil, J.; Shimon, L. J. W.; Lahav, M.; Leiserowitz, L. Growth and Dissolution of Organic Crystals with "Tailor-Made" Inhibitors-Implications in Stereochemistry and Materials Science. *Angew. Chemie Int. Ed. English* **1985**, *24*, 466–485.

(13) DeYoreo, J. J.; Vekilov, P. G. Principles of Crystal Nucleation and Growth. *Rev. Mineral. Geochemistry* **2003**, *54*, 57–93.

(14) Kubota, N. Effect of Impurities on the Growth Kinetics of Crystals. *Cryst. Res. Technol.* **2001**, *36*, 749–769.

(15) Alonzo, D. E.; Raina, S.; Zhou, D.; Gao, Y.; Zhang, G. G. Z.; Taylor, L. S. Characterizing the Impact of Hydroxypropylmethyl Cellulose on the Growth and Nucleation Kinetics of Felodipine from Supersaturated Solutions. *Cryst. Growth Des.* **2012**, *12*, 1538–1547.

(16) Ilevbare, G. a.; Liu, H.; Edgar, K. J.; Taylor, L. S. Inhibition of Solution Crystal Growth of Ritonavir by Cellulose Polymers – Factors Influencing Polymer Effectiveness. *CrystEngComm* **2012**, *14*, 6503–6514.

(17) Ilevbare, G. A.; Liu, H.; Edgar, K. J.; Taylor, L. S. Maintaining Supersaturation in Aqueous Drug Solutions: Impact of Di Ff Erent Polymers on Induction Times. *Cryst. Growth Des.* **2013**, 740–751.

(18) Schram, C. J.; Beaudoin, S. P.; Taylor, L. S. Impact of Polymer Conformation on the Crystal Growth Inhibition of a Poorly Water-Soluble Drug in Aqueous Solution. *Langmuir* **2015**, *31*, 171–179.

(19) Schram, C. J.; Taylor, L. S.; Beaudoin, S. P. Influence of Polymers on the Crystal Growth Rate of Felodipine – Correlating Adsorbed Polymer Surface Coverage to Solution Crystal Growth Inhibition. *Langmuir* **2015**, *31*, 11279–11287.

(20) Holder, G. a.; Winkler, J. Crystal-Growth Poisoning of N-Paraffin Wax By Polymeric Additives and Its Relevance to Polymer Crystallization Mechanisms. *Nature* **1965**, *207*, 719–721.

(21) Land, T. A.; Martin, T. L.; Potapenko, S.; Palmore, G. T.; De Yoreo, J. J. Recovery of Surfaces from Impurity Poisoning during Crystal Growth. *Nature* **1999**, *399*, 442–445.

(22) Gratz, A. J.; Hillner, P. E. Poisoning of Calcite Growth Viewed in the Atomic Force Microscope (AFM). *J. Cryst. Growth* **1993**, *129*, 789–793.

(23) Schram, C. J.; Smyth, R. J.; Taylor, L. S.; Beaudoin, S. P. Understanding Crystal Growth Kinetics in the Absence and Presence of a Polymer Using a Rotating Disk Apparatus. *Cryst. Growth Des. (In Review)*.

(24) Wu, S. Calculation of Interfacial Tension in Polymer Systems. *J. Polym. Sci. Part C Polym. Symp.* **1971**, *34*, 19–30.

(25) Macrae, C. F.; Edgington, P. R.; McCabe, P.; Pidcock, E.; Shields, G. P.; Taylor, R.; Towler, M.; van de Streek, J. Mercury: Visualization and Analysis of Crystal Structures. *J. Appl. Cryst.* **2006**, *39*, 453–457.

(26) Holmberg, K.; Jonsson, B.; Kronberg, B.; Lindman, B. *Surfactants and Polymers In Aqueous Solutions, 2nd Ed.*; John Wiley & Sons, LTD: Chichester, 2003.

(27) Christina, B.; Taylor, L. S.; Mauer, L. J. Physical Stability of L -Ascorbic Acid Amorphous Solid Dispersions in Different Polymers : A Study of Polymer Crystallization Inhibitor Properties. *Food Res. Int.* **2015**, *76*, 867–877.

(28) Trasi, N. S.; Taylor, L. S. Effect of Polymers on Nucleation and Crystal Growth of Amorphous Acetaminophen. *CrystEngComm* **2012**, *14*, 5188–5197.

(29) Chen, J.; Ormes, J. D.; Higgins, J. D.; Taylor, L. S. Impact of Surfactants on the Crystallization of Aqueous Suspensions of Celecoxib Amorphous Solid Dispersion Spray Dried Particles. *Mol. Pharm.* **2015**, *12*, 533–541.

(30) Williams, H. D.; Trevaskis, N. L.; Charman, S. a; Shanker, R. M.; Charman, W. N.; Pouton, C. W.; Porter, C. J. H. Strategies to Address Low Drug Solubility in Discovery and Development. *Pharmacol. Rev.* **2013**, *65*, 315–499.

CHAPTER 7. CONCLUSIONS AND RECOMMENDATIONS FOR FUTURE WORK

In the work presented in the preceding chapters of this dissertation, the impact of adsorbed polymers on crystal growth inhibition was studied. Several important conclusions were made from the results of this work. It was found that crystal growth in the presence of polymers impacted the kinetics of solute integration onto the crystal lattice. Another conclusion was that adsorbed polymer conformation greatly impacted the effectiveness of polymers as crystal growth inhibitors. The adsorbed conformation was affected by certain polymer properties such as ionization state and hydrophobicity. Finally, it was found that polymers impacted crystal morphology and crystal growth mechanism. These conclusions and the results that led to them open up many new questions and possibilities for future studies.

In Chapter 3, the kinetics of felodipine crystallization was impacted by the presence of HPMCAS. Specifically, the kinetic constants for the integration steps, k_r and r were shown to change. It was speculated that the change in r, the integration order, could be due to change in growth mechanism when polymers are present. The work of Chapter 6 provided evidence that the presence of polymers can indeed change growth mechanism. However, a definite link between integration order and growth mechanism has not yet been made. Therefore, it is recommended that the integration kinetics for systems with different growth mechanisms be studied in order to confirm this correlation.

The work presented in Chapters 4 and 5 showed that polymers that adsorbed in a coiled globule formation had reduced inhibitory impact compared to polymers that adsorbed in an extended chain conformation. This is because the globule formation leaves many growth sites open and available on the crystal for drug growth units to adsorb. In contrast, more growth sites are blocked when the polymer is more evenly distributed on the surface. Accordingly, in Chapter 5, polymer fractional surface coverage was shown to correlate linearly to polymer effectiveness.

This work served as a proof-of-concept for this correlation between surface coverage and polymer effectiveness. The ultimate goal is that the correlation can be used to aid in polymer selection during drug product formulation. However, it is not practical for pharmaceutical companies to measure the surface coverage for every drug-polymer combination in order to predict effectiveness.

Therefore, it is recommended that this work be expanded upon to include other active pharmaceutical ingredients (API) and an even broader range of polymers. If other APIs with properties similar to felodipine are found to exhibit a very similar correlation when studied with the same group of polymers, then that correlation would be proven to be predictive for new drug compounds with properties similar to felodipine.

Next, another set of model compounds that exhibit different properties from the set already studied could be assessed in order to build up a model correlation to describe polymer effectiveness for new drugs similar to that set. Expanding the study in this fashion would build up a robust framework in order to predict polymer effectiveness.

Another finding of the work in Chapter 4 was that HPMCAS adsorption was shown to adsorb to multiple crystal faces with various surface chemistries. Thus, it was concluded that HPMCAS adsorption was non-specific. It is possible that this non-specificity is due to the fact that HPMCAS has both hydrophilic and hydrophobic groups. For the polymers, such as PVP that are very hydrophilic, or PVAc that are very hydrophobic, it is still unclear whether these polymers will selectively adsorb to faces that exhibit properties similar to their own.

Therefore, another recommendation for future work is to study polymer adsorption onto amorphous drug surfaces. Using these surfaces, it is possible to control for surface chemistry because it is homogeneous. It is hypothesized that hydrophobic polymers would be more likely to adsorb to the more hydrophobic APIs and vice versa. This study would provide valuable insight into polymer adsorption specificity.

In Chapter 6, it was concluded that growth environment greatly impacted crystal growth rates. When poisoned crystalline surfaces of felodipine were exposed to supersaturated solutions containing HPMCAS, the growth rates were consistently slower than when they were exposed to solutions with no HPMCAS. Furthermore, when SDS was present in solution during growth, felodipine growth rates increased compared to the pure system.

Therefore, it is recommended that the impact of growth environment be explored further. In particular, it would be interesting to simulate the conditions of the stomach or GI tract in both the FaSSIF and FeSSIF states. These studies could

determine if other components present in the digestive system such as bile salts have an impact on polymer adsorption or conformation.

Finally, in the work presented in this dissertation, properties such as polymer concentration as well as API supersaturation remained constant within each study in order to keep the experiments controlled. The exception to this was the study in Chapter 5, in which PVPVA adsorption was studied at a higher polymer concentration. It was found that doubling the polymer concentration increased polymer surface coverage, but not by a factor of two. PVPVA adsorbed in the globule conformation at both the lower and higher concentrations, and the higher concentration increased the number of globules, but not the size of them. The latter is certainly a possibility, as is the suggestion that polymer concentration could change the adsorbed conformation altogether. Therefore it would be interesting to study the impact of polymer concentration on adsorbed conformation. The evidence from one system is not enough to draw any certain conclusions. Furthermore, it would be interesting to study the impact of API concentration on polymer conformation. These suggestions for future studies would greatly enhance our understanding of the impact of polymers on crystal growth inhibition.

APPENDICES

Appendix A. ASSESSING THE STABILIZATION POTENTIAL OF VARIOUS POLYMERS FOR SPRAY-DRIED AMORPHOUS LACTOSE

This appendix is a preprint with minor modifications of a manuscript submitted with the same title by: Caitlin J. Schram, Tony Howes, and Stephen P. Beaudoin. It describes research completed at the University of Queensland under the Purdue-UQ Research Exchange Grant.

A.1 Abstract

A large proportion of pharmaceutical compounds have poor aqueous solubility, hindering their bioavailability. Formulating these compounds as amorphous solids, using methods such as spray drying, can improve their solubility and enhance delivery. Additives, such as polymers, are often utilized to stabilize amorphous solids, therefore it is necessary to evaluate how they can influence crystallization behavior. In this study, the stabilization potential of five different polymers was assessed, with the goal of examining the impact of both functional group chemistry and backbone structure. It was found that PAA and PVP were the best crystallization inhibitors due to their functional group chemistries.

A.2 Introduction

More than 75% of active pharmaceutical ingredients (API) currently under development have poor aqueous solubility[1]. This poses a problem for oral therapeutics due to decreased bioavailability[2]. Utilizing the amorphous form of the drug, which has a

higher overall free energy than the crystalline form, is an effective method to alleviate solubility issues and therefore improve drug delivery[3,4].

Recent literature has described methods that attempt to stabilize the inherently unstable amorphous form and prevent crystallization[2]. One such method is the addition of polymers to the system. The ability of polymers to stabilize an amorphous API has been attributed to several factors including decreased molecular mobility and the formation of specific drug-polymer interactions[5–7]. Thus, the formation of a solid drug-polymer dispersion, in which the API is dispersed as an amorphous material within a polymeric matrix, is reported as an effective means of inhibiting crystallization[8–10]. Amorphous solid dispersions can be prepared in a number of ways[8]. Spray drying is one such method that has proven to produce amorphous material due to rapid conversion of a liquid solution to a dry powder by evaporation[11].

Although not an API, lactose is chosen as the model for this study due to its well-documented crystallization properties[12–15] as well as its wide use as an excipient in solid dosage forms[16]. Due to its thermodynamic instability, amorphous lactose will crystallize over time when exposed to a humid environment. Amorphous lactose is extremely hygroscopic. Its molecules are configured such that hydrogen bonding sites are exposed[13]. As these sites bind to the water molecules in the air, the water content in the solid increases and the glass transition temperature (T_g) of the solid decreases. When the T_g drops below the experimental temperature, the lactose will crystallize[17]. In other words, exposure to humid air lowers the activation energy barrier towards crystallization[12]. Thus, the extent of lactose crystallization increases with increasing RH and time[13].

In this study, α-lactose monohydrate was spray dried with a number of polymers and exposed to humid air in order to assess the effectiveness of each polymer at inhibiting lactose crystallization. Previous studies have indicated that the polymers that form stronger hydrogen bonds with the compound can more effectively stabilize an amorphous system[18–20]. Other studies have suggested that polymers that can decrease the molecular mobility of the compound by increasing its T_g will be effective[21]. Each of the polymers used in this study were selected solely based on their structure, with the intention of examining the effect of functional groups and backbone structure on a polymer's ability to interact with lactose and inhibit crystallization.

A.3 Materials and methods

A.3.1 Materials

α-lactose monohydrate (Mw 360.31 g mol^{-1}), Poly(vinylpyrrolidone) (PVP, Mw 40,000 g mol^{-1}), and polyacrylonitrile (PAN, Mw 150,000 g mol^{-1}) were purchased from Sigma-Aldrich (Sydney, Australia). Poly(acrylic acid) (PAA, Mv ~450,000 g mol^{-1}), Poly(ethylene succinate) (PES, ave Mw 10,000 g mol^{-1}), and Poly(trimellitic anhydride chloride-*co*-4,4'-methylenedianiline) (PTM, Mw not given) were purchased from Sigma-Aldrich (St Louis, MO, USA). Figure A.1 shows the molecular structures of the polymers and lactose. Saturated salt solutions of K_2CO_3 and NaCl were used to generate air of 44 and 75% RH.

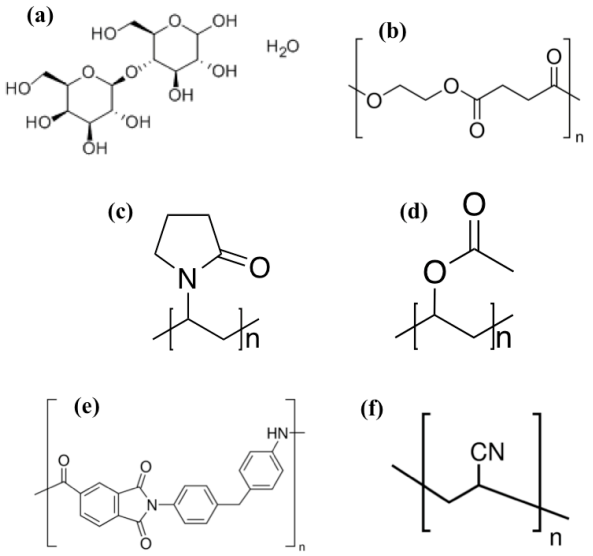

Figure A.1. Chemical structures of (a) α-lactose monohydrate, (b) PES, (c) PAA, (d) PVP, (e) PTM, and (f) PTN

A.3.2 Spray Drying

Pure α-lactose monohydrate or a mixture of lactose and 20% (w/w) polymer was added to DI water to give a solution containing 20g solid/100mL solution. The solutions were spray dried using a Buchi B-290 Mini Spray Dryer (Buchi Labortechnik AG, Switzerland). The process conditions, given in Table A.1, were constant for all experiments, except for the lactose/PAA composite, which was spray-dried at a lower inlet temperature due to the low decomposition temperature of PAA. To ensure rapid drying of this sample at the lower inlet T, the feed rate was also lowered. The spray-dried powders were stored in a desiccator for 24 hours before being moved to RH chambers where they were stored for 3 or 10 days.

Table A.1. Spray drying process conditions

Parameters	**Settings**
Feed flow (ml/min)	8.5
Inlet temperature (°C)	185
Drying gas volume flow (m^3/h)	35

A.3.3 Assessment of crystallinity

X-ray diffraction (XRD) patterns were obtained using a D8 Advance X-ray Powder Diffractometer (Bruker Corporation, Billerica, MA), to assess the crystalline content of each sample before and after storage at 44% and 75% RH. Samples were also assessed using a differential scanning calorimeter (DSC) (Q10, TA instruments, New Castle, DE, USA, aluminium non-hermetically sealed pans, calibration with indium). Samples were heated from 30°C to 260°C at a rate of 10°C/min. DSC has been shown to be a suitable semiquantitative method to determine the crystallinity of lactose[22]. XRD and DSC were performed on the pure spray dried lactose sample and each of the 7 spray dried lactose/polymer composites before and after storage in controlled relative humidity environments.

A.4 Results and discussion

A.4.1 Properties of spray-dried powders before storage

X-ray diffraction patterns for spray-dried lactose and composite particles before storage are shown in Figure A.2. Each pattern shows broad and diffuse maxima, indicating that all spray-dried samples were amorphous.

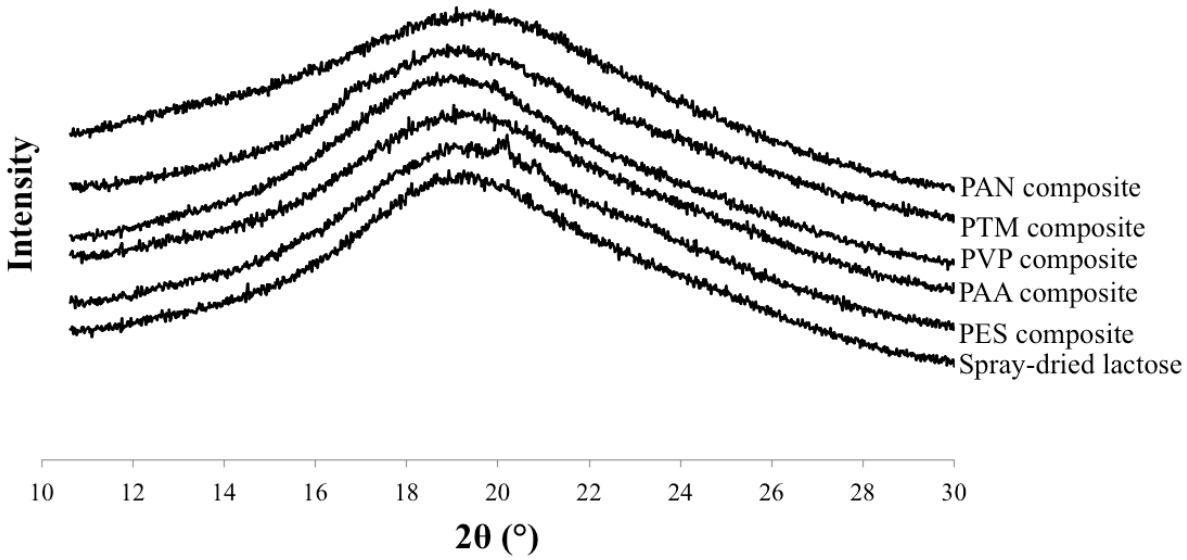

Figure A.2. XRD patterns of spray-dried lactose and lactose/polymer composites before storage

DSC thermograms of the spray-dried materials before storage are shown in comparison to α-lactose monohydrate in Figure A.3. The thermogram of crystalline α-lactose monohydrate exhibits a broad endothermic peak at ~150 °C, signifying dehydration of crystalline water[12,22]. In contrast, pure spray dried lactose shows an exothermic reaction at ~103 °C, signifying the crystallization event[12,22]. The five spray-dried composites also exhibit the exothermic peak typical of an amorphous material, however this peak is shifted to a higher temperature for each of the composites (up to ~130 °C), indicating that the incorporation of polymers requires more energy for

crystallization to occur. This has been observed in previous studies of spray-dried lactose/PVP composites[23].

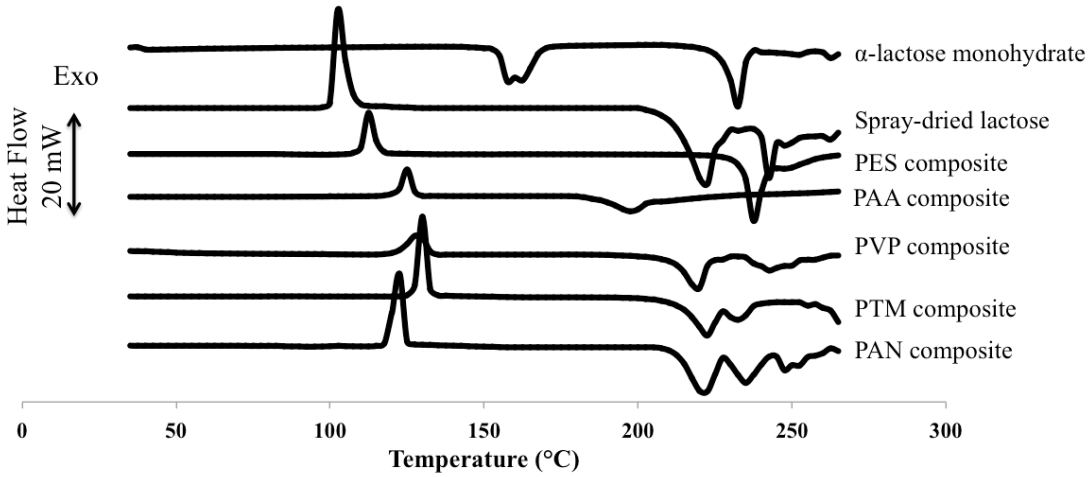

Figure A.3. DSC thermograms of spray-dried lactose and lactose/polymer composites before storage.

Spray drying and recrystallization of lactose can result in mutarotation of α-lactose to β-lactose[13]. The two forms differ in the orientation of a hydroxyl group on the glucose unit[24]. The mechanism of mutarotation occurs via an intermediate aldehyde form. This mechanism can be modelled as a first order reaction in which proton transfer, assisted by a water molecule, and the opening of the pyranosidic ring occur simultaneously[25].

It can be seen from Figure A.3 that both α-lactose monohydrate and pure spray-dried lactose exhibit an endothermic heat of fusion peak at ~222 °C, indicative of the alpha form. Spray-dried lactose also shows a very small β peak at 230°C, demonstrating that a small amount of mutarotation has occurred upon crystallization. This is as expected since lactose is dissolved in aqueous solution before spray drying, and the two isomeric forms are both present in aqueous solution in a reversible equilibrium[24]. The spray-dried

composites each exhibit a different ratio of the α and β forms upon re-crystallization compared to pure spray-dried lactose. The effect of polymers on mutarotation will be discussed further in Sections A.4.3 and A.4.4.

A.4.2 Impact of Polymers on Lactose Crystallization

In order to assess the stabilizing effect of polymeric additives on lactose crystallization, each of the spray-dried samples were exposed to air of 44% and 75% relative humidity for three days. The critical RH for lactose crystallization has been reported as between 43 and 45% RH[26]. The XRD patterns for each sample are shown in Figure A.4. The patterns are displayed with the diffractogram of a-lactose monohydrate for comparison. The diffractograms show that all samples possess some degree of crystallinity, and that as expected, the samples exposed to 75% RH have higher and sharper peaks, and therefore possess a higher degree of crystallinity than the samples exposed to 44% RH due to the increased crystallization driving force at the higher relative humidity.

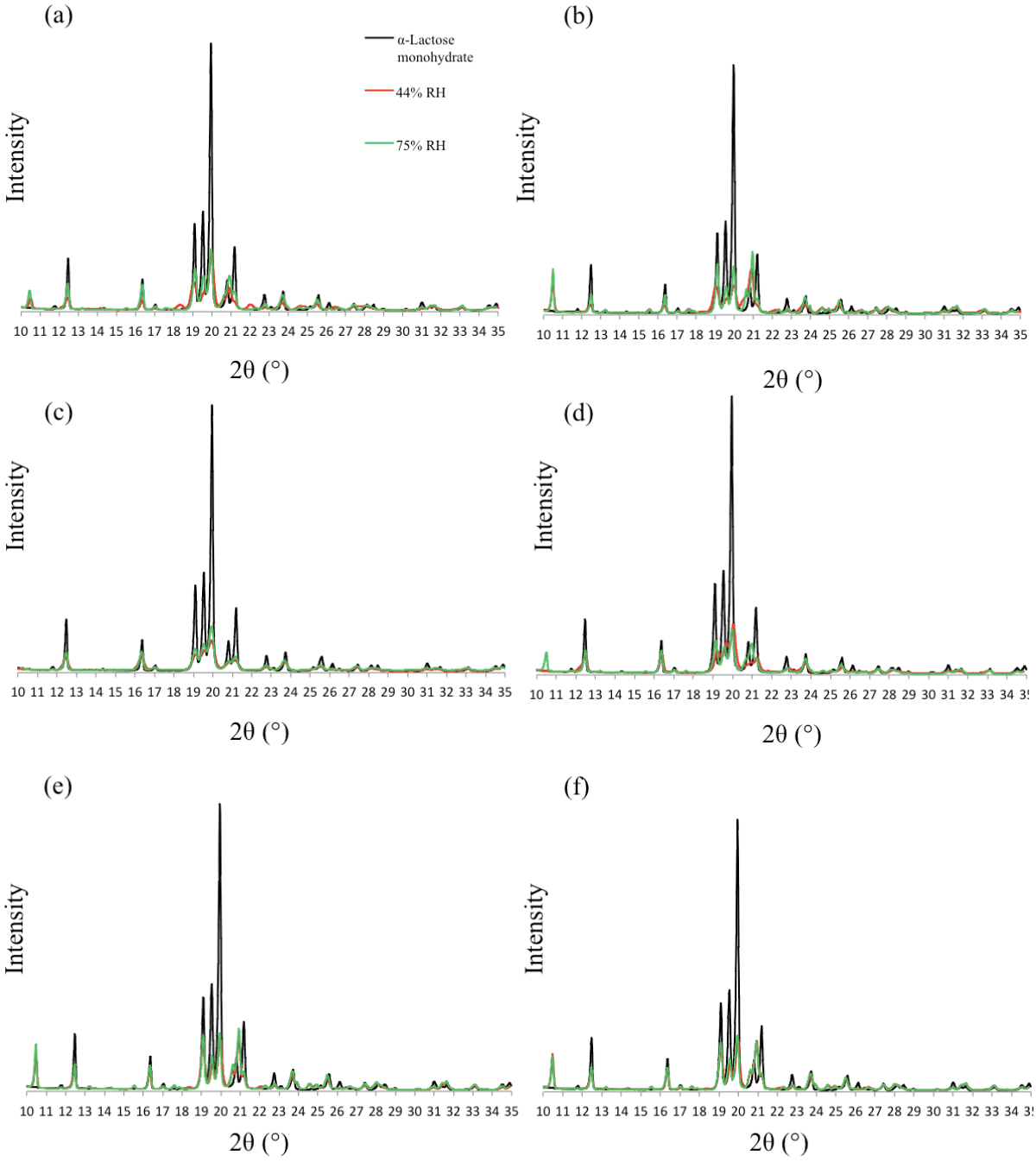

Figure A.4. X-ray diffraction patterns after storage at 44% (red) and 75% (green) relative humidity of spray-dried (a) pure lactose, and spray-dried composites containing (b) PES, (c) PAA, (d) PVP, (e) PTM, and (f) PAN. Diffractograms are compared to crystalline α-lactose monohydrate (black).

The percent of lactose crystallized at 75% RH for each sample (calculated relative to α-lactose monohydrate) are displayed in Table A.2. It can be seen that the composite spray-dried with PAA has the lowest percent crystallinity, indicating that PAA is the most effective crystallization inhibitor. For the samples exposed to 75% RH, the order of effective inhibitors is: PAA > PVP > PES > PAN > PTM.

Table A.2. Calculated % Crystallinity of lactose

Sample	% Crystallinity
Pure lactose	55.5
PES composite	50.6
PAA composite	39.8
PVP composite	45.5
PTM composite	53.8
PAN composite	51.9

All freshly spray-dried composites were also stored for 10 days at 75% RH. These samples along with the samples stored at 44% and 75% RH for 3 days were characterized with DSC, and the results are shown in Figure A.5. It can be seen that the thermograms for samples stored at 75% RH for 10 days compared to 75% RH for 3 days look very similar for all samples. This implies that there were not many changes in stability during storage over the longer term.

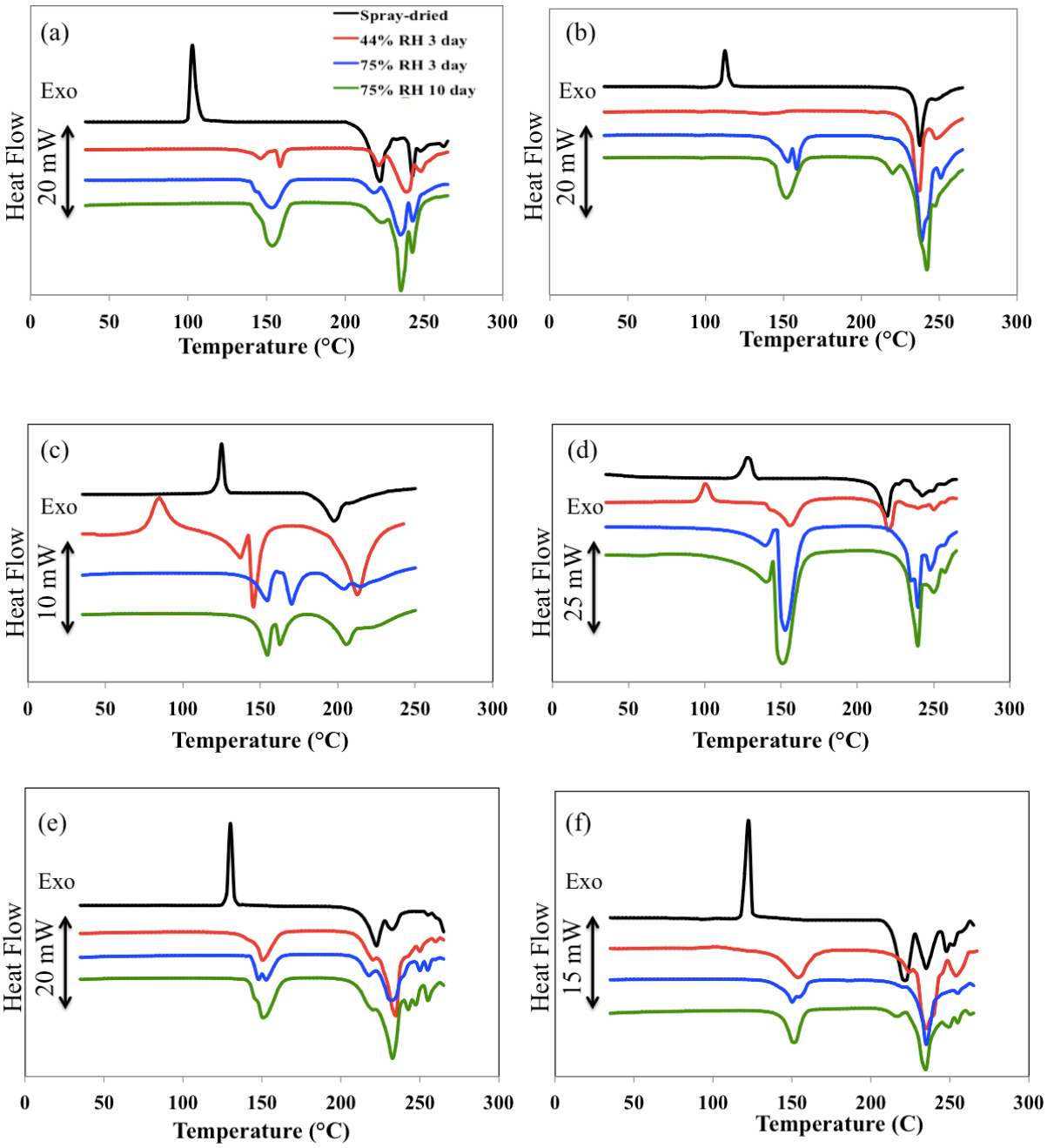

Figure A.5. DSC thermograms of spray-dried (a) pure lactose, and spray-dried composites containing (b) PES, (c) PAA, (d) PVP, (e) PTM, and (f) PAN. Characterization was performed before storage (black) and after storage at 44% RH for 3 days (red), at 75% RH for 3 days (blue), and at 75% RH for 10 days (green).

The DSC thermograms of pure lactose after storage (Figure A.5a) exhibit dehydration peaks around 150°C, which increase in magnitude as RH increases, as expected due to higher % crystallinity. The dual dehydration peaks indicate the presence of two types of hydrates[17]. Composites with PTM and PAN (Figures A.5e and A.5f) have similar DSC thermograms compared to the pure lactose samples at all three storage conditions. This is not surprising given that the XRD results indicate that these two polymers had little effect on lactose crystallization. The DSC thermograms of PAA and PVP composites (Figures A.5c and A.5d) stored at 44% RH for 3 days both exhibit an exothermic peak indicative of amorphous material, similar to the spray-dried sample before storage. These results agree with the XRD results, which indicated that PVP and PAA were the most effective stabilizers.

A.4.3 Assessment of Lactose Mutarotation

The XRD diffractograms of recrystallized pure lactose (Figure A.5a) show peaks at 10.5° and 21°, both of which are not present in the α-lactose monohydrate spectrum. Peaks at these two diffraction angles are characteristic of the β form[27]. Therefore, it is evident that mutarotation occurs upon recrystallization of spray-dried lactose, in agreement with the DSC results discussed in Section A.4.1. Previous studies have shown a similar result[13] and it could be due to high spray-drying temperatures. Similarly, the XRD patterns of lactose spray dried with PES (Figure A.4b), PTM (Figure A.4e), and PAN (Figure A.4f), also show evidence of mutarotation for both storage conditions. Interestingly, lactose spray-dried with PAA (Figure A.4c) does not mutarotate to the β form upon recrystallization, and lactose spray-dried with PVP (Figure A.4d) is only

present in the β form when exposed to 75% RH. The DSC thermograms of the samples (Figure A.5) after storage show similar results, whereby the β form (endothermic peak at ~240°C) dominates for all stored samples, except PAA composites, and PVP composites stored at 44% RH.

These results suggest that mutarotation is linked to stability. PAA was determined to be the best stabilizer, and there is no evidence of transformation to the β form for lactose spray-dried with PAA. PVP was the second best stabilizer and composites with PVP remained in the α form at the lower relative humidity. All other samples, which were not stabilized as effectively by the polymers, transformed to the β form upon crystallization. This will be explored further in Section A.4.4.

A.4.4 Assessment of polymer structure on stabilization

The ranking for crystallization inhibition was: PAA > PVP > PES > PAN > PTM. Comparing this order to the polymer molecular structures shown in Figure A.1, it is clear that there is no significant effect of polymer backbone structure on stability. PTM was the polymer studied which did not have a chain backbone. It was hypothesized that its ring-structured backbone could increase its stabilization potential because it could more effectively hinder the mobility of lactose molecules, slowing their arrangement into a lattice structure. Because of its larger backbone structure, PTM also had the highest T_g. It was thought that this should increase the T_g of the lactose composite and therefore slow crystallization. However, since it was the least effective stabilizer, the results indicated that functional group chemistry, not backbone structure or T_g, is the most important factor.

PAA and PVP were the most effective crystallization inhibitors. Both polymers contain a C=O group, which is a strong hydrogen bond acceptor. Trasi *et al.* have shown evidence using FTIR of hydrogen bonding between the carbonyl groups of PAA and PVP and the –OH group of acetaminophen[19]. It can be seen from Figure 1 that lactose contains numerous –OH groups, a strong hydrogen bond donor group. As stated in Section A.2, crystallization of lactose in humidity occurs *via* binding of water to the exposed –OH groups[13]. Thus, it can be concluded that PAA and PVP are able to hydrogen bond strongly to these groups, inhibit the interactions between lactose and water, and therefore slow crystallization. This conclusion aligns with the mutarotation results discussed in Section A.4.3. Water molecules assist the proton transfer step during mutarotation[25]. Since polymers that are able to form strong hydrogen bonds with lactose are inhibiting the interaction of lactose with water molecules, it follows that they would also inhibit mutarotation.

A.5 Conclusions

The ability of five different polymers to stabilize spray-dried amorphous lactose was assessed. It was found that PAA and PVP were the best crystallization inhibitors. The results suggest that polymer functional group chemistry is more important than polymer backbone structure for crystallization inhibition. PAA and PVP both have strong hydrogen bond acceptor groups, thus they are able to interact strongly with lactose and inhibit the interaction of lactose with water. This allows the polymers to stabilize the amorphous material and slow crystallization.

References

(1) Williams, H. D.; Trevaskis, N. L.; Charman, S. a; Shanker, R. M.; Charman, W. N.; Pouton, C. W.; Porter, C. J. H. Strategies to Address Low Drug Solubility in Discovery and Development. *Pharmacol. Rev.* **2013**, *65*, 315–499.

(2) Blagden, N.; de Matas, M.; Gavan, P. T.; York, P. Crystal Engineering of Active Pharmaceutical Ingredients to Improve Solubility and Dissolution Rates. *Adv. Drug Deliv. Rev.* **2007**, *59*, 617–630.

(3) Yu, L. Amorphous Pharmaceutical Solids: Preparation, Characterization and Stabilization. *Adv. Drug Deliv. Rev.* **2001**, *48*, 27–42.

(4) Hancock, B. C.; Zografi, G. Characteristics and Significance of the Amorphous State in Pharmaceutical Systems. *J. Pharm. Sci.* **1997**, *86*, 1–12.

(5) Taylor, L. S.; Zografi, G. Spectroscopic Characterization of Interactions Between PVP and Indomethacin in Amorphous Molecular Dispersions. *Pharm. Res.* **1997**, *14*, 1691–1698.

(6) Bhugra, C.; Pikal, M. J. Role of Thermodynamic, Molecular, and Kinetic Factors in Crystallization From the Amorphous State. *J. Pharm. Sci.* **2008**, *97*, 1329–1349.

(7) Matsumoto, T.; Zografi, G. Physical Properties of Solid Molecular Dispersions of Indomethacin with Poly(vinylpyrrolidone) and Poly(vinylpyrrolidone-Co-Vinyl-Acetate) in Relation to Indomethacin Crystallization.pdf, 1999, 1722–1728.

(8) Leuner, C.; Dressman, J. Improving Drug Solubility for Oral Delivery Using Solid Dispersions. *Eur. J. Pharm. Biopharm.* **2000**, *50*, 47–60.

(9) Crowley, K. J.; Zografi, G. The Effect of Low Concentrations of Molecularly Dispersed Poly(vinylpyrrolidone) on Indomethacin Crystallization from the Amorphous State. *Pharm. Res.* **2003**, *20*, 1417–1422.

(10) Trasi, N. S.; Taylor, L. S. Effect of Additives on Crystal Growth and Nucleation of Amorphous Flutamide. *Cryst. Growth Des.* **2012**, *12*, 3221–3230.

(11) Ré, M.-I. Formulating Drug Delivery Systems by Spray Drying. *Dry. Technol.* **2006**, *24*, 433–446.

(12) Price, R.; Young, P. M. Visualization of the Crystallization of Lactose from the Amorphous State. *J. Pharm. Sci.* **2004**, *93*, 155–164.

(13) Haque, M. K.; Roos, Y. H. Crystallization and X-Ray Diffraction of Spray-Dried and Freeze-Dried Amorphous Lactose. *Carbohydr. Res.* **2005**, *340*, 293–301.

(14) Herrington, B. L. Some Physicochemical Properties of Lactose. *J. Dairy Sci.* **1934**.

(15) Schmitt, E. a.; Law, D.; Zhang, G. G. Z. Nucleation and Crystallization Kinetics of Hydrated Amorphous Lactose above the Glass Transition Temperature. *J. Pharm. Sci.* **1999**, *88*, 291–296.

(16) Chidavaenzi, O. C.; Buckton, G.; Koosha, F. The Effect of Co-Spray Drying with Polyethylene Glycol 4000 on the Crystallinity and Physical Form of Lactose. *Int. J. Pharm.* **2001**, *216*, 43–49.

(17) Angberg, M. Lactose and Thermal Analysis with Special Emphasis on Microcalorimetry. **1995**, *248*.

(18) Kestur, U. S.; Taylor, L. S. Role of Polymer Chemistry in Influencing Crystal Growth Rates from Amorphous Felodipine. *CrystEngComm* **2010**, *12*, 2288.

(19) Trasi, N. S.; Taylor, L. S. Effect of Polymers on Nucleation and Crystal Growth of Amorphous Acetaminophen. *CrystEngComm* **2012**.

(20) Christina, B.; Taylor, L. S.; Mauer, L. J. Physical Stability of L -Ascorbic Acid Amorphous Solid Dispersions in Different Polymers : A Study of Polymer Crystallization Inhibitor Properties. *Food Res. Int.* **2015**, *76*, 867–877.

(21) Van den Mooter, G.; Wuyts, M.; Blaton, N.; Busson, R.; Grobet, P.; Augustijns, P.; Kinget, R. Physical Stabilisation of Amorphous Ketoconazole in Solid Dispersions with Polyvinylpyrrolidone K25. *Eur. J. Pharm. Sci.* **2000**, *12*, 261–269.

(22) Gombás, Á.; Kata, M.; Jr, G. R.; Erõs, I. QUANTITATIVE DETERMINATION OF CRYSTALLINITY OF A-LACTOSE MONOHYDRATE BY DSC. *J. Therm. Anal. Calorim.* **2002**, *68*, 503–510.

(23) Berggren, J.; Alderborn, G. Effect of Polymer Content and Molecular Weight on the Morphology and Heat- and Moisture-Induced Transformations of Spray-Dried Composite Particles of Amorphous Lactose and Poly(vinylpyrrolidone). *Pharm. Res.* **2003**, *20*, 1039–1046.

(24) Dos Reis Coimbra, J. S.; Teixeira, J. A. *Engineering Aspects of Milk and Dairy Products*; CRC Press: Boca Raton, 2009.

(25) Silva, A. M.; da Silva, E. C.; da Silva, C. O. A Theoretical Study of Glucose Mutarotation in Aqueous Solution. *Carbohydr. Res.* **2006**, *341*, 1029–1040.

(26) Berggren, J.; Alderborn, G. Long-Term Stabilisation Potential of Poly(vinylpyrrolidone) for Amorphous Lactose in Spray-Dried Composites. *Eur. J. Pharm. Sci.* **2004**, *21*, 209–215.

(27) Buma, T. J.; Wiegers, G. A. X-Ray Powder Patterns of Lactose and Unit Cell Dimensions of Beta-Lactose. *Netherlands Milk Dairy J.* **1967**, *21*, 208–213.

Appendix B. SUPPORTING DATA

This appendix shows the desupersaturation profiles measured using UV-vis spectrometry. The slopes of these profiles were used to generate the data points of the growth rate figures presented in this dissertation. Each data point is the average of three profiles, each multiplied by the volume of the solution. The raw data filenames are given for the UV data as well as all AFM data presented in this dissertation.

B.1 Data for Figures 3.2 and 3.5

a) 01-30-2015_RDAexpPure_200rpm_60-12-T25

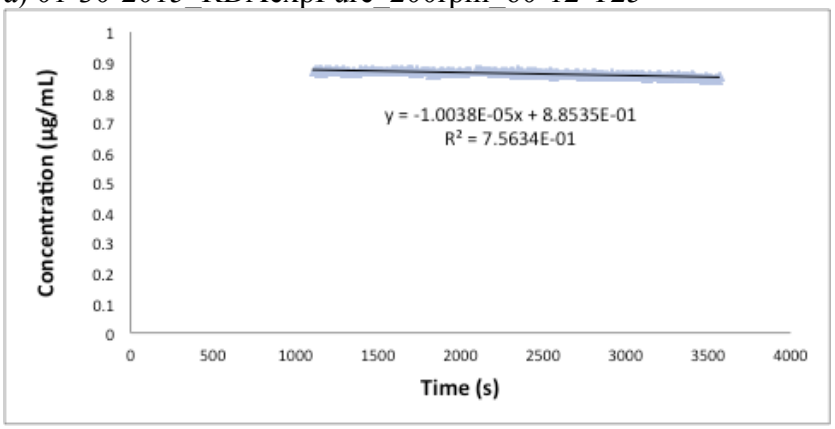

b) 01-30-2015_RDAexpPure2_200rpm_60-12-T25

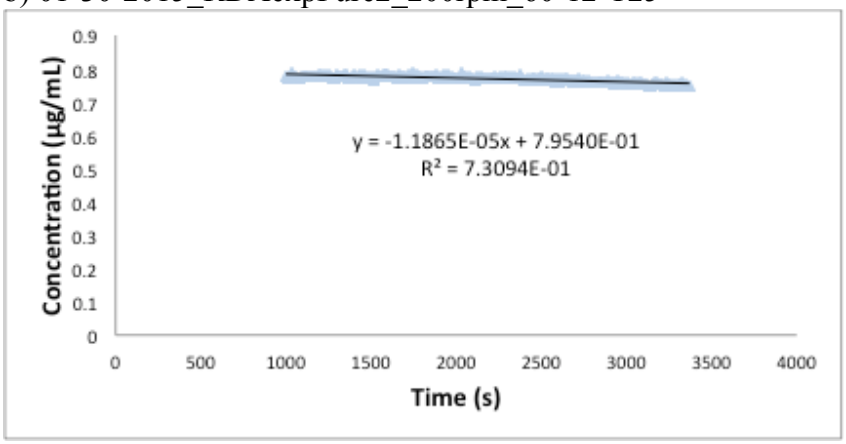

c) 01-31-2015_RDAexpPure_200rpm_60-12

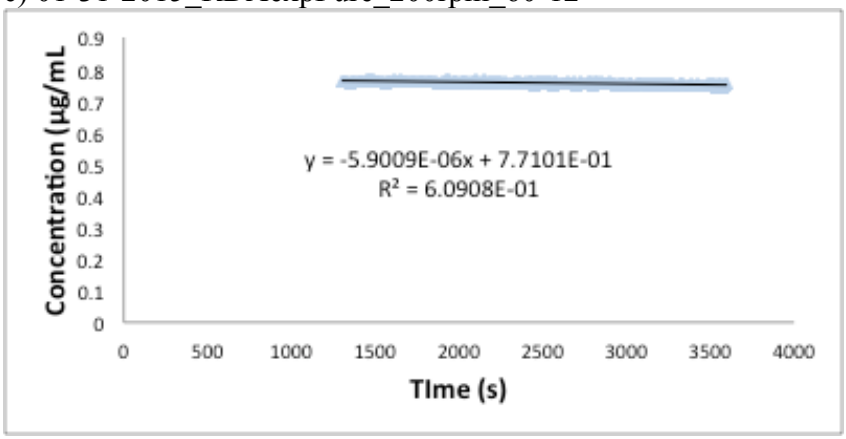

Figure B.1. (a-c) Desupersaturation profiles for pure felodipine (S of 4, no polymers present). **ω = 200 rpm.**

a) 11112014_RDAexp_500rpm_Sof4

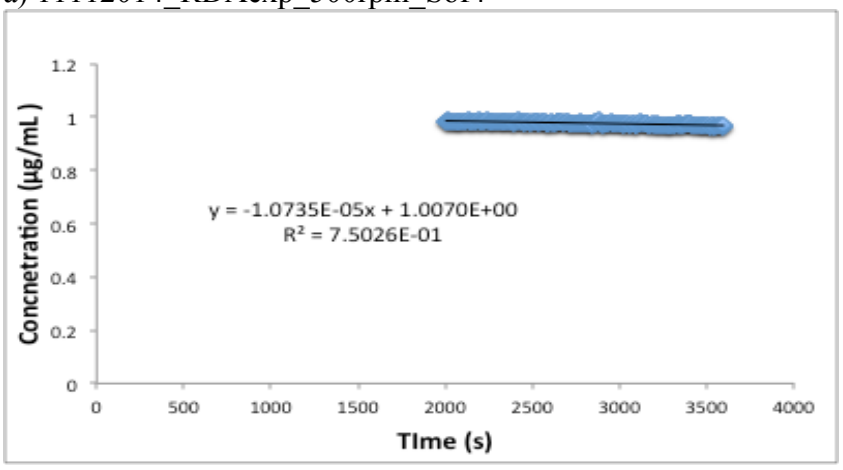

b) 12012014_RDAexp_500rpm_Sof4

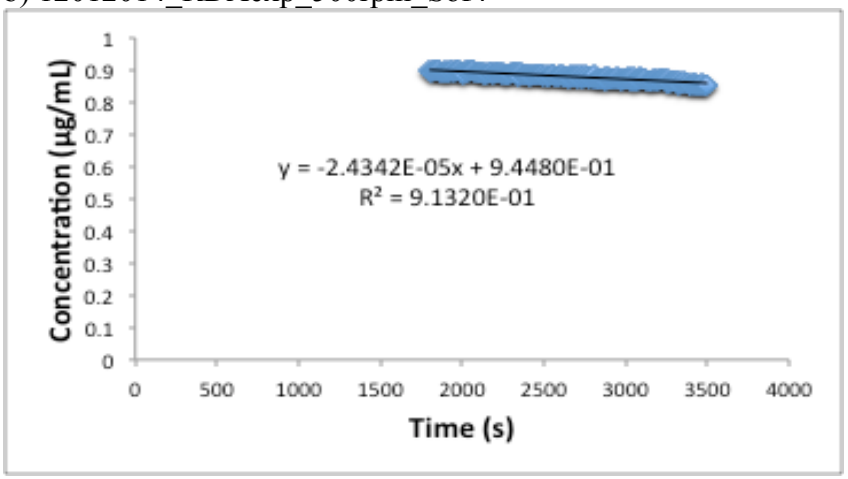

c) 01-30-2015_RDAexpPure_500rpm_60-12-T25

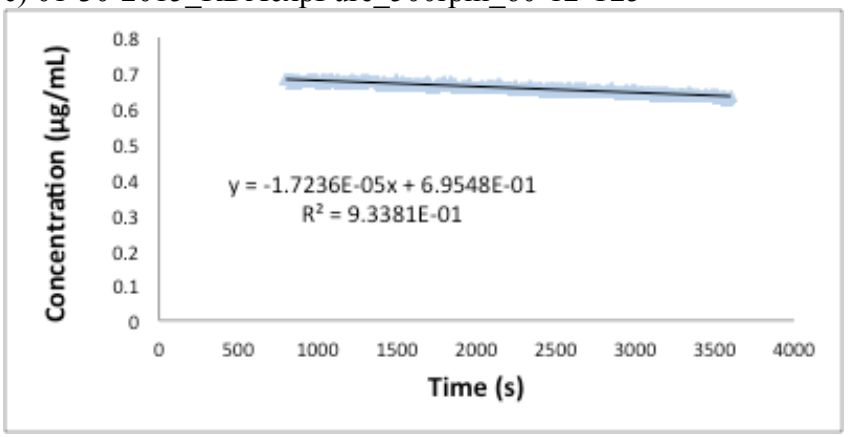

Figure B.2. (a-c) Desupersaturation profiles for pure felodipine (S of 4, no polymers present). **ω = 500 rpm.**

a) 11102014_RDAexp_1000rpm_Sof4

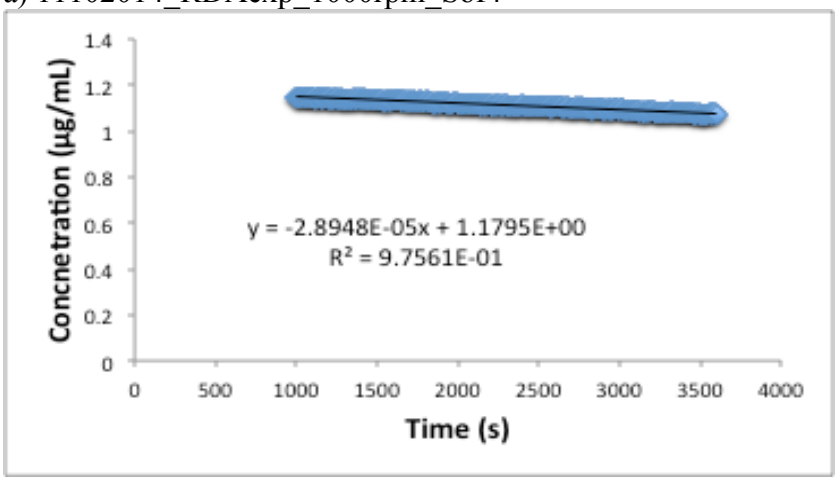

b) 09042015_RDAexp_Sof4_1000rpm

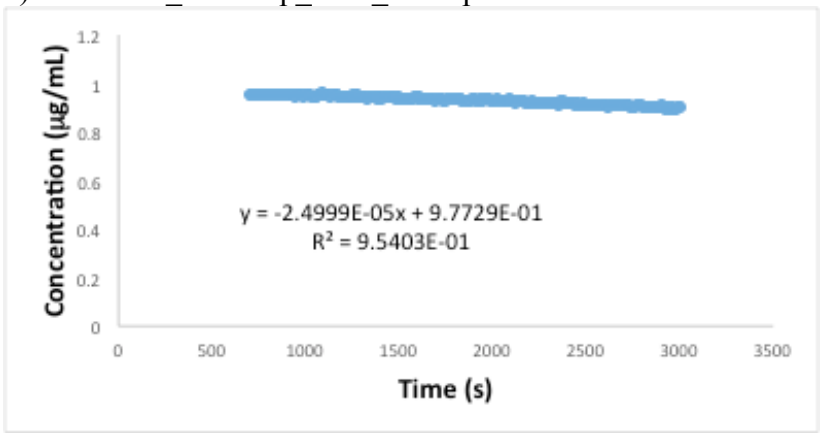

c) 09042015_RDAexp_Sof4_1000rpm_2

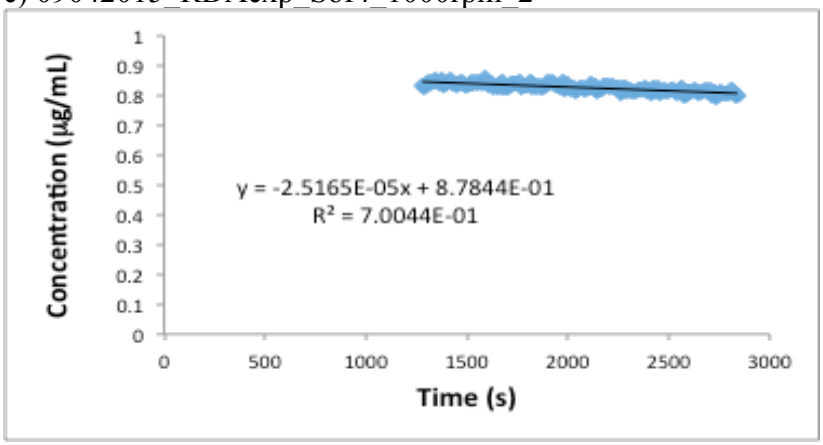

Figure B.3. (a-c) Desupersaturation profiles for pure felodipine (S of 4, no polymers present). **ω = 1000 rpm.**

a) 12012014_RDAexp_1500rpm_Sof4

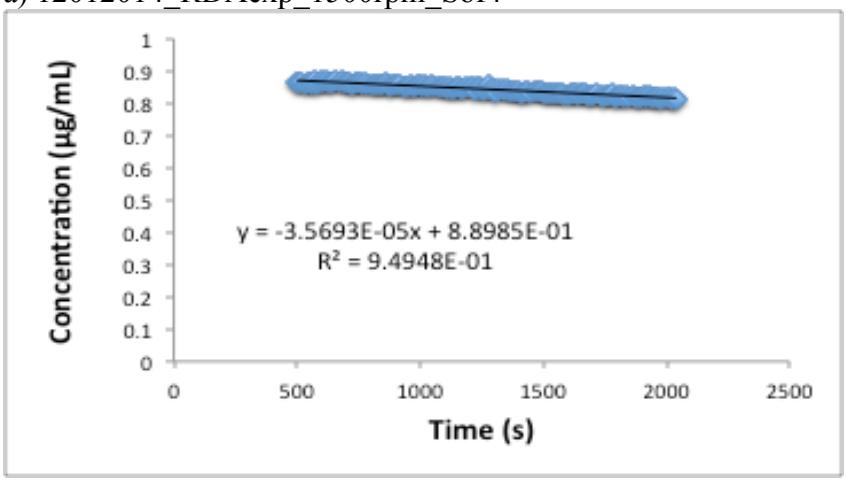

b) 06252015_RDAexp_Sof4_1500rpm

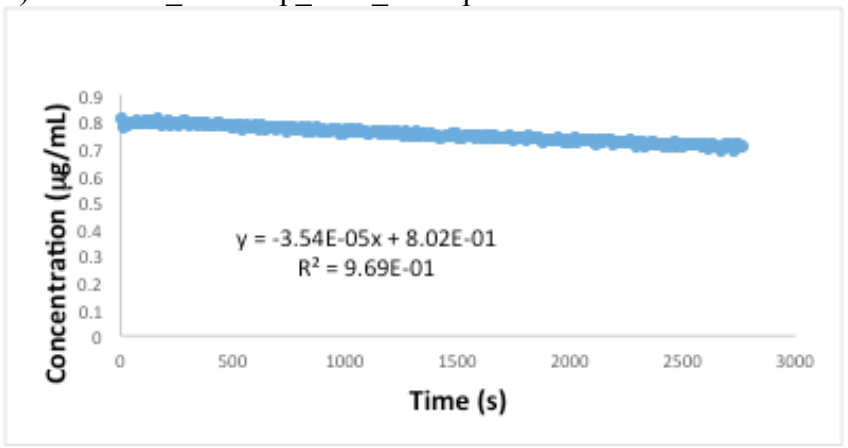

c) 09042015_RDAexp_Sof4_1500rpm

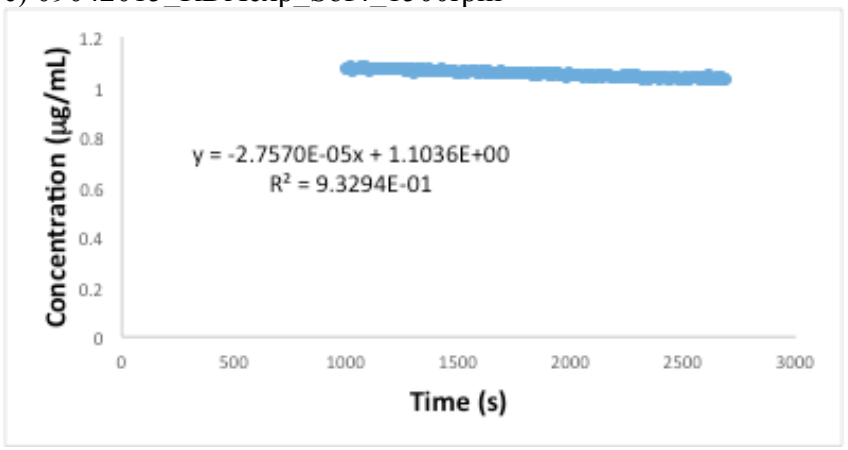

Figure B.4. (a-c) Desupersaturation profiles for pure felodipine (S of 4, no polymers present). **ω = 1500 rpm.**

a) 12022014_RDAexp_2000rpm_Sof4_2

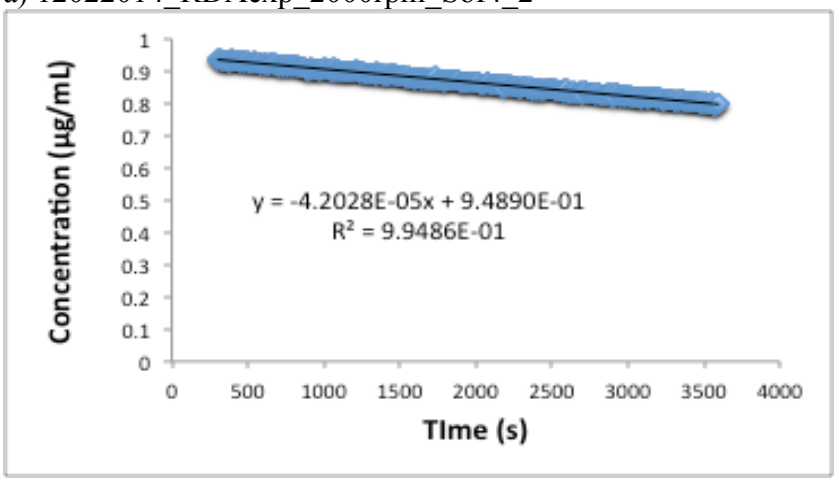

b) 07152015_RDAexp_Sof4_2000rpm

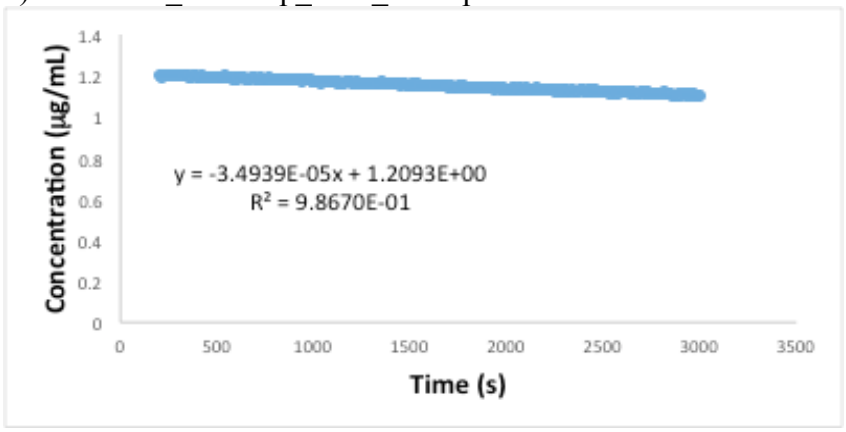

c) 01-31-2015_RDAexpPure_2000rpm_60-12

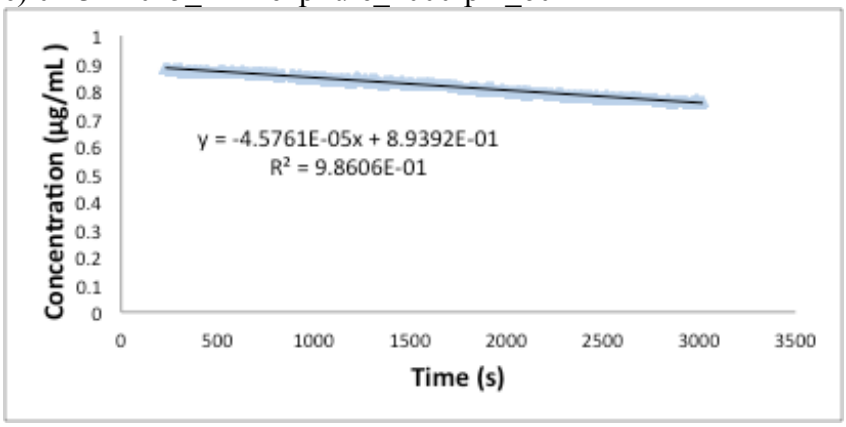

Figure B.5. (a-c) Desupersaturation profiles for pure felodipine (S of 4, no polymers present). **ω = 2000 rpm.**

a) 11102014_RDAexp_3000rpm_Sof4

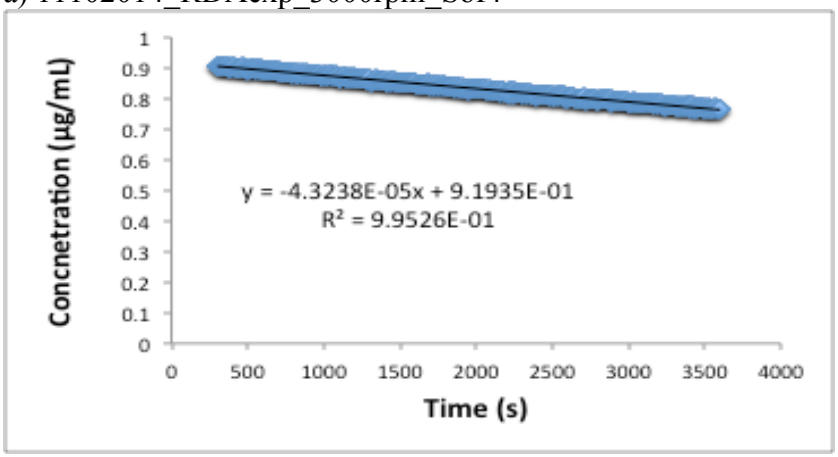

b) 11112014_RDAexp_3000rpm_Sof4

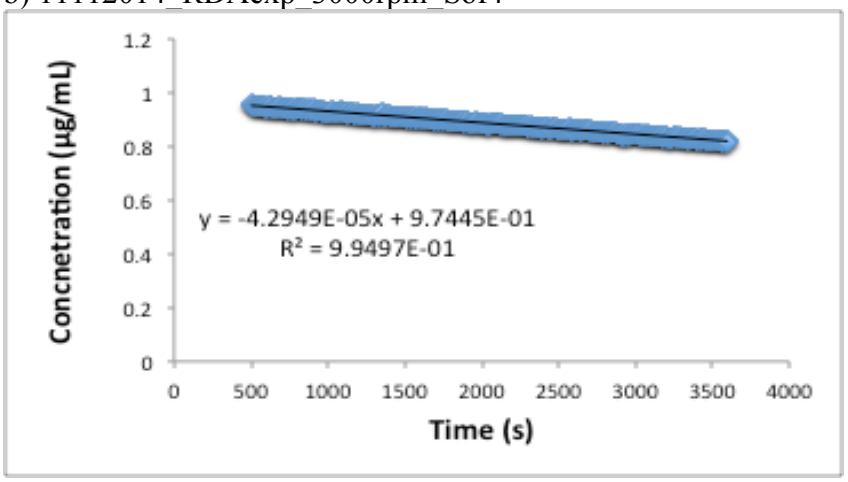

c) 08052015_RDAexp_Sof4_3000rpm

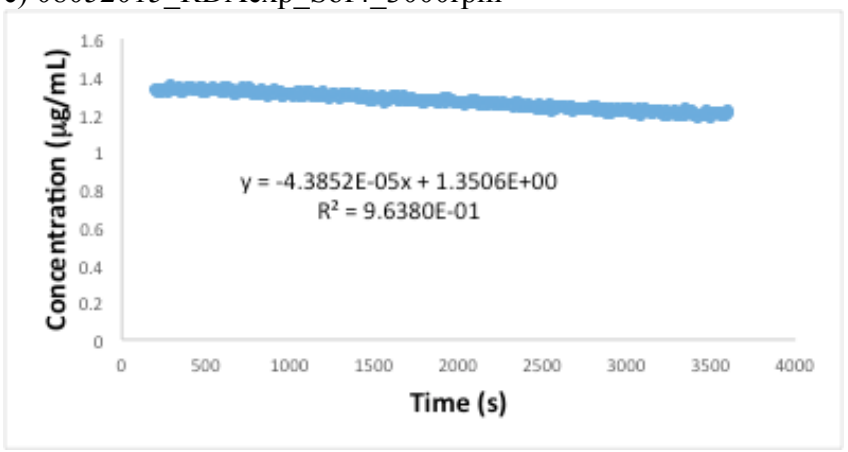

Figure B.6. (a-c) Desupersaturation profiles for pure felodipine (S of 4, no polymers present). **ω = 3000 rpm.**

a) 11112014_RDAexp_4000rpm_Sof4

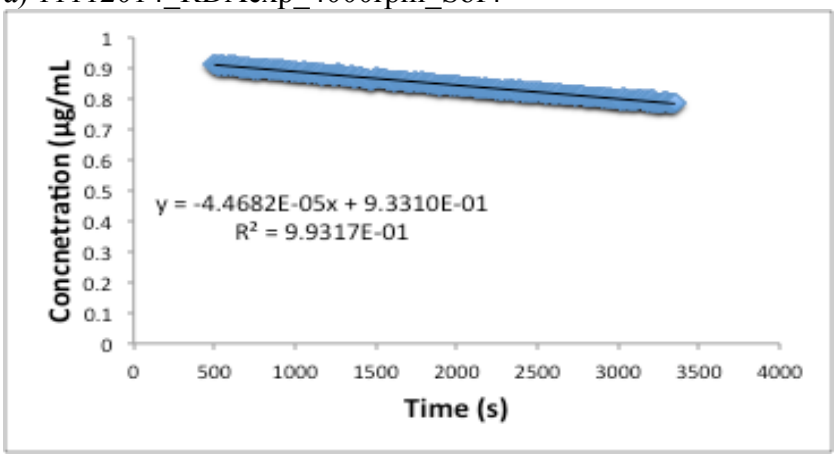

b) 08122015_RDAexp_Sof4_4000rpm

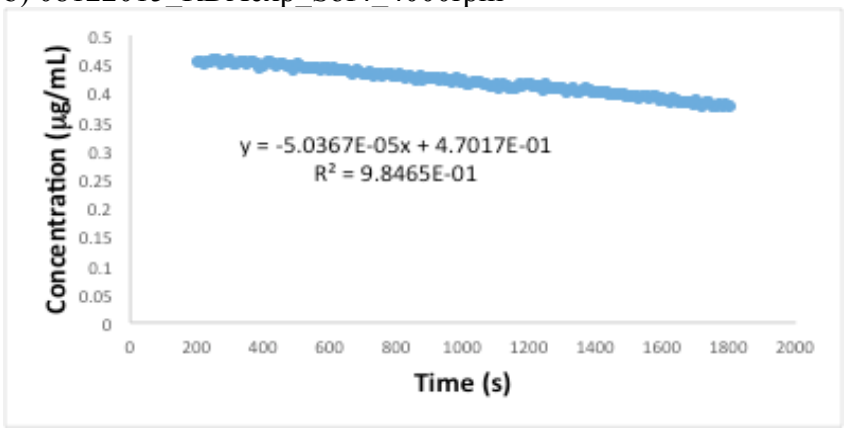

c) 09042015_RDAexp_Sof4_4000rpm_2

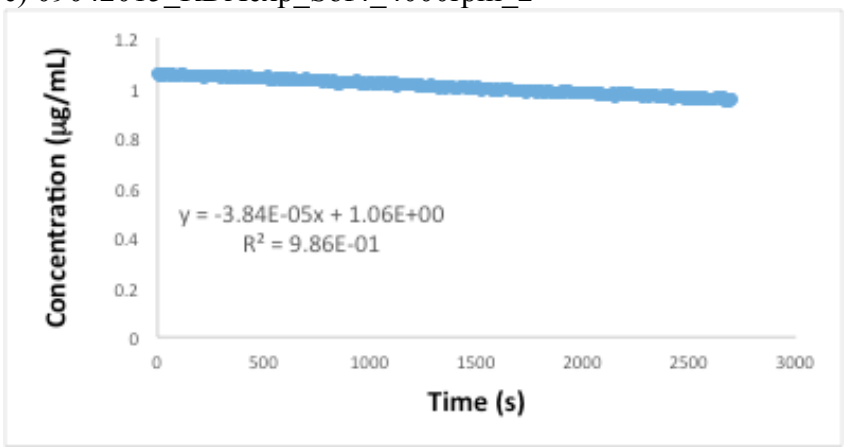

Figure B.7. (a-c) Desupersaturation profiles for pure felodipine (S of 4, no polymers present). **ω = 4000 rpm.**

a) 12-07-2014_60-12-T25_5000rpm

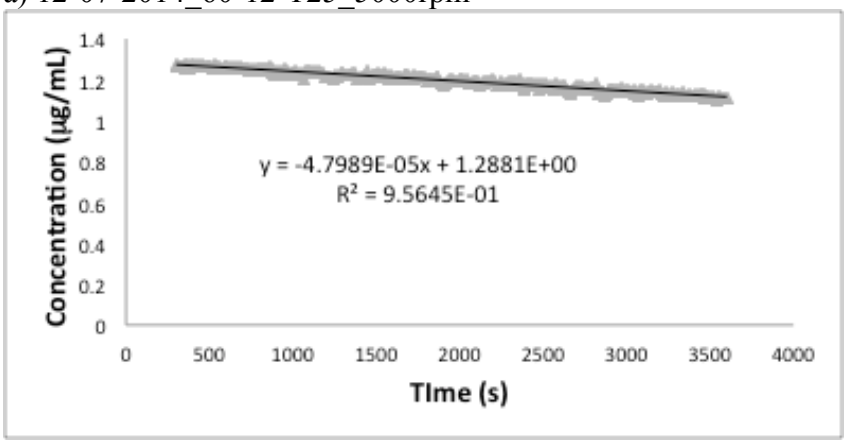

b) 12-07-2014_60-12-T25_5000rpm(2)

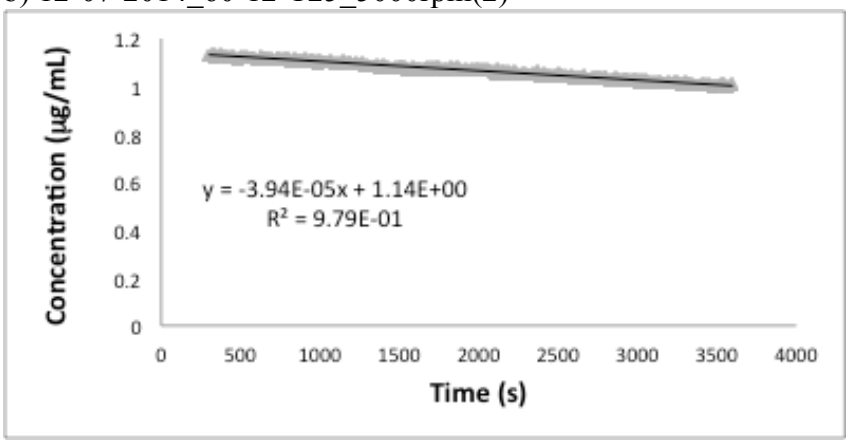

c) 12192014_RDAexp_5000rpm_Sof4(2)

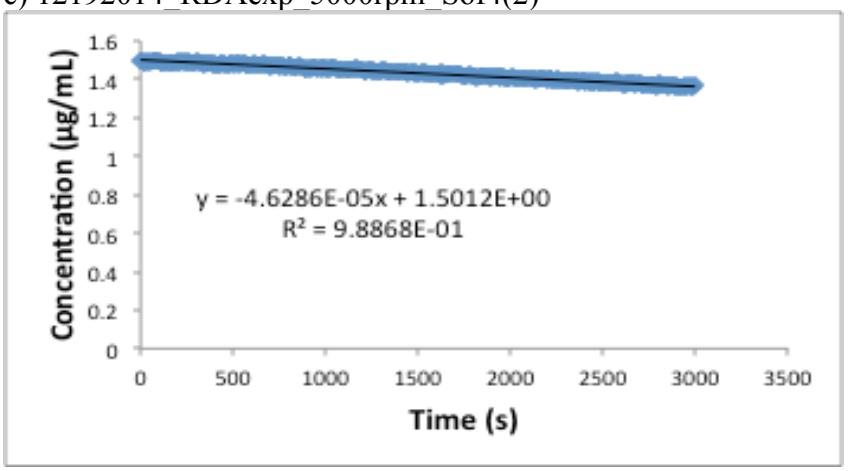

Figure B.8 (a-c) Desupersaturation profiles for pure felodipine (S of 4, no polymers present). **ω = 5000 rpm.**

a) 10172014_RDAexp_6000rpm_Sof4(2)

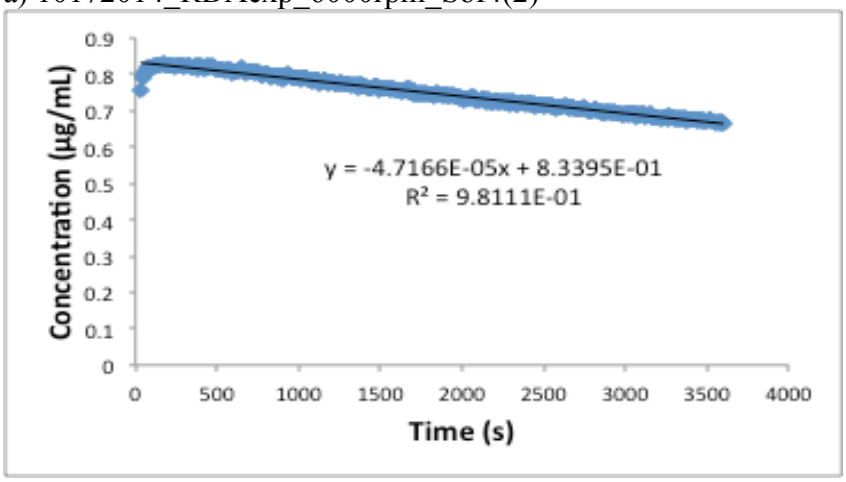

b) 11112014_RDAexp_6000rpm_Sof4

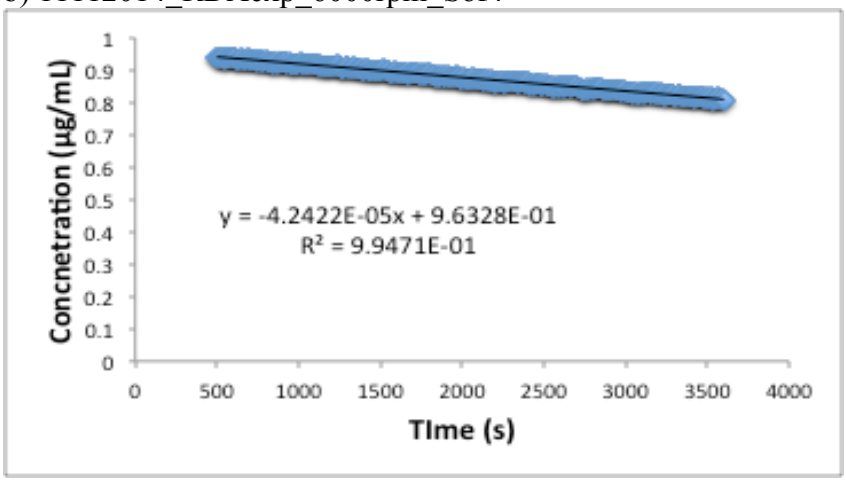

c) 01-25-2015_RDAexpPure_6000rpm_60-12-T25

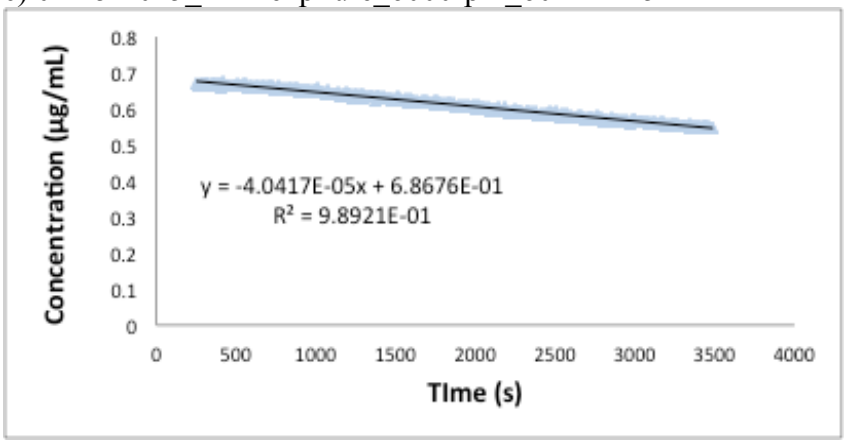

Figure B.9. (a-c) Desupersaturation profiles for pure felodipine (S of 4, no polymers present). **ω = 6000 rpm.**

a) 04-02-2015_RDAexpHPMCAS_200rpm_60-12-T25 and 04-02-2015_RDAexpHPMCAS_200rpm_60-12-T25(1.2)

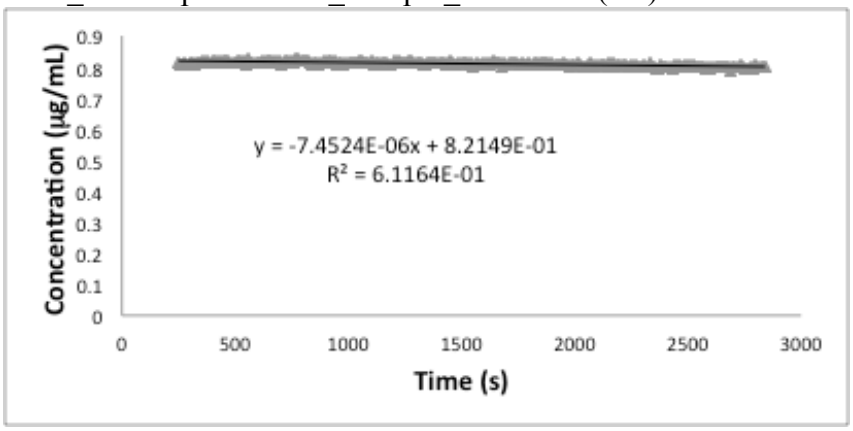

b) 05272015_RDAexp_Sof4_200rpm_wHPMCAS

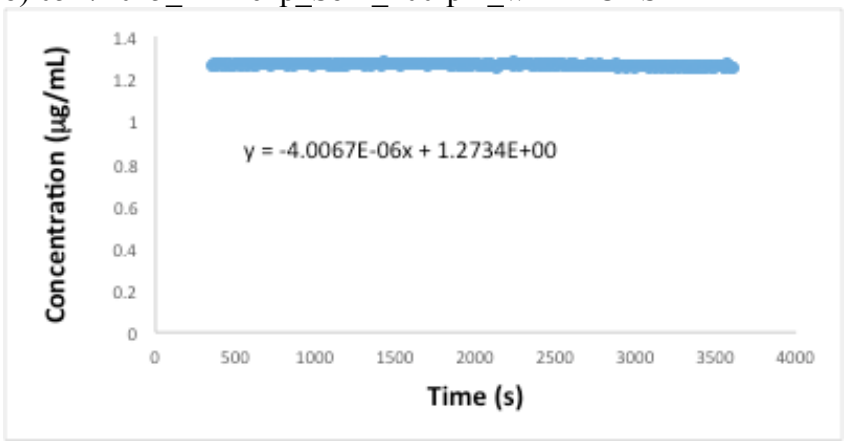

c) 06122015_RDAexp_Sof4_200rpm_wHPMCAS

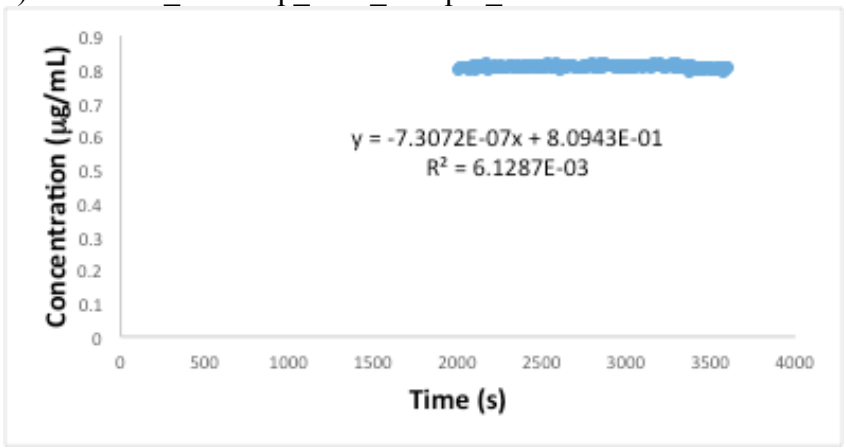

Figure B.10. (a-c) Desupersaturation profiles for felodipine (S of 4) with 5 µg/mL **HPMCAS** present in solution. **ω = 200 rpm.**

a) 02-17-2015_RDAexpHPMCAScomp_500rpm_60-12-T25

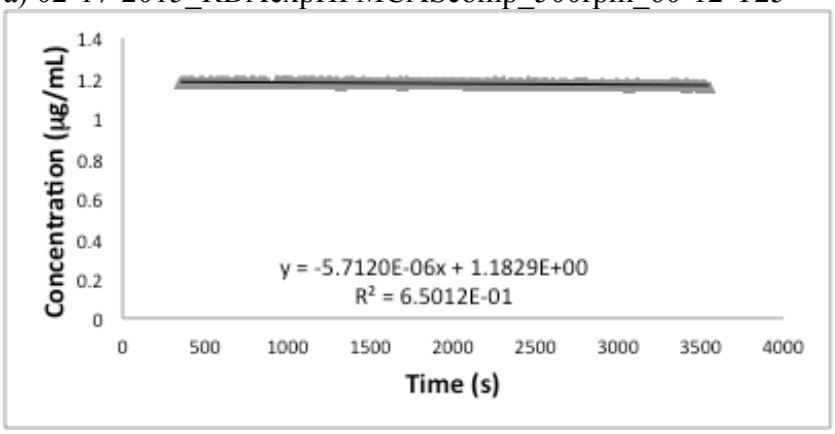

b) 11122014_RDAexp_500rpm_Sof4_wHPMCAS

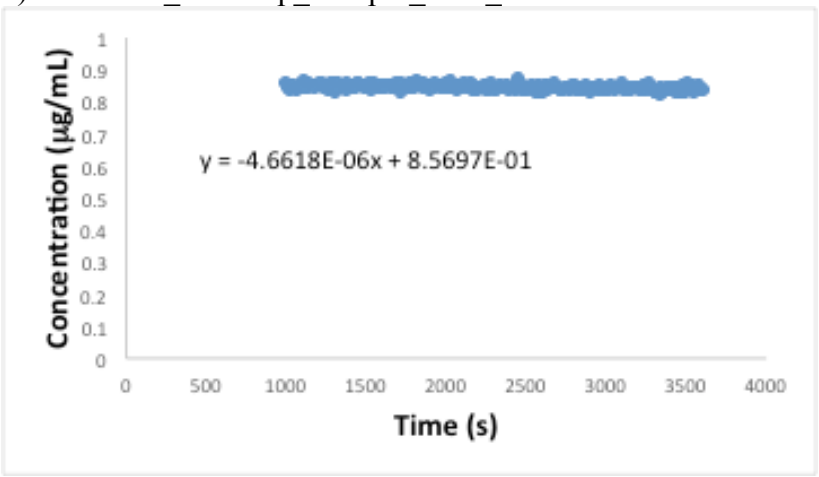

c) 05282015_RDAexp_Sof4_500rpm_wHPMCAS

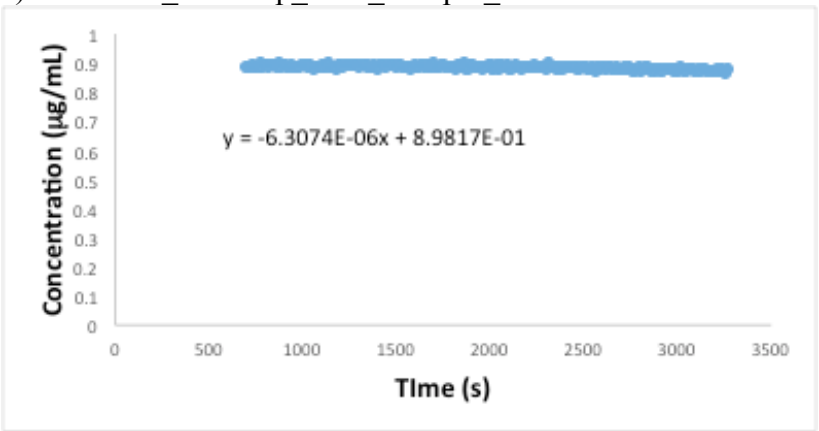

Figure B.11. (a-c) Desupersaturation profiles for felodipine (S of 4) with 5 µg/mL **HPMCAS** present in solution. **ω = 500 rpm.**

a) 11122014_RDAexp_1000rpm_Sof4_wHPMCAS

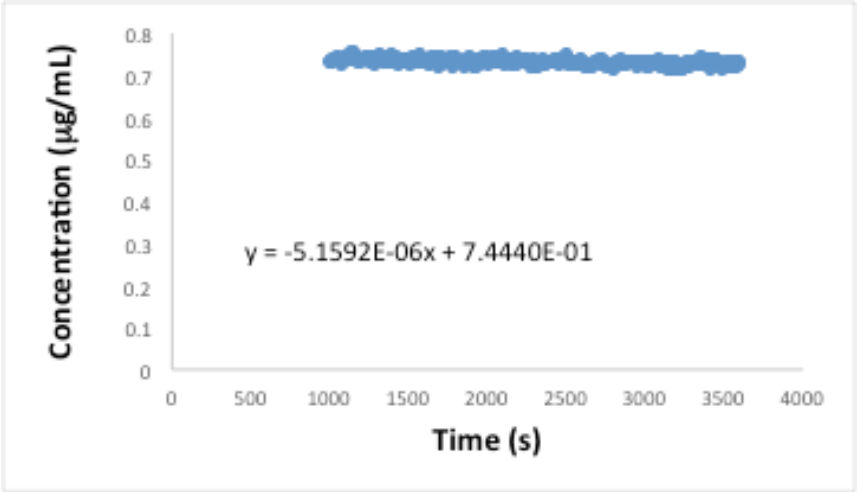

b) 03-03-2015_RDAexpHPMCAS2_1000rpm_60-12-T25

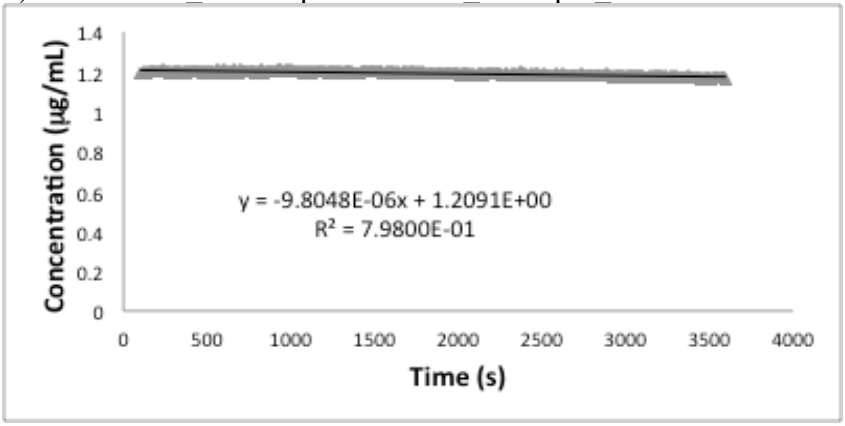

c) 03-03-2015_RDAexpHPMCAS_1000rpm_60-12-T25

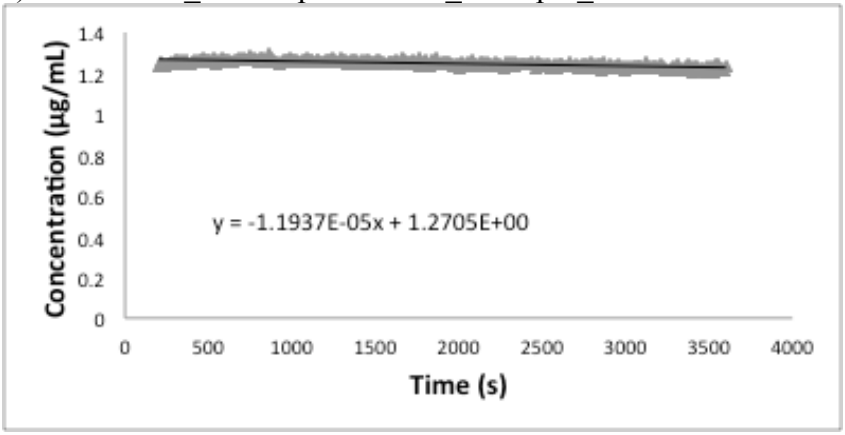

Figure B.12. (a-c) Desupersaturation profiles for felodipine (S of 4) with 5 µg/mL **HPMCAS** present in solution. **ω = 1000 rpm.**

a) 11132014_RDAexp_1500rpm_Sof4_wHPMCAS

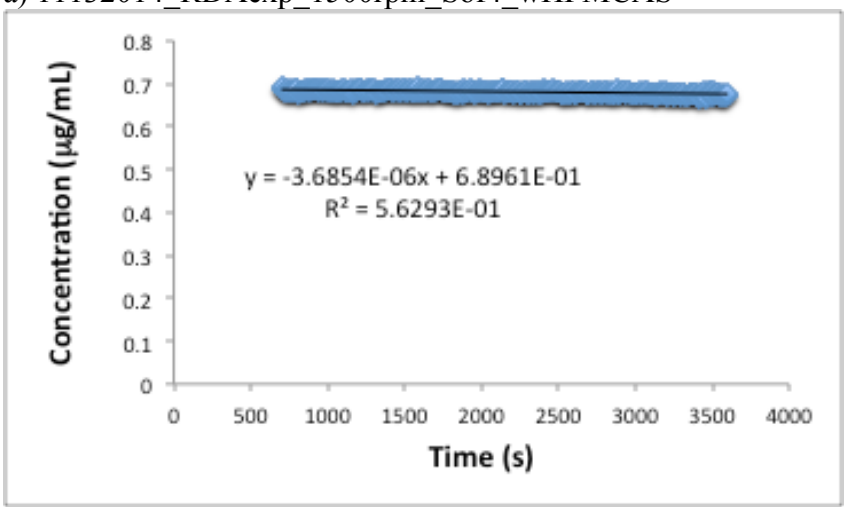

b) 12232014_RDAexp_1500rpm_Sof4_wHPMCAS

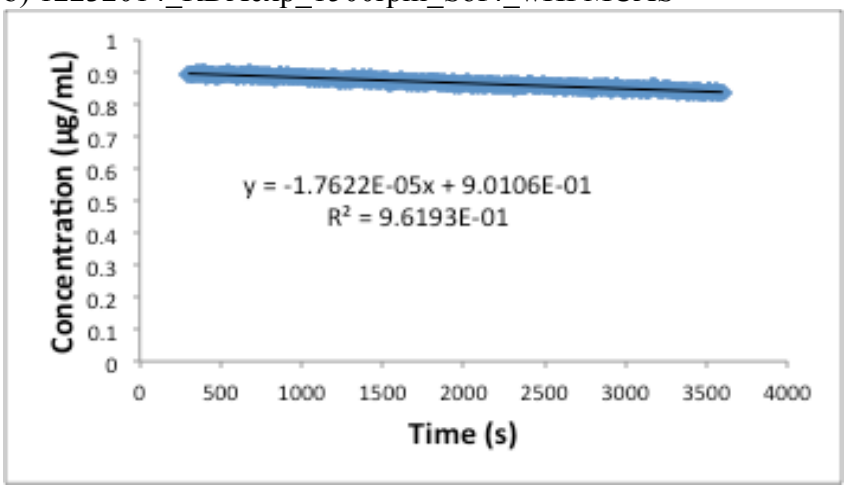

c) 02182015_RDAexp_1500rpm_Sof4_wHPMCAS

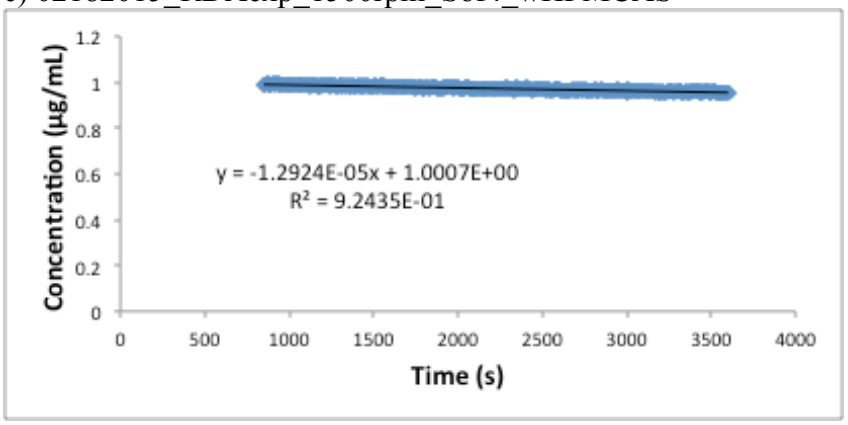

Figure B.13. (a-c) Desupersaturation profiles for felodipine (S of 4) with 5 µg/mL **HPMCAS** present in solution. **ω = 1500 rpm.**

a) 11142014_RDAexp_2000rpm_Sof4_wHPMCAS_2

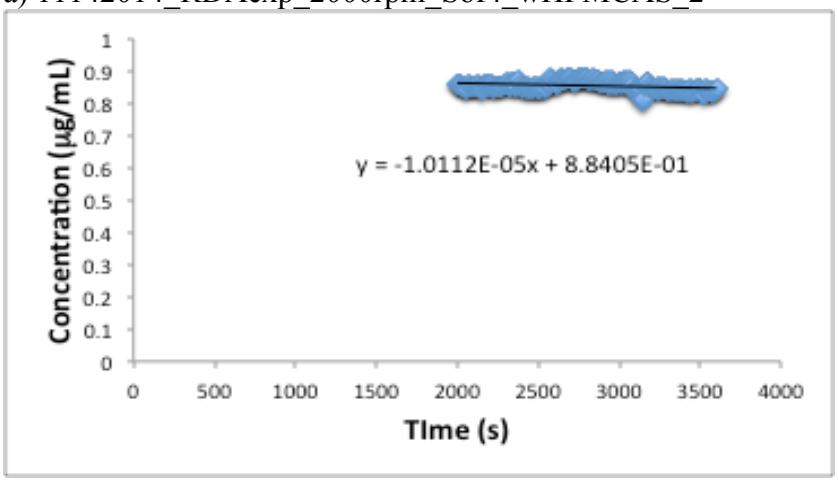

b) 12232014_RDAexp_2000rpm_Sof4_wHPMCAS

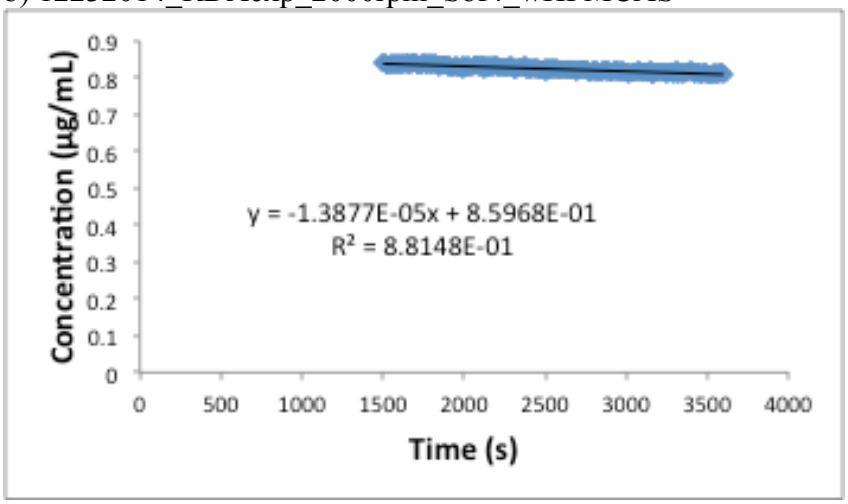

c) 08272015_RDAexp_Sof4_2000rpm_wHPMCAS

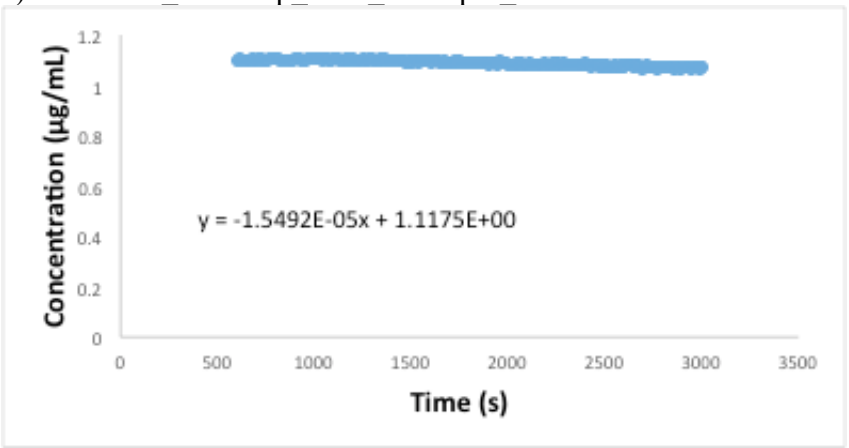

Figure B.14. (a-c) Desupersaturation profiles for felodipine (S of 4) with 5 µg/mL HPMCAS present in solution. **ω = 2000 rpm.**

a) 11122014_RDAexp_3000rpm_Sof4_wHPMCAS(2)

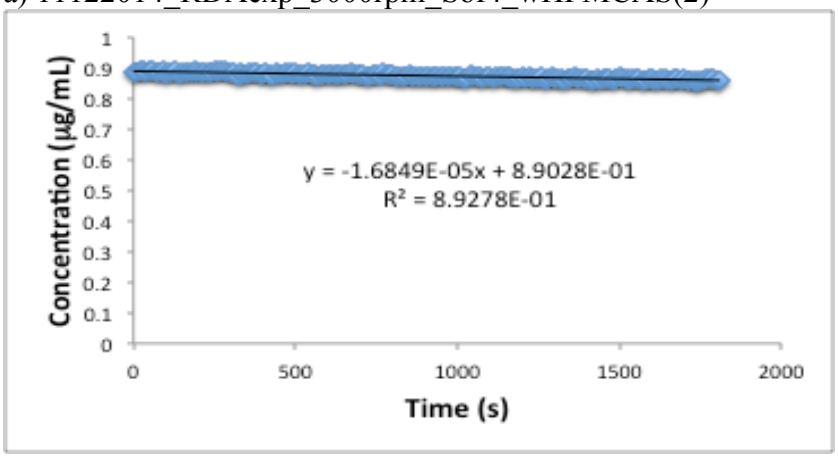

b) 02-26-2015_RDAexpHPMCAScomp_3000rpm_60-12-T25

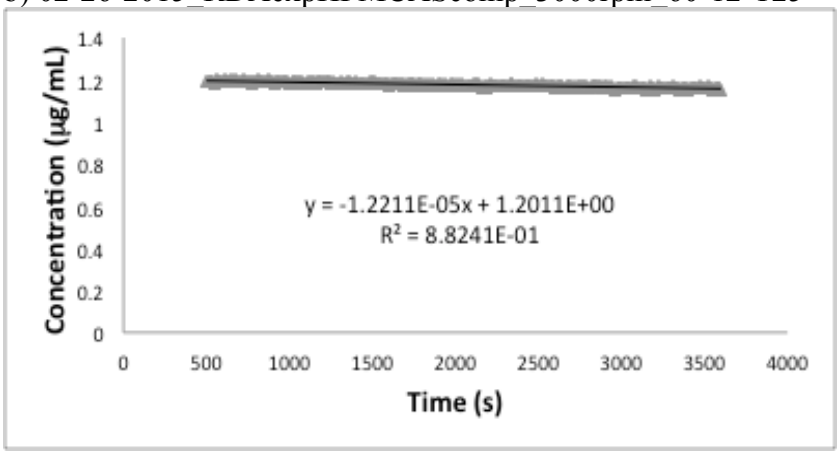

c) 09082015_RDAexp_Sof4_3000rpm_wHPMCAS_2

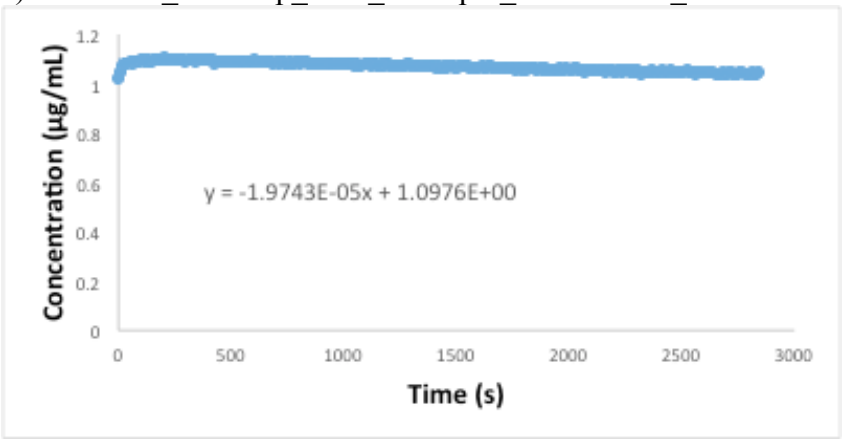

Figure B.15. (a-c) Desupersaturation profiles for felodipine (S of 4) with 5 µg/mL HPMCAS present in solution. **ω = 3000 rpm.**

a) 12222014_RDAexp_4000rpm_Sof4_wHPMCAS(2)

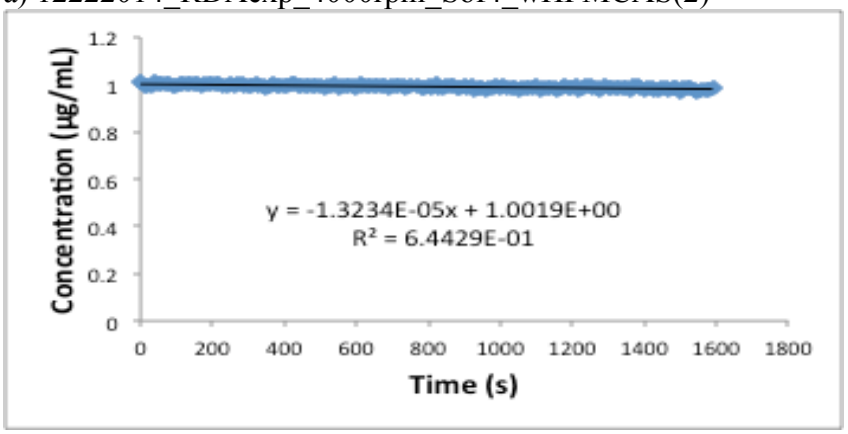

b) 02-26-2015_RDAexpHPMCAScomp2_4000rpm_60-12-T25

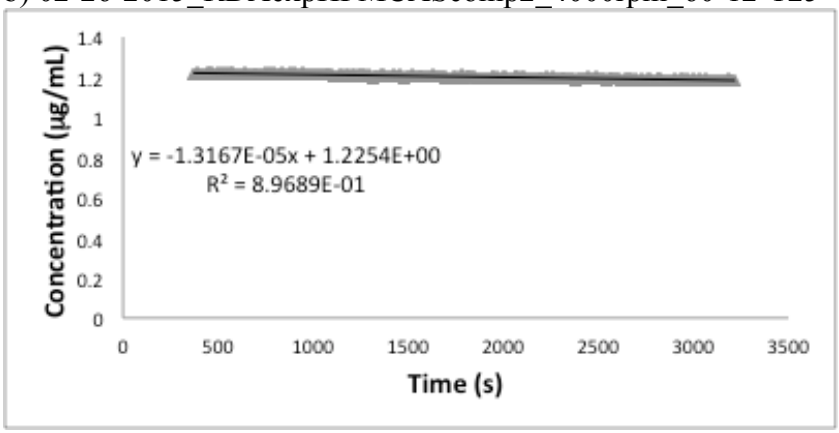

c) 05272015_RDAexp_Sof4_4000rpm_wHPMCAS

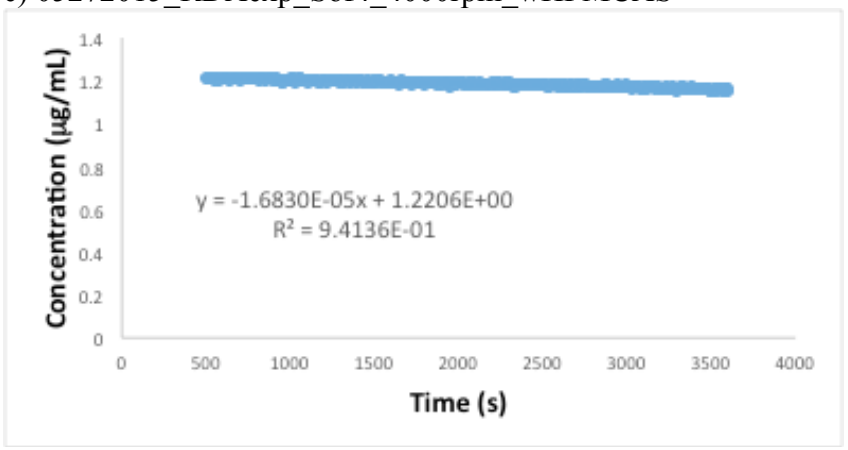

Figure B.16. (a-c) Desupersaturation profiles for felodipine (S of 4) with 5 µg/mL HPMCAS present in solution. **ω = 4000 rpm.**

a) 03-03-2015_RDAexpHPMCAS_5000rpm_60-12-T25

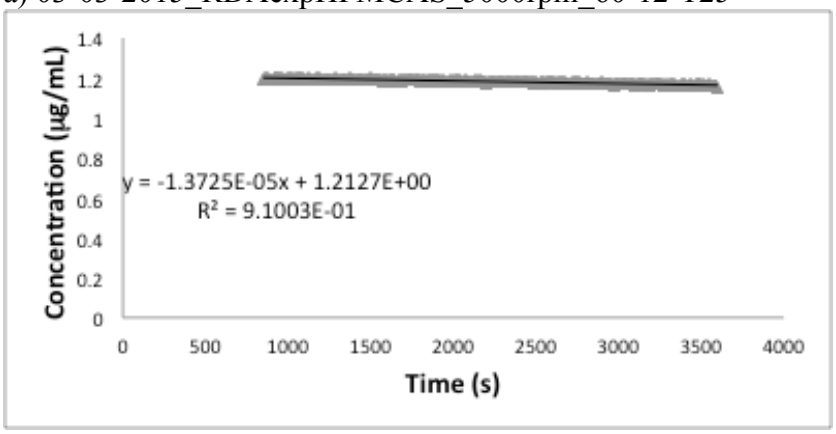

b) 05222015_RDAexp_Sof4_5000rpm_wHPMCAS_2

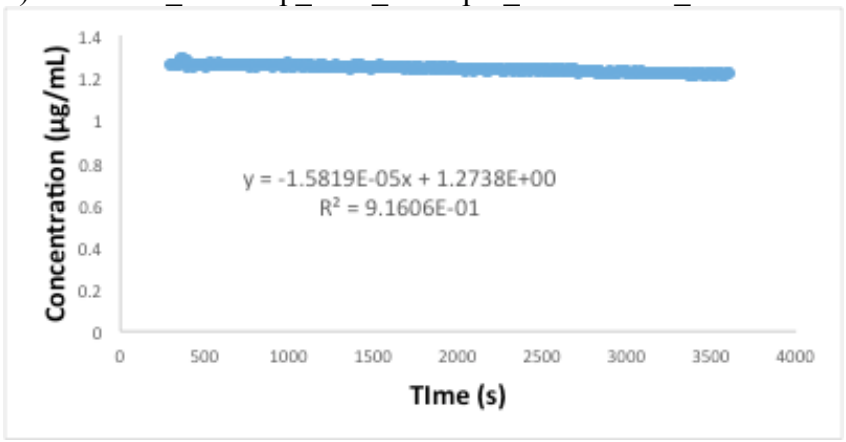

c) 05222015_RDAexp_Sof4_5000rpm_wHPMCAS_3

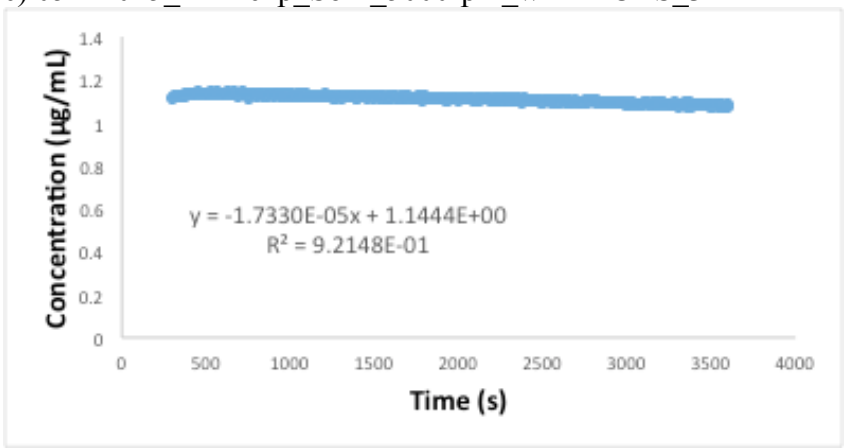

Figure B.17. (a-c) Desupersaturation profiles for felodipine (S of 4) with 5 µg/mL HPMCAS present in solution. **ω = 5000 rpm.**

a) 11122014_RDAexp_6000rpm_Sof4_wHPMCAS

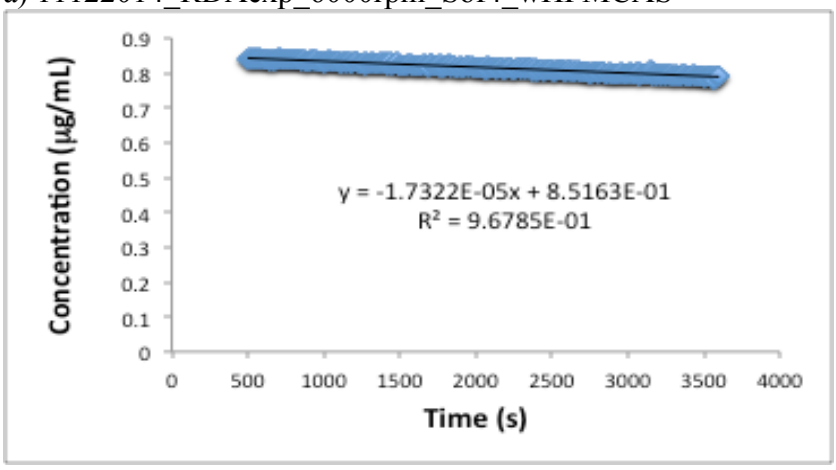

b) 12222014_RDAexp_6000rpm_Sof4_wHPMCAS

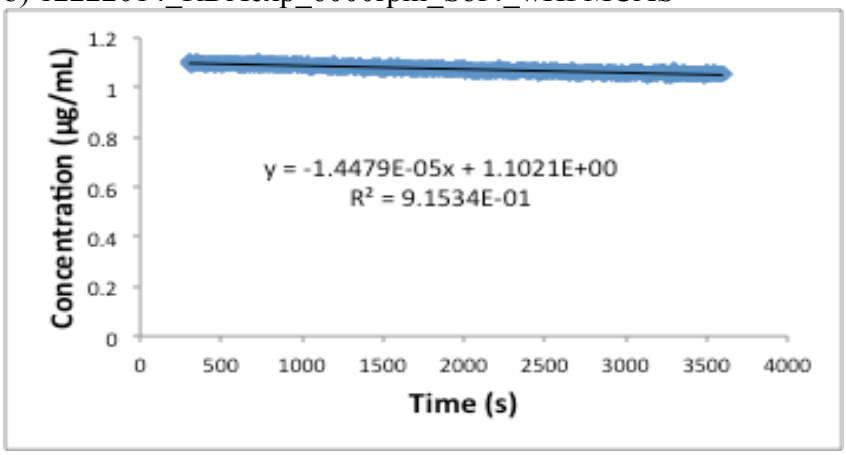

c) 04072014_RDAexp_6000rpm_Sof4_wHPMCAS_2 and 04072014_RDAexp_6000rpm_Sof4_wHPMCAS_2(2)

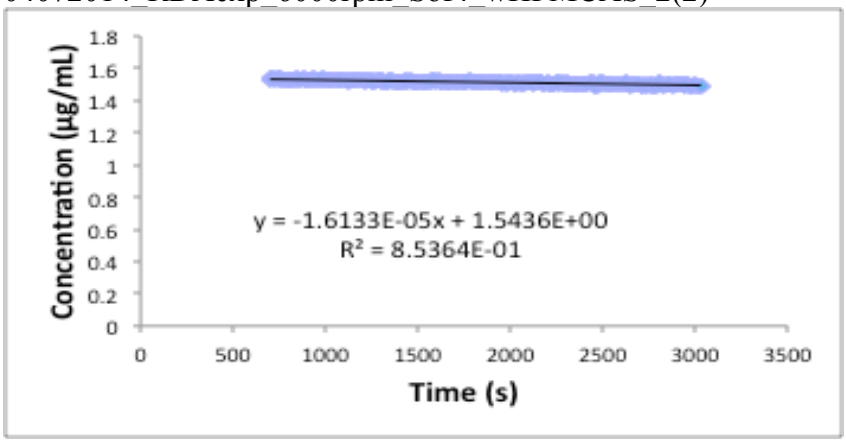

Figure B.18. (a-c) Desupersaturation profiles for felodipine (S of 4) with 5 µg/mL HPMCAS present in solution. **ω = 6000 rpm.**

B.2 Data for Figure 3.3

a) 08122015_RDAexp_Sof2_4000rpm

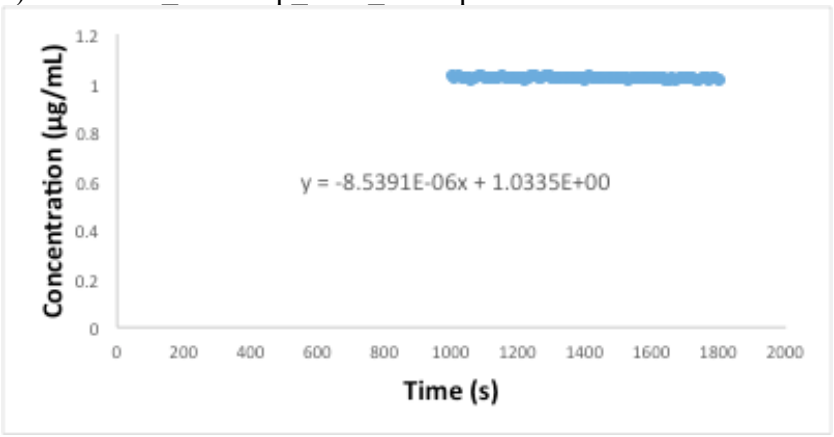

b) 08122015_RDAexp_Sof2_4000rpm_2

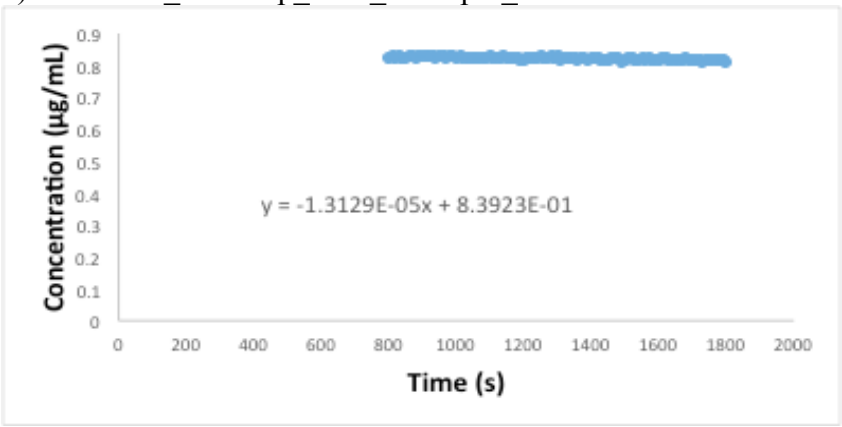

c) 08262015_RDAexp_Sof2_4000rpm

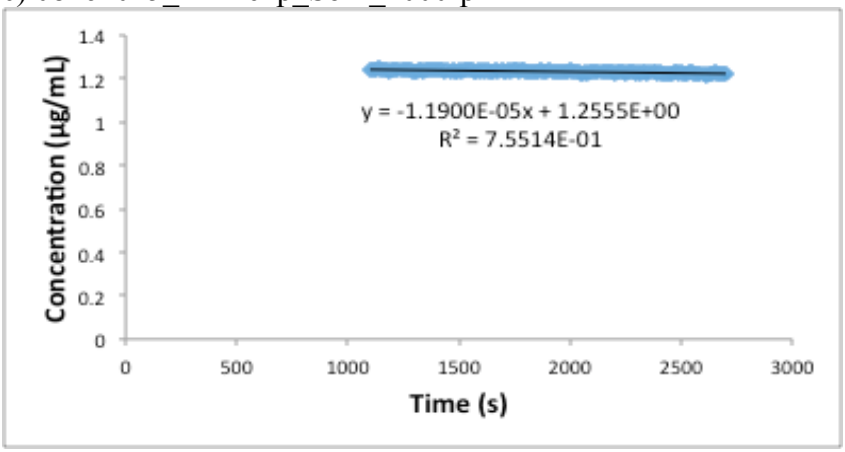

Figure B.19. (a-c) Desupersaturation profiles for felodipine (**S of 2**, no polymers present). ω = 4000 rpm**.**

a) 07312015_RDAexp_Sof3_4000rpm

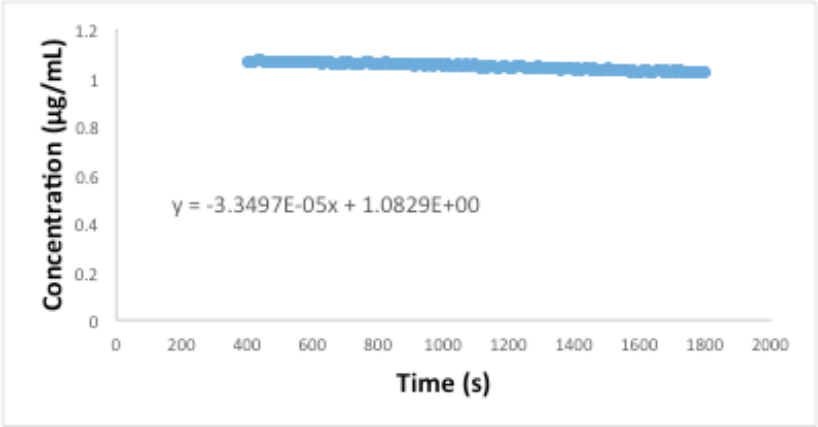

b) 08032015_RDAexp_Sof3_4000rpm

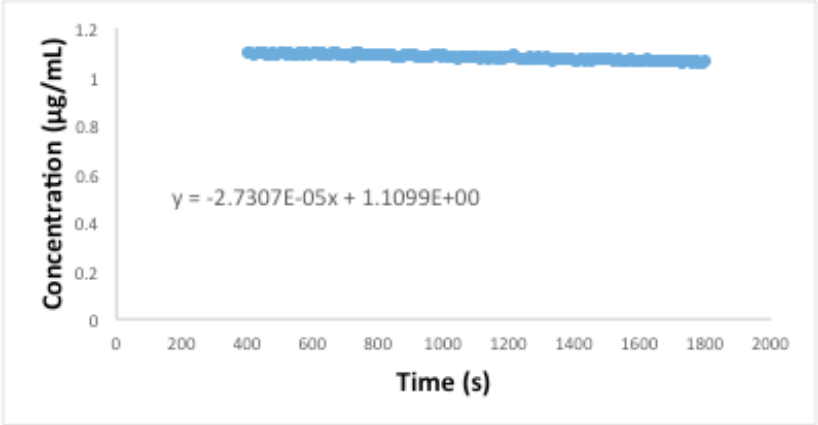

c) 09082015_RDAexp_Sof3_4000rpm

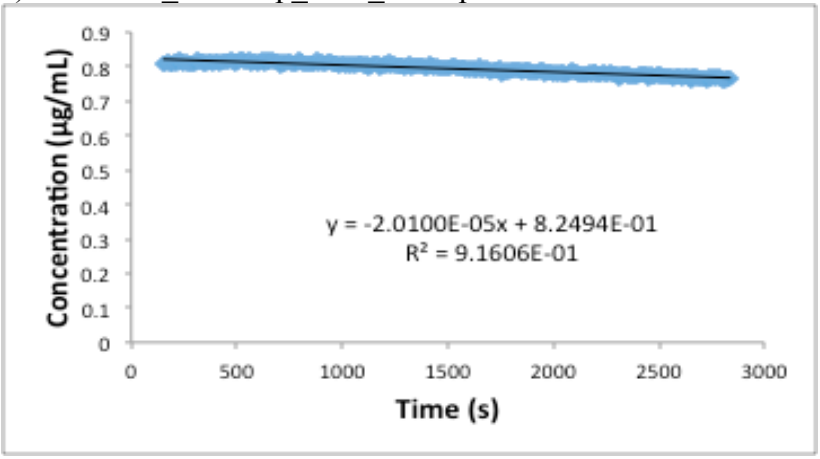

Figure B.20. (a-c) Desupersaturation profiles for felodipine (**S of 4**, no polymers present). ω = 4000 rpm**.**

a) 07312015_RDAexp_Sof5_4000rpm

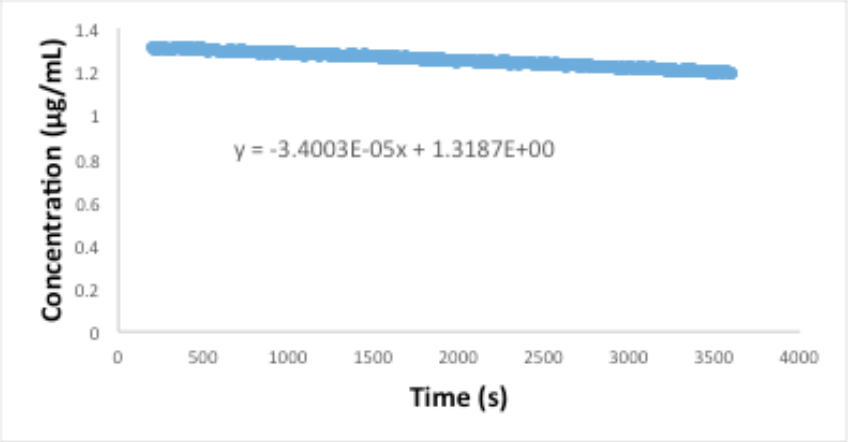

b) 08032015_RDAexp_Sof5_4000rpm

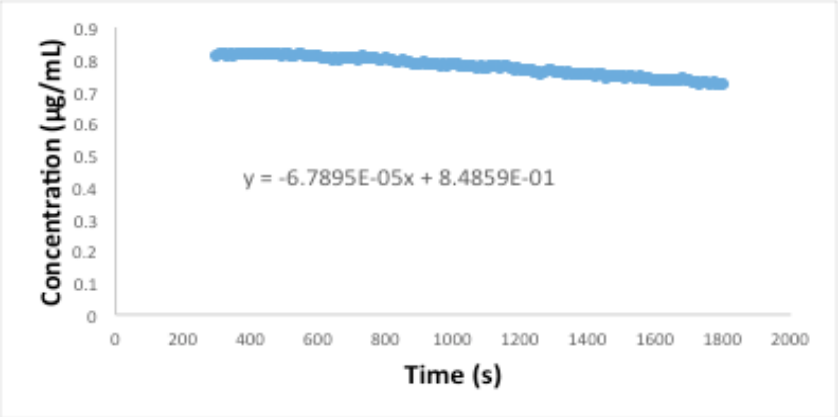

c) 08122015_RDAexp_Sof5_4000rpm

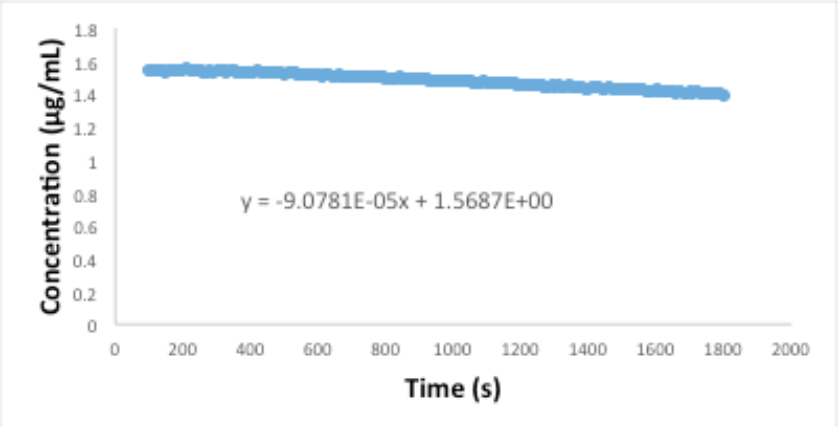

Figure B.21. (a-c) Desupersaturation profiles for felodipine (**S of 5**, no polymers present). ω = 4000 rpm**.**

a) 07312015_RDAexp_Sof6_4000rpm_2

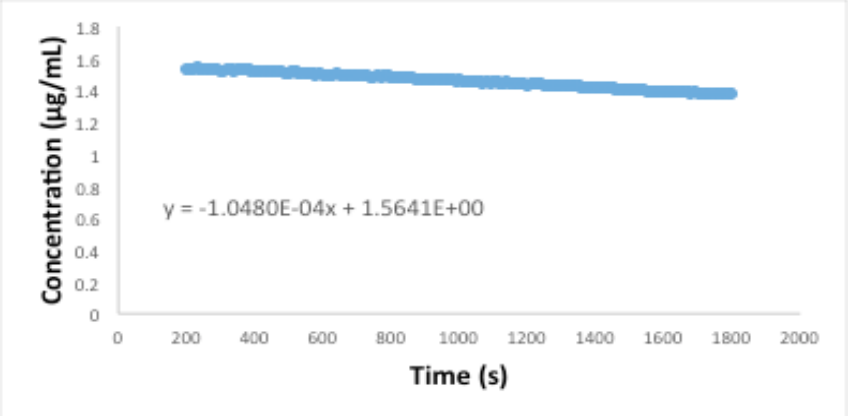

b) 08122015_RDAexp_Sof6_4000rpm

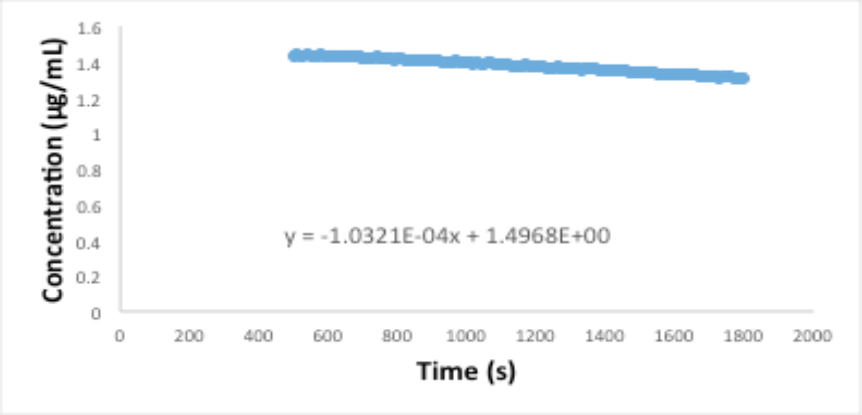

c) 07172015_RDAexp_Sof6_4000rpm

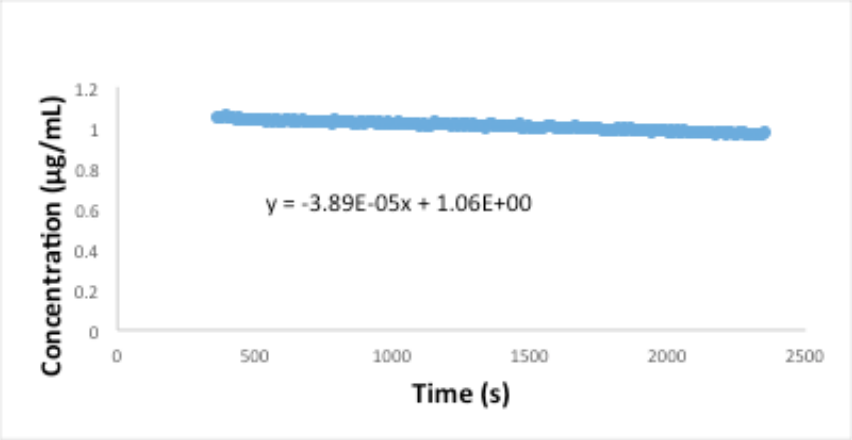

Figure B.22. (a-c) Desupersaturation profiles for felodipine (**S of 6**, no polymers present). ω = 4000 rpm**.**

B.3 Data for Figure 4.2

a) From RS data

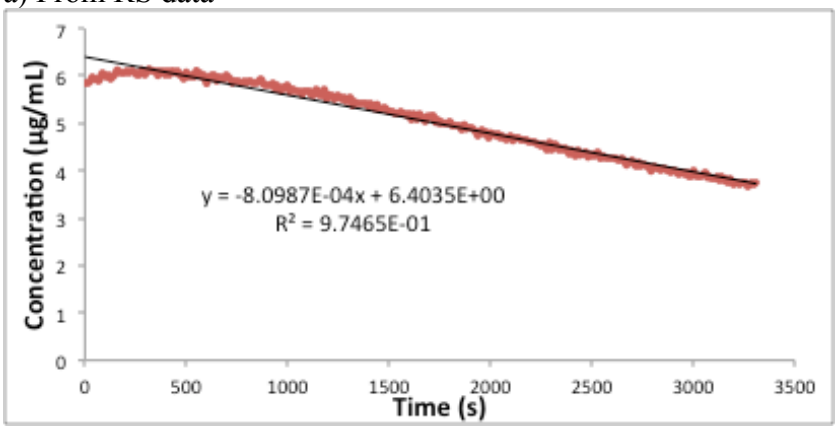

b) From RS data

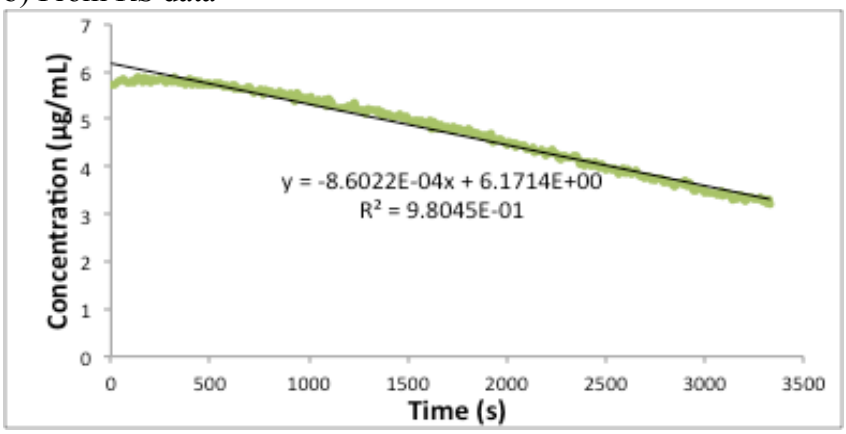

c) From RS data

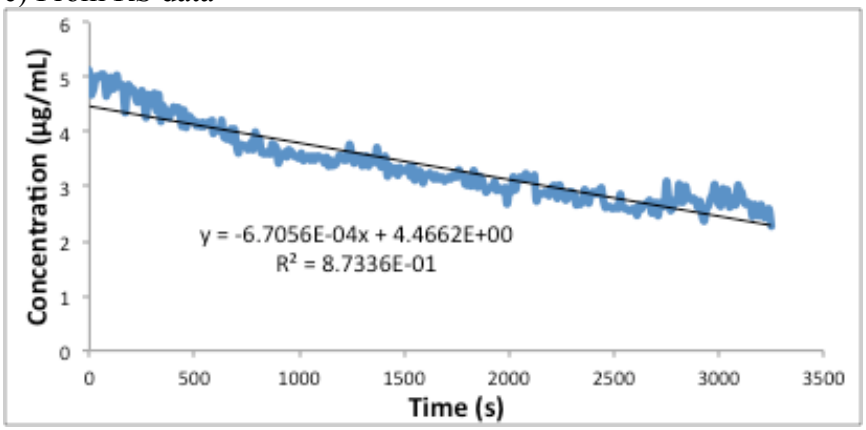

Figure B.23. (a-c) Desupersaturation profiles for felodipine (S of 8, no polymers present) at **pH 6.8**. ω = 1000 rpm**.**

a) From RS data

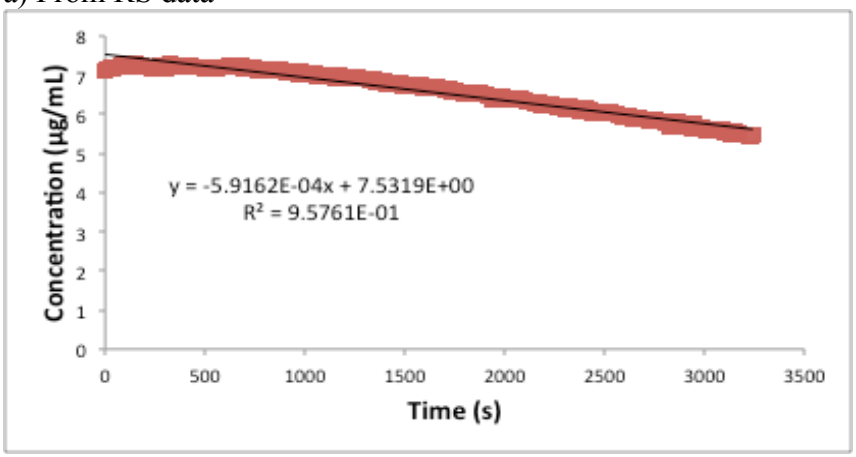

b) From RS data

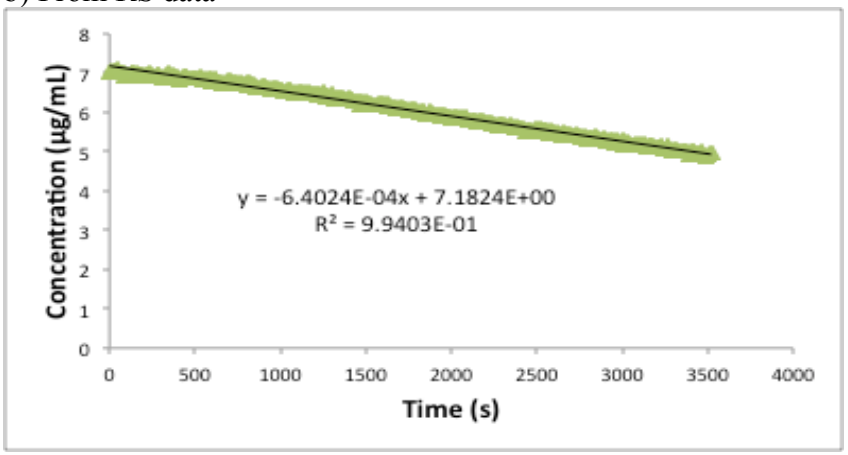

c) From RS data

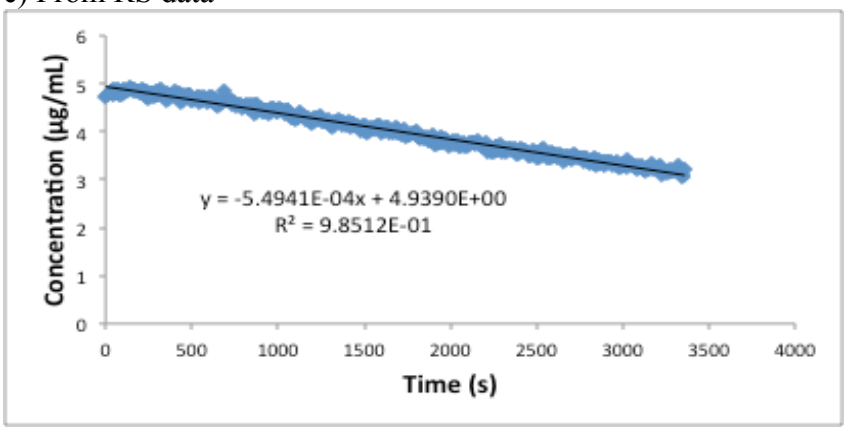

Figure B.24. (a-c) Desupersaturation profiles for felodipine (S of 8) with 5 µg/mL **HPMCAS** present in solution at **pH 3**. ω = 1000 rpm**.**

a) From RS data

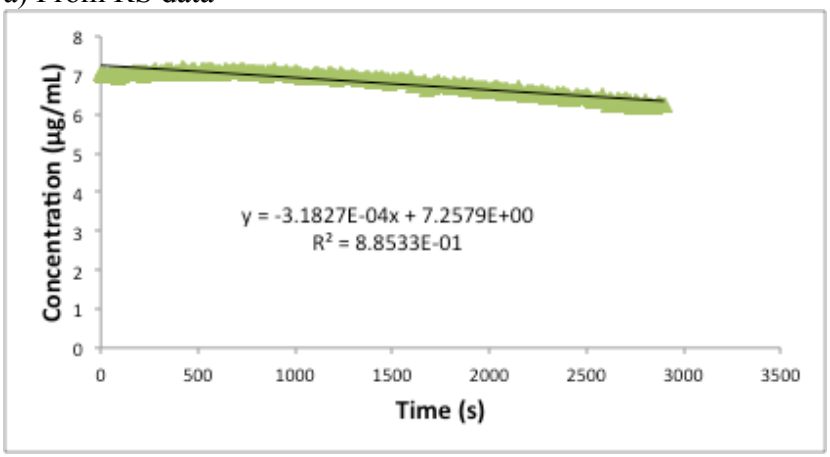

b) From RS data

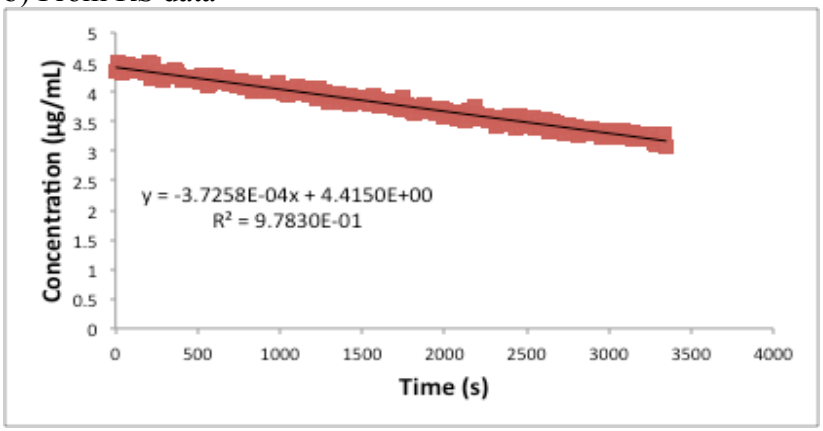

c) From RS data

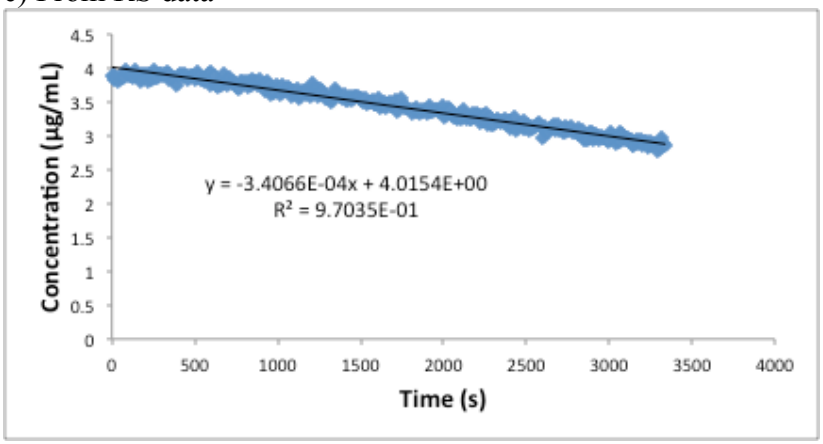

Figure B.25. (a-c) Desupersaturation profiles for felodipine (S of 8) with 5 µg/mL **HPMCAS** present in solution at **pH 6.8**. ω = 1000 rpm**.**

B.4 Data for Figure 5.1

a) 01092015_RDAexp_6000rpm_Sof4_wPAA_2

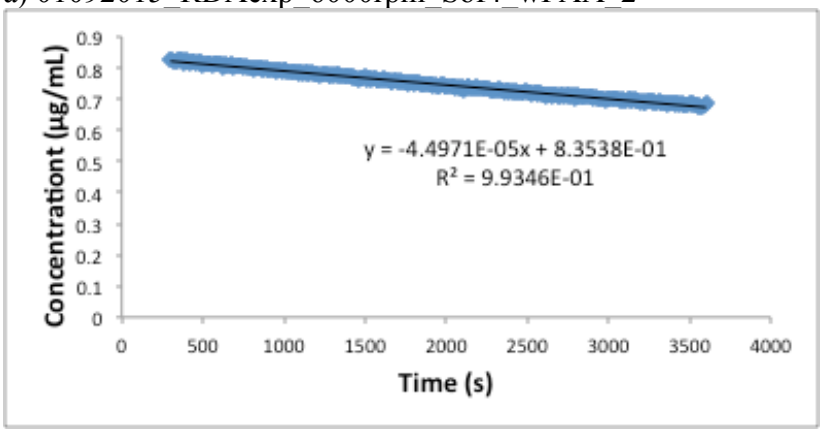

b) 01092015_RDAexp_6000rpm_Sof4_wPAA_4

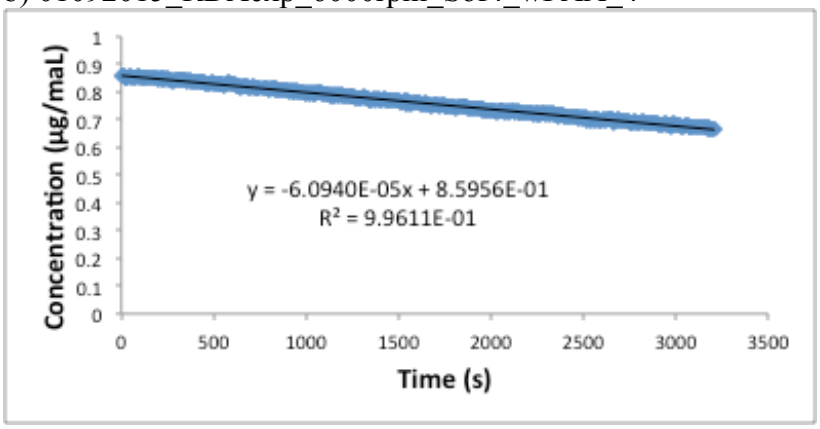

c) 03312015_RDAexp_6000rpm_Sof4_wPAA and 03312015_RDAexp_6000rpm_Sof4_wPAA(2)

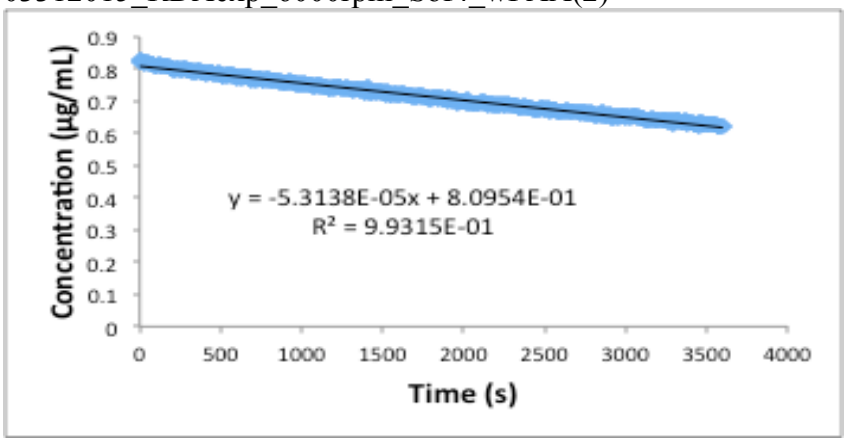

Figure B.26. (a-c) Desupersaturation profiles for felodipine (S of 4) with 5 µg/mL **PAA** present in solution. ω = 6000 rpm**.**

a) 11142014_RDAexp_6000rpm_Sof4_wPVP

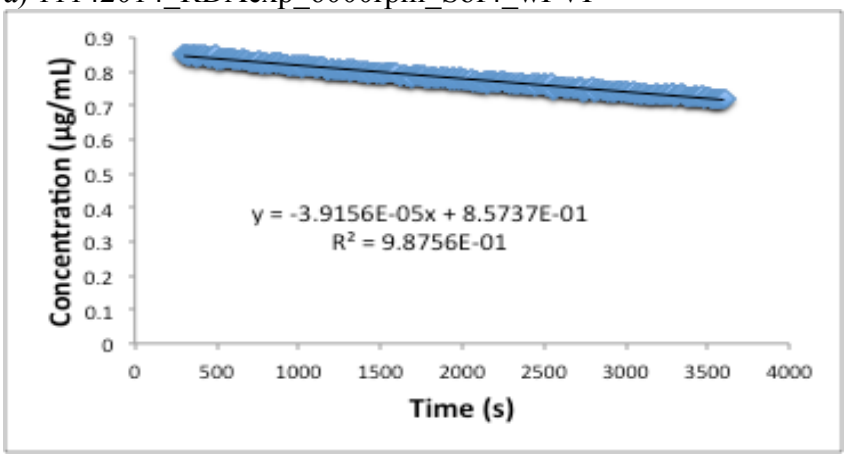

b) 02112015_RDAexp_6000rpm_Sof4_wPVP

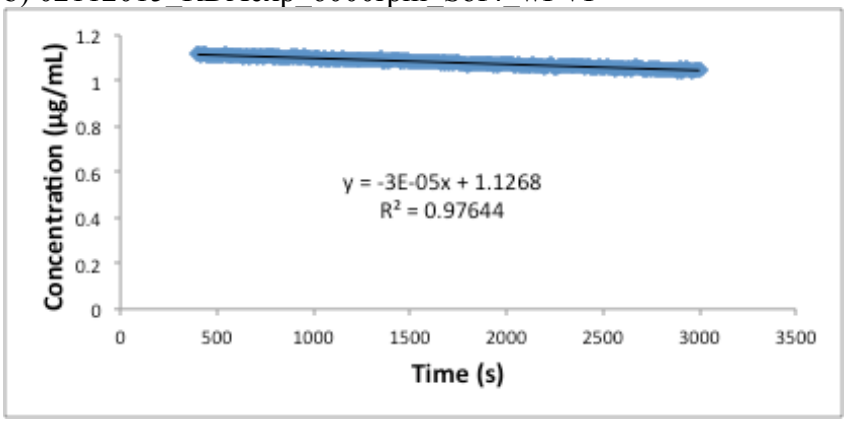

c) 02202015_RDAexp_6000rpm_Sof4_wPVP

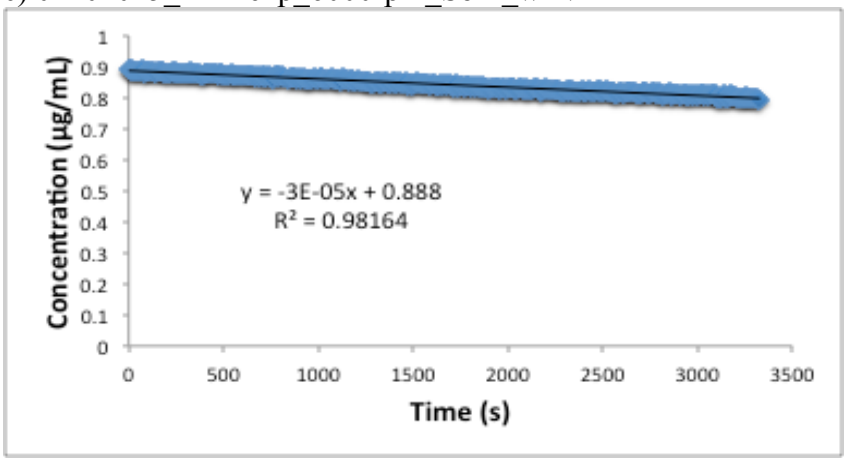

Figure B.27. (a-c) Desupersaturation profiles for felodipine (S of 4) with 5 µg/mL **PVP** present in solution. ω = 6000 rpm**.**

a) 01262015_RDAexp_6000rpm_Sof4_wPVPVA_2

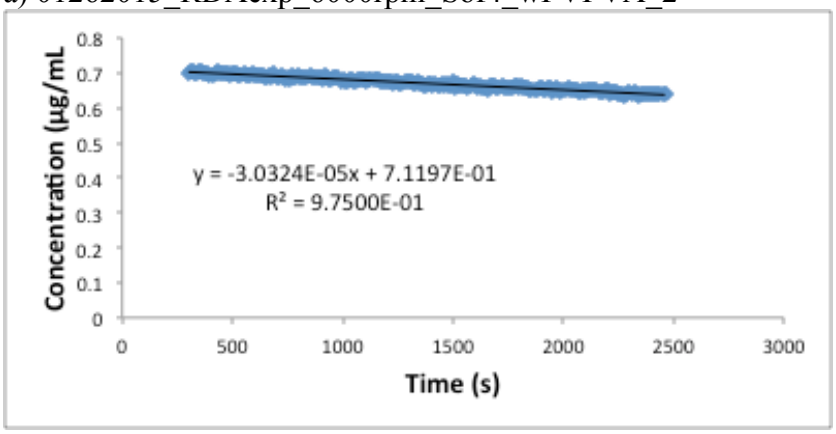

b) 01262015_RDAexp_6000rpm_Sof4_wPVPVA and 01262015_RDAexp_6000rpm_Sof4_wPVPVA(2)

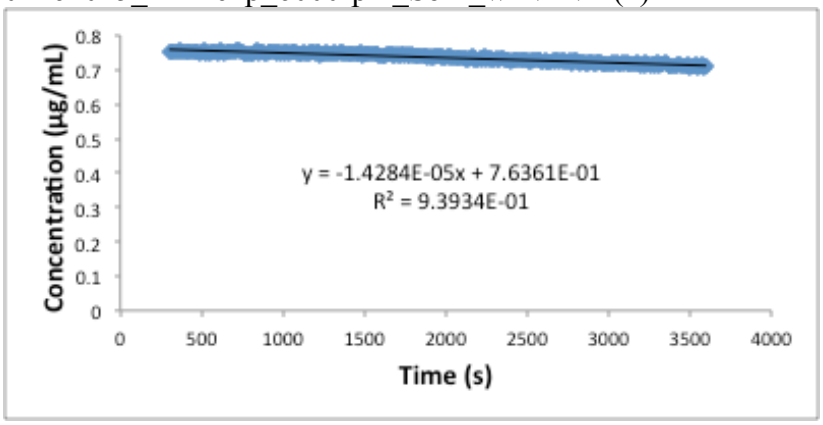

c) 02182015_RDAexp_6000rpm_Sof4_wPVPVA_3

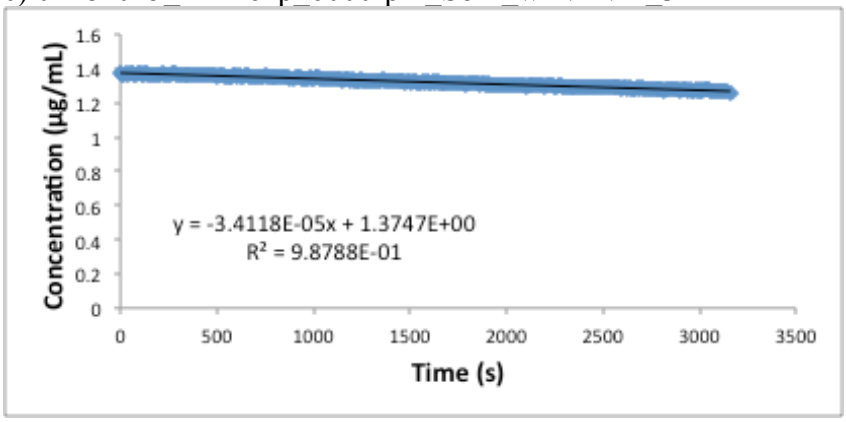

Figure B.28. (a-c) Desupersaturation profiles for felodipine (S of 4) with 5 µg/mL **PVPVA** present in solution. ω = 6000 rpm**.**

a) 02112015_RDAexp_6000rpm_Sof4_wHPMC_2(3)

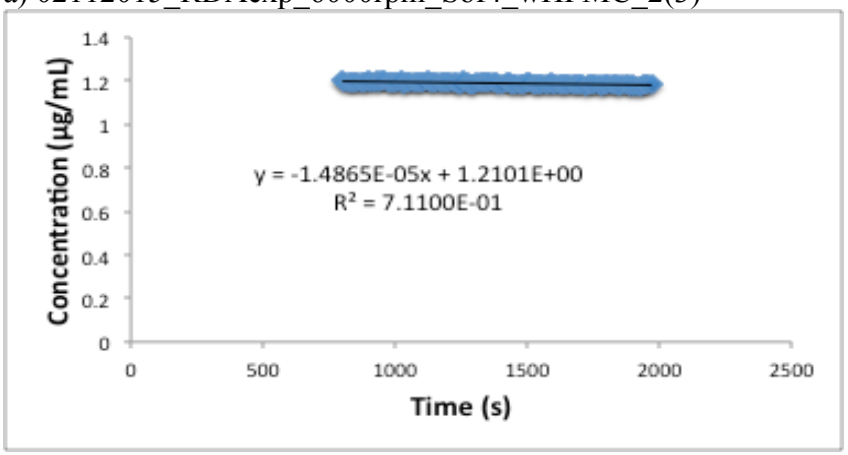

b) 02112015_RDAexp_6000rpm_Sof4_wHPMC_3

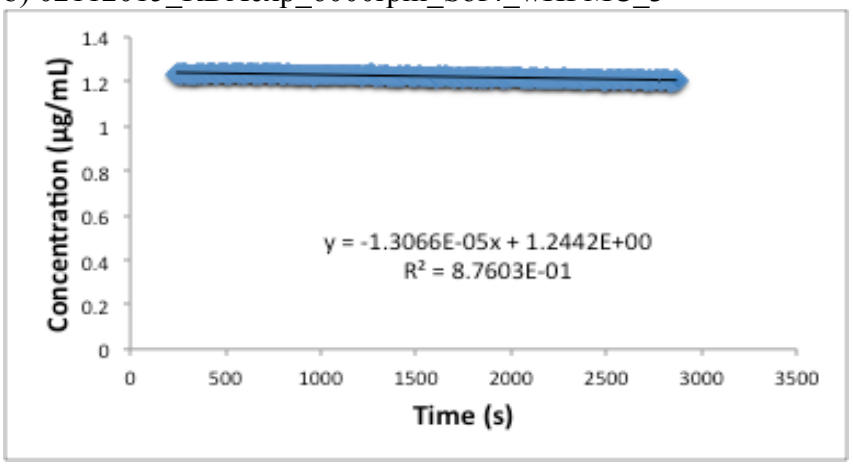

c) 02202015_RDAexp_6000rpm_Sof4_wHPMC_3

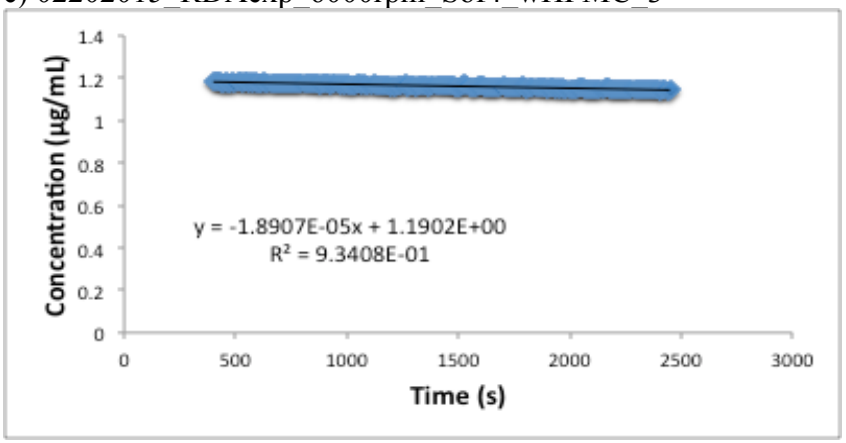

Figure B.29. (a-c) Desupersaturation profiles for felodipine (S of 4) with 5 µg/mL **HPMC** present in solution. ω = 6000 rpm**.**

a) 11132014_RDAexp_6000rpm_Sof4_wP2VP

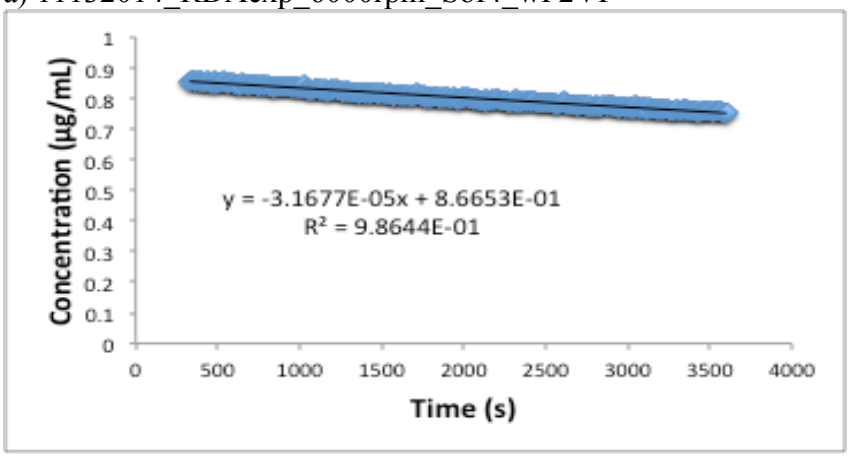

b) 03252015_RDAexp_6000rpm_Sof4_wP2VP

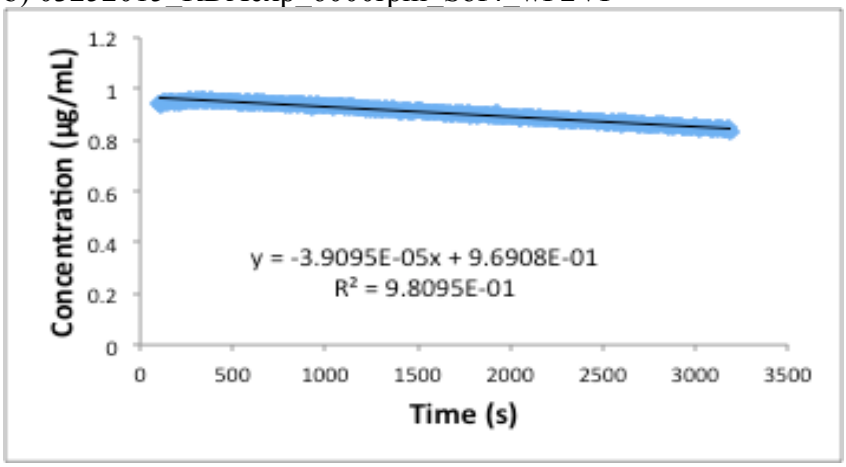

c) 03252015_RDAexp_6000rpm_Sof4_wP2VP_2

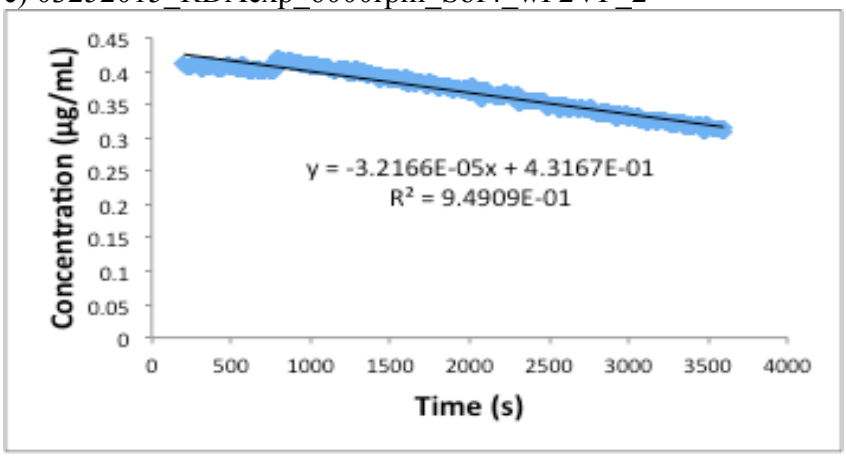

Figure B.30. (a-c) Desupersaturation profiles for felodipine (S of 4) with 5 µg/mL **P2VP** present in solution. ω = 6000 rpm**.**

a) 01212015_RDAexp_6000rpm_Sof4_wPVAc

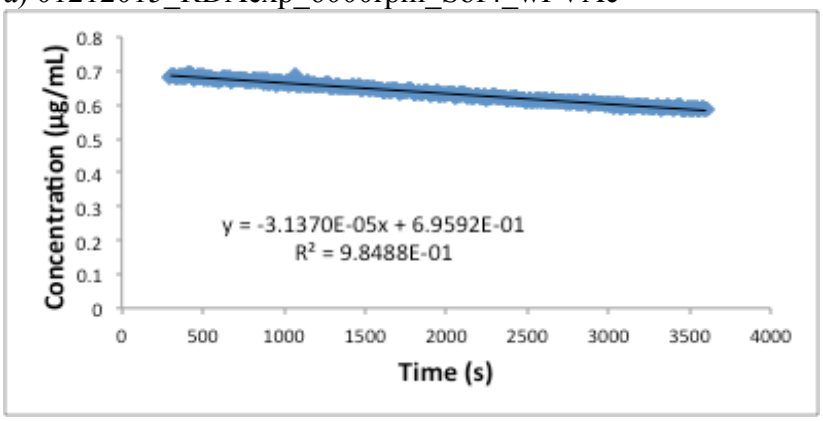

b) 01292015_RDAexp_6000rpm_Sof4_wPVAc_4

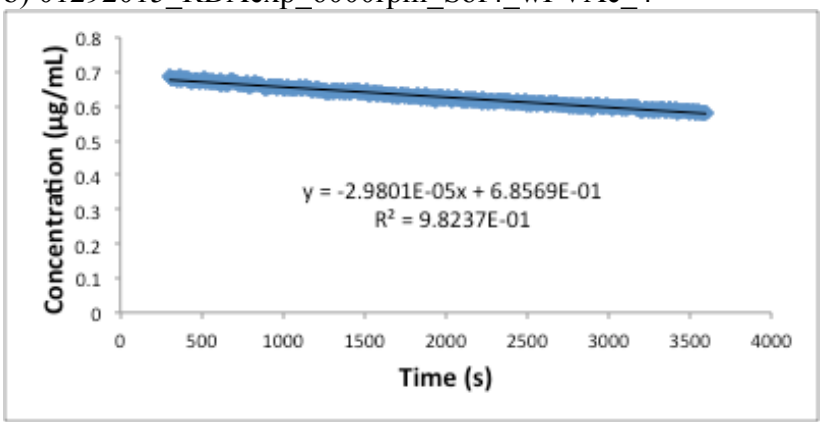

c) 04072014_RDAexp_6000rpm_Sof4_wPVAc and
04072014_RDAexp_6000rpm_Sof4_wPVAc(2) and
04072014_RDAexp_6000rpm_Sof4_wPVAc(3)

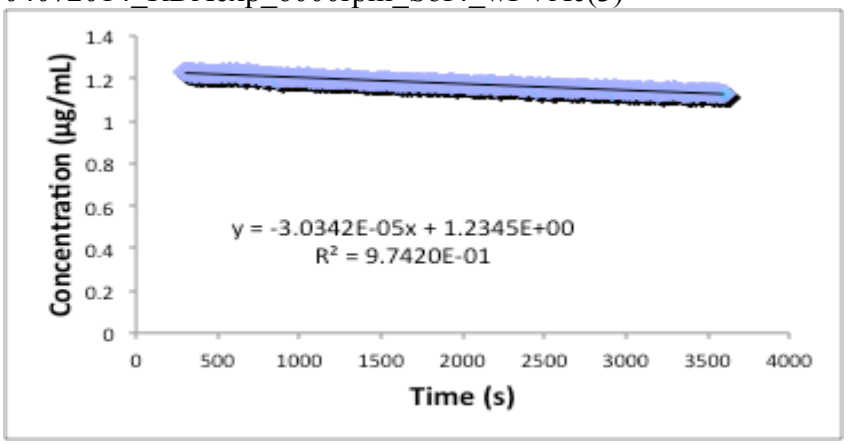

Figure B.31. (a-c) Desupersaturation profiles for felodipine (S of 4) with 5 µg/mL **PVAc** present in solution. ω = 6000 rpm**.**

B.5 Data for Figure 5.3

a) 03102015_RDAexp_6000rpm_Sof4_wPVPVA_10ug

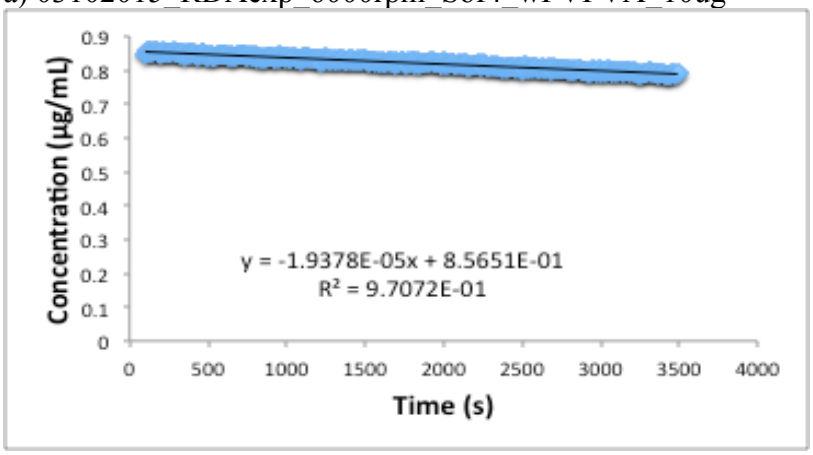

b) 03102015_RDAexp_6000rpm_Sof4_wPVPVA_10ug_2

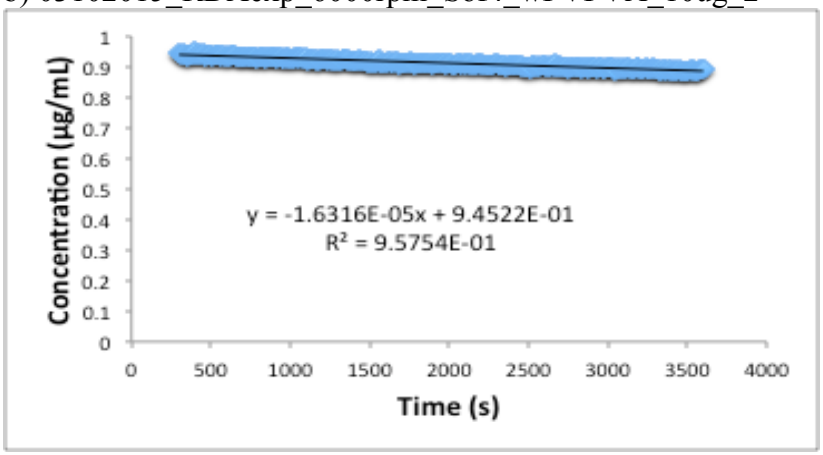

c) 03102015_RDAexp_6000rpm_Sof4_wPVPVA_10ug_3

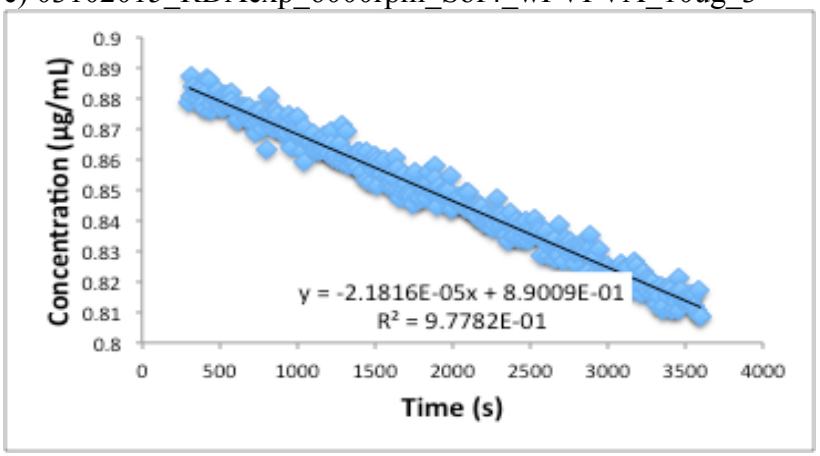

Figure B.32. (a-c) Desupersaturation profiles for felodipine (S of 4) with **10 µg/mL PVPVA** present in solution. ω = 6000 rpm**.**

a) 03112015_RDAexp_6000rpm_Sof4_wPVPandPVAc_5ug_2

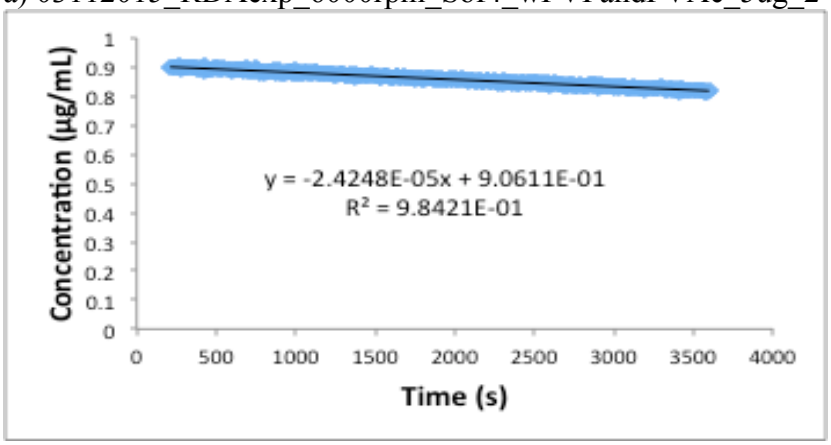

b) 03112015_RDAexp_6000rpm_Sof4_wPVPandPVAc_5ug_3

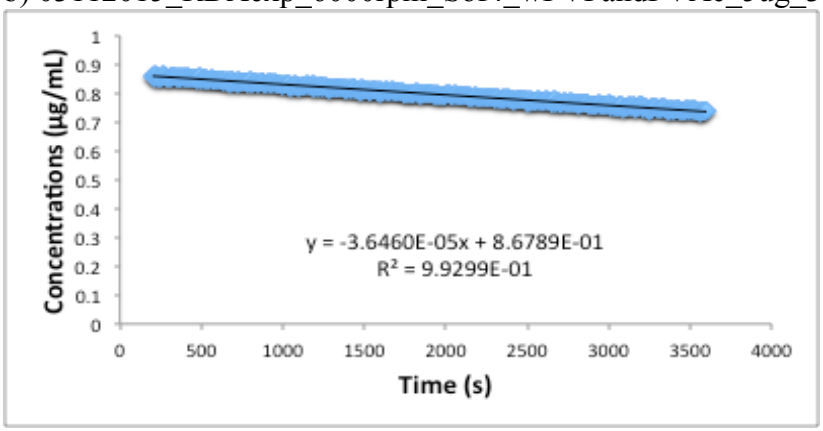

c) 03132015_RDAexp_6000rpm_Sof4_wPVPandPVAc_5ug_4 and 03132015_RDAexp_6000rpm_Sof4_wPVPandPVAc_5ug_4(2) and 03132015_RDAexp_6000rpm_Sof4_wPVPandPVAc_5ug_4(3)

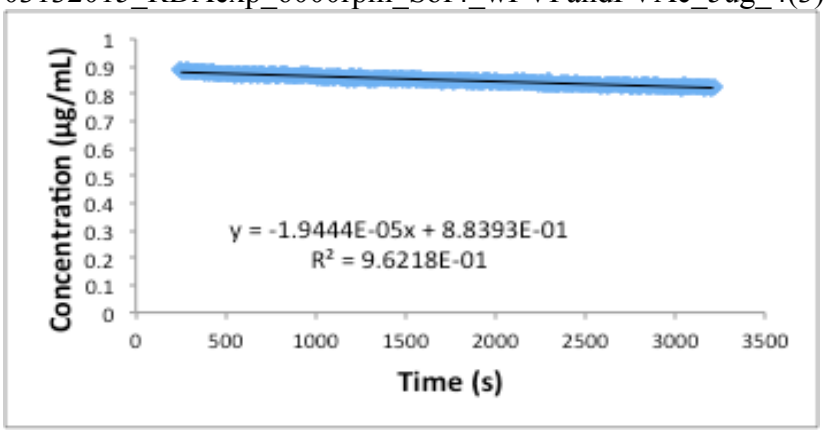

Figure B.33. (a-c) Desupersaturation profiles for felodipine (S of 4) with 5 µg/mL **PVP & PVAc** present in solution. ω = 6000 rpm**.**

a) 02252015_RDAexp_6000rpm_Sof4_wPVPandPVAc

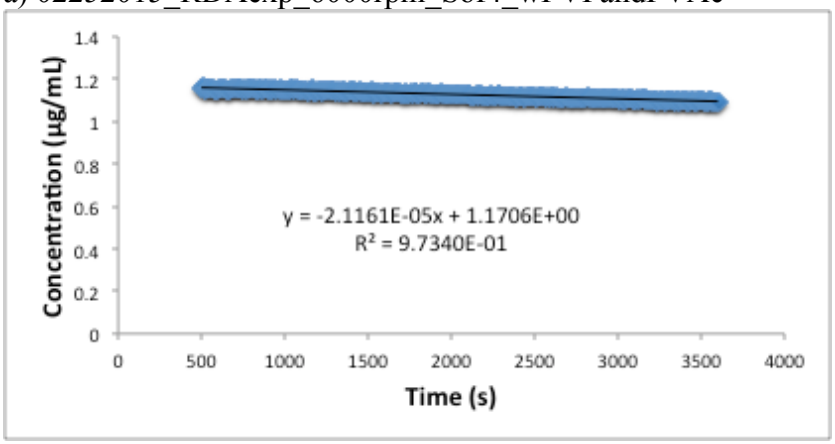

b) 02252015_RDAexp_6000rpm_Sof4_wPVPandPVAc_2

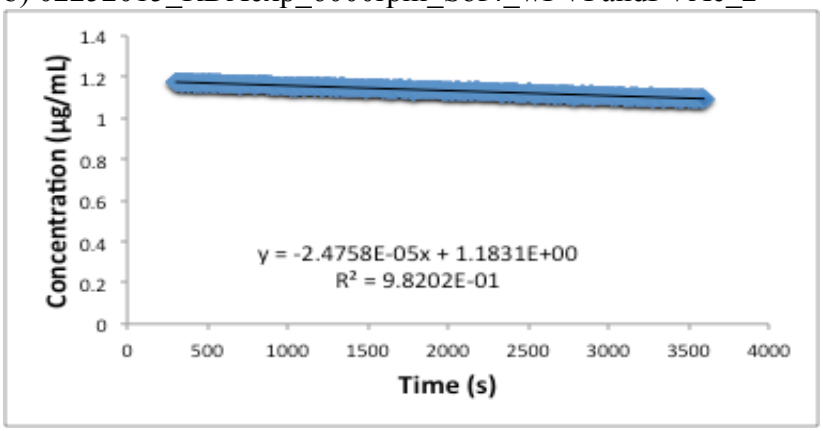

c) 03102015_RDAexp_6000rpm_Sof4_wPVPandPVAc_10ug and 03102015_RDAexp_6000rpm_Sof4_wPVPandPVAc_10ug_2

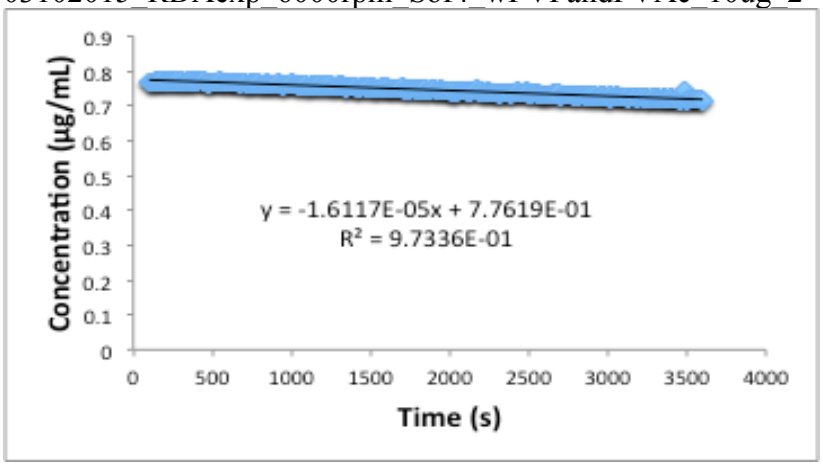

Figure B.34. (a-c) Desupersaturation profiles for felodipine (S of 4) with **10 µg/mL PVP & PVAc** present in solution. ω = 6000 rpm**.**

B.6 Data for Figures 6.2, 6.3, 6.5, and 6.7

a) 07012015_RDAexp_Sof4_3000rpm_afterHPMCAS_freshbuffer

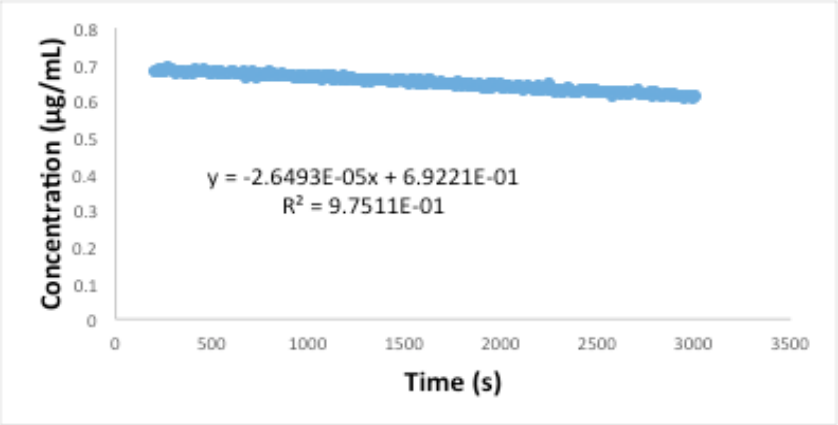

b) 07012015_RDAexp_Sof4_3000rpm_afterHPMCAS_freshbuffer_2

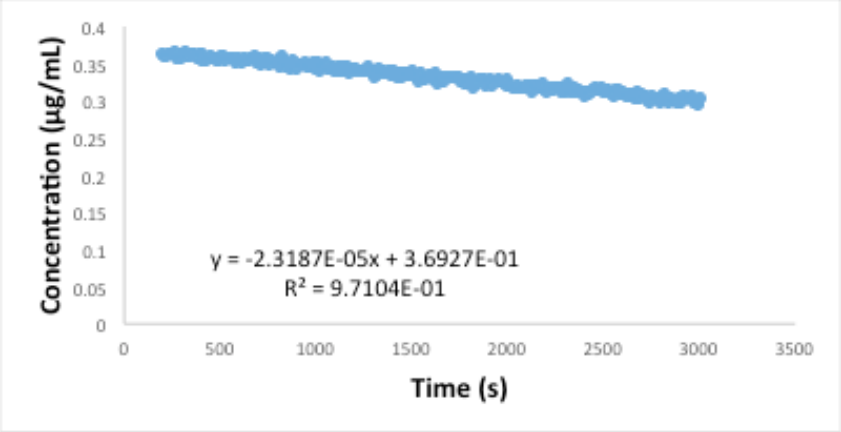

c) 07082015_RDAexp_Sof4_3000rpm_afterHPMCAS_freshbuffer

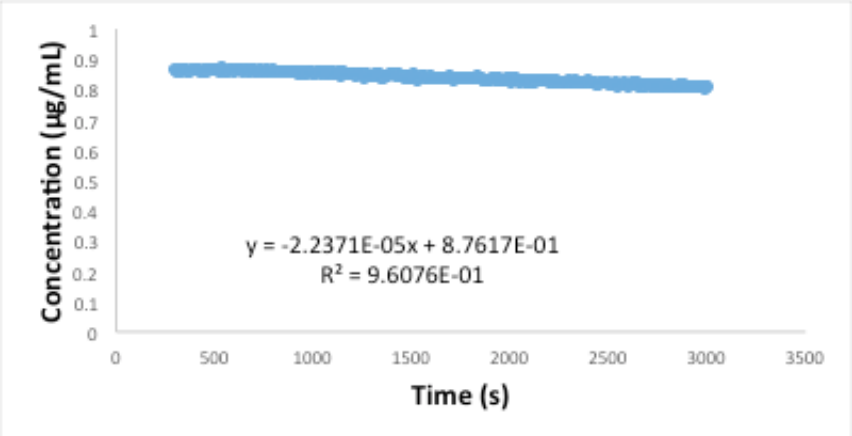

Figure B.35. (a-c) Desupersaturation profiles for felodipine (S of 4) prepared using **method *(ii)***. Growth was measured with **no polymer** present. ω = 3000 rpm**.**

a) 08262015_RDAexp_Sof4_3000rpm_afterHPMCAS_freshbuffer_aftergrowth

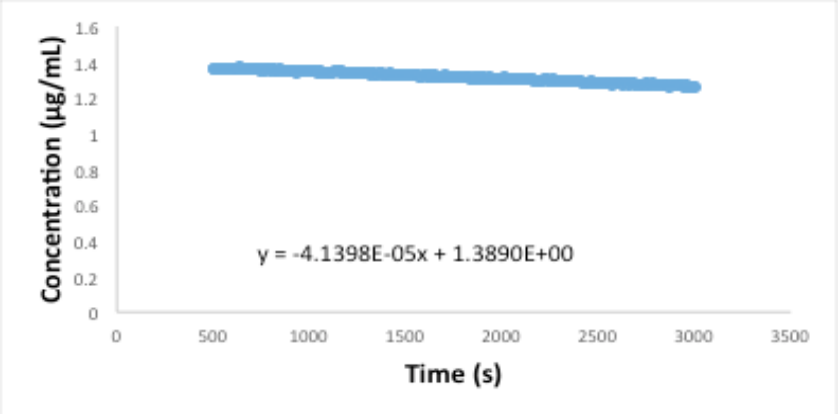

b) 08262015_RDAexp_Sof4_3000rpm_afterHPMCAS_freshbuffer_aftergrowth_2

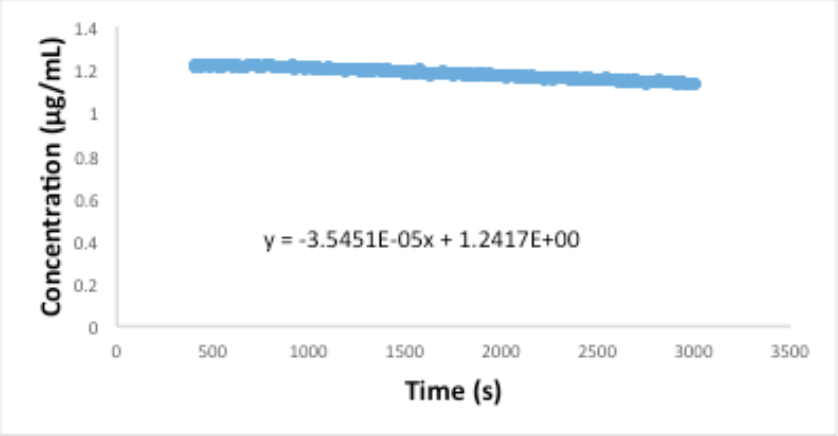

c) 08262015_RDAexp_Sof4_3000rpm_afterHPMCAS_freshbuffer_aftergrowth_3

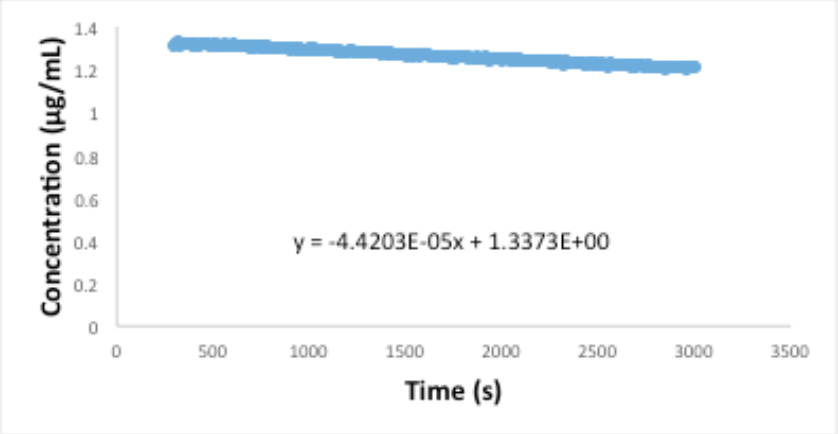

Figure B.36. (a-c) Desupersaturation profiles for felodipine (S of 4) prepared using **method *(ii)***. Growth was measured with **no polymer** present, **2nd growth** experiment. ω = 3000 rpm**.**

a) 12032014_RDAexp_3000rpm_Sof4_wHPMCAS_pre

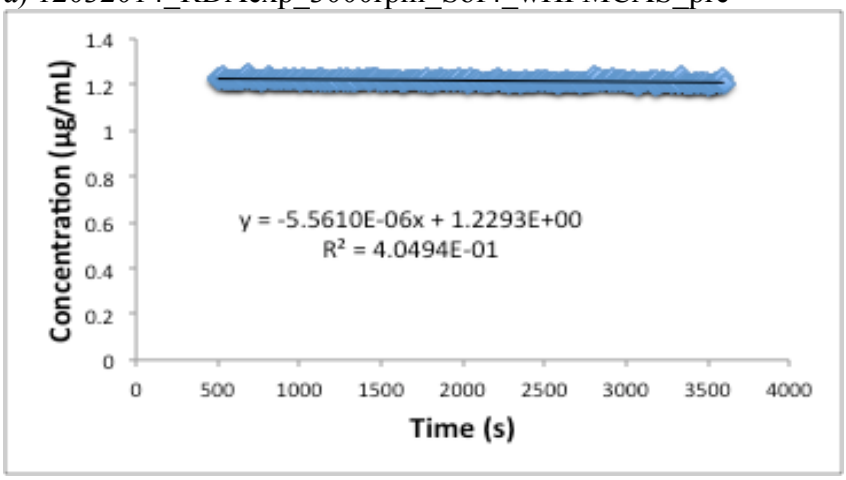

b) 06092015_RDAexp_Sof4_3000rpm_afterHPMCAS_same soln

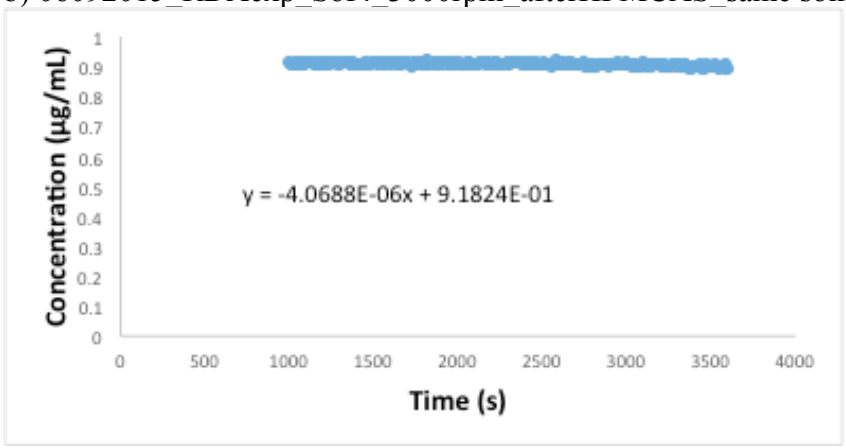

c) 08042015_RDAexp_Sof4_3000rpm_afterHPMCAS_samesoln

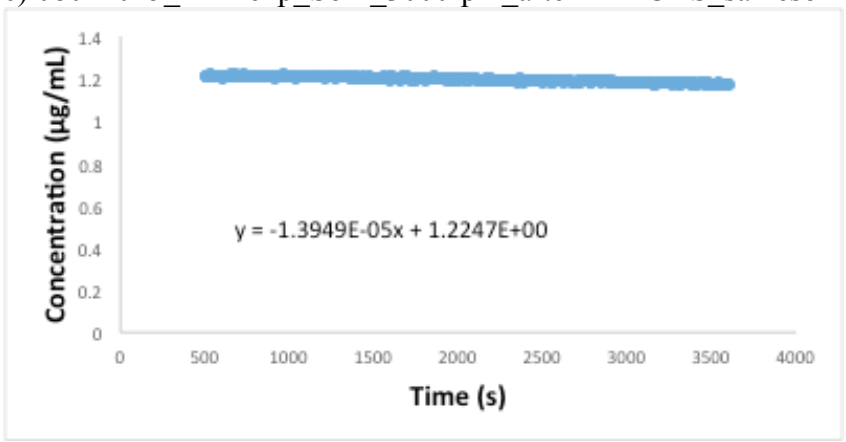

Figure B.37. (a-c) Desupersaturation profiles for felodipine (S of 4) prepared using **method *(ii)***. Growth was measured with 5 µg/mL **HPMCAS** present in solution. ω = 3000 rpm**.**

a) 07012015_RDAexp_Sof4_3000rpm_seedgrowthwHPMCAS_freshbuffer

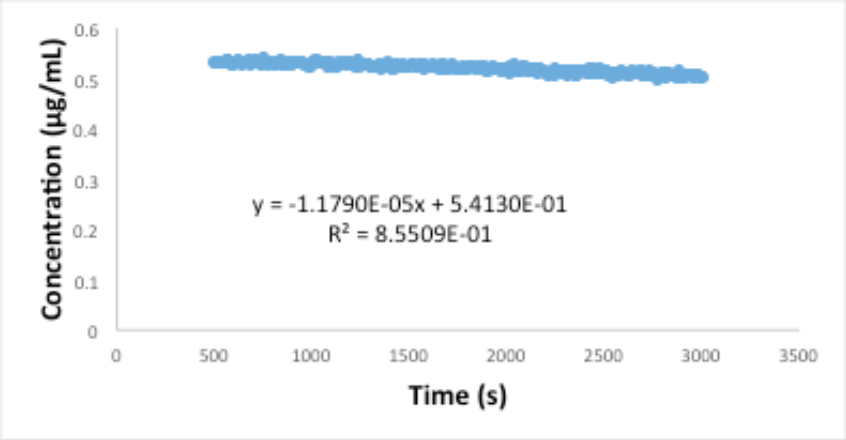

b) 07012015_RDAexp_Sof4_3000rpm_seedgrowthwHPMCAS_freshbuffer_2

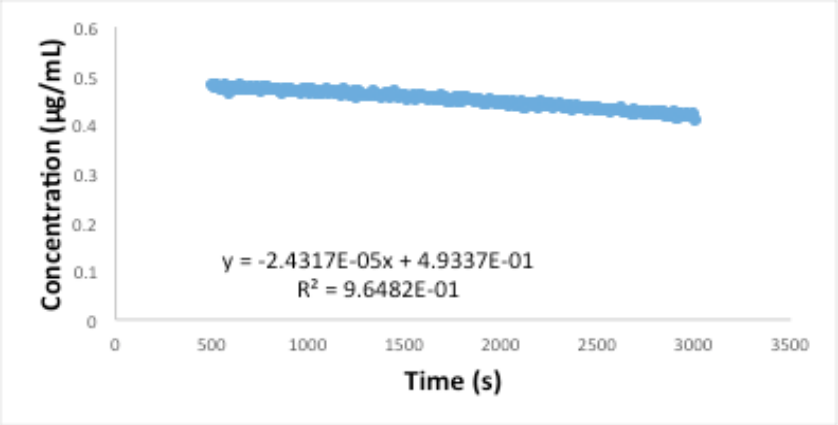

c) 07082015_RDAexp_Sof4_3000rpm_seedgrowthwHPMCAS_freshbuffer_2

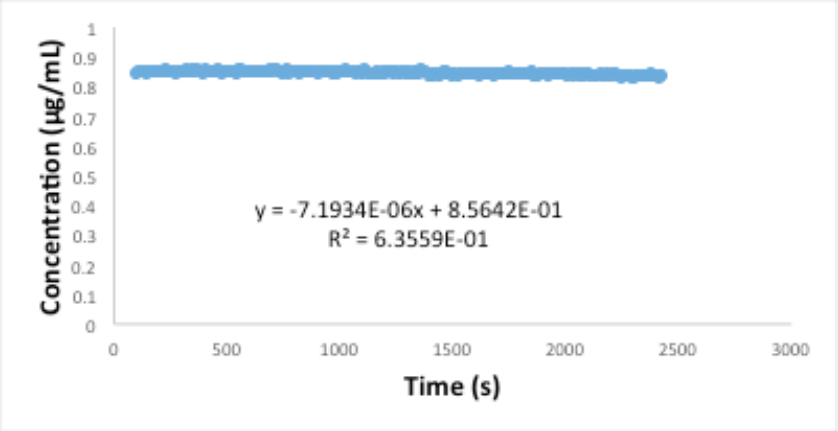

Figure B.38. (a-c) Desupersaturation profiles for felodipine (S of 4) prepared using **method *(iii)***. Growth was measured with **no polymer** present. ω = 3000 rpm**.**

a) 06262015_RDAexp_Sof4_3000rpm_seedgrowthwHPMCAS_samesoln

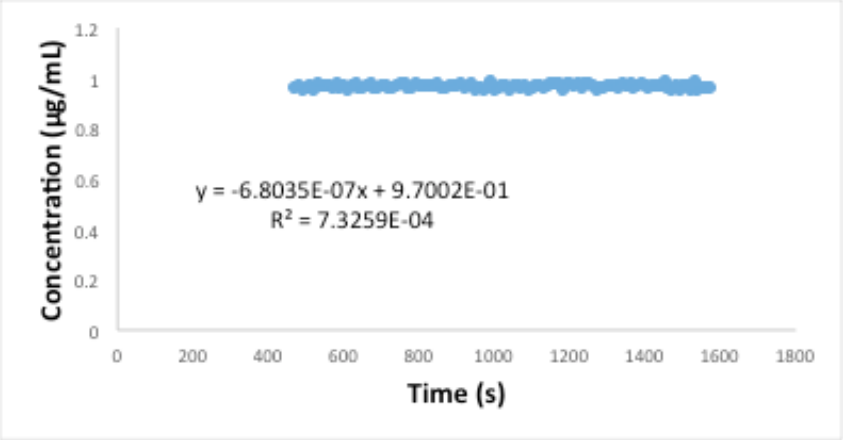

b) 06302015_RDAexp_Sof4_3000rpm_seedgrowthwHPMCAS_samesoln

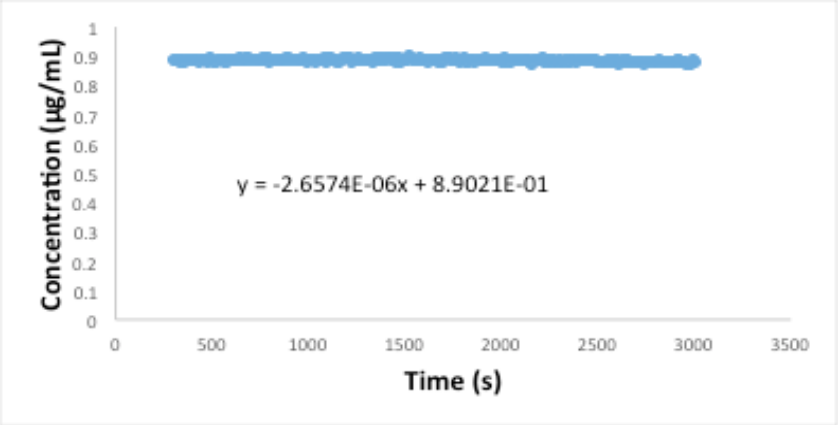

c) 06302015_RDAexp_Sof4_3000rpm_seedgrowthwHPMCAS_samesoln_2

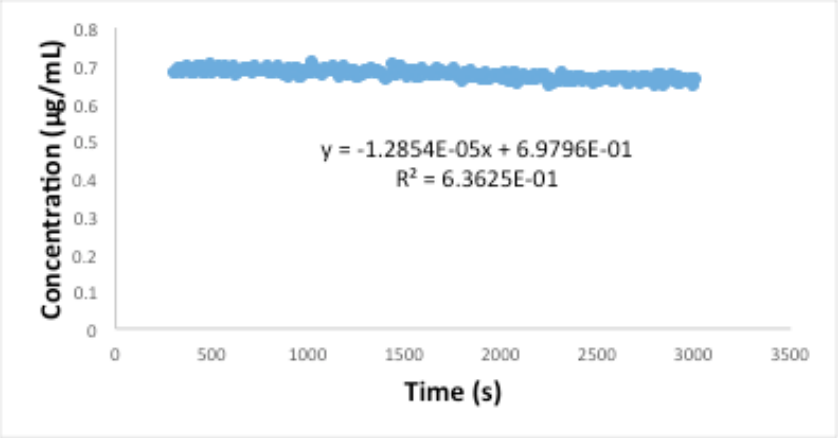

Figure B.39. (a-c) Desupersaturation profiles for felodipine (S of 4) prepared using **method *(iii)***. Growth was measured with 5 µg/mL **HPMCAS** present in solution. ω = 3000 rpm**.**

a) 08272015_RDAexp_Sof4_3000rpm_soliddisp10

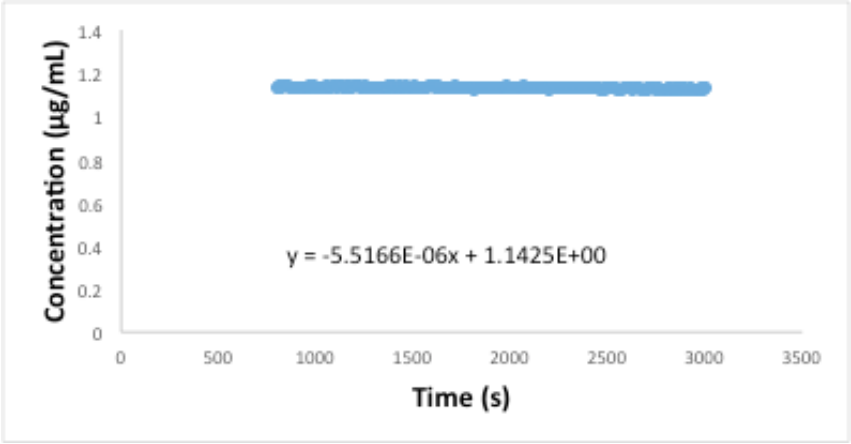

b) 08272015_RDAexp_Sof4_3000rpm_soliddisp10_2

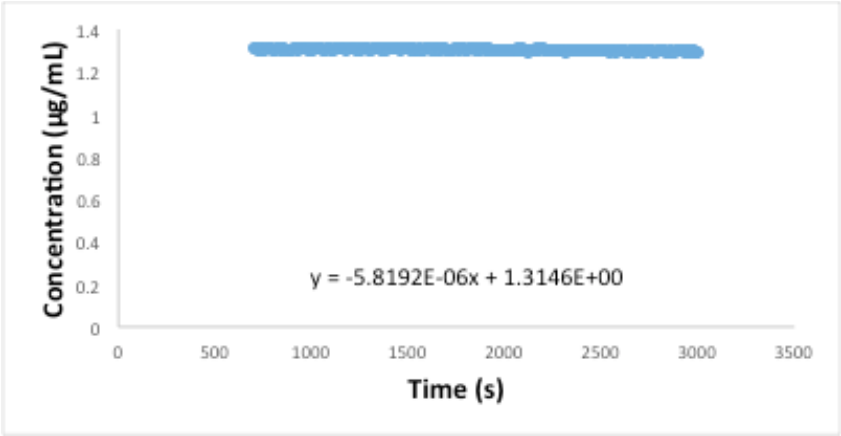

c) 08272015_RDAexp_Sof4_3000rpm_soliddisp10_3

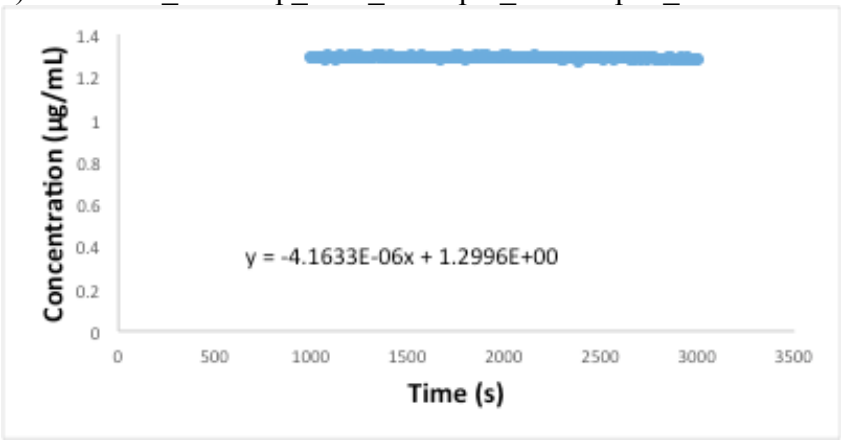

Figure B.40. (a-c) Desupersaturation profiles for felodipine (S of 4) prepared using **method *(iv)***. Growth was measured with **no polymer** present. ω = 3000 rpm**.**

a) 09082015_RDAexp_Sof4_3000rpm_soliddisp_polysoln

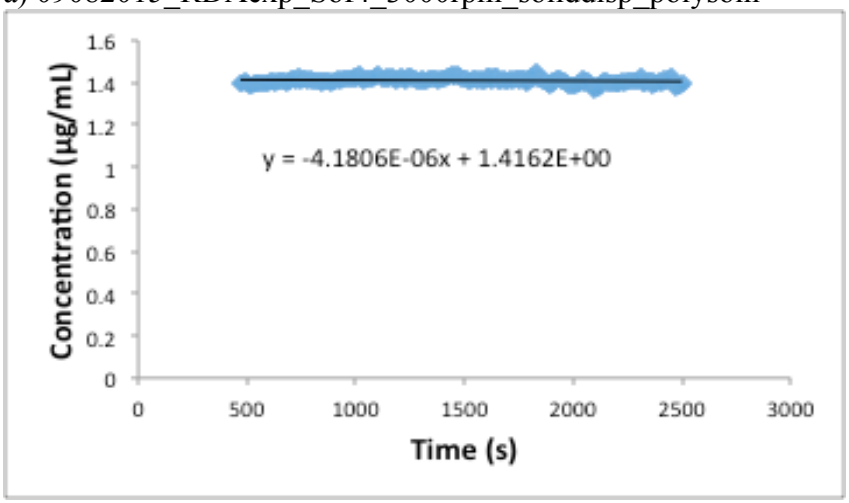

b) 09082015_RDAexp_Sof4_3000rpm_soliddisp_polysoln_2

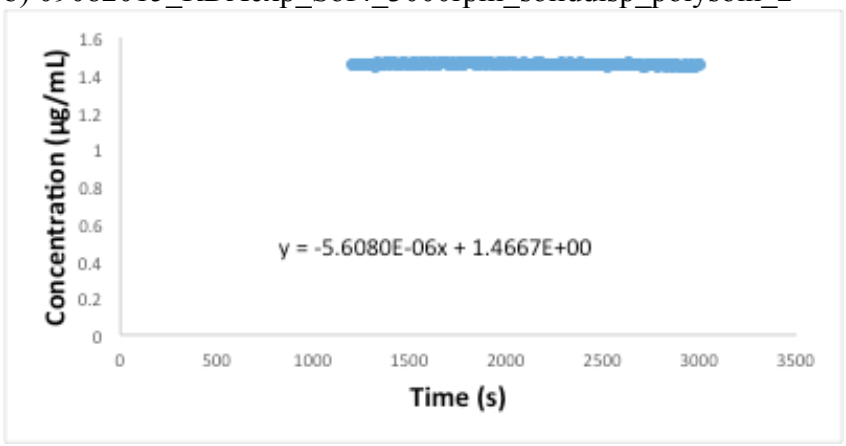

c) 09082015_RDAexp_Sof4_3000rpm_soliddisp_polysoln_3

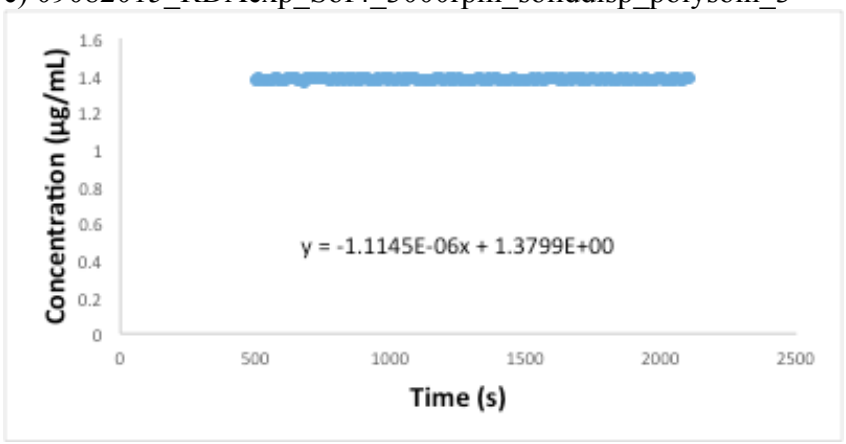

Figure B.41. (a-c) Desupersaturation profiles for felodipine (S of 4) prepared using **method (*iv*)**. Growth was measured with 5 µg/mL **HPMCAS** present in solution. ω = 3000 rpm**.**

B.7 Data for Figure 6.10

a) 08192015_RDAexp_Sof4_3000rpm_wHPMCASandSDS_2

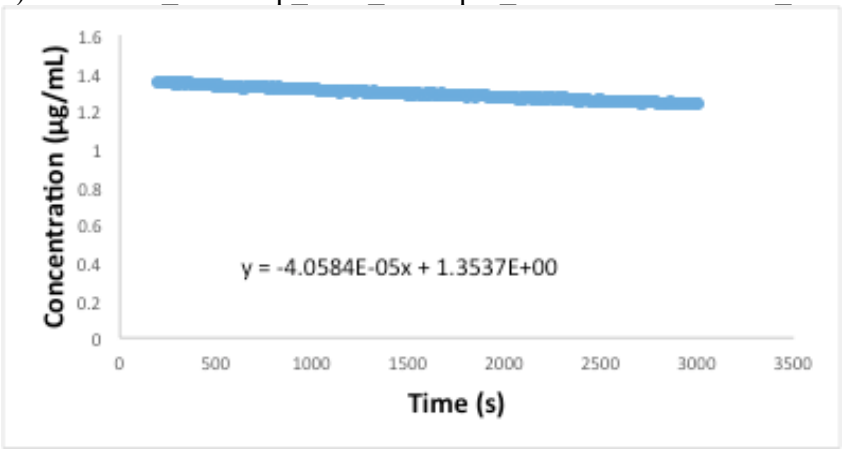

b) 08192015_RDAexp_Sof4_3000rpm_wHPMCASandSDS_3

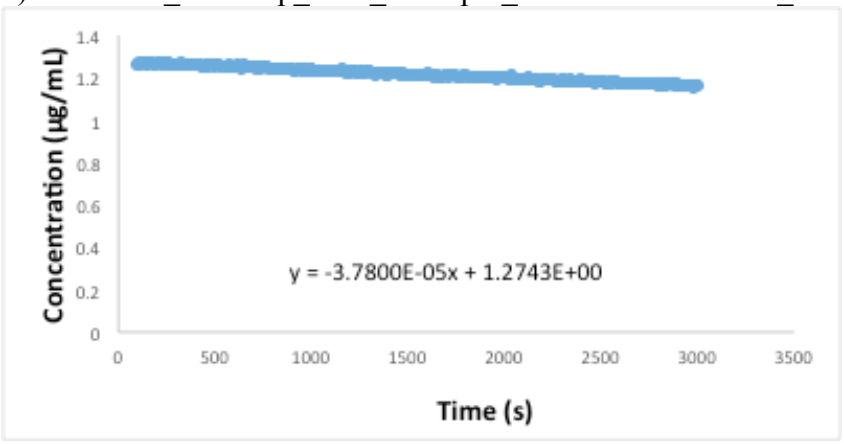

c) 08192015_RDAexp_Sof4_3000rpm_wHPMCASandSDS_4

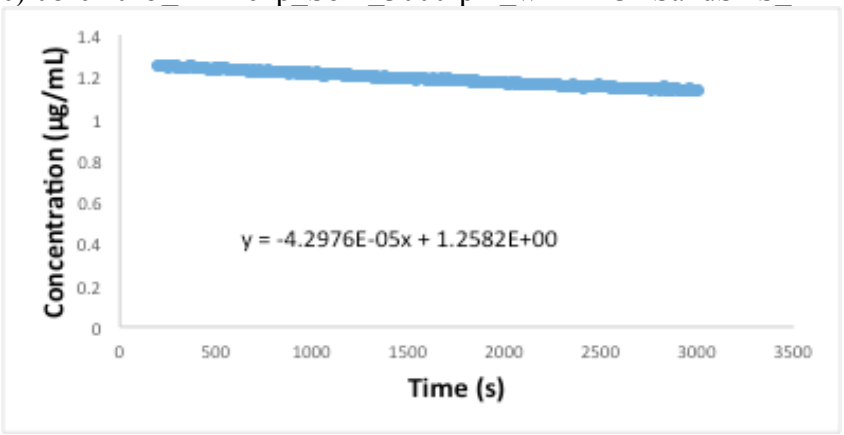

Figure B.42. (a-c) Desupersaturation profiles for felodipine (S of 4) with 5 µg/mL **HPMCAS** and 100 µg/mL **SDS** 5µg/mL present in solution. ω = 3000 rpm**.**

a) 09212015_RDAexp_Sof4_3000rpm_felodipineSDS

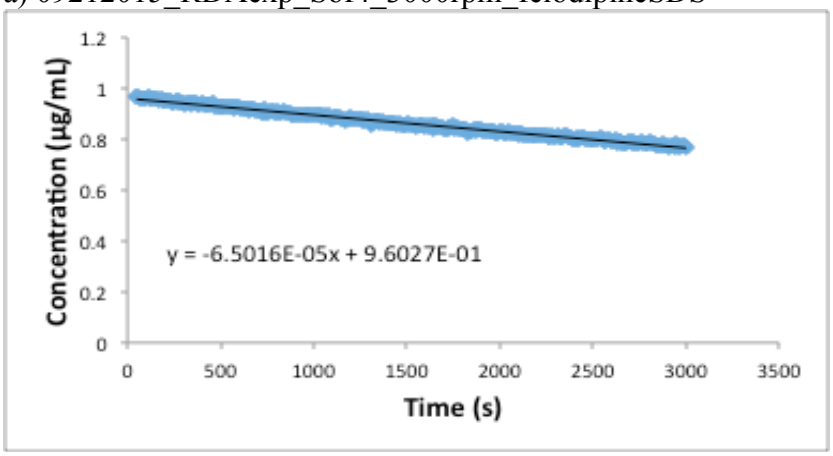

b) 09212015_RDAexp_Sof4_3000rpm_felodipineSDS_2

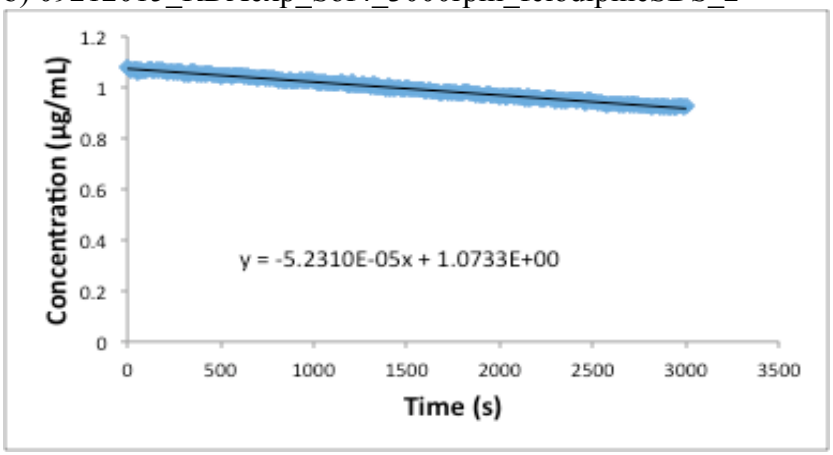

c) 09212015_RDAexp_Sof4_3000rpm_felodipineSDS_3

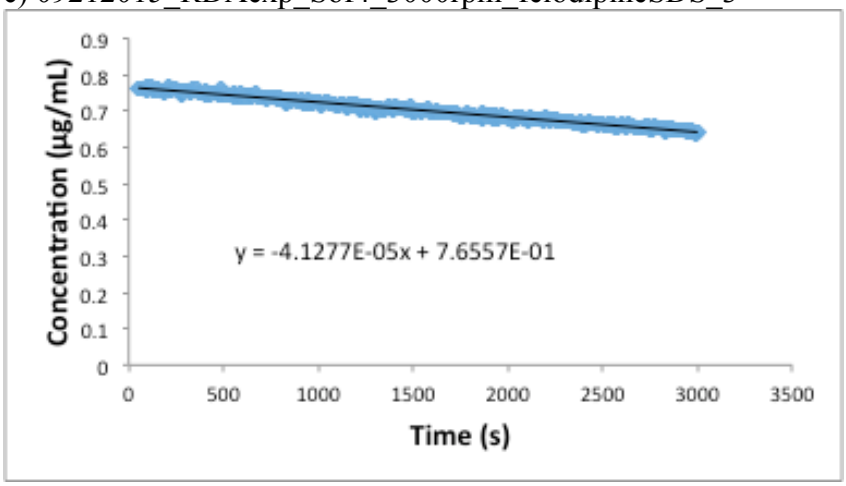

Figure B.43. (a-c) Desupersaturation profiles for felodipine (S of 4) with 100 µg/mL **SDS** present in solution. ω = 3000 rpm**.**

B.8 AFM and IR-AFM Data

Table B.1. AFM Data Filenames

Figure	Filename
4.3a	cjs_20130716_NPG_c_felodipineHPMCAS_liq_pH3_2um_3.000
4.3b	cjs_20130724_NPG_c_felodipineHPMCAS_liq_pH6.8_2um_3.000
4.3c	cjs_20140205_NPG_c_felodipine_liq_pH6.8_2um_4.003
4.4a	cjs_20130724_NPG_c_felodipineHPMCAS_liq_pH6.8_500nm_3.000
4.4b	cjs_20130716_NPG_c_felodipineHPMCAS_liq_pH3_500nm_2.001
4.4c	cjs_20131030_NPG_c_felodipineHPMCAS_liq_pH3_2um_1.004
4.6a/c	cjs_20131030_NPG_c_felodipineHPMCAS_liq_pH3_2um_1.005
4.6b/d	cjs_20131030_NPG_c_felodipineHPMCAS_liq_pH6.8_2um_1.002
4.7	cjs_20131220_felodipineHPMCAS H6 Spectra w markers
4.8a	cjs_20131208_1209_felodipineHPMCAS_IR
4.8b	cjs_20131220_felodipineHPMCAS_1700_IR4
4.8c	cjs_20131220_felodipineHPMCAS_1720_IR6
4.9	cjs_20131030_NPG_c_felodipineHPMCAS_liq_pH3_2um_1.002
5.2a	cjs_20150506_SNL_c_felodipinePAA_liq_1um_3.000 crop750
5.2b / 5.4a	cjs_20150206_NPG_c_felodipinePVP_liq_2um_3.001 crop750
5.2c / 5.4g	cjs_20150221_SNL_c_felodipineHPMCAS_liq_1um_2.002 crop750
5.2d / 5.4c	cjs_20150122_NPG_c_felodipinePVAc_liq_2um_3.000 crop750
5.2e	cjs_20150505_SNL_c_felodipine_liq_1um_2.004 crop750
5.4b	cjs_20150317_SNL_c_felodipineP2VP_liq_1um_2.001 crop750

5.4d	cjs_20150217_SNL_c_felodipinePVPVA_liq_1um_2.000 crop750
5.4e	cjs_20150303_SNL_c_felodipinePVPandPVAc_liq_1um_2.000 crop750
5.4f	cjs_20150605_NPG_c_felodipinePVPVA10_2_liq_3um_1.000 crop750
5.4h	cjs_20150217_SNL_c_felodipineHPMC_liq_1um_2.001 crop750
6.4a	cjs_20150811_NPG_c_felodipine_aftergrowth_liq_1um_1.001
6.4b	cjs_20150807_NPG_c_felodipine_wHPMCAS_aftergrowth_liq_1um_4.002
6.4c	cjs_20150807_NPG_c_felodipine_afterHPMCAS_aftergrowth_freshbuffer_liq_1um_1.002
6.4d	cjs_20150811_NPG_c_felodipine_afterHPMCAS_aftergrowth_samesoln_liq_1um_2.002
6.6a	cjs_20150722_NPG_c_felodipine_liq_5um_2.000
6.6b	cjs_20150722_NPG_c_felodipine_seedgrowthwHPMCAS_liq_5um_4.000
6.8a	cjs_20150722_NPG_c_felodipine_seedgrowthwHPMCAS_liq_1um_3.000
6.8b / 6.9	cjs_20150917_NPG_c_felodipineHPMCAS_soliddisp_liq_1um_2.001
6.11a	cjs_20150505_SNL_c_felodipine_liq_1um_2.004
6.11b	cjs_20150221_SNL_c_felodipineHPMCAS_liq_1um_2.003
6.11c	cjs_20150901_SNL_c_felodipineHPMCAS&SDS_liq_1um_2.001

VITA

VITA

Caitlin Joy Schram was born in Royal Oak, Michigan, on January 2, 1989, the daughter of Tim and Vicki Schram. After finishing first in her high school class in 2007, she began studying chemical and biomolecular engineering at Johns Hopkins University, receiving the degree of Bachelor of Science in May, 2011. She entered the graduate program in the School of Chemical Engineering at Purdue University in August, 2011, receiving her Doctor of Philosophy degree in December, 2015. She then began working as a scientist in the Process Analytical Technology group at Vertex Pharmaceuticals in Boston, Massachusetts, in January 2016.

.

PUBLICATIONS

PUBLICATIONS

- Schram, C.J.; Beaudoin, S.P.; Taylor, L.S. Impact of Polymer Conformation on the Crystal Growth Inhibition of a Poorly Water-Soluble Drug in Aqueous Solution. *Langmuir* **2015**, *31*, 171-179.

- Schram, C.J.; Taylor, L.S.; Beaudoin, S.P. Influence of Polymers on the Crystal Growth Rate of Felodipine – Correlating Adsorbed Polymer Surface Coverage to Solution Crystal Growth Inhibition. *Langmuir* **2015**, *31*, 11279 – 11287.

- Schram, C.J.; Smyth, R.J.; Taylor, L.S.; Beaudoin, S.P. Understanding Crystal Growth Kinetics in the Absence and Presence of an Impurity Using a Rotating Disk Apparatus. *Cryst. Growth Des. In Review*.

- Schram, C.J.; Beaudoin, S.P.; Taylor, L.S. Polymer Inhibition of Crystal Growth by Surface Poisoning. *Cryst. Growth Des. In Review.*

- Schram, C.J.; Howes, T.; Beaudoin, S.P. Assessing the Stabilization Potential of Various Polymers for Spray-Dried Amorphous Lactose. *In Preparation*.